

Heterogeneous input in a subduction system & its effect on plate boundary processes

Structural analysis of the
Osa Mélange, SW Costa Rica

by

Alexander P. Clarke

JUNE 2018

*A thesis submitted for the degree
of Doctor of Philosophy*



Department of Earth Sciences
Royal Holloway, University of London

THIS PAGE INTENTIONALLY LEFT BLANK.

“ What we saw of the broken rocks, consisting inainly of greywackes, limestones, and the Steinmann trinity, rivalled in abandoned disarray Puck’s most mischievous attempts to puzzle and confuse mere mortal man. ”

Bailey & McCallien (1950)

I, Alexander Peter Clarke, hereby declare that this thesis and the work contained within are entirely my own, unless stated otherwise. Chapter 5.6 contains an early draft preview of a co-authored paper intended for publication. Chapters 6 – 8 are a collection of co-authored papers which are either published, submitted for publication, or awaiting submission for publication. I am responsible for the data collection and analysis throughout this thesis, and for primary authorship of all 4 of the included papers; detailed statements of my contributions to each of the co-authored papers are included on the cover page of each paper.

Signed:

A handwritten signature in black ink, appearing to read 'Alexander Peter Clarke', written in a cursive style.

Dated: 22nd November 2018

ABSTRACT

The Middle America Subduction Zone is the type example of an erosive margin; i.e. material is removed from the forearc and incorporated into the subduction channel. The Osa Mélange (SW Costa Rica) occupies the forearc of this subduction zone and is currently being tectonically eroded. This mélangé consists of blocks of altered basalt, chert, and carbonate within a volcanoclastic pelitic matrix. Using field study, microstructural analysis, rock physics, and numerical modelling, we have characterised the geological history of this mélangé and determined the pattern of its future deformation.

This mélangé originated on the incoming plate by mass wasting from a seamount chain into its flexural moat. Flexural moats are major sites of oceanic sedimentation and may contain up to 3 km of sediment. Sediment thickness at the trench is a fundamental control on whether the subduction zone is erosive or accretionary, therefore subduction of a flexural moat may promote localised accretion, even if the subduction zone is otherwise erosive. The Osa Mélangé is the first recognised example of an accreted seamount moat.

Mélanges are commonly envisaged as strong, stiff blocks within a weak, compliant matrix; however triaxial deformation experiments on an altered basalt megablock and its surrounding volcanoclastic matrix show that the matrix of the Osa Mélangé is now stronger and stiffer than the blocks. Compliant blocks in stiffer matrix make the rock unit more prone to fracture, therefore low block-to-matrix ratios do not always promote aseismic creep. Whether fractures form in blocks or matrix depends on the difference in strength and difference in Young's modulus. Failure in one block promotes failure in its neighbours and surrounding matrix, priming the subduction interface for through-going rupture.

As the mélangé is tectonically eroded by hydrofracturing of the hanging wall, the style of incorporation is controlled by its fabric and rheology. Where aspect ratios are low, weaker material is comminuted into the plate boundary interface, whereas high aspect ratios, reactivate pre-existing weaknesses to form blocks in the subduction channel composed of both lithologies.

THIS PAGE INTENTIONALLY LEFT BLANK.

ACKNOWLEDGEMENTS

Firstly, I would like to thank my supervisor, Paola Vannucchi, for all her help and advice over the last four years and for her comments and suggestions which have vastly improved this thesis. Paola provided the starting point for this project and followed its evolution and development while allowing me the academic freedom to explore the avenues of research that most interested me. I am also very thankful to Jason Morgan for his guidance and very stimulating discussions, culminating in several of the key ideas in this thesis. Enormous thanks go to Audrey Ougier-Simonin (BGS) for her support and assistance with the physical properties and laboratory aspects of this project. I would also like to thank Christina Manning for her support as my Advisor and for helping me with my geochemical analysis. I am also thankful to Luca Menegon and Euan Nisbet for a stimulating viva examination.

This PhD project would not have got off the ground without funding from the RHUL Earth Sciences Department Research Committee and the Geological Society of London. I would also like to thank Robert Hall and the South East Asia Research Group, as well as Euan Nisbet for their generous monetary support. I am also very grateful to Kevin D'Souza, Dan Parsonage, and Sue Woods for helping with numerous logistical matters. I am also deeply appreciative of the work done by Margaret Collinson on behalf of the postgraduates in our department and for her sage advice in my times of need.

My undying gratitude goes to Lotte Leclézio, Helen Loxely-Blount, and Humarrah Sheikh for being the best friends anyone could ask for and for supporting me throughout this project; without them I certainly would not have completed this thesis. Enormous thanks go to Sandy Drymoni who has been a great and supportive friend and who I have bounced many ideas off during this PhD. I am also hugely grateful to David Cavell for his support and friendship, stimulating discussions, and for proof-reading Chapter 2. I would like to thank Loren Snow for their support and understanding these past few years and for starting the chain of events that led to my interest in *mélanges*. I am also thankful to Nathaniel Forbes Inskip and Kayode Adeoye-Akinde

for their stimulating discussions and for helping me learn how to use COMSOL Multiphysics.

Big thanks also go to Amy Gough, Rebecca Brownlow, Amy Tuck-Martin, Adam Creaser, Eddy Evans, Zoë Matthews, and many others for enjoyable tea breaks when I needed them the most. Numerous other members of the postgraduate community in the Earth Sciences department at RHUL are also thanked for their kindness and help with myriad issues. I would also like to thank Hayley Hunt for proofreading Chapter 3 and ensuring the explanations therein are understandable to those outside of the field. Thank you also to Charlotte Ball and Chris Stocker who provided me with places to stay while conducting my experiments at the BGS. I also thank Christof Liebermann, Zoë Matthews (again) and other denizens of 5 Runnymede Court for putting up with me during the final stages of this thesis. I am also very thankful to the members of my St John Ambulance unit – especially Will Dommett and Amandine Donovan – for providing me with a break from geology when the work became too much.

Finally, I am tremendously grateful to my parents, Sue and Andy Clarke, for their never-ending support and assistance and for helping me in so many ways to complete this thesis. This PhD would not have been possible without them.

TABLE OF CONTENTS

CHAPTER 1. Introduction	17
1.1. <i>Aims and Outline of this Thesis</i>	18
CHAPTER 2. Regional Geology	21
2.1. <i>Geographical and Geological Configuration of the Osa Peninsula and Surrounding Areas</i>	21
2.2. <i>Previous Interpretations of the Formation of the Osa Melange</i>	28
2.3. <i>Tectonic history of Central America and the Caribbean in the Mesozoic and Cenozoic</i>	38
2.4. <i>Summary of regional geology</i>	63
CHAPTER 3. The Subduction Zone Plate Boundary Interface:	65
3.1. <i>The Subduction Channel</i>	65
3.2. <i>Accretion and Erosion</i>	73
3.3. <i>Slip on the Plate Boundary</i>	81
3.4. <i>Summary of subduction zone background</i>	93
CHAPTER 4. Mélanges	95
4.1. <i>History of the term</i>	96
4.2. <i>Different definitions proposed</i>	112
4.3. <i>Use of the term “Mélanges” in this thesis</i>	114
CHAPTER 5. Methodology	117
5.1. <i>Field methods</i>	117
5.2. <i>Light microscopy methods</i>	121
5.3. <i>Rock mechanics methods</i>	122
5.4. <i>Numerical modelling methods</i>	131
5.5. <i>Geochemical methods</i>	133
5.6. <i>Image analysis methods</i>	134
CHAPTER 6. Seamount chain – subduction zone interactions:	149

CHAPTER 7. Weak Blocks in a Strong Matrix:	150
7.1. <i>Abstract</i>	150
7.2. <i>Introduction</i>	151
7.3. <i>Geology of the Osa Mélange</i>	154
7.4. <i>Experimental Deformation of Blocks and Matrix</i>	158
7.5. <i>Numerical Modelling</i>	160
7.6. <i>Interpretation & Implications</i>	163
7.7. <i>Conclusions</i>	166
7.8. <i>References</i>	168
7.9. <i>Supplementary Material</i>	171
CHAPTER 8. Deformation history of the Osa Mélange, SW Costa Rica, and the influence of its rheology and complex fabric on subduction erosion in Central America	176
8.1. <i>Abstract</i>	177
8.2. <i>Introduction</i>	177
8.3. <i>Methods</i>	179
8.4. <i>Geology of the Osa Mélange</i>	180
8.5. <i>Multi-Stage Evolution of the Osa Mélange</i>	196
8.6. <i>Conclusions</i>	205
8.7. <i>References</i>	206
8.8. <i>Supplementary Material</i>	210
CHAPTER 9. Provenance of the Osa Mélange Blocks	214
9.1. <i>Introduction</i>	214
9.2. <i>Results</i>	218
9.3. <i>Discussion</i>	226
9.4. <i>Conclusion</i>	231
CHAPTER 10. Discussion	234
10.1. <i>How and where did the Osa Mélange form?</i>	234
10.2. <i>Is the Osa Mélange really a mélange?</i>	263
10.3. <i>What is the relationship between the Osa Mélange and the Caribbean Large Igneous Complex?</i>	266
10.4. <i>What is the effect of mélangé fabrics and rheology on slip at the plate boundary?</i>	270
10.5. <i>Critical evaluation of research process and recommendations for future work</i>	280

CHAPTER 11. Conclusion	300
CHAPTER 12. References	302
APPENDIX 1. Geochemical Data	336
APPENDIX 2. Structural Anisotropy Data	338
APPENDIX 3. Triaxial Experiment Data	342

THIS PAGE INTENTIONALLY LEFT BLANK.

LIST OF FIGURES, EQUATIONS & TABLES

CHAPTER 2. REGIONAL GEOLOGY

- FIG. 2.1. Geological map of the Osa Peninsula 22
- FIG. 2.2. Map of nearby geological features on the Caribbean and Cocos Plates 24
- FIG. 2.3. Comparison between different models of Osa Melange formation 30
- FIG. 2.4. Two competing models of origin and emplacement of the Caribbean plateau 40
- FIG. 2.5. In situ model of Caribbean formation 45
- FIG. 2.6. Geological map southern Central America showing arc fronts 50
- FIG. 2.7. Structural evolution of the Osa Melange 51
- FIG. 2.8. Stratigraphy of the Fila Costena 52
- FIG. 2.9. Breakup of the Farallon Plate and the evolution of the Cocos-Nazca Spreading Centre 55
- FIG. 2.10. Stratigraphy of the Charco Azul Group 59

CHAPTER 3. THE SUBDUCTION ZONE PLATE

BOUNDARY INTERFACE

- FIG. 3.1. Anatomy of a subduction channel 66
- FIG. 3.2. Deformation mechanisms and styles at different depths within the subduction channel 67
- FIG. 3.3. Model of tectonic erosion 71
- FIG. 3.4. Global map of subduction zone margins showing the distribution of erosive and accretionary subduction zones 72
- FIG. 3.5. Graph of sediment thickness vs convergence rate 78
- FIG. 3.6. Cross sections of idealised accretionary and erosive margins 80
- FIG. 3.7. Depths of different types of slip activity in a subduction zone 82
- EQUATION 3.1. Equation that relates rupture area to seismic energy release. 85

FIG. 3.8. Scaling laws showing the relationship between seismic moment and duration for regular earthquakes and slow earthquakes	86
FIG. 3.9. Schematic diagram of the plate boundary surface showing the heterogenous distribution of slip	87
FIG. 3.10. Graph showing the relative occurrence of megathrust earthquakes at thickly and thinly sedimented trenches.	90
FIG. 3.11. Diagram demonstrating the principle of velocity weakening and velocity strengthening behaviour	91
FIG. 3.12. Inferred relationship between block-in-matrix ratios and seismic style	93

CHAPTER 4. MÉLANGES

FIG. 4.1. Selection of Greenly's (1919) sketches	97
FIG. 4.2. Systems for classifying mélange units	104
FIG. 4.3. Genetic classification system of mélanges formed in different tectonic settings	106
FIG. 4.4. Hierarchical subdivision of mélange units used in this thesis	114

CHAPTER 5. METHODOLOGY

EQUATION 5.1. Equation to calculate dry density	123
EQUATION 5.2. Equation to calculate saturated density	123
EQUATION 5.3. Equation to calculate particle density	123
FIG. 5.1. Experimental setup to measure density and porosity using the saturation buoyancy test	124
EQUATION 5.4. Equation to calculate porosity	125
FIG. 5.2. Setup for the cell for triaxial strength test	126
FIG. 5.3. Photograph of the full setup for triaxial strength tests	127
EQUATION 5.5. Equation to calculate uncorrected point load strength	129
FIG. 5.4. Setup for the point load strength test	130
EQUATION 5.6. Equation to calculate size-corrected point load strength	131
EQUATION 5.7. Equation to calculate uncorrected point load strength	131
FIG. 5.5. Model geometry	132
FIG. 5.6. Process of discerning structural anisotropy	137

- FIG. 5.7. Figure showing 3 examples of structural anisotropy for synthetic data 138
- FIG. 5.8. Different domains within an image showing two distinct orientations 140
- FIG. 5.9. Examples of structural anisotropy analysis performed on photos from the Osa Mélange 143
- FIG. 5.10. Detailed geological map of the Gwna Mélange at Llanbadrig, northern Anglesey 144

CHAPTER 6. SEAMOUNT CHAIN – SUBDUCTION

ZONE INTERACTIONS

- FIG. 1. Gravity maps showing scale of seamount flexural moats 149
- FIG. 2. Geological map of Osa mélange 149
- FIG. 3. Conceptual model of frontal accretion of seamount moat sediments 149
- FIG. DR1. Geological map of the San Pedrillo Unit of the Osa mélange 149
- FIG. DR2. Typical appearance of the Cocolito Package 149
- FIG. DR3. Typical appearance of the Punta Marengo Package 149
- FIG. DR4. Typical appearance of the Bahia Drake Package 149
- FIG. DR5. Volume estimates of flexural moats and the Osa Mélange 149

CHAPTER 7. WEAK BLOCKS IN A STRONG MATRIX

- FIG. 7.1. Geological map of the San Pedrillo Unit of the Osa Mélange 152
- FIG. 7.2. Field photos and photomicrographs of blocks and matrix in the Punta Marengo Package 153
- FIG. 7.3. Photographs and schematic illustrations of the volcanoclastic matrix and altered basalt 155
- FIG. 7.4. Stress – strain graph showing the results of triaxial deformation experiments 157
- FIG. 7.5. Numerical modelling results 159
- FIG. 7.6. Graph showing which component will fail first with different rheological properties 162
- TABLE SUPPLEMENT 1. Summary of mechanical results 172

FIG. SUPPLEMENT 1. Photographs of samples after
experimental deformation 173

CHAPTER 8. DEFORMATION HISTORY OF THE OSA MÉLANGE, SW
COSTA RICA, AND THE INFLUENCE OF ITS RHEOLOGY AND COM-
PLEX FABRIC ON SUBDUCTION EROSION IN CENTRAL AMERICA

FIG. 8.1. Geological map of the Osa Peninsula 178
FIG. 8.2. Geological map of the San Pedrillo Unit 181
FIG. 8.3. Photographs and data for the Punta
Marenco Package 183
FIG. 8.4. Map of San Pedrillo Unit showing
strength of rocks 187
FIG. 8.5. Photographs and data for the Cocolito Package 189
FIG. 8.6. Photographs and data from the Bahia
Drake Package 192
FIG. 8.7. Photographs and data from the
Campanario Package 194
FIG. 8.8. Photographs of the Punta San Pedrillo Unit 195
FIG. 8.9. Illustrative diagram showing the three phases of Osa
Mélange evolution 197
FIG. 8.10. Schematic illustration of different styles of incorpora-
tion into the subduction channel 202
TABLE 8.1. Rock Mechanics Results 212

CHAPTER 9. PROVENANCE OF THE OSA MÉLANGE BLOCKS

FIG. 9.1. Geological map of the Osa Peninsula 215
FIG. 9.2. Photomicrographs of the lithologies analysed in this
geochemical pilot study 216
FIG. 9.3. Series discrimination diagrams 217
FIG. 9.4. Harker diagrams 219
FIG. 9.5. Normalised multi-element (spider) diagrams 223
FIG. 9.6. Spider diagrams showing footprints of
comparison units 225
FIG. 9.7. Tectonic discrimination diagrams 227
FIG. 9.8. Diagram illustrating the problems with proposed prove-
nances of Osa dacites 230

CHAPTER 10. DISCUSSION

- FIG. 10.1. Cross section through a seamount complex showing sedimentary facies 247
- FIG. 10.2. Unified model of Osa Mélange formation 253
- FIG. 10.3. Style of deformation expected in material that has been frontally accreted and underplated 257
- FIG. 10.4. Heterogeneity of subduction channel composition and processes 259
- FIG. 10.5. Outcrop patterns of the Nicoya and Herradura complexes 267
- FIG. 10.6. Sketch of the relative locations of the Nicoya and Inner Osa Igneous Complex oceanic plateaus in the Campanian 268
- FIG. 10.7. Mechanisms of material addition to the subduction channel 270
- FIG. 10.8. Reorientation of blocks into plane of weakness 271
- FIG. 10.9. Relationship between the angle of stress maxima and the aspect ratio of the block 277
- TABLE 10.1. Length of subduction zones worldwide that are subducting large high relief features 289

THIS PAGE INTENTIONALLY LEFT BLANK.

CHAPTER 1. INTRODUCTION

Erosive subduction zones constitute approximately half of all modern subduction zones (Clift and Vannucchi, 2004), and yet the influence of upper plate material into the subduction system on plate boundary processes remains poorly explored, in contrast to the influence of incoming plate material. Upper plate material is typically mechanically stronger, lithified, and may display a tectonic fabric largely absent from incoming plate sediments (Clift and Vannucchi, 2004). Similarly, while it is acknowledged the erosive and accretionary behaviour can change along the length of the trench – controlled largely by sediment volume in the trench – perturbations causing localised accretion in response to locally thick sediment packages on the incoming plate have not been described. This thesis addresses these matters.

For this thesis, we elected to focus our study on the Osa Peninsula in southwestern Costa Rica as it is located only a few kilometres from the erosive Middle America Subduction Zone and is one of the few locations in the world where the outer portion of the active forearc is subaerially exposed. The Middle America Subduction Zone is the type locality for erosive subduction zones and has been the target of 2 IODP expeditions, IODP Exp. 334 (Vannucchi *et al.*, 2011) and IODP Exp. 344 (Harris *et al.*, 2012). The Osa Peninsula is subaerially exposed due to the subduction of the Cocos Ridge occurring immediately outboard of the Osa Peninsula, which has caused significant uplift in combination with increased basal erosion.

This peninsula exposes the Osa Mélange, which is a chaotic block-in-matrix rock unit composed of blocks of basalt, chert and carbonate in a volcanoclastic pelitic matrix. This is one of several accreted terranes on the Pacific margin of Central America that was originally formed above the Galapagos hotspot. This mélange also occupies the hanging wall of the Middle America Subduction Zone, meaning that it is currently being tectonically incorporated into the subduction channel.

This thesis addresses the processes and setting of mélange formation, characterises the deformation history and structural

INTRODUCTION

fabric, and hypothesises as to the active and future deformation as it is incorporated into the subduction channel.

1.1. AIMS AND OUTLINE OF THIS THESIS

While erosive subduction zones represent approximately half of the world's subduction zones (Clift and Vannucchi, 2004), the effect of pre-existing fabrics in the upper plate on incorporation and deformation within the subduction channel has remained hitherto unstudied. This study aims to address this oversight by characterising the structure and rheology of the Osa Melange, first prior to subduction, and then during and after it was accreted, and modelling the influence of this heterogeneity on the deformation at the plate interface. To do so, this study aims to answer the following questions:

- How and where did the Osa Melange form?
- What is the strength of the blocks and matrix in the Osa Melange and how have they evolved through time?
- How does the degree of heterogeneity within the subduction channel affect the style of slip within the plate boundary interface?
- How do the changing block and matrix rheologies affect the style of slip within the plate boundary interface?
- How does the differential strength of materials in the forearc affect their incorporation into the subduction channel?
- How do the different tectonic fabrics in the Osa Melange affect their incorporation into the subduction channel?

To provide a background and context for this study, Chapter 2 introduces the locations and tectonostratigraphic units that will be discussed throughout this thesis and details the geological history of the Central American region from the Cretaceous onwards, while Chapter 3 discusses the processes operating at the subduction zone plate interface and introduces recent advancements in this field, and Chapter 4 provides a detailed introduction to the study of melanges and includes an extended note on the history of the development of the term “melange”. Chapter 5 details the methodologies employed by this study, including the standard methodologies of geological research and the novel techniques detailed in Chapter 5.6. Chapter 6 (“Seamount chain – subduction zone interactions: Implications for

accretionary and erosive subduction zone behavior”) presents my hypothesis for the environment of formation of the Osa Mélangé and invokes a hitherto not-proposed location where subduction accretion may occur. Chapter 7 (“Weak Blocks in a Strong Matrix: the effects of rheological inversion on subduction zone seismicity”) addresses how the rheologies of the blocks and matrix change with increasing deformation and burial and how this influences seismicity at the plate boundary. Chapter 8 (“Deformation history of the Osa Mélangé, SW Costa Rica, and the influence of its rheology and complex fabric on subduction erosion in Central America”) presents a comprehensive study of how the rheology and anisotropy of the mélangé vary throughout the rock unit and what this means for the style of reincorporation into the subduction channel during subduction erosion. Chapter 9 addresses the high degree of pervasive alteration and questions the efficacy of geochemical analysis to discern the provenance of these rocks. Chapter 10 contains an extended discussion of the ideas presented in this thesis and critically evaluates the work done. Finally, Chapter 11 presents the thesis conclusions.

Chapter 6 has already been published (Clarke *et al.*, 2018), Chapter 7 has been submitted to the Journal of Geophysical Research, and Chapter 8 is awaiting submission to Tectonics. As such, these chapters contain their own introductions, methodologies, results, discussions and conclusions relevant to the subject matter they contain. It is the author’s intention that the ideas contained in Chapter 5.6 (“Quantitative characterisation of mélangé fabrics using image analysis: a simple method for determining structural anisotropy from field photos”) and Chapter 9 (“Provenance of the Osa Mélangé Blocks”) be written for publication at a later date pending additional data collection outside of the scope of this doctoral project.

THIS PAGE INTENTIONALLY LEFT BLANK.

CHAPTER 2. REGIONAL GEOLOGY

This chapter provides an introduction to the geology of the Osa Peninsula and its surrounding features in order to provide geological context for the ideas presented in this thesis. Firstly, notable nearby features on the Caribbean, Cocos and Nazca plates are introduced. Secondly, proposed ideas about the formation of the rocks of the Osa Peninsula are described, with detailed introduction and discussion of the two dominant hypotheses. Finally, the geological history of the Osa Peninsula and its surrounding features is described in detail.

2.1. GEOGRAPHICAL AND GEOLOGICAL CONFIGURATION OF THE OSA PENINSULA AND SURROUNDING AREAS

2.1.1. *The Osa Peninsula*

The Osa Peninsula is situated in south-western Costa Rica and protrudes into the Pacific ocean (Fig. 2.1). The peninsula has a length of 57 km, a width of 28 km at its widest point, and covers an area of ~1500 km². It is connected to mainland Costa Rica in the north and separated from the mainland in the west by the Golfo Dulce. The peninsula is densely forested by rainforest flora – >700 species of tree and 4 – 5000 species of plant – and provides a habitat for 124 species of mammal, 71 species of reptile, 46 species of amphibian, 375 species of bird, and 8000 species of insect (Barrantes *et al.*, 1999 [Spanish] cited in Almeyda Zambrano *et al.*, 2010; Sanchez-Azofeifa *et al.*, 2002). The terrain consists of lowland hills with a maximum altitude of ~780 m (Berangé and Thorpe, 1988; Government of Costa Rica, 1965) cut by several rivers and streams. Due to the hot, humid climate enjoyed by the peninsula, exposed rocks deteriorate quickly by tropical weathering and the only natural exposure of fresh rock is found in river valleys and around the coast. Large areas of the peninsula are occupied by protected land (Fig. 2.1b) – predominantly the Corcovado National Park (425 km² [Almeyda Zambrano *et al.*, 2010]), within which there are no roads accessible by car, permits are required for sampling, and visitors must be accompanied by registered guides. The majority of roads on the peninsula are

REGIONAL GEOLOGY

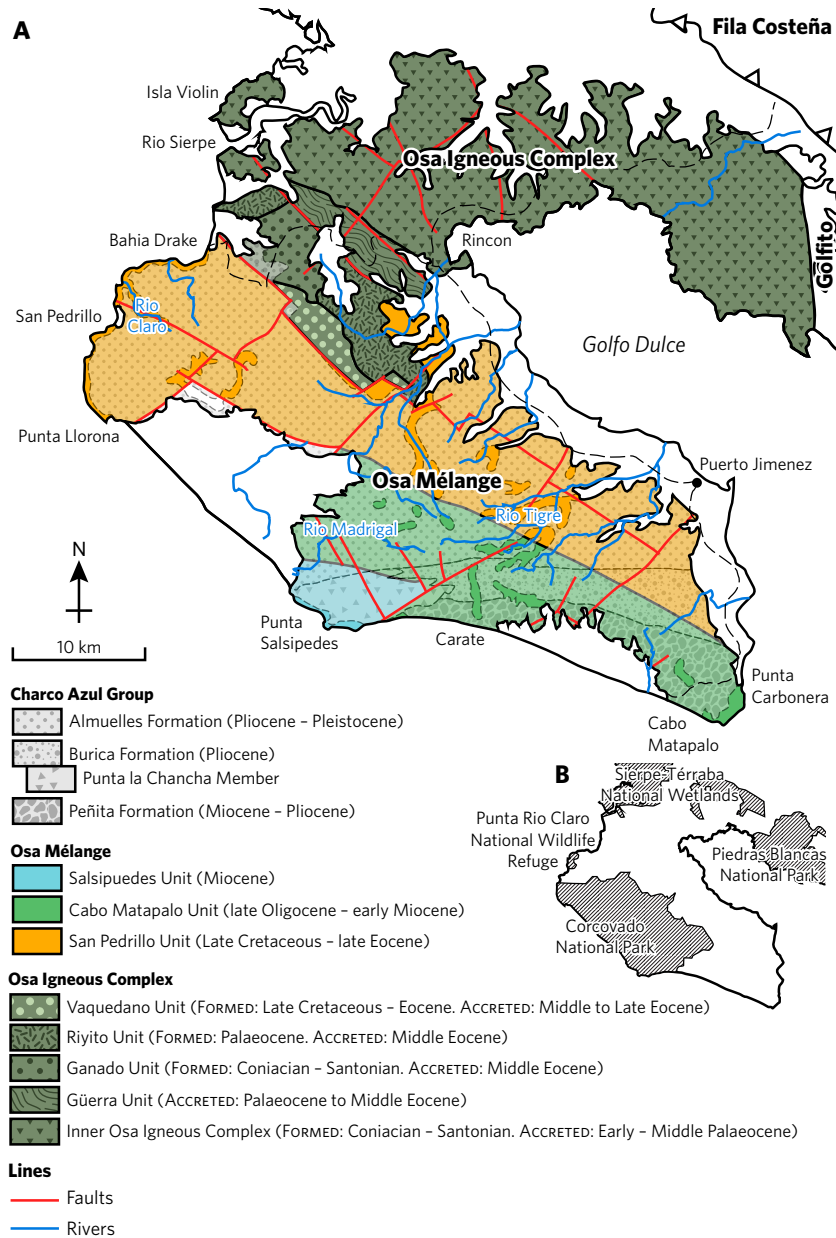


FIG. 2.1. **A:** Geological map of the Osa Peninsula showing the outcrop distribution of the Osa Mélange, Osa Igneous Complex, and the overlying Charco Azul Group, and their constituent units. The Charco Azul Group is shown semi-transparent to allow the sub-cropping boundaries between the units of the Osa Mélange to be visible (modified from Di Marco *et al.*, 1994; Vannucchi *et al.*, 2006; and Buchs *et al.*, 2009). **B:** Map showing the area of protected land within the Osa Peninsula (modified from Salom-Pérez *et al.*, 2007).

unpaved and rivers must be crossed by ford. To the north-east of the peninsula lies the ~3 km², densely forested Caño island. The peninsula has a population of ~14,000 (as of the 2011 census [Instituto Nacional de Estadística y Censos, 2011]) and approximately one fourth of the population is employed in the industry of tourism, as the Osa Peninsula is both a popular location of internal tourism and attracts international tourism primarily in the form of eco-tourism and backpacking. Major infrastructure investment primarily facilitates this tourism and transport links away from popular tourist sites are poor (Forastelli and Aguilar, 2013).

The Osa Peninsula consists of a basement divided into two units. The inner portion – termed the Osa Igneous Complex (Buchs *et al.*, 2009), consists of deformed pillow basalts, massive basalts, gabbros and cherts – while the outer portion – termed the Osa Mélange – is an intensely deformed mixture of basalt, carbonate, sandstone and mudstone (Vannucchi *et al.*, 2006). This is overlain by faulted and tilted early Pliocene – recent cover sediments. Palaeosols found at the unconformity at the base of these sediments contain a placer gold deposit that – along with a modern placer deposit found in the beds of the peninsulas rivers and streams – has been exploited by indigenous and artisanal miners since ~700 A.D (Naughton, 1993).

The Osa Mélange has been divided into three distinct mélange units by Di Marco *et al.* (1995) on the basis of their lithology and – later – the timing of their accretion (Fig. 2.1). The largest, innermost and oldest of these units, the San Pedrillo Unit, is exposed on the northeastern coastline, Caño Island, and in the river valleys of the Rio Claro and Rio Tigre (Vannucchi *et al.*, 2006) (Fig. 2.1). This is composed predominantly of dark grey volcanoclastic pelites and altered basalts and contains packages rich in chert and (mostly deep water) carbonate. The Cabo Matapalo Unit, exposed on the south coast near Cabo Matapalo (Fig. 2.1), consists of a high proportion of recrystallised carbonate blocks within a dark grey pelitic matrix, with mafic mega-blocks being present in the north of this unit. The Salsipuedes Unit, exposed only on Punta Salsipuedes (Fig. 2.1) – located within the Corcovado National Park – is the smallest unit and is described as consisting mostly of deformed carbonate, although access restrictions have prevented thorough investigation of this unit (Di Marco *et al.*, 1995).

REGIONAL GEOLOGY

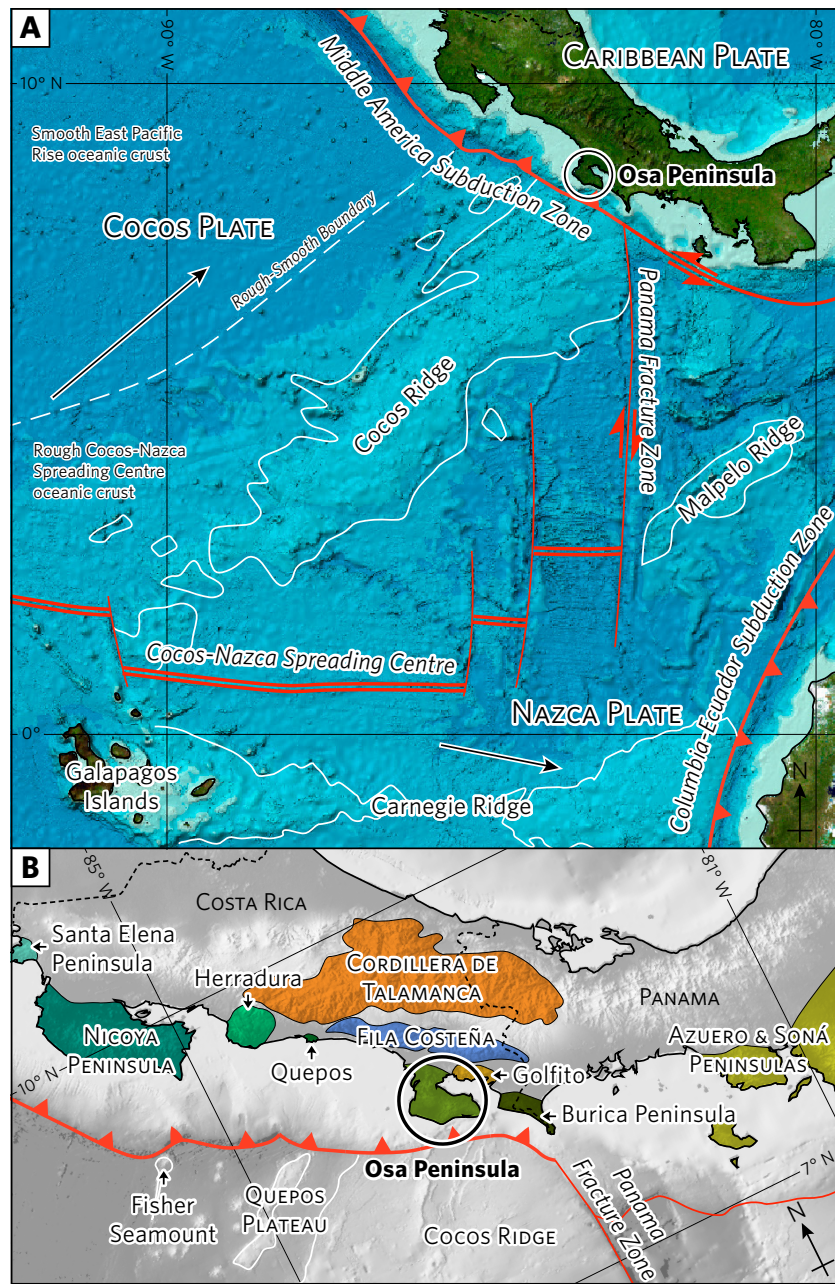


FIG. 2.2. **A:** Map of the Central American and eastern Pacific region showing the position of the Osa Peninsula and notable nearby crustal-scale features on the Cocos and Nazca plates mentioned later in this thesis. White arrows indicate convergence vectors. Base-map from GEBCO _2014 (Weatherall *et al.*, 2015). **B:** Map of Costa Rica and western Panama overlain with the locations and outcrop extents of major regional-scale features on the Caribbean and Cocos plates. Base-map from Ryan *et al.* (2009).

2.1.2. Nearby Features on the Cocos Plate

The Osa Peninsula lies landwards of the Middle America Subduction Zone where the subducting Caribbean plate subducts the Cocos Plate and the Galapagos-derived Cocos Ridge. Subduction of this ridge causes significant shallowing of the angle of the subducting slab to near flat off-shore Osa, which is compared to the $\sim 65^\circ$ at the Costa Rican – Nicaraguan border, considered as typical for this subduction zone (Protti *et al.*, 1995; Gardner *et al.*, 2013). The Middle America Subduction Zone is the type example of an “erosive” subduction zone (the subduction erosion tectonic process is described in detail in Chapter 3.2) which accounts for approximately half of modern subduction zones (Clift and Vannucchi, 2004). The Osa Peninsula forms the forearc of this subduction zone where it has been uplifted due to subduction of the Cocos Ridge. Material derived from the base of this forearc is entrained into the subduction plate boundary interface and as such represents a major influence on the physical properties of this subduction channel (the subduction channel concept is introduced in Chapter 3.1) (Vannucchi *et al.*, 2006).

The Cocos Ridge is an ~ 1000 km long aseismic ridge extending from the Cocos-Nazca Spreading Centre near the Galapagos Islands to the Middle America Trench off-shore the Osa Peninsula. It is 250 – 500 km wide, stands ~ 2000 m off the normal ocean floor and is up to 3 times thicker than normal oceanic crust, with most of the additional thickness attributed to the lower crust (Walther *et al.*, 2003). This ridge represents the trace of the Galapagos hotspot on the Cocos Plate and is mirrored on the Nazca Plate by the Carnegie Ridge (Fig. 2.2); these two ridges – along with the isthmus of Panama – define the borders of the Panama Basin. The hotspot trace here is defined by a ridge formed by near-continuous magmatism – as opposed to a line of discrete seamounts – due to the interaction between the Galapagos hotspot and the Cocos-Nazca Spreading Centre (Walther *et al.*, 2003). Basalts from the northern section of the Cocos Ridge have compositions similar to ocean island basalts (OIB), whereas the central and southern sections have compositions intermediate between OIB and normal mid-ocean ridge basalt (Hoernle *et al.*, 2000).

Located ~ 80 km to the south-east of the Osa Peninsula – near the peninsula of Burica – lies the triple junction between the

REGIONAL GEOLOGY

Caribbean, Cocos, and Nazca plates (Fig. 2.2). The boundary between the Cocos and Nazca plates in this region is a dextral transform fault known as the Panama Fracture Zone (PFZ). This fracture zone consists of four distinct linear troughs and remains seismically active (Lowrie *et al.*, 1979; Adamek *et al.*, 1988).

To the north of the Cocos Ridge, the oceanic plate is ~40% covered by seamounts, which form notable reentrant structures as they collide with the Costa Rican margin (Ranero and von Huene, 2000). This oceanic crust was formed at the Cocos-Nazca Spreading Centre (CNS) following the breakup of the Farallon Plate. Notable morphological features on this rough oceanic crust are the Quepos plateau and the Fisher Seamount and Ridge (Fig. 2.2b) (Fisher *et al.*, 2004). Further north, offshore the Nicoya Peninsula, the oceanic plate has a smoother morphology and was formed at the East Pacific Rise (EPR) prior to Farallon breakup (Ranero and von Huene, 2000; Barckhausen *et al.*, 2001). Several-km-long normal faults produced by bending of the incoming plate prior to subduction are found adjacent to, and parallel – sub-parallel with, the trench. These are present on both the CNS-produced crust and the EPR-produced crust, although they extend a greater distance away from the trench in the EPR-produced crust (Ranero *et al.*, 2005).

2.1.3. Nearby Features on the Caribbean Plate

The Caribbean plate is largely underlain by the Caribbean Large Igneous Province, forming a widespread basement across the plate. This is principally composed of an oceanic plateau, several accreted plateaus and other volcanic edifices (as represented in the Nicoya Complex), and uplifted “normal” oceanic crust (Kerr *et al.*, 2003). Located atop this plate are two major arc systems: the Central American Arc along the western margin, and the Greater and Lesser Antilles along the eastern margin (e.g. Hastie *et al.*, 2010; Montes *et al.*, 2012).

The Osa Peninsula is one of several promontories along the Pacific margin of southern Central America (Fig. 2.2) which is composed largely of basaltic material. These promontories either represent accreted seamounts (e.g. Quepos, western central Costa Rica [Hauff *et al.*, 2000b] and Azuero, central southern Panama [Buchs *et al.*, 2011]), oceanic plateaus accreted to the Caribbean

plate (e.g. Nicoya, northwestern Costa Rica [Hauff *et al.*, 2000b]; Burica, southwestern Costa Rica [Buchs, 2008]), accretionary prisms (e.g. Santa Elena, northwestern Costa Rica [Baumgartner and Denyer, 2006] and Azuero, central southern Panama [Buchs, 2008]), or a Cretaceous – Palaeogene volcanic arc (e.g. Azuero and Soná, central southern Panama [Buchs *et al.*, 2011]). As such, all of these promontories were formed by accretion of material on the Farallon/Cocos plates mostly formed at the Galapagos hotspot (Hauff *et al.*, 2000b).

Inland of the Osa Peninsula, on the northeastern side of Golfo Dulce (Fig. 2.1), lies the Golfito Complex (Fig. 2.2b); comprised of Late Cretaceous basaltic – trachyandesite lavas, volcanoclastics, and hemi-pelagic limestones. Crucially, no plutonic rocks or felsic-composition rocks have been reported from this complex. This was interpreted by Hauff *et al.* (2000b) as an accreted oceanic plateau or Caribbean Large Igneous Province basement. However, Buchs *et al.* (2010) show that this complex contains igneous rocks with compositions ranging from plateau-like to arc-like and interpret that this complex represents the earliest stages of arc development – a so-called “proto-arc” – atop an oceanic plateau forming part of the Caribbean Large Igneous Complex shortly after the initiation of the Middle America Subduction Zone.

Located further inland from the Osa Peninsula is the Fila Costeña range (Fig. 2.2b), interpreted as a fold-and-thrust belt formed by inversion of the 2 – 4 km thick Eocene – Holocene inner forearc basin in the latest Pliocene to recent, following the arrival of the Cocos Ridge to the Middle America Subduction Zone (Fisher *et al.*, 2004). Fisher *et al.* (2004) reported that this unit contains upper Eocene shallow water limestones which grade into Oligocene – middle Miocene volcanoclastic turbidites (see Fig. 2.8) displaying an overall coarsening upwards succession from marls at their base to conglomerates at their top. This is conformably overlain by Miocene shallow marine – fluvial conglomerate, sandstones, and mudstones. A formation of Pliocene marine mudstone overlies this succession and is itself overlain by lava flows, lahars, and pyroclastics dated at 1 – 4 Ma (de Boer *et al.*, 1995). Finally, discontinuous Pleistocene and Holocene fluvial and marine terraces cap this unit.

REGIONAL GEOLOGY

Yet further inland lies the Miocene – Pleistocene volcanic arc of the Cordillera de Talamanca (Fig. 2.2b). This represents an ~175 km long region of elevated topography (up to >3500 m; the highest mountains in Central America [Fisher *et al.*, 2004]) which exposes granitoids and intermediate composition plutonic rocks largely absent from arcs in central and northern Costa Rica and western Panama. The Cordillera de Talamanca also represents a gap in active volcanism. Cessation of magmatism is inferred to be the result of slow and highly oblique subduction of the Nazca Plate following formation of the Panama Fracture Zone (Morell, 2015) and uplift is attributed to subduction of the Cocos Ridge (e.g. Kolarsky *et al.*, 1995; Abratis, 1998).

2.2. PREVIOUS INTERPRETATIONS OF THE FORMATION OF THE OSA MELANGE

2.2.1. Early Models

Early studies (e.g. Dengo 1962; Berrangé and Thorpe, 1988) of the Osa Peninsula did not distinguish between the Osa Mélange and the Osa Igneous Complex, and regarded the rocks of the Osa Peninsula as a component of the Nicoya Complex – an igneous complex exposed on the Nicoya Peninsula, NW Costa Rica (Fig. 2.2b) and along the Pacific coast of Costa Rica – which is commonly interpreted as a component of the Caribbean Large Igneous Province (Berrangé and Thorpe, 1988). Dengo (1960 [Spanish] cited in Berrangé and Thorpe, 1988; 1962) was the first to describe the geology of the Osa Peninsula and recognised the major lithologies. Azéma *et al.* (1981; 1982; 1983 [Spanish] cited in Berrangé and Thorpe, 1988), and Lew (1983a, b cited in Berrangé and Thorpe, 1988) determined biostratigraphical ages ranging from Upper Campanian to Upper Miocene for the sedimentary rocks within what is now recognised as the Osa Mélange.

Baumgartner *et al.* (1986 cited in Buchs *et al.*, 2009) were the first to distinguish between the predominantly basaltic Osa Igneous Complex and the more disrupted Osa Mélange; which they termed the “Osa Caño Accretionary Complex”. They interpreted that the mélange formed in the Eocene as an accretionary prism which was composed of mass-wasted blocks derived from the forearc.

Berrangé and Thorpe (1988) described these rocks as an obducted segment of ocean crust formed in a Cretaceous to Early Eocene back-arc basin (Fig. 2.3a). The sedimentary component of these rock units was said to have been interstratified with the basalts prior to diagenesis due to the injections of sediment into the basalt. They inferred that this back-arc basin formed on an overriding Cocos plate above a south-west dipping subduction zone. Obduction of this back-arc would have occurred during a reversal of the subduction polarity in the Oligocene followed by uplift in the Middle Pliocene. When describing rocks near San Pedrillo — where the Osa Mélange is now recognised to outcrop and where Baumgartner *et al.* (1986 cited in Buchs *et al.*, 2009) reported a sedimentary mélange — they describe intense fracturing and shearing which likely destroyed primary igneous features such as pillow structures. Where they do recognise the presence of mélange, it is only in the “limestone breccia”, which they regard as having a tectonic origin.

Berrangé and Thorpe’s (1988) attribution of the rocks of the Osa Peninsula to a back-arc environment was based on the analysis of trace-element geochemistry and position on TiO_2 – Zr, Ti–Zr–Sr, and Ti–Zr–Y diagrams (Pearce and Cann, 1973). Most samples analysed were collected from areas now known to be outcrops of the Osa Igneous Complex; however, two samples were collected from Carate (Fig. 2.1a) which is now known to expose the Cabo Matapalo Unit of the Osa Mélange. Only one sample was collected *in situ* and this is geochemically distinct from the other samples analysed with significant enrichment of incompatible elements and steeply negative REE* patterns.

The olistostromal interpretation of Baumgartner *et al.* (1986 cited in Buchs *et al.*, 2009) was later expanded upon by Di Marco (1994) and Di Marco *et al.* (1995) who subdivided the mélange into 3 distinct units: the San Pedrillo Unit in the north and northwest, the Cabo Matapalo Unit in the east, and the Sal-sipuedes unit in the south. Di Marco *et al.* (1995) report the results

* “Rare earth” elements. Sc, Y, La, Ce, Pr, Nd, Pm, Sm, Eu, Gd, Tb, Dy, Ho, Er, Tm, Yb, Lu. La – Sm are classified as “light” rare earth elements (LREEs) and Eu – Lu — in addition to Y — are classified as “heavy” rare earth elements (HREEs).

REGIONAL GEOLOGY

A: Berrange and Thorpe (1988)

B: Meschede et al. (1999)

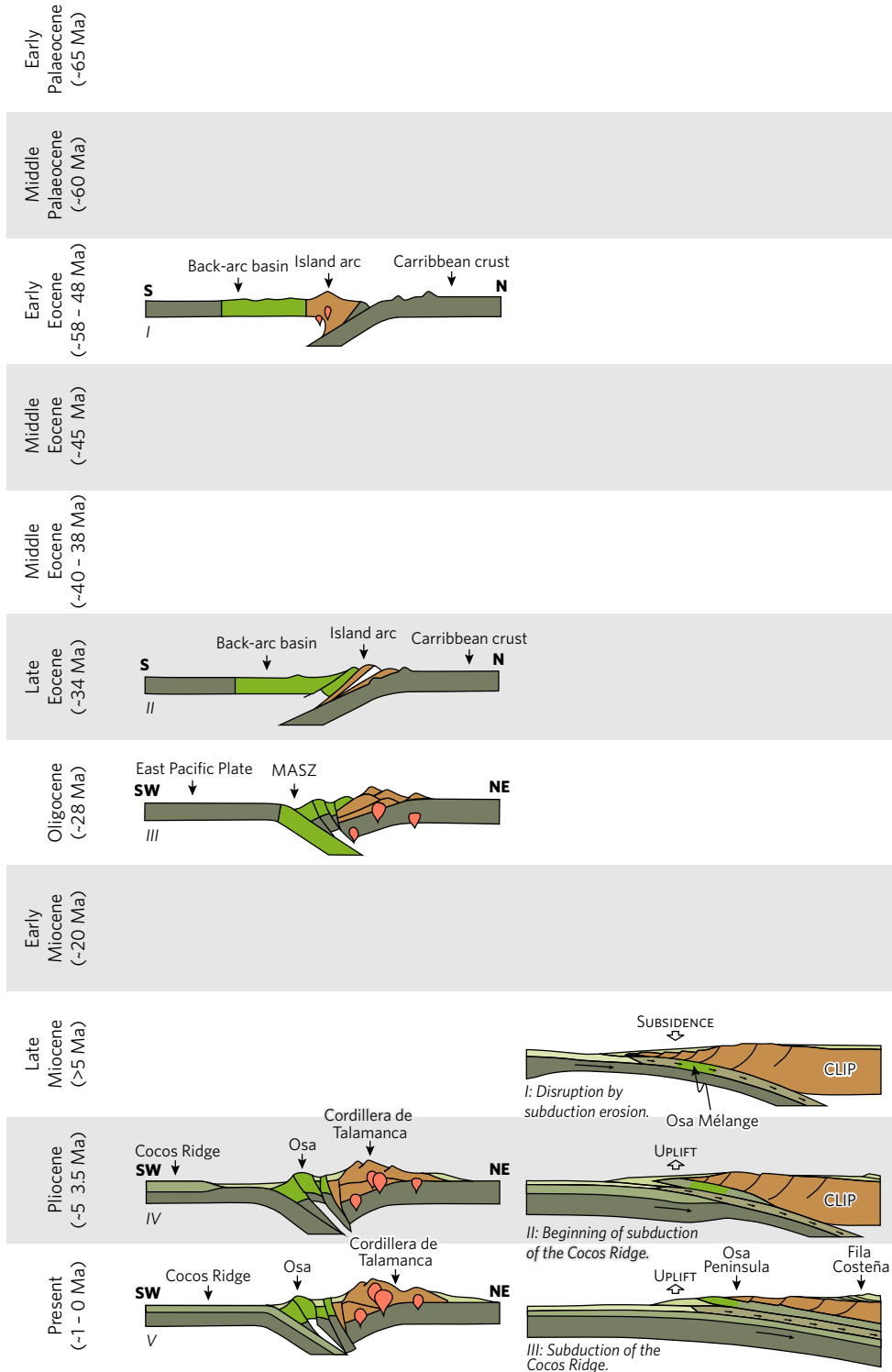
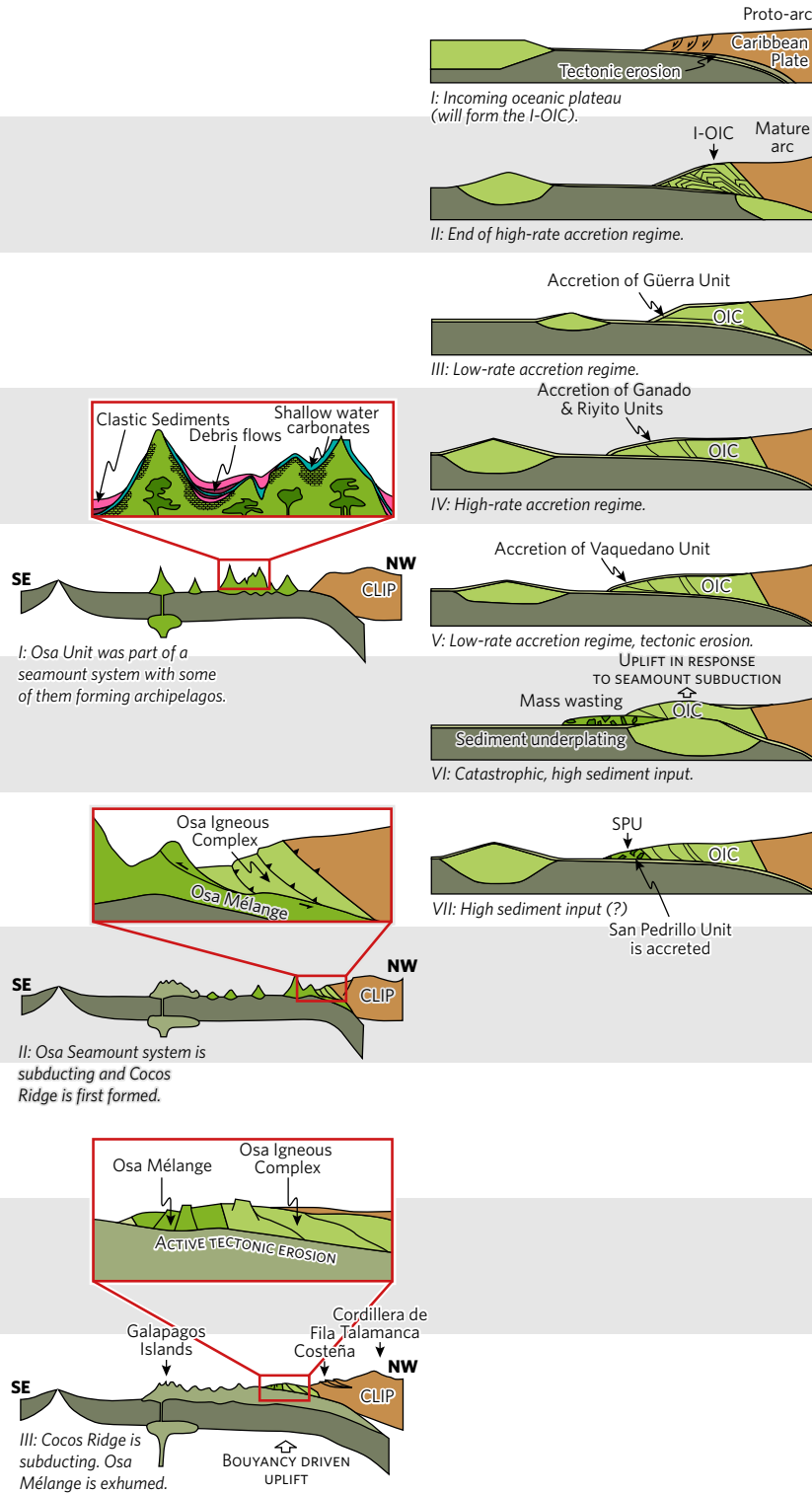


FIG. 2.3. (Caption overleaf.)

C: Vannucchi et al. (2006)

D: Buchs et al. (2009)



REGIONAL GEOLOGY

Fig. 2.3. (CONTINUED) Comparison between the formation models for the rocks of the Osa Peninsula, modified from **A:** Berrange and Thorpe (1998), **B:** Meschede *et al.* (1999), **C:** Vannucchi *et al.* (2006), and **D:** Buchs *et al.* (2009) with each step correlated in time.

of detailed fieldwork and describe the *mélange* as consisting predominantly of “highly deformed turbidites and hemi-pelagic and pelagic sediments” containing large blocks of basalt, dolerite, gabbro and felsic rocks in a volcanoclastic greywacke matrix. Di Marco *et al.* (1995) interpreted that this formed by trench-fill sedimentation in the Palaeogene – early Neogene which mixed with tectonically off-scraped basalt from the upper surface of the subducting oceanic plate.

Contrary to the olistostromal interpretation of Baumgartner *et al.* (1986 cited in Buchs *et al.*, 2009) and Di Marco *et al.* (1995), Meschede *et al.* (1999) proposed an interpretation of the *mélange* based on the observation that a high proportion of the *mélange* consisted of tectonically dismembered basalt (Fig. 2.3b). They proposed that the *mélange* was formed by Neogene tectonic erosion of the upper plate consisting of basalts derived from the Caribbean Large Igneous Province and a volcanic arc built atop it. They described the basalts – which they estimated represents 80 – 90% of the *mélange* – as brecciated to the point of cataclasis with deformation concentrated within numerous shear zones. They proposed that following the arrival of the Cocos Ridge to the subduction zone, the Osa *Mélange* was uplifted to its present position.

Higher precision trace-element and isotope geochemistry by Hauff *et al.* (2000b) showed that the basalts of the Osa Peninsula – as well as Quepos, Gorgona, and large parts of the Caribbean Large Igneous Province – were sourced from the Galapagos hotspot. Hauff *et al.* (2000b) did not distinguish between samples collected from the Osa *Mélange* and the Osa Igneous Complex; however, one sample was collected from Golfo Dulce, an area later interpreted by Vannucchi *et al.* (2006) to expose the Osa *Mélange*. However, Di Marco *et al.* (1995) and Buchs *et al.* (2009) tentatively ascribe the rocks in this area to the Osa Igneous Complex. This sample is geochemically similar to other samples in the Osa Igneous Complex and shares $^{143}\text{Nd}/^{144}\text{Nd}$ and $^{208}\text{Pb}/^{204}\text{Pb}$

isotope values similar to Gorgona Komatiites (Buchs *et al.*, 2016). No inference is made by Hauff *et al.* (2000b) between the source of the basalts in the Osa Igneous Complex and the provenance of the basalt blocks in the Osa Mélange.

Following the recognition that the igneous rocks of the Osa Peninsula have a Galapagos seamount geochemical affinity, two models have been proposed to explain the formation of the Osa Mélange. Vannucchi *et al.* (2006) proposed that the mélange was formed by tectonic dismemberment of subducting seamounts and transferred directly from the subducting plate to the overriding plate (hereby referred to as the “direct accretion model”), whereas Buchs *et al.* (2009) proposed that the seamounts were accreted, then eroded back into the trench to form the mélange, before being re-accreted to overriding plate (hereby referred to as the “trench fill model”).

2.2.2. Direct Accretion Model

The data from Hauff *et al.* (2000b) was interpreted by Vannucchi *et al.* (2006) to suggest that the basalt blocks in the Osa Mélange were derived from seamounts formed above the Galapagos hot-spot and that both the Osa Mélange and the Osa Igneous Complex represent a series of accreted seamounts. In this hypothesis, the two rock units formed from different structural levels of the same seamount system which was largely intact prior to subduction. The flanks of these seamounts, including their sedimentary cover, experienced extensive tectonic dismemberment during subduction to form the mélange, while the upper section is subject to less shear and forms the Osa Igneous Complex (Fig. 2.3c). Based on dating by Berrangé *et al.* (1989) and Hauff *et al.* (2000b), they determined that these seamounts were formed in the late Cretaceous to Miocene and accreted from the Eocene to Miocene. In this hypothesis, both the Osa Mélange and the Osa Igneous Complex were directly accreted to the forearc at approximately the same time.

Vannucchi *et al.* (2006) interpret that although the first pervasive phase of deformation occurred during subduction, a precursor phase of ocean floor metamorphism and veining suggest that the initial environment of formation was tectonically or

REGIONAL GEOLOGY

magmatically active, consistent with a seamount. Slope instabilities resulted in isolated slump deposits and debris flows in the lower portion of this seamount. Due to the presence of shallow water carbonates in the Osa Igneous Complex, they interpret that the tops of these seamounts either achieved or approached subaerial exposure. Conversely, the presence of deep-water carbonates and debris flows in the Osa Mélange – which are absent from the Osa Igneous Complex – is used as the primary evidence for the mélange and igneous complex being formed of different structural levels of the seamount system.

Upon subduction, the upper portions of these seamounts were thrust trenchward and frontally accreted, forming the Osa Igneous Complex. Thrusting and related deformation associated with frontal accretion result in the thrust-bound lens-like internal structure of the Osa Igneous Complex (Buchs *et al.*, 2009). At the same time, the lower portion of the seamounts is underthrust and buried to a depth of 4 – 8 km. As the first pervasive phase of deformation recorded in the Osa Mélange is layer-parallel extension – producing boudinage, pinch and swell structures, and matrix injections – Vannucchi *et al.* (2006) interpreted that dismemberment of the seamount flanks occurred after the seamounts had been underthrust. Immediately prior to the mélange being underplated to the forearc, the deformation style shifted to layer-parallel compression – producing cleavage and buckle-folding – which was followed by SSW-trending thrusting and the formation of shear zones and the shear fabric during accretion. A final phase of SSE-trending deformation is associated with the changing stress fields around subducting seamounts; recorded in localised foliation, mineral lineations and fault plane lineations. Arrival of the Cocos Ridge at ~2.5 Ma resulted in uplift and exhumation of the mélange and extensive sub-vertical, dip-slip faulting at a variety of scales to accommodate the irregular morphology of the subducted Cocos Ridge. These faults form two approximately perpendicular sets and show multiple generations of slickenlines and slickenfibres indicative of reactivation and inversion as different morphological features on the Cocos Ridge are subducted below them.

This model is predicated on a lack of terrigenous material in the mélange and the observation that the mélange contains a high proportion of basalt. Seamount flanks – from which Vannucchi

et al. (2006) interpret the Osa Mélange formed – are dominantly zones of sediment bypass, not sediment deposition (Leslie *et al.*, 2002), and where sediments are stored on the seamount flank, they do not constitute a large fraction of the seamount volume (Garcia and Davis, 2001). Additionally, transport of large blocks of terrigenous material outside of the trench and onto the flanks of a seamount is energetically unfeasible.

Although Vannucchi *et al.* (2006) interpret Hauff *et al.*'s (2000b) geochemical data as indicating that the basalt blocks in the Osa Mélange originate from Galapagos-derived seamounts, this is not the only interpretation. Firstly, the sample upon which Vannucchi *et al.* (2006) base their interpretation is not unambiguously sourced from the Osa Mélange – as Di Marco *et al.* (1995) and Buchs *et al.* (2009) tentatively report exposures of the Osa Igneous Complex in this area – and may therefore not give information about the provenance of the mélange blocks. Secondly, a Galapagos signature to these blocks does not preclude an overriding plate origin, as the overriding plate consists of the Caribbean Large Igneous Province which also bears a Galapagos signature. Despite this, subsequent workers (e.g. Alvarado *et al.*, 2009) have also asserted that the Osa Mélange contains blocks derived from Galapagos seamounts while citing Hauff *et al.* (2000b), despite this interpretation being made by Vannucchi *et al.* (2006).

2.2.3. Trench Fill Model

In contrast to Vannucchi *et al.* (2006), Buchs *et al.* (2009) expand on the olistostromal hypothesis of Baumgartner *et al.* (1986 cited in Buchs *et al.*, 2009) and Di Marco *et al.* (1995) with a detailed and multidisciplinary description of the mélange and igneous complex. This interpretation is based on the observation that a high proportion of the material in the Osa Mélange is detrital sediment and the basaltic blocks share geochemical similarity to the Osa Igneous Complex. Their analysis of 10 basalt blocks from the San Pedrillo Unit of the Osa Mélange show REE patterns and concentrations allowing them to be associated with distinct units within the Osa Igneous Complex.

They interpret that the Osa Igneous Complex accreted from a subducting oceanic plateau in the middle Palaeocene to form the

Inner Osa Igneous Complex, and a chain of seamounts in the late Palaeocene – middle Eocene to form the units of the outer Osa Igneous Complex, resulting in an accretionary prism formed in a similar manner to proposed by Vannucchi *et al.* (2006) (Fig. 2.3d). In contrast to Vannucchi *et al.*'s (2006) hypothesis of direct accretion of the Osa Mélange, Buchs *et al.* (2009) propose that mass wasting from the accreted Osa Igneous Complex into the Middle America Trench produced the Osa Mélange, which was then itself accreted. Alongside mass-wasted blocks from the Osa Igneous Complex, they report that the Osa Mélange trench-fill also contained intermediate-composition blocks derived from a volcanic arc and pelagic and shelf carbonates derived from the forearc. Finally, the arrival of the Cocos Ridge results in uplift and the formation of high angle faults in the accreted mélange in a similar manner to that proposed by Vannucchi *et al.* (2006).

The relative proportion of basalt and sediments in this mélange is a consistent topic of contention between workers. Meschede *et al.* (1999) and Vannucchi *et al.* (2006) reported that basalt is the most abundant component of the mélange. While Berrangé and Thorpe's (1988) do not explicitly address the proportion of different lithologies, their description of the sediments as “interstratified with the basalts” implies that the basalts were the larger fraction. However, Di Marco *et al.* (1995) and Buchs *et al.* (2009) report that the fraction of basalts is subordinate to the fraction of sediments. The high degree of pervasive fracturing and alteration reported by all authors is likely the cause of this discrepancy, and Buchs *et al.* (2009) notes that due to this “it may locally be particularly hard to make a distinction between the matrix and the blocks.”

Despite citing the presence of intermediate-composition blocks as indicative of mélange formation adjacent to an arc, the extreme paucity of this material throughout much of the mélange challenges the trench fill interpretation. It also remains unexplained how megablocks of these lithologies can be transported to the trench without any similar material being deposited in the forearc basin which is now preserved as the Fila Costeña fold and thrust belt (Fisher *et al.*, 2004). Buchs *et al.* (2009) attribute these rocks to an arc on the basis of negative Nb anomalies and positive Pb anomalies, both typical of the slab-derived fluid component of

arc magmas (e.g. Baier *et al.*, 2008; Manea *et al.*, 2014), however, the lack of significant enrichment in large-ion lithophile elements (LILE) relative to high-field-strength elements (HFSE) – which is also typical of such magmas – is not commented on. Buchs *et al.* (2009) also do not address the possibility of these blocks not being derived from a contemporaneous arc, but an older arc system, the roots of which may have been in the hanging wall of the erosive subduction zone and available to be incorporated into the mélangé by return-flow (the return-flow process is introduced in Chapter 3.1.1) in the subduction channel (Cloos and Shreve, 1988b). This may explain the presence of the plutonic rock (described as a monzonite) that Buchs *et al.* (2009) report which would be unlikely to be exposed at the surface of an active arc. Additionally, while intermediate-composition rocks are rare in seamount systems, they have been known to occur within large ocean islands (e.g. MacDonald and Katsura, 1964; Willbold, 2009), which is another possibility not addressed by Buchs *et al.* (2009). Despite Buchs *et al.* (2009)'s assertion that “the cores of the biggest igneous olistoliths remained surprisingly well preserved”, the thin section they show to illustrate this displays significant brecciation and alteration and so their variable incompatible element patterns – in particular their positive Pb anomaly – may also be attributable to alteration by sediment-derived fluids within the subduction zone, rather than to a primary feature (c.f. Buchs *et al.*, 2009).

Despite widespread agreement among workers (e.g. Vannucchi *et al.*, 2006; Alvarado *et al.*, 2009) that the basalt blocks within the Osa Mélangé share the same Galapagos seamount source as the Osa Igneous Complex, this is based on geochemical analysis of a maximum of 15 blocks (Berrangé and Thorpe, 1988; Hauff *et al.*, 2000b; Buchs *et al.*, 2009). 3 blocks analysed are of intermediate composition and have been attributed to the arc (Buchs *et al.*, 2009). The Galapagos-affinity of the basalts in the Osa Igneous Complex has been more thoroughly established (Hauff *et al.*, 2000b; Buchs *et al.*, 2009). The association between the Osa Mélangé and the Osa Igneous Complex is strengthened by the obvious geographical proximity between the Osa Mélangé and the Osa Igneous Complex. The pervasive sub-greenschist metamorphism and zeolite and calcite veining within blocks in the Osa

REGIONAL GEOLOGY

Mélange – common surrounding seamounts as ocean floor metamorphism (e.g. Spooner and Fyfe, 1973) and also present in the Osa Igneous Complex (Buchs *et al.*, 2009) – is further evidence that these two units share a provenance. Geochemical evidence from the igneous blocks is therefore not essential to assign a Galapagos provenance to these blocks.

2.3. TECTONIC HISTORY OF CENTRAL AMERICA AND THE CARIBBEAN IN THE MESOZOIC AND CENOZOIC

The prevailing history of southern Central America throughout the Cretaceous and Cenozoic is north-eastwards movement of Pacific volcanic edifices – likely all products of the Galapagos-hot-spot – until subduction and occasional accretion at the Central American margin. The Osa Peninsula represents one of a great number of these allochthonous terranes that outcrop around the Caribbean and South American region.

2.3.1. Pre-Cretaceous tectonic background

Early to mid-Mesozoic rifting and spreading between North and South America during the breakup of Pangaea resulted in the formation of the inter-American ocean basin (e.g. Dietz and Holden, 1970; Kerr *et al.*, 2003; Beutel, 2009), creating the region now occupied by Central America and the Caribbean. This basin connected to the newly-formed Atlantic Ocean. Continental rifting began at ~190 Ma, causing initial separation of North America and South America and the continental crustal blocks that now occupy the Central American and Caribbean regions (Pindell and Kennan, 2009). Continental rifting in these two seaways gave way to ocean crust formation at ~158 Ma, leading to the development of two oceanic regions – the Colombian Marginal Seaway in the west and the Proto-Caribbean Seaway in the east – at ~148 Ma, which were separated by the southern tip of the Yucatan Block until the earliest Cretaceous (Pindell and Kennan, 2009).

2.3.2. Cretaceous

2.3.2.1. Formation and emplacement of the Caribbean Large Igneous Province

Most workers agree that the Caribbean Large Igneous Province (CLIP) was erupted onto the Farallon Plate to the west of the Inter-American ocean basin (e.g. Duncan and Hargraves, 1984; Burke, 1988; Kerr *et al.*, 2003; Hoernle *et al.*, 2004; Pindell and Kennan, 2009; Serrano *et al.*, 2011). The earliest magmatism in the CLIP occurred at -139 Ma in the Nicoya Peninsula (Hoernle *et al.*, 2004), followed by eruption of 112.7 Ma lavas in Curaçao (Wright and Wyld, 2011). More-or-less continuous magmatism occurred throughout the Late Cretaceous, with three main pulses of activity at 90 – 88 Ma, 82 – 80 Ma, and 76 – 74 Ma. (Serrano *et al.*, 2011). This long history of magmatism is incompatible with the short pulse of magmatism predicted by eruption of a mantle plume head, as proposed by Duncan and Hargraves (1984), but rather several diffuse eruptions associated with a long-lived plume (Hoernle *et al.*, 2004; Serrano *et al.*, 2011).

Two dominant models exist to explain the formation and emplacement of the Caribbean Large Igneous Province between the Americas. Burke (1988) and subsequent workers (e.g. Kerr *et al.*, 2003; Hastie *et al.*, 2010, 2013) infer that the CLIP formed on the Farallon Plate above the Galapagos Hotspot and migrated towards and into the gap between the Americas, eventually jamming the subduction zone and causing polarity reversal of the existing subduction zone and subduction initiation behind the Caribbean plateau (sometimes referred to as the Caribbean-Colombian Oceanic Plateau [Kerr *et al.*, 2003]) in the Turonian – Campanian (Fig. 2.4a)(Hastie *et al.*, 2013). Alternatively, (Pindell *et al.*, 1992, 2005, 2006; Pindell and Kennan, 2009) proposed that the CLIP formed after a subduction reversal in the Hauterivian – Albian and erupted onto the Farallon plate between the Americas which was the upper plate subducting the proto-Caribbean sea before subduction initiation along the western CLIP margin separated the Caribbean plate from the Farallon plate (Fig. 2.4b) (e.g. Pindell and Kennan, 2009). In contrast to these models, James (2002; 2005; 2006) proposed that the Caribbean Large Igneous Province

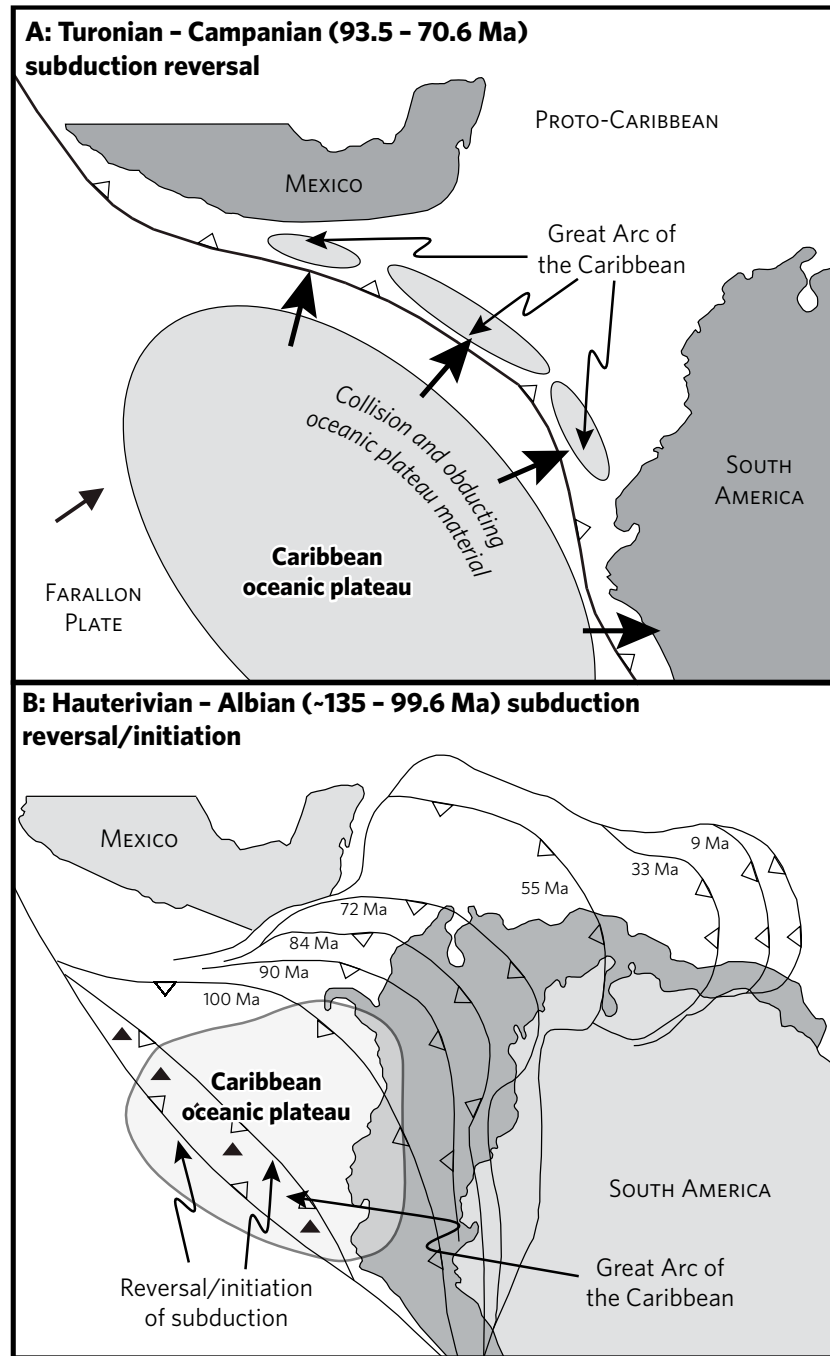


FIG. 2.4. Two competing models for the origin and emplacement of the Caribbean oceanic plateau between the Americas (from Hastie et al., 2013). **A:** The Turonian - Campanian subduction reversal model (e.g. Burke, 1988; Kerr et al., 2003) showing the Caribbean oceanic plateau jamming the subduction zone beneath the Great Arc of the Caribbean and causing subduction reversal. (Caption continued on opposite page.)

was not formed in the Pacific domain and subsequently accreted and was instead formed entirely *in situ* between the Americas by oceanic spreading at triple junctions in the absence of a mantle plume or slab window to promote extraordinary magmatism.

The Caribbean Large Igneous Province is composed of a diverse range of basaltic igneous products, ranging from slightly enriched to strongly depleted, and including one of the few examples of Phanerozoic komatiites on Isla Gorgona off the western coast of Colombia (Echeverría & Aitken, 1980; Serrano *et al.*, 2011). The presence of komatiites within the CLIP has been used by Nisbet *et al.* (1993), Kerr *et al.* (1996), Hauff *et al.* (2000b), and Herzberg *et al.* (2007) as evidence of extraordinary mantle temperatures (1550 – 1600°C [Herzberg *et al.*, 2007]) within the Galapagos plume while, conversely, the presence of hydrous fluid inclusions within olivines in the komatiites has been used by Kamenetsky *et al.* (2010) and Serrano *et al.* (2011) to suggest the involvement of subduction zone fluids in the high degree of mantle melting necessary to produce komatiites. Basalts sharing similar geochemistry to the Gorgona komatiites, although lacking the characteristic spinifex texture, have been reported by Buchs *et al.* (2016) in the Osa Igneous Complex, and komatiite-like lavas with micro-spinifex texture and geochemistry enriched in LREE and HFSE have been reported by (Alvarado *et al.*, 1997) in Tortugal, Costa Rica.

2.3.2.1.1. Turonian – Campanian (93.5 – 70.6 Ma) Subduction Reversal

Most models of Caribbean formation suggest that the Caribbean Large Igneous Province originated as an oceanic plateau on the Farallon plate outboard of the Americas and was subsequently accreted into its present location (e.g. Kerr *et al.*, 2003). In this

Fig. 2.4. (CONTINUED) **B:** The Hauterivian – Albian subduction reversal model showing eastwards advancement of the Great Arc of the Caribbean, the development of the Caribbean oceanic plateau on the overriding plate, and initiation of the Middle America Subduction Zone on the western margin of the plateau.

REGIONAL GEOLOGY

model, flood basalt magmatism extruded onto the Farallon plate at ~92 – 88 Ma above the Galapagos hotspot (Kerr *et al.*, 2003 and references therein). The Galapagos plume is strongly implicated as the source for CLIP magmatism on the basis of isotope geochemistry, the presence of high MgO lavas, and the large volumes of melt products (e.g. Hauff *et al.*, 2000b; Kerr *et al.*, 2003).

Debate exists as to whether the Caribbean Large Igneous Province is derived from a singular oceanic plateau (e.g. Burke, 1988; Kerr *et al.*, 2003; Serrano *et al.*, 2011) or whether it is composed of an amalgam of volcanic edifices produced above the Galapagos hotspot and accreted to each other (Hoernle *et al.*, 2004). Inclusion of volcanic edifices not produced by the Galapagos hotspot into a mostly Galapagos-produced Caribbean Large Igneous Province has also been proposed (Kerr and Tarney, 2005). These accreted sections of the CLIP are commonly regarded to include the Nicoya and Gorgona Complexes (Hoernle *et al.*, 2004; Serrano *et al.*, 2011). Portions of the Caribbean Large Igneous Province interpreted to have been accreted to the Caribbean plate extend from Guatemala in the north to Ecuador in the south (Hoernle *et al.*, 2004 and references therein). Such accreted units may be genetically related to the main CLIP plateau exposed in the east and formed prior to the initiation of the Middle America Subduction Zone. However, no regular geographic pattern of ages is present within the CLIP (Serrano *et al.*, 2011).

At this time, a well-established eastwards-dipping subduction zone occupied the western margin of the Americas, where the Farallon plate was being subducted beneath the Columbian Marginal Seaway and the Proto-Caribbean Seaway in Central America. The arc above this subduction zone, referred to as the “Great Arc of the Caribbean” by Burke (1988), is the precursor to the Greater Antilles Arc.

The attempted subduction of the Caribbean plateau at this subduction zone at ~85 Ma (Kerr, *et al.*, 2003) jammed the subduction zone, resulting in a polarity reversal on the eastern margin of the Caribbean plateau behind the Greater Antilles arc and the initiation of the Middle America Subduction Zone on the western (trailing) margin of the plateau (e.g. Burke, 1988; Kerr *et al.*, 2003; Hastie *et al.*, 2010). This occurred because the Caribbean plateau was too thick (>20 km thick) and buoyant to be subducted (Kerr *et*

al., 2003; Saunders *et al.*, 1996). The Middle America Subduction Zone nucleated within the western extremity of the Caribbean Large Igneous Province, leaving the Nicoya Complex – and possibly the Osa Igneous Complex (Pindell and Kennan, 2009) – on the Farallon Plate from which it was subsequently accreted to the Caribbean Plate (Hoernle *et al.*, 2004).

2.3.2.1.2. Hauterivian – Albian (~135 – 99.6 Ma) Subduction Reversal

An alternative hypothesis, proposed by Pindell *et al.* (1992) and expanded upon by Pindell *et al.* (2005; 2006) and Pindell and Kennan (2009), is that the Caribbean Large Igneous Province erupted in the Pacific domain but partially between the Americas. They propose that at ~125 – 114 Ma, the portion of the Western Pangaea Subduction Zone in the Central American region underwent a polarity reversal into a southwest-dipping subduction above the nascent Caribbean Arc. The timing of this polarity reversal is constrained by the timing of uplift of high pressure/low temperature metamorphic rocks rimming the Caribbean plate, including the Siuna Mélange in Nicaragua (Flores *et al.*, 2015), the Motagua mélange in Guatemala (Bruechner *et al.*, 2009), and the Blue Mountain schists in Jamaica (Abbot and Bandy, 2008). To the north and south of this region – along the North American plate, the Chortis block (a continental block in the Central American region), and the South American plate – the subduction zone continued to dip eastwards. This subducted the oceanic crust of the Columbian Marginal Seaway as the trench advanced eastwards towards its present position at the Greater Antilles (Pindell and Kennan, 2009). Subduction of the spreading ridges within the Columbian Marginal Seaway and the Proto-Caribbean Seaway lead to the development of a slab gap beneath the Farallon/nascent Caribbean Plate to the south of Hispaniola. This slab gap had the dual effect of inhibiting arc development in the central eastern Caribbean and allowing the rise of the Galapagos Plume unimpeded by subducting slabs (Pindell and Kennan, 2009). Serrano *et al.* (2011) and Pindell *et al.* (2006) suggest that the presence of this slab window alone may be sufficient to explain the formation of

the Caribbean Large Igneous Province – including the komatiites in Gorgona – without the involvement of the Galapagos plume.

Eruption of flood basalt magmatism that formed the Caribbean Large Igneous Province occurred at ~92 – 88 Ma – with a minor later phase occurring at 76 – 72 Ma – above the Galapagos hotspot (Kerr *et al.*, 2003 and references therein). Pindell and Kennan (2009) determined on the basis of palinspastic reconstructions and hotspot drift paths that the Galapagos hotspot occupied a position within the Caribbean interior at 92 Ma, at the inception of CLIP magmatism. This erupted onto the eastern Farallon plate which lay between the Americas and occupied a position close to its present location.

As spreading between the American plates ceased following the eruption of the Caribbean Large Igneous Complex, the space into which the eastern tip of Farallon had been moving stopped expanding. Continued plate convergence caused the Farallon plate in the Caribbean region to become kinematically incompatible with the Farallon plate in the Pacific domain. At this point (~85 Ma), subduction initiated – likely along former transform faults near the western edge of the CLIP – as the nascent Caribbean plate overrode the thinner, older, and less buoyant Farallon plate (Pindell and Kennan, 2009).

2.3.2.1.3. *In situ* formation

In contrast to models which interpret the Caribbean Large Igneous Province being formed within the Pacific realm and separated from the Farallon Plate with the initiation of the Middle America Subduction Zone, Frisch *et al.* (1992) and others (Meschede and Frisch, 1998; James, 2002; 2005; 2006; 2009) propose that the Caribbean Large Igneous Province was formed *in situ* between the Americas. James (2002; 2005; 2006; 2009) regard the Caribbean region as an aulacogen of the Atlantic until the Aptian (Fig. 2.5). He infers that the extraordinary thickening of the oceanic crust was accomplished by magmatism at a triple junction between the Caribbean and Gulf of Mexico spreading centres in the absence of a mantle plume and that subduction at the Greater Antilles did not initiate until after the Aptian. James advocates this model as he regards the block rotations, subduction polarity reversals, and mantle plumes invoked by other models (e.g. Burke,

1988; Pindell and Kennan, 2009) to be “geometrically unlikely and needlessly complex”. He notes that the Caribbean Plate has a similar geometry to the Scotia and Banda Sea Plates which are formed by oceanic spreading, and therefore infers a similar origin (James 2002; 2005; 2006).

However, this model does not account for the well-established Galapagos-hotspot geochemical affinity of CLIP basalts (e.g. Hauff *et al.*, 1997; 2000a, b; Hoernle *et al.*, 2002; 2004; Kerr *et al.*, 2003), does not provide an explanation for the occurrence of the Galapagos hotspot and the formation of the Osa Igneous Complex at ~89 – 84 Ma (Buchs *et al.*, 2009), and is inconsistent with Pindell and Kennan’s (2009) reconstruction of the Galapagos plume’s location during the Cretaceous. Oceanic spreading at a mid-ocean ridge, even at a triple junction, does not typically produce sufficient volumes of magma to achieve subaerial exposure or oceanic crust that is >20 km thick. James (2005) makes reference to Iceland as an example of thickened oceanic crust formed above a mid-ocean ridge without acknowledging the role of a mantle plume in its development (e.g. Fitton *et al.*, 1997) or

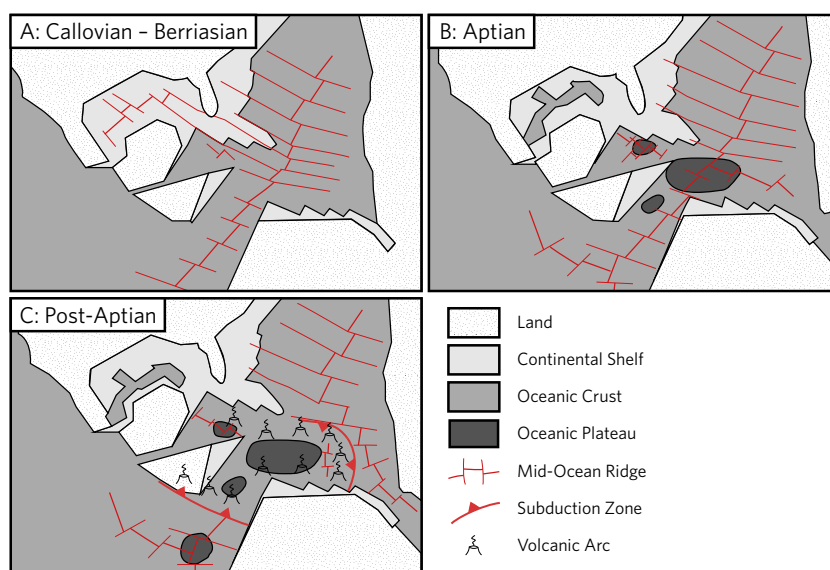


FIG. 2.5. *In situ* model of Caribbean formation (from James, 2006) showing large volumes of magma production at triple junctions resulting in the formation of the Caribbean oceanic plateau (B), before subduction at the Lesser Antilles and Middle America subduction zones after the Aptian separates the Caribbean Plate from the Atlantic and Pacific plates.

alternative hypotheses (e.g. Foulger and Anderson, 2005) which infer extraordinary processes to explain the high volumes of magmatism. Since this model infers that major MOR spreading ceased in the Aptian, later stage magmatism in the CLIP – the majority of which occurred in the Late Cretaceous (Serrano *et al.*, 2011) – is explained by back-arc spreading, which is incompatible with the crustal thickening this magmatism resulted in. This model also supposes that subduction along the western margin of the Americas and in the inter-American region did not initiate until the Aptian, despite widespread evidence of an Inter-American island arc existing from the earliest Cretaceous (e.g. Mann *et al.*, 1991; Mitchell, 2003; Pindell and Kennan, 2009 and references therein).

2.3.2.2. *Initiation of the Middle America Subduction Zone*

Most models agree that the Middle America Subduction Zone initiated as a westwards-dipping subduction zone on the western margin of the Caribbean Large Igneous Province at ~84 Ma; after the main phase of CLIP magmatism. This subduction zone separated the downgoing Farallon plate from new overriding Caribbean Plate (e.g. Burke, 1988; Hoernle *et al.*, 2002; Kerr *et al.*, 2003; Pindell and Kennan, 2009). This subduction zone is inferred to initiate along a former transform fault towards the edge of the Caribbean flood basalt province but potentially leaving some Galapagos products – such as portions of the Osa Igneous Complex and Nicoya Complex – on the Farallon side of the subduction zone Pindell and Kennan (2009).

Late Cretaceous volcanic rocks exposed throughout the Pacific coasts of Costa Rica, Panama and northernmost Colombia record the presence of earliest arc development along the south-western margin of the Caribbean Plate. The basement of this arc – exposed on Azuero Peninsula – is entirely composed of oceanic plateau with no continental fragments (Buchs *et al.*, 2010), and suggests that plateau-related magmatism ceases at 89 – 85 Ma. Development of this arc indicates that subduction along the western edge of the Caribbean plate initiated in the late Campanian (~75 – 73 Ma). Remnants of this arc are exposed in Golfito, southwestern Costa Rica, Azuero, southern Panama, and San Blas, eastern Panama (Buchs *et al.*, 2010; Montes *et al.*, 2012). This arc has been referred to as the Azuero Marginal Complex (Buch *et al.*,

2010), the Sona-Azuero Arc (Wegner *et al.*, 2011), and the Campanian – Eocene Belt (Montes *et al.*, 2012) and represents a single linear arc front during the Campanian (~75 – 73 Ma) – Eocene (~38 Ma) which has been segmented by later strike-slip faulting (Montes *et al.*, 2012).

Arc rocks in this belt show a geochemical trend from oceanic plateau-like to supra-subduction zone arc-like and consist of basaltic to trachyandesitic lavas, hemipelagic limestones, and volcanoclastic sediments (Buchs *et al.*, 2010 and references therein), with early arc-derived sediment being deposited in the Costa Rican back-arc in the upper Campanian (Mende, 2001 [German] cited in Buchs *et al.*, 2010). While not exposed in Golfito, intermediate composition plutons dated to ~ 67.6 – 41.1 Ma (de Boer *et al.*, 1995; Montes *et al.*, 2012) are found elsewhere in Costa Rica and in Azuero Peninsula, Panama.

2.3.2.3. *Formation of Inner Osa Igneous Complex Plateau*

The earliest basaltic volcanism in the oceanic plateau that would become the Inner Osa Igneous Complex occurred at ~89 – 84 Ma, prior to the initiation of the Middle America Subduction Zone at 88 Ma and overlapping with eruption of the Caribbean Large Igneous Complex (Buchs *et al.*, 2009). This has led Pindell and Kennan (2009) to speculate that this plateau may have been part of the same broad volcanic edifice that formed the Caribbean Large Igneous Complex prior to subduction initiation leaving portions of this edifice on the Farallon plate while the majority of the plateau occupied the nascent Caribbean plate. Unlike the Azuero Plateau in southwestern Panama, the Inner Osa Igneous Complex lacks any arc-related volcanics or intrusives, which demonstrates that the Inner Osa Igneous Complex occupied the incoming Farallon plate following initiation of the Middle America Subduction Zone, prior to its accretion to the Costa Rican forearc (Buchs *et al.*, 2009). The Coniacian – Santonian ages for the inception of magmatism on this plateau are derived from biostratigraphy, as Buchs *et al.* (2009) demonstrated that the 78 – 44 Ma age obtained by $^{40}\text{Ar}/^{39}\text{Ar}$ dating by Berrangé *et al.* (1989) was derived from samples that had undergone argon loss, as outcrops of the Osa Igneous Complex in Burica reporting an Eocene age on the basis

of $^{40}\text{Ar}/^{39}\text{Ar}$ dating are stratigraphically overlain by well-dated, Palaeocene volcanoclastic sediments of the Pavones Formation (Buchs *et al.*, 2009). This plateau is predominantly composed of massive, columnar jointed, or pillow lava and sills, displaying flat REE patterns suggesting a high fraction of melting consistent with eruption of an oceanic plateau and/or hotspot magmatism. However, rare interbedded cherts are present and facilitate biostratigraphic dating (Buchs *et al.*, 2009).

2.3.2.4. *Formation of Osa Seamounts*

The outer Osa Igneous Complex originated as a chain of seamounts produced by the Galapagos hotspot after formation of the oceanic plateaus that form the Inner Osa Igneous Complex and the Caribbean Large Igneous Complex (Duncan and Hargraves, 1984; Buchs *et al.*, 2009; Pindell and Kennan, 2009). Based on palinspastic reconstructions and hotspot drift paths, Pindell and Kennan (2009) determine that the locus of the Galapagos hotspot was positioned just off the Caribbean margin on the Farallon plate in the early – mid Palaeogene. Eruptive ages of the units within the Osa Igneous Complex are poorly resolved as biostratigraphic data from interbedded sediments is sparse and the rocks are shown to have undergone significant argon loss during their history (Buchs *et al.*, 2009).

The Güerra Unit marks the contact between the Inner Osa Igneous Complex and the Outer Osa Igneous Complex and is interpreted by Buchs *et al.* (2009) as forming after the formation of the Inner Osa Igneous Complex and before the accretion of the Outer Osa Igneous Complex on the basis of its geometrical relationships. Similar to the Inner Osa Igneous Complex, the Ganado Unit consists of basaltic and basaltic-andesitic lavas intruded by basalt, dolerite and gabbroic dykes which also display a Coniacian – Santonian age (~89 – 84 Ma) and plateau affinities. However, Buchs *et al.* (2009) demonstrate on the basis of geochemistry (Nb – Y ratios) that these two units are genetically dissimilar. The Riyito and Vaquedano units were erupted as seamounts and both contain basaltic pillow lavas and sheet flows interbedded with sediments. Sedimentary rocks form a minor (<3%) component of the Riyito Unit and mostly consist of volcanoclastic turbidites containing reworked clasts of lava. The Vaquedano

Unit contains xenoliths of pelagic limestones and is interbedded with detrital sediments. Biostratigraphic ages for this unit range from the Campanian to the Middle Eocene (Buchs *et al.*, 2009). Biostratigraphic ages for chert and limestone blocks within the San Pedrillo Unit of the Osa Mélange indicate that the sedimentary cover of these seamounts was deposited from the Campanian to middle Eocene, prior to accretion of these seamounts (Buchs *et al.*, 2009 and references therein).

2.3.3. Palaeogene

2.3.3.1. Formation of other nearby seamounts

With the cessation of large-scale, plateau-like magmatism associated with the Caribbean Large Igneous Province in the Late Cretaceous, Galapagos products took the form of seamounts of various scales. This included the later units within the outer Osa Igneous Complex, such as the Vaquedano Unit (Buchs *et al.*, 2009) and the accreted seamount complexes of Quepos and Herradura (Denyer and Gazel, 2009). Herradura, the larger of the two complexes, formed in the Maastrichtian to middle Eocene and consists of pillow basalts and intrusives interlayered with volcanoclastic and epiclastic sediments (Arias, 2003; Denyer and Gazel, 2009). This complex lies structurally landwards of the Nicoya Complex but is not considered part of the CLIP due to its seamount-related geochemistry (Denyer and Gazel, 2009). Quepos is a smaller seamount complex formed at 65.0 – 59.4 Ma (Sinton *et al.*, 1997; Hauff *et al.*, 2000; Hoernle *et al.*, 2002) and consisting of vesicular pillow basalts and intrusives.

2.3.3.2. Development of the Campanian – Eocene arc belt

Arc magmatism continued in the Campanian – Eocene arc belt, with increasing maturity of the arc system, until ~38 Ma (Montes *et al.*, 2012). In San Blas — a strongly folded and faulted complex of massive basalts, pillow basalts, basaltic andesites, volcanoclastic rocks, cherts and limestones in the east of the Campanian – Eocene arc belt — latest Maastrichtian – middle Eocene granitoid plutons intruded the earlier plateau and arc rocks, while Palaeocene basaltic and rhyolitic lavas were erupted (Montes *et al.*, 2012).

REGIONAL GEOLOGY

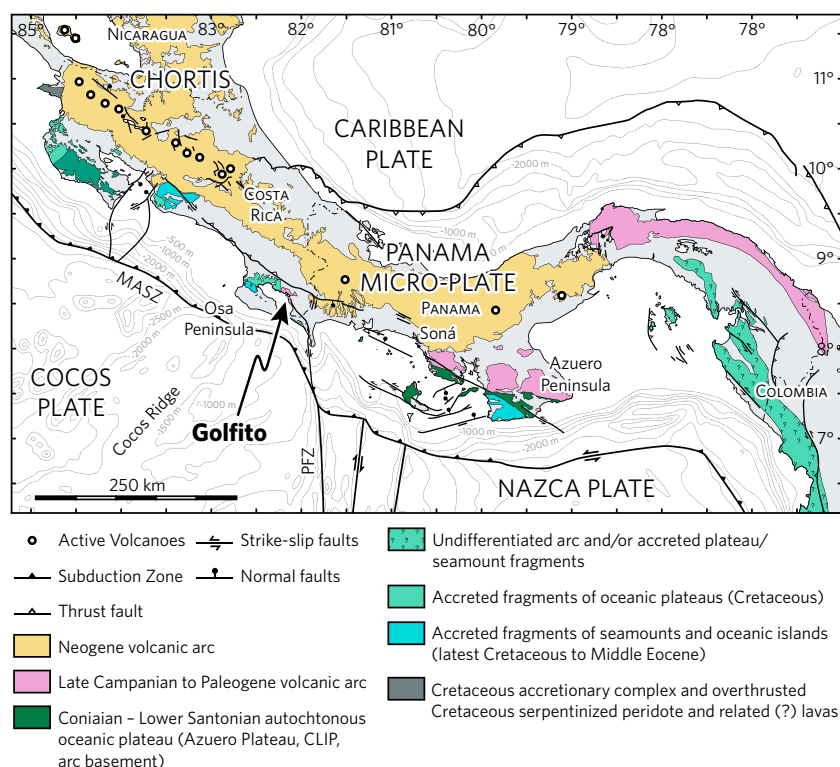


FIG. 2.6. Geological map of southern Central America showing the Miocene - recent arc belt (yellow), the Campanian - Eocene arc belt (pink), and accreted terranes (blue and green) (modified from Buchs *et al.*, 2010; Montes *et al.*, 2012).

Uplift at ~47 – 42 Ma exposed these plutonic roots in Panama and Colombia (Montes *et al.*, 2012).

As the Golfito Complex represents the location of the arc during subduction initiation and was later located at the toe of the forearc in the middle Palaeocene to be juxtaposed against the Inner Osa Igneous Complex (Fig. 2.6), significant subduction erosion must have occurred along this margin in the late Cretaceous to early Palaeocene. This suggests subduction erosion is the normal behaviour of this margin. The switch to accretion with the arrival of the Osa plateau and seamounts suggests that the seamount systems themselves triggered the change from erosion to accretion, rather than enhancing erosion (c.f. Clift and Vannucchi, 2004).

Arc magmatism resumed at ~28 Ma to the northeast of the Campanian – Eocene arc belt, defining the earliest stages of the

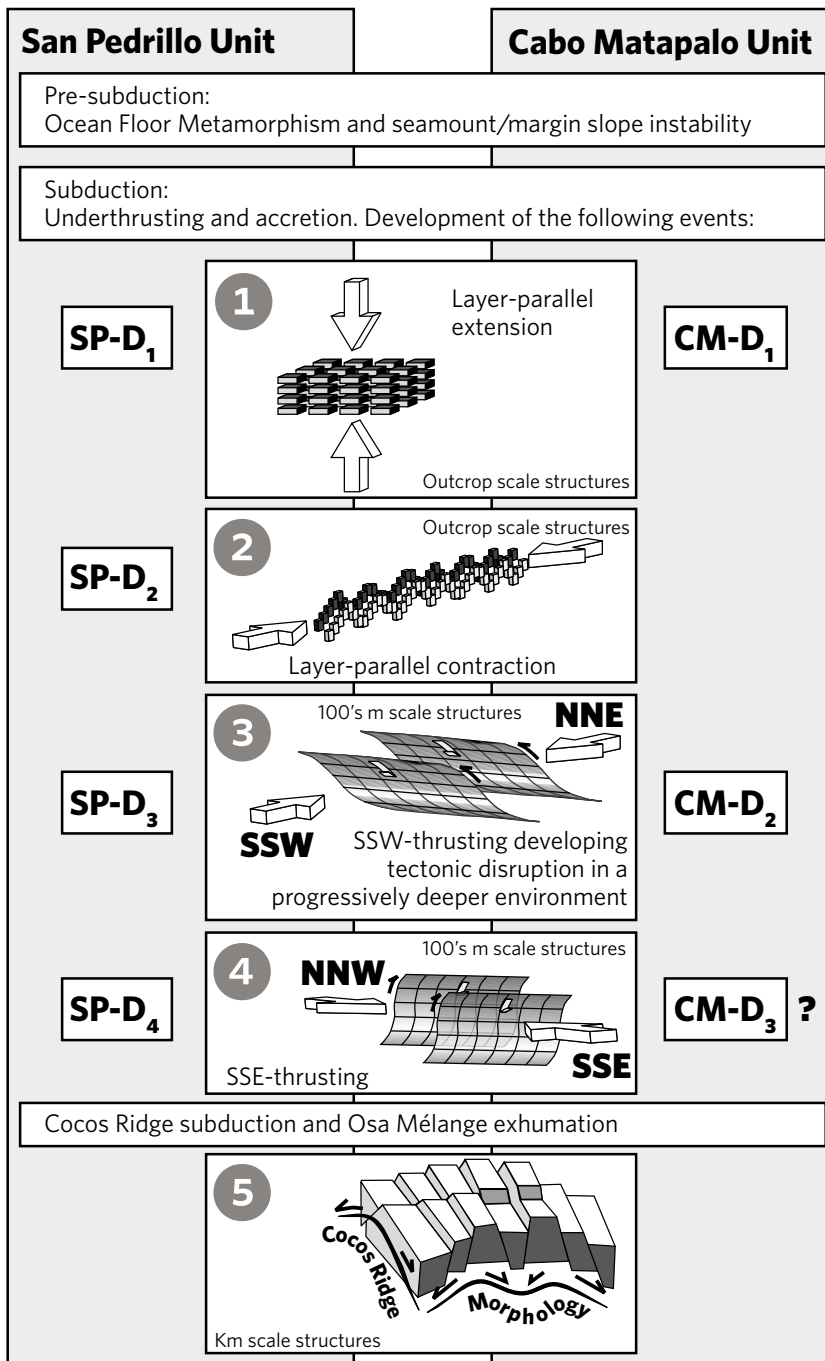


FIG. 2.7. Structural evolution of the fabric within the Osa Mélange showing 5 dominant phases of deformation effecting the San Pedrillo Unit and 4 phases effecting the Cabo Matapalo Unit (from Vannucchi *et al.*, 2006).

REGIONAL GEOLOGY

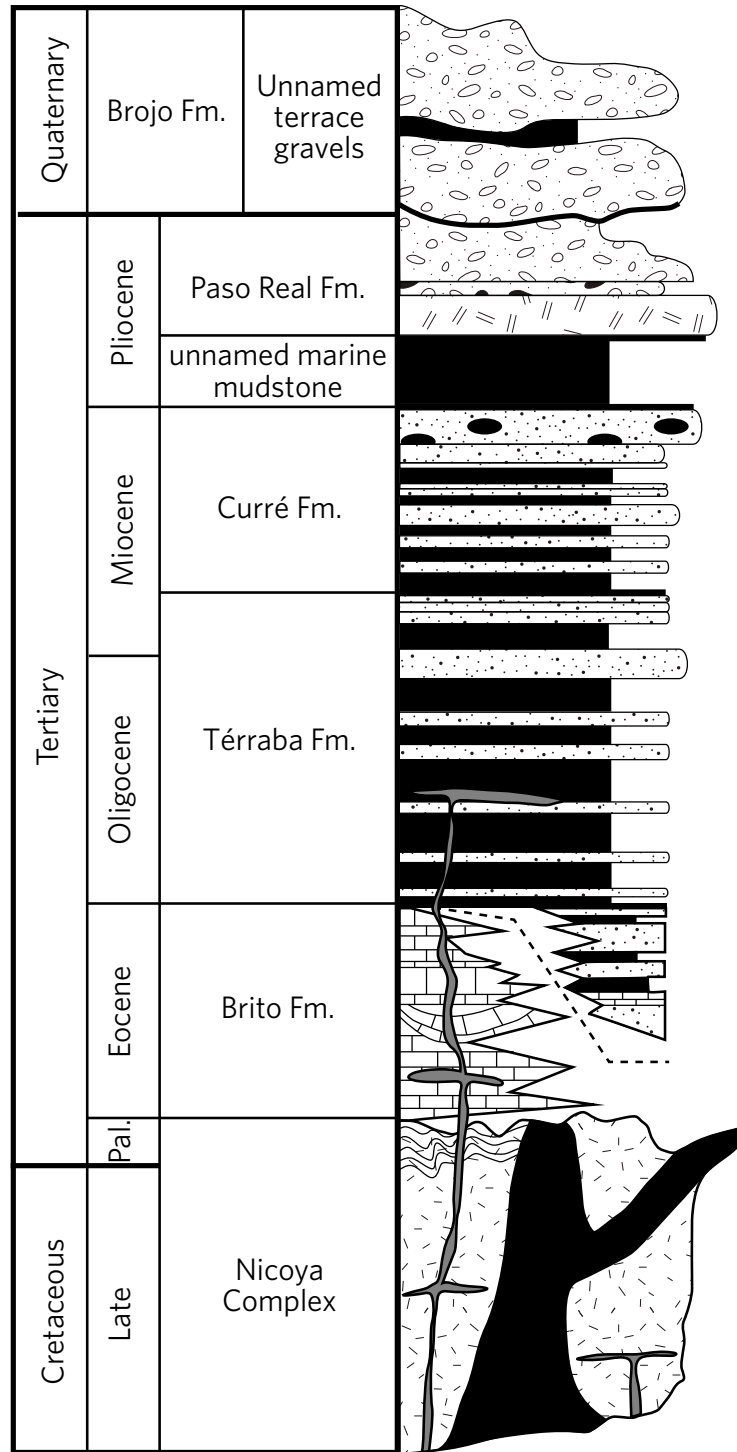


Fig. 2.8. Stratigraphy of the Fila Costeña (from Fisher *et al.*, 2004) showing the evolution of sedimentary facies in the southern Central American forearc through time.

predominantly Miocene – recent arc found across Costa Rica and western Panama (Fig. 2.6) (Montes *et al.*, 2012).

At ~24 Ma, the mature Central American arc – subaerially exposed since at least the Oligocene – collided with the South American continent, preventing the restart of magmatism over the San Blas Complex. At this time, Central and South America remained separated by ~200 km straits with water depths >1.2 km, allowing significant exchange of water masses and marine organisms between the Pacific Ocean and the Caribbean Sea (Newkirk and Martin, 2009; Montes *et al.*, 2012; Osborne *et al.*, 2014).

2.3.3.3. *Accretion of the Osa seamounts*

By the middle Palaeocene, the oceanic plateau that would become the Inner Osa Igneous Complex reached the Middle America Subduction Zone and began to be accreted. This accretion occurred by pervasive thrust faulting and dismemberment of the plateau and its sparse cover of pelagic sediments into fault-bounded lenses which are internally relatively undeformed. (Buchs *et al.*, 2009). At ~58 – 48 Ma, the first of the train of seamounts, now forming the Güerra Unit, was wholly underthrust and subducted to the depth of prehnite – pumpellyite to greenschist metamorphism before being underplated to the accretionary prism of the Inner Osa Igneous Complex (Buchs *et al.*, 2009). During this time (~51 Ma), the San Pedrillo Unit of the Osa Mélange began to be accreted (Vannucchi *et al.*, 2006). Vannucchi *et al.* (2006) interpreted that accretion of the Osa Mélange predominantly occurred by underplating to the base of the Osa Igneous Complex (Fig. 2.7). Subduction and accretion of seamount edifices continued coeval with accretion of the Osa Mélange, with the Ganado and Riyito Units being accreted at ~45 Ma and the Vaquedano Unit – the terminal unit of the Osa Igneous Complex – being accreted at ~38 Ma (Buchs *et al.*, 2009). Accretion of the San Pedrillo Unit ceased at ~31 Ma (Vannucchi *et al.*, 2006).

2.3.3.4. *Fila Costeña forearc basin*

With the shut-off of the Campanian – Eocene arc belt and the subsidence of the forearc, the Térraba forearc basin formed, which existed until the Quaternary when it underwent inversion to

produce the Fila Costeña fold and thrust belt (Fisher *et al.*, 2004). Early deposition in this basin preceded the development of the Miocene – recent arc belt (Fig. 2.8), therefore any volcanic or volcanoclastic debris deposited at this time was derived from the Golfito arc, while most Miocene and post-Miocene volcanics are derived from the Cordillera de Tamanca. This early (middle to late Eocene) sedimentation produced the Brito Formation, consisting of shallow water limestones interbedded with bioclastic and volcanoclastic turbidites (Fisher *et al.*, 2004). This is overlain by a coarsening upwards succession of volcanoclastic turbidites in the Oligocene to lower Miocene Terraba Formation, and the shallow marine or fluvial/lacustrine conglomerates, sandstones and mudstones of the Miocene Curré Formation. Overlying this is a Pliocene marine mudstone and the Pliocene Paso Real Formation, consisting of lahars, pyroclastics and lava flows. Pre-Miocene gabbroic intrusions cut the older section of this succession (Fisher *et al.*, 2004).

2.3.4. Miocene

2.3.4.1. Breakup of Farallon Plate and the evolution of the Cocos-Nazca Spreading Centre

The beginning of the Miocene saw the breakup of the Farallon Plate into the Cocos Plate in the north and the Nazca Plate in the south (Meschede and Barckhausen, 2001). At about this time, the Pacific-Farallon spreading ridge collided with North America, ceasing further subduction and seafloor spreading and coupling the North American and Pacific plates (Handschumacher, 1976). This coupling resulted in major tectonic reorganisation causing the Farallon plate to break along a pre-existing fracture zone (Hey, 1977; Handschumacher, 1976) over the Galapagos hotspot (Meschede and Barckhausen, 2001).

The Cocos-Nazca spreading centre (CNS), which initially formed with the breakup of the Farallon Plate at 23 Ma, has undergone three ridge-jumps over its 23 Ma history (Fig. 2.9). The initial ridge configuration (CNS-1, from Meschede and Barckhausen [2001]) existed from 23 Ma until 19.5 Ma and featured a ridge axis at ~60° to north. At this time, the Galapagos hotspot was situated to the north of the spreading centre on the Cocos

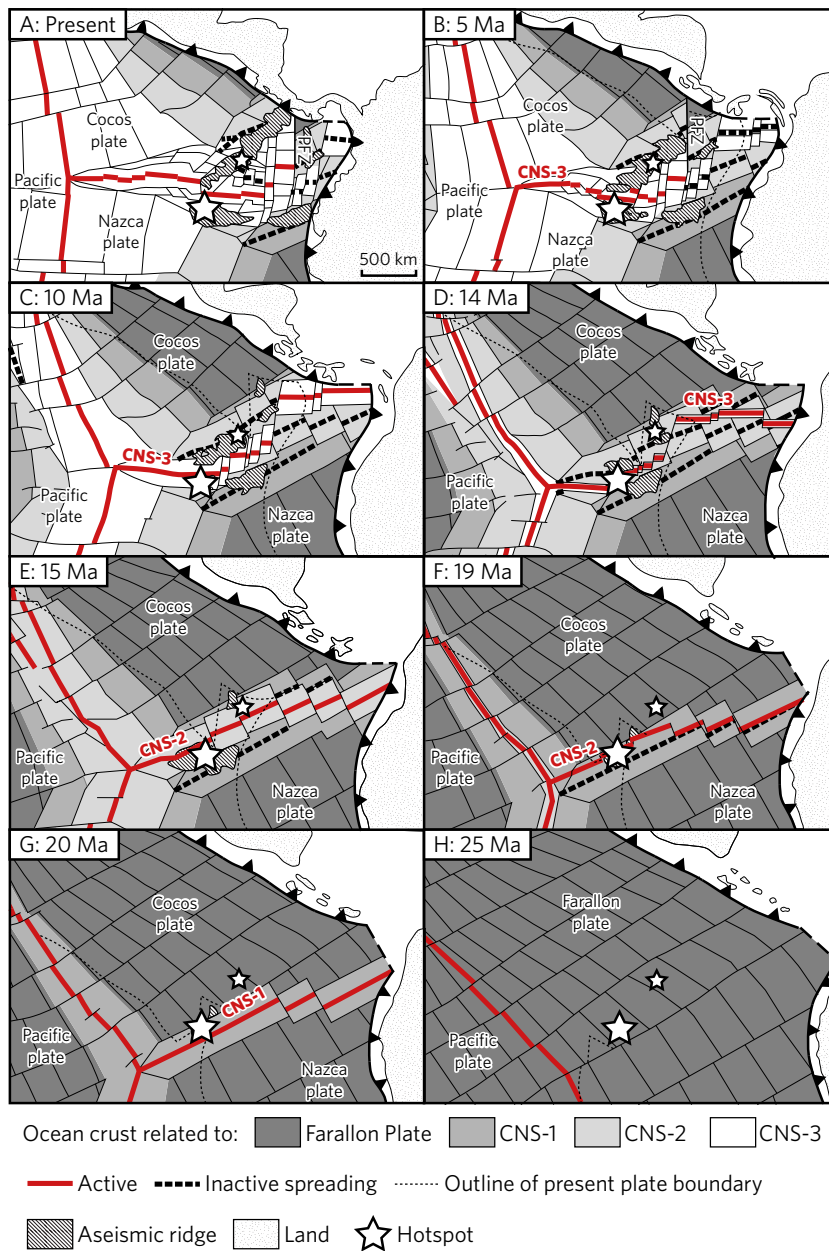


FIG. 2.9. Breakup of the Farallon Plate and the evolution of the Cocos-Nazca Spreading Centre (CNS) and Panama Fracture Zone (PFZ) through time (modified from Meschede and Barckhausen, 2001).

Plate. At 19.5 Ma, the Cocos-Nazca spreading centre shifted to the north (CNS-2, from Meschede and Barckhausen [2001]) and lay approximately coincident with the Galapagos hotspot with a ridge axis at $\sim 70^\circ$ to North. At 14.7 Ma, following northwards migration

REGIONAL GEOLOGY

of the spreading centre relative to the hotspot, the Cocos-Nazca spreading centre jumped southwards to again be approximately coincident with the Galapagos hotspot (CNS-3, from Meschede and Barckhausen [2001]); this ridge is now sometimes referred to as the Galapagos Spreading Centre. This new ridge had an axis trending approximately east – west. Continued northwards migration of the spreading centre relative to the hotspot has resulted in the hotspot being again located to the south of the spreading centre where it has produced the Galapagos Islands (Meschede and Barckhausen, 2001).

Formation of the Panama Fracture Zone at ~8.5 Ma caused cessation of spreading along the eastern-most sections of the Cocos-Nazca Spreading Centre and the transference of portions of the eastern Cocos Plate – including the Malpelo and Coiba Ridges – to the Nazca Plate (Meschede and Barckhausen, 2001; Morell, 2015). Formation of the Panama Fracture Zone also resulted in significantly slower (37 mm/a compared with 81 mm/a of the Cocos Plate) and more oblique subduction beneath Panama (Morell, 2015). The high degree of obliquity between the direction of Nazca plate motion before and after Panama Fracture Zone formation lead to short-lived spreading (~4 – 1 Ma) along the PFZ-parallel Morgan Rift to the east of the Panama Fracture Zone (Morell, 2015).

2.3.4.2. *Formation of the Cocos Ridge*

Meanwhile, the Cocos Ridge – presently subducting beneath the Osa Peninsula – began to be formed as an aseismic ridge and part of the trace of the Galapagos hotspot on the Cocos Plate at ~20 – 22 Ma (Meschede and Barckhausen, 2001 and references therein). Due to its position on the opposite (northern) side of the present-day Cocos-Nazca spreading centre from the present-day centre of Galapagos magmatism, Meschede *et al.* (1998) interpreted that the Cocos Ridge was formed by a second centre of hotspot magmatism located to the north of the primary Galapagos hotspot. They also suggested that the present-day Malpelo Ridge off the coast of Panama formed the oldest part of this ridge system – termed the Cocos-Malpelo Ridge – until dextral strike-slip movement the Panama Fracture Zone cut this ridge. However, Meschede and Barckhausen (2001) interpret that Cocos Ridge

formed above the Galapagos hotspot which – due to its position on the Cocos-Nazca spreading centre – deposited material onto both the Cocos Plate (forming the Cocos Ridge) and the Nazca Plate (forming the Carnegie Ridge). Meanwhile, the Malpelo Ridge formed above a second magmatic centre ~500 km northeast of the Galapagos hotspot. The 14.7 Ma northwards ridge-jump on the Cocos-Nazca spreading centre decreased the amount of hotspot magma being deposited on the Cocos Plate to form the Cocos Ridge while simultaneously increasing the amount of hotspot-magma contributing to the Carnegie Ridge on the Nazca Plate (Meschede and Barckhausen, 2001).

2.3.4.3. Deposition of Cabo Matapalo Unit and Salsipuedes Unit

From the late Oligocene into the Miocene, the Cabo Matapalo and Salsipuedes units were deposited, with the Cabo Matapalo Unit being formed from ~27 – 19.5 Ma (Vannucchi *et al.*, 2006 and references therein). These differ from the earlier San Pedrillo Unit by having an increased proportion of limestones over pelites and basalts and containing significantly lower proportions of chert; these limestones contain partially recrystallised fragments of pelagic fossils (Vannucchi *et al.*, 2006). The presence of dykes with no contact metamorphism, and abundant injection structures and sedimentary dykes, suggests intrusion and overpressure while the rocks were still unlithified.

2.3.4.4. Accretion of the Cabo Matapalo and Salsipuedes units

Subsequently, the Cabo Matapalo accreted at ~11 Ma, followed by the Salsipuedes Unit. The Cabo Matapalo unit underwent an initial deformation phase consisting of layer-parallel extension responsible for extensive boudinage and pinch-and-swell structures, followed by a second phase of thrust faulting and shearing responsible for the development of recumbent folds and major thrust faults (Fig. 2.7). The Cabo Matapalo Unit lacks a phase of layer-parallel compression unrelated to thrusting, as seen in the San Pedrillo Unit (Vannucchi *et al.*, 2006). Similar detailed analysis of the Salsipuedes Unit has not been conducted due to the extreme lack of accessible exposure.

REGIONAL GEOLOGY

2.3.4.5. *Development of the Miocene – recent arc belt*

While minor magmatism northeast of the Campanian – Eocene arc began in the Oligocene, widespread arc development initiated in the early Miocene. This arc front remains active and is responsible for the present volcanism in southern Central America from Guatemala to western Panama, including the Cordillera de Talamanca (Montes *et al.*, 2012). These arcs seal some of the gaps in the Campanian – Eocene belt and contribute to the development of the land bridge between North and South America (Montes *et al.*, 2012). These arcs predominantly produce andesitic lavas and dacitic – rhyolitic pyroclastic flows, with ignimbrites present in the Cordillera de Guanacaste in northern Costa Rica (Abratis, 1998).

The formation of the Panama Fracture Zone at ~8.5 Ma significantly slowed subduction east of the fracture zone and produced strike-slip motion along a portion of the Central American margin (Mechede & Barckhausen, 2001; Morell, 2015). The initial position of the Panama triple junction at the time of formation was offshore the southeastern Nicoya Peninsula, from which it has migrated eastwards to its current position (Morell, 2015). The highly oblique subduction in this region after the formation of the Panama Fracture Zone resulted in cessation of the calc-alkaline magmatism in the Cordillera de Talamanca and adjacent Cordillera Central de Panama (Morell, 2015).

2.3.4.6. *Beginning of the Panama Isthmus*

Recent work (e.g. Kirby and MacFadden, 2005; Kirby *et al.*, 2008; Montes *et al.*, 2012; Bacon *et al.*, 2015) has revealed that the isthmus of Panama closed significantly earlier than was previously recognised: within the early – middle Miocene. While debate continues as to whether this represents the Panama isthmus *sensu stricto*, arc collision, significantly reduced water flow, and migration of land mammals have been established within the Miocene.

The earliest evidence of migration of land mammals is at ~20 Ma. As any pre-Pliocene land bridge which may have existed was likely ephemeral – e.g. the ~23 – 20 Ma and 8 – 6 Ma land bridges proposed by Bacon *et al.* (2015) – it is proposed by O’Dea *et al.* (2016) that these animals migrated by rafting and that the slow pace of this migration prior to the Pliocene is the result of

strong currents in the Central American straits. It is also suggested that migrating fauna may have been insufficiently adapted to the climate or competition on their new continent (O’Dea *et al.*, 2016 and references therein).

The sigmoidal shape of the Panamanian land mass was produced by oroclinal bending accommodated by discrete sinistral strike-slip faults and rotation of relatively rigid blocks at ~38 Ma (Montes *et al.*, 2012). This deformation – accompanied by uplift in surrounding basins – closed the Culebra Strait in the Canal Basin area of Panama and establish a land connection between North America and Panama by 19 Ma (Kirby and MacFadden, 2005; Kirby *et al.*, 2008) allowing North American faunal migration onto the newly formed Central American peninsula. At this time, North and Central America remained separated from South America by the Central American Seaway to the east of Panama (Kirby *et al.*, 2008). However, by ~15 Ma, this seaway was beginning to close (Kirby *et al.*, 2008; Montes *et al.*, 2012) and flow of deep water masses between the Pacific Ocean and the Caribbean Sea ceased by 9.2 Ma (Newkirk and Martin, 2009; Osborne *et al.*, 2014).

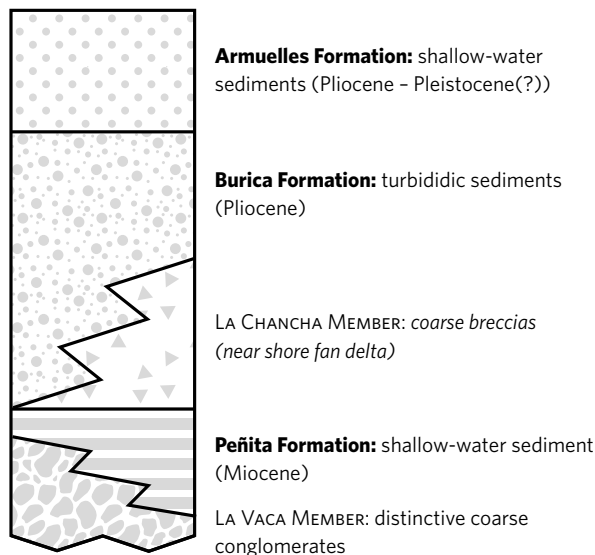


FIG. 2.10. Stratigraphy of the Charco Azul Group of the Osa and Burica peninsulas (modified from Buchs *et al.*, 2009) showing the variation in sedimentary facies through time.

2.3.5. Pliocene

2.3.5.1. Deposition of cover sediments on the Osa Peninsula

Forearc slope sediments of the Charco Azul Group began to be deposited on the Osa Peninsula in the early Pliocene (Fig. 2.10). The unconformity between these slope sediments and the basement of the Osa Igneous Complex and Osa Mélange is marked by palaeosols hosting placer gold deposits, indicating subaerial exposure of the forearc. At the same time, the late Palaeocene – Eocene Pavones Formation – consisting of shallow water limestones and silicic pelagic limestones containing detrital clasts of quartz, zoned plagioclase, and green amphibole – was being deposited on Burica Peninsula (Buchs *et al.*, 2009).

Forearc subsidence due to subduction erosion led to the submergence of the Osa Peninsula and the development of a fan-delta depositing the conglomerates of the La Vaca Member (Coates *et al.*, 1992). Continued subsidence and retreat of the delta resulted in the deposition of green-blue litharenite- and siltstone-bearing turbidites of the Piñata Formation (Vannucchi *et al.*, 2006; Buchs *et al.*, 2009). Conformably overlying this are the fine-grained turbidites and calc-turbidites of the Burica Formation which contain large-scale slumps and channels filled with conglomerates derived from the Cordillera de Talamanca and the Osa Mélange (Coates *et al.*, 1992; Vannucchi *et al.*, 2006). Overlying these are further green-blue early Pleistocene turbiditic siltstones, litharenites and conglomerates of the Armuelles Formation deposited as the forearc was once again uplifted (Coates *et al.*, 1992; Buchs *et al.*, 2009). The Charco Azul Group represents a sequence from shallow marine to deep marine, to shallow marine again (Vannucchi *et al.*, 2006). This vertical movement exceeds what can be expected due to eustatic sea level changes and corresponds well to the local tectonics of the margin (Vannucchi *et al.*, 2006). Finally, variably sorted and poorly consolidated sandstones of the Pleistocene – recent Marengo Formation and Puerto Jiménez Group have been interpreted by Vannucchi *et al.* (2006) to reflect rapid pulses of uplift and subsidence on a scale faster than eustatic sea level variations.

2.3.5.2. *Completion of the Panama Isthmus*

Separation between the Pacific Ocean and the Caribbean Sea water masses definitively stopped in the Pliocene, as has been recognised since Saito (1976) and Keigwin (1978). Large-scale exchange of shallow and intermediate seawater ceased at ~4 Ma, and all surface water connections were severed by 2.76 Ma (O’Dea *et al.*, 2016 and references therein). This final closure of all seaways and the establishment of a continuous land bridge between North and South America has been regarded as the Panama Isthmus *sensu stricto* by O’Dea *et al.* (2016) who restrict the use of the term “isthmus” to only contiguous, entirely subaerial connection between continents. This final closure potentially triggered glaciations in the northern hemisphere (e.g. Burton *et al.*, 1997; Haug *et al.*, 2001; Lear *et al.*, 2003) and facilitated accelerated migrations of biota (Marshall *et al.*, 1982; Jackson *et al.*, 1993). This closure occurred through the gradual emergence of the San Blas Complex throughout the Neogene following the collision between the Central American peninsula and South America and eustatic sea level fall promoted by widespread glaciations in the northern hemisphere (O’Dea *et al.*, 2016).

2.3.6. *Quaternary*

2.3.6.1. *Subduction of the Cocos Ridge*

At ~2.5 Ma, the Cocos Ridge impacted the Middle America Subduction Zone and began to subduct under the Osa Peninsula (e.g. Vannucchi *et al.*, 2013; Morell, 2015). The subduction of this thickened oceanic crust caused rapid tectonic erosion at the base of the forearc, a landward shift in the trench axis, normal faulting and uplift of the Osa Peninsula, inversion of the Fila Costeña basin, uplift of the Cordillera de Talamanca, and detachment of the Panama micro-plate from the Caribbean Plate (Fisher *et al.*, 2004; Vannucchi *et al.*, 2006, 2013; Morell, 2015). Continued subduction of the Cocos Ridge caused dramatic thinning of the wedge to ~3 km below the coastline – down from 12 – 14 km of crust under the Nicoya Peninsula – which resulted in long-term subsidence of the margin (Vannucchi *et al.*, 2013). The angle of subduction has correspondingly shallowed due to subduction of the thickened

REGIONAL GEOLOGY

crust of the Cocos Ridge, from $>65^\circ$ off-shore Santa Elena to sub-horizontal beneath the Osa Peninsula (Protti *et al.*, 1995). This change in the angle of subduction is accommodated by the Quesada Sharp Contortion, a tear or bend in the slab corresponding to the position of the Cocos Ridge, as revealed by the location of the Wadati-Benioff Zone beneath Costa Rica (Protti *et al.*, 1994).

The timing of Cocos Ridge subduction is widely debated with estimates ranging from ~ 8 Ma (e.g. Abratis and Wörner, 2001; Gazel *et al.*, 2009) to ~ 0.5 Ma (Gardner *et al.*, 1992). Most datasets suggest a late Pliocene – Pleistocene age for this event (e.g. Fisher *et al.*, 2004; Vannucchi *et al.*, 2006, 2013; Morell, 2015), although the 8 – 5 Ma cessation of magmatism in the Cordillera de Talamanca – attributed to flat subduction of the Cocos Ridge – has been used to suggest a late Miocene age for Cocos Ridge subduction (e.g. Abratis and Wörner, 2001). However, Morell (2015) demonstrated that the ~ 8 – 5 Ma cessation of magmatism is best explained by highly oblique convergence after the ~ 8.5 Ma formation of the Panama Fracture Zone, meaning that a ~ 2.5 Ma age is favoured for initiation of Cocos Ridge subduction.

2.3.6.2. Rise of the Fila Costeña

As a result of Cocos Ridge subduction, the Térraba forearc basin underwent inversion to produce the Fila Costeña fold and thrust belt during the Quaternary (Morell, 2015). This inversion resulted in a minimum of ~ 17 km of horizontal shortening (about 45% of the width) of the Térraba basin (Fisher *et al.*, 2004). Fisher *et al.* (2004) demonstrated that the direction of deformation within this belt was primarily orthogonal to the Central American margin and lacks any significant strike-slip component. Extensive Quaternary-age fluvial deposits are present within this range, and form terraces recording the uplift history of the region (Fisher *et al.*, 2004).

2.3.6.3. Uplift of the Cordillera de Talamanca

The subduction of the Cocos Ridge also caused uplift of the Cordillera de Talamanca at 3 – 1 Ma, exposing its plutonic roots. This is evidenced by the extent of the uplifted area closely corresponding to the width and position of the Cocos Ridge off-shore. The uplift of this arc also resulted in the inversion and uplift of

Limón back thrust belt in eastern Costa Rica at 1.6 Ma (Morell, 2015). Sparse Quaternary adakite volcanoes in the Cordillera de Talamanca and Cordillera Central de Panama – such as Volcán Barú in western Panama – have been interpreted as the product of a slab window due to the subduction of a segment of the Cocos-Nazca Spreading Centre (e.g. Johnston and Thorkelson, 1997; Abratis and Wörner, 2001) or a slab tear at the Panama Fracture Zone (e.g. Morell *et al.*, 2013).

2.4. SUMMARY OF REGIONAL GEOLOGY

The Osa Mélangé is one of many products of the Galapagos hotspot accreted in Central America during the Cenozoic. The subduction of Galapagos products is a major driver for the tectonics on the southwestern margin of the Caribbean Plate, and has produced several accreted terranes along the Costa Rican and Panamanian coasts, promoted uplift of the Osa Peninsula and the Fila Costeña fold and thrust belt, and caused long-term forearc subsidence and trench retreat due to subduction erosion. Both Vannucchi *et al.* (2006) and Buchs *et al.* (2009) propose that the Osa Mélangé formed from material derived from a chain of Galapagos seamounts now accreted landwards of mélangé as the Osa Igneous Complex. Chapters 6 and 8 of this thesis expand on these hypotheses and refine the interpretation of mélangé formation.

THIS PAGE INTENTIONALLY LEFT BLANK.

CHAPTER 3. THE SUBDUCTION ZONE PLATE BOUNDARY INTERFACE:

Processes and their implications

The subduction zone plate boundary interface is an area of significant geological interest but is largely inaccessible to direct observation due to the extreme depths at which they are located. Few drilling projects (e.g. Sakaguchi *et al.*, 2011) have succeeded in sampling the plate boundary interface and those that have only reached the up-dip extremity of this zone. As such, the subduction zone plate interface is studied by geophysical means (e.g. Sage *et al.*, 2006), analogue and numerical modelling (e.g. Gerya *et al.*, 2002; Warren *et al.*, 2008), and the study of fossil plate interfaces (e.g. Vannucchi *et al.*, 2008). Recent advancement in seismic and GPS monitoring technologies have allowed study of movement on this plate interface and the recognition of a broad spectrum of seismic and aseismic slip (Ide *et al.*, 2007).

This chapter introduces the concept of the subduction channel, describes the tectonic processes of subduction erosion and subduction accretion, and explores the spectrum of seismic and aseismic slip possible on the subduction zone fault.

3.1. THE SUBDUCTION CHANNEL

The subduction channel – first postulated by Shreve and Cloos (1986) – is a viscously deforming shear zone located between the down-going and the overriding plates in a subduction zone reaching from the frontal thrust at the trench to the asthenosphere (Gerya and Stockhert, 2002; Gerya *et al.*, 2002; Warren *et al.*, 2008). This layer accommodates the majority of the shear strain associated with the subduction process. In its upper sections, this layer is most commonly comprised of poorly consolidated marine sediment derived from the top of the incoming plate, along with lithified blocks of upper-plate material in the case of erosive subduction zones (Vannucchi *et al.*, 2012) or a gouge of tectonically abraded material (Cowan, 1985). This chaotic distribution of blocks within a more tractable matrix is analogous to exhumed mélanges, and subduction channels have been interpreted as the

THE SUBDUCTION ZONE PLATE BOUNDARY INTERFACE

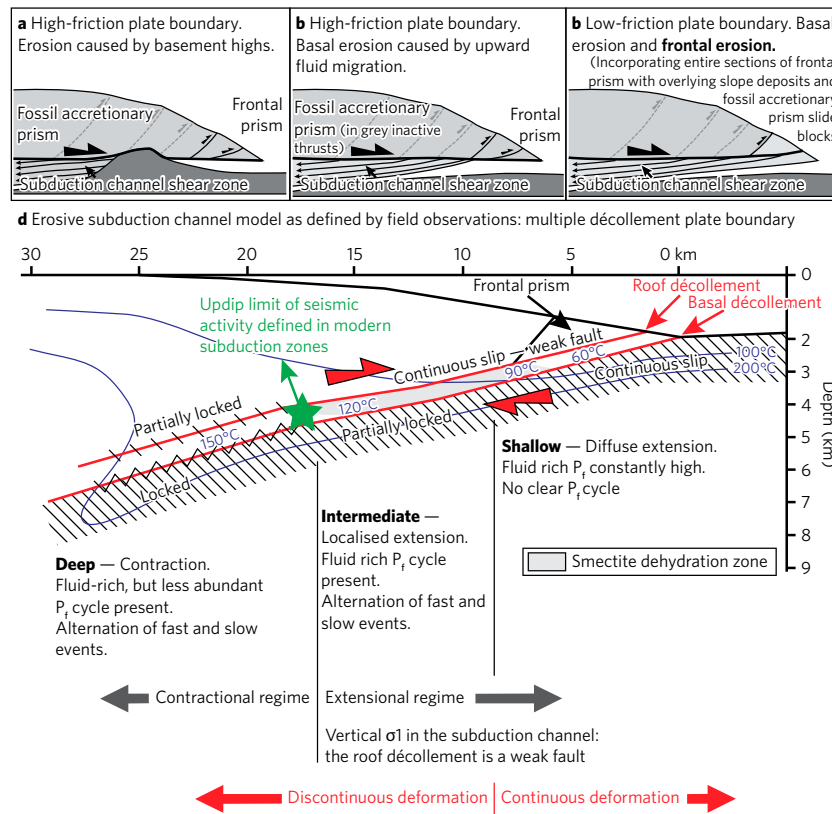


FIG. 3.1. Anatomy of a subduction channel (from Vannucchi *et al.*, 2008) showing **A**: subduction erosion as a response of the subduction channel shear zone to subduction of a basement high (high friction). **B**: Subduction erosion as a result of hydrofracturing the upper plate (low friction). **C**: Low friction subduction erosion cutting through the toe of the margin to incorporate blocks from the upper plate. **D**: Systematic anatomy of a subduction channel (based on data from the Apennines and Costa Rica) showing the upper and lower décollement surfaces, and the deformation and mechanisms active at each depth, including the position of the seismogenic zone.

setting of formation of several mélanges, including the Franciscan Mélange (Shreve and Cloos, 1986; Krohe, 2017), the Shimanto Belt in Japan (Kitamura *et al.*, 2005; Bachmann *et al.*, 2009b), and the Sestola–Vidiciatico unit of the Apennines in Italy (Vannucchi *et al.*, 2008). This poorly consolidated layer acts as a lubricant along the subduction zone, contributing to the weakening the plate interface, and allowing the process of subduction and terrestrial-style plate tectonics (Duarte *et al.*, 2015). This channel has been

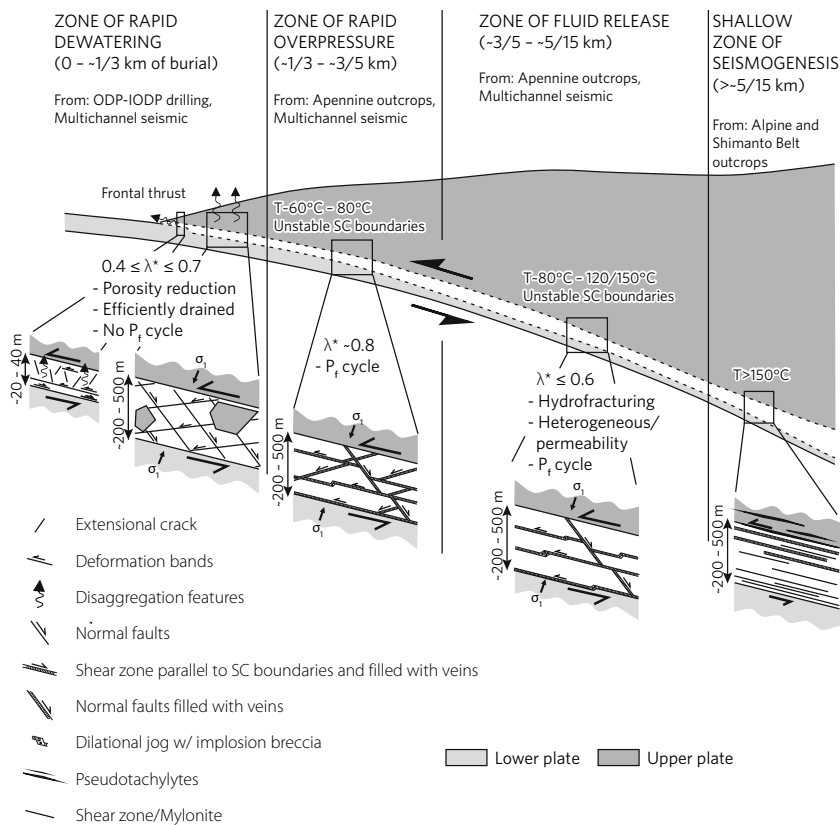


FIG. 3.2. Deformation mechanisms and styles at different depths within the subduction channel up to the onset of the seismogenic zone (from Vannucchi *et al.*, 2012).

imaged by seismological studies as a thin low-velocity zone along the plate surface (e.g. Sage *et al.*, 2006), numerically modelled (Gerya *et al.*, 2002; Warren *et al.*, 2008), and observed in the field in uplifted fossil subduction complexes (Vannucchi *et al.*, 2008). The thickness of these subduction channels is highly variable within and between subduction zones, ranging from ~20 m to ~1000 m (Vannucchi *et al.*, 2012).

Subduction channels consist of an inlet below the frontal thrust of the subduction zone through which oceanic sediment is subducted, a roof décollement defining the base of the upper plate, and a basal décollement defining the top of the subducting plate. These surfaces have been observed in field studies of fossil subduction channels (Kitamura *et al.*, 2005; Vannucchi *et al.*, 2008; Bachmann *et al.*, 2009) and by high resolution seismic

analysis (Collot *et al.*, 2011). The position of the subduction channel's boundaries migrate with time as the roof décollement rises into the upper plate, entraining material in the subduction zone hanging wall, or lowers as the subduction channel material indurates and becomes attached to the upper plate; these concepts of material being added (accreted) or removed (eroded) from the upper plate during subduction is introduced in detail in Chapter 3.2. Shear within the subduction channel is heterogeneously distributed with zones of shear localisation within the broader channel, with some shear deformation potentially affecting the base of the upper plate and the top of the subducting plate. Typically, strain localises within the finer-grained, clay-rich material, rather than the sandier material (Vannucchi *et al.*, 2012). The subduction channel is not of uniform thickness and can pinch and swell to accommodate subduction of intermittently increased sediment or seamounts (Sage *et al.*, 2006; Vannucchi *et al.*, 2012). As sediment is subducted and buried, compaction and dewatering can result in a significant reduction in material volume, causing a non-simple shear component to deformation within the subduction channel, which may promote the instabilities in the subduction channel boundaries that result in subduction erosion (Vannucchi *et al.*, 2012).

Vannucchi *et al.* (2012) subdivided the upper 15 km of the subduction channel into 4 zones on the basis of the dominant processes acting on material within the channel (Fig. 3.2). Material in zone 1 undergoes rapid dewatering as it passes below the frontal thrust. The input material in this zone is typically unconsolidated sediment with a high pore-fluid content. Water released in this zone drains upwards into the toe of the forearc and along the subduction channel to the trench and maintains a largely stable fluid pressure. This process results in the primary lithification of the subducted sediment — causing a reduction in porosity from ~50% to ~25% — and resulting in progressively more localised concentrations of strain. Zone 1 has a sharply defined upper boundary, but the lower boundary is more diffuse. In this zone, deformation is primarily accomplished by rotation and frictional slip of the grains (Karner *et al.*, 2003). In this zone, the dominant surface of slip is a semi-permeable barrier to upwards-migrating

fluid flow, while the adjacent, less strained, brecciated portion acts as an effective conduit for through-going fluids. This zone already exhibits development of both roof and basal surfaces of enhanced slip, as shown by Vannucchi *et al.* (2008), with the basal surface concentrating the most shear strain. Deformation in this zone concentrates within materials which are unlithified, with rigid blocks being spared deformation. This zone primarily undergoes compaction and layer-parallel extensional deformation and fracturing in a rhomb-shaped fracture network generally not accompanied by mineralisation (Vannucchi *et al.*, 2012).

By the time material reaches zone 2, it has been consolidated and lithified such that it can sustain discrete fractures accommodating extensional deformation. This zone also features high fluid pressures with defined cycles of fluid pressures – indicating inefficient drainage of this zone – resulting in widespread mineral precipitation of veins. Temperatures within this zone have been modelled by Grevenmeyer *et al.* (2004) and Harris *et al.* (2010a, b) to be ~60 – 100°C. Fracturing in zone 2 also occurs as a rhomb-shaped network of mutually cross-cutting normal faults and extensional fractures along with channel-parallel shear zones and may cut through both blocks and matrix. Hydrofracturing is common within this zone, increasing the secondary porosity and permeability of the subduction channel and facilitating fluid-flow. In this zone, the basal shear zone acts as a pathway for fluid migration from greater depths into shallower portions of the subduction zone.

The material within zone 3 has undergone total lithification and consolidation, has a porosity of ~10%, and now exhibits a volume approximately half that of when it was first subducted. Calahorrano *et al.* (2008) and Ranero *et al.* (2008) calculate that temperatures within this zone range from ~80 – 150°C. The upper limits of these temperatures trigger metamorphic dehydration from mineral-bound sources of water, facilitate the process of pressure-solution, and promote the change from aseismic to seismic strain. In zone 3, over-pressured fluids as part of a fluid-pressure cycle drain effectively, either into zone 2 or through splay-faults into and through the forearc (Vannucchi *et al.*, 2012). Due to this complete lithification, slip planes cut through matrix and blocks, suggesting near-homogenous frictional properties.

This zone also sees the first occurrence of seismogenic structures in the form of dilational jogs* containing implosion breccias (Vannucchi *et al.*, 2012).

Zone 4 is defined as the up-dip limit of the seismogenic zone and is characterised by high fluid pressure and fluid pressure cycles accompanied by seismic slip producing pseudotachylites along the roof décollement and in the upper plate. This region still features extensional fractures, but the shear zones develop into mylonites with increasing depth. In this region, the majority of shear is localised along the roof décollement and the upper portion of the subduction channel features sufficiently high fluid pressures to cause hydrofracturing. The high permeability contrast between the base of the upper plate and the subduction channel at this depth promotes hydrofracturing of the hanging wall facilitating subduction erosion (von Huene *et al.*, 2004; Vannucchi *et al.*, 2012).

3.1.1. Return Flow

Within this channel, strain kinematics can differ significantly from other shear zones, as sediment carried downwards by the subducting slab may begin to flow upwards due to its own buoyancy; a process known as return-flow (Cloos and Shreve, 1988a; Warren *et al.*, 2008; Zheng *et al.*, 2013; Krohe, 2017). This process – originally interpreted to operate only within the top 15 km of the subduction zone system (Cloos and Shreve, 1988a) – is now believed to allow recovery of material subducted to depths greater than 100 km (Gerya *et al.*, 2002). This process is likely not ubiquitous in subduction zones, but has been proposed to have occurred – amongst other locations – in the Franciscan subduction zone, explaining the presence of blueschist-facies blocks within a lower grade matrix (Krohe, 2017). This process and term has been used to describe the two related phenomena of ascent of individual blocks – which are typically assumed to be free-floating (Cloos and Shreve, 1988a; Krohe, 2017) – and the exhumation of

* Rhomboidal cracks produced by slip-parallel extension at a releasing bend on the fault surface, often filled by vein material or breccia.

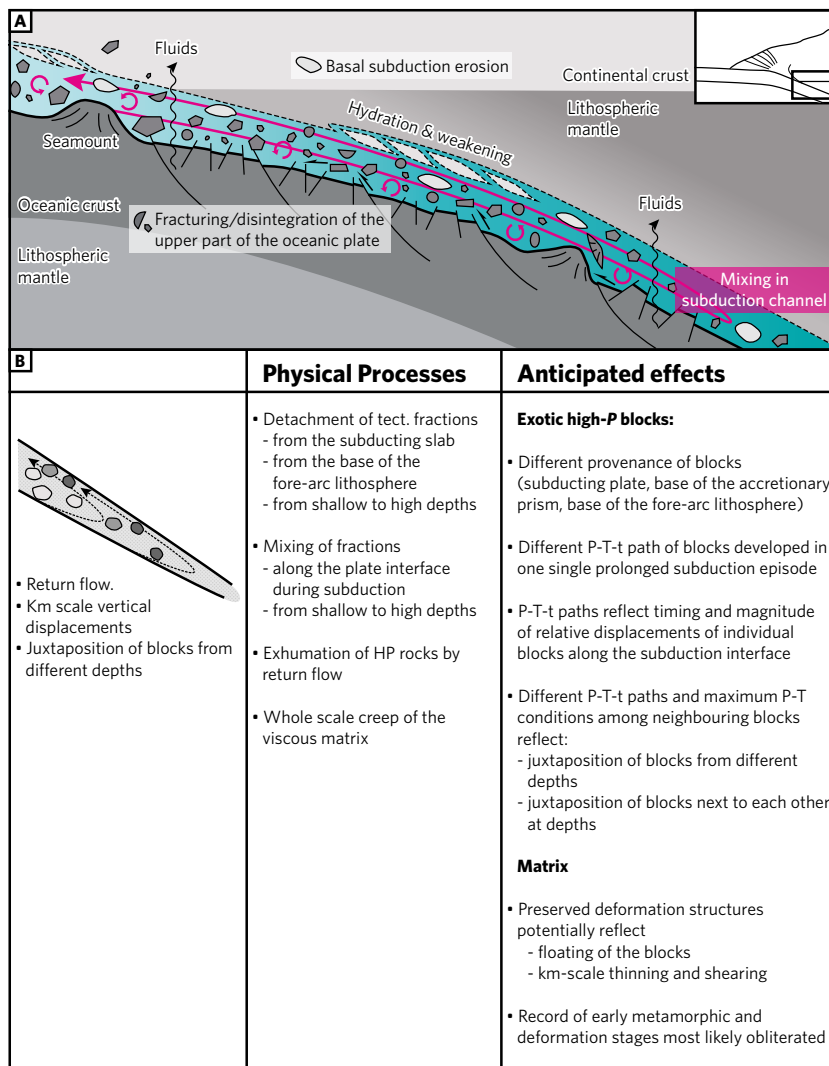


FIG. 3.3. **A:** Model of tectonic erosion coupled with fragmentation of the downgoing slab to tectonically mix materials from both plates within the subduction channel (from Krohe, 2017). This includes buoyancy-related return flow of material along the upper surface of the subduction channel. **B:** The expected processes and the resultant features expected to be recorded in fossil subduction channels.

crustal-scale slices of subducted material (Gerya *et al.*, 2002; Warren *et al.*, 2008; Zheng *et al.*, 2013).

The driving force behind this uplift of material is the buoyancy of the material itself, which acts against the shear traction between the downgoing slab and the overriding plate. This buoyancy becomes the dominant force acting on the blocks once they become kinematically decoupled from the downgoing plate and

THE SUBDUCTION ZONE PLATE BOUNDARY INTERFACE

acts to return the material to a neutral buoyancy (Gerya *et al.*, 2002; Warren *et al.*, 2008). This process has been well modelled by analogue (Chemenda *et al.*, 1996, 2000) and numerical experiments (Gerya *et al.*, 2002; Warren *et al.*, 2008) which have interpreted that the process is geodynamically possible.

Warren *et al.* (2008) and Zheng *et al.* (2013) applied the subduction channel concept to continental subduction to explain the rapid burial and subsequent exhumation of high pressure and ultra-high pressure rocks found within orogenic belts. Exhumation of high and ultra-high pressure rocks within a subduction channel allows for uplift without invoking processes of slab break-off or extensive surface erosion (Warren *et al.*, 2008).

Despite this modelling and the apparent simplicity of uplift along the path of the subduction zone fault, the concept of return flow remains controversial, as blocks previously believed to have been incorporated via tectonic erosion of the upper plate and exhumed into the lower-metamorphic-grade matrix in which they are now found, have since been reinterpreted as olistoliths derived from a previously exposed metamorphic complex (Wakabayashi, 2011, 2012; Krohe, 2017).

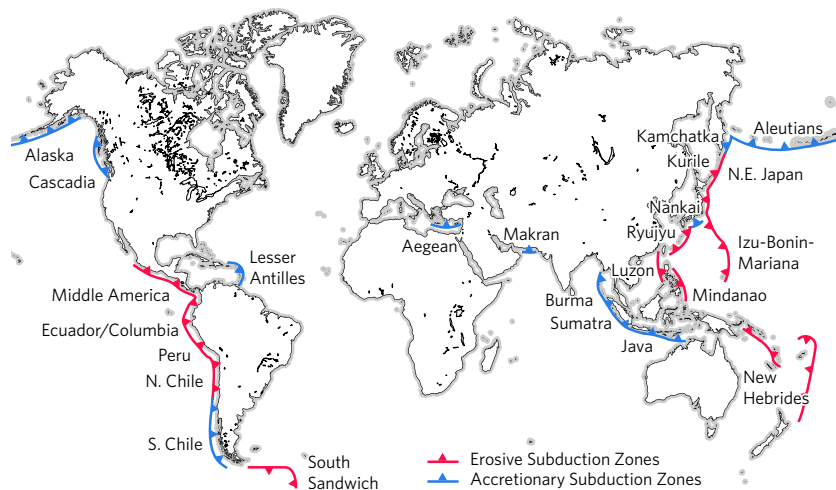


FIG. 3.4. Global map of subduction zone margins showing the distribution of erosive and accretionary subduction zones (modified from Clift and Vannucchi, 2004).

3.2. ACCRETION AND EROSION

Subduction zone margins may be broadly categorised into two groups, accretionary and erosive, on the basis of whether they are contributing material to the forearc or removing material from the forearc. Approximately half (~57%) of global subduction zones by length are defined as erosive margins (Clift and Vannucchi, 2004). This fundamental difference in the processes operating within the subduction zone influences the structure and morphology of the margin. It is important to note that both material removal and material addition may be occurring at once in the same subduction zone, either a) alternating in time, b) changing with depth, or c) changing along strike due to localised or short-term perturbations in the subduction system, such as subduction of a seamount. As such, whether a subduction zone is categorised as accretionary or erosive is defined by Clift and Vannucchi (2004) on the basis of active growth or shrinkage of the forearc wedge, not by the presence or absence of particular features. At a global scale, significantly more material is removed from the forearc by tectonic erosion than is added by accretion; however, despite this, most subduction systems – including several erosive margins – are net contributors to the production of new crust due to the high volume of magmatism at the arc (Clift and Vannucchi, 2004).

3.2.1. *What is subduction accretion?*

Subduction accretion is the transfer of material from the incoming plate to the overriding plate in a subduction zone. This process occurs either by off-scraping of sediment at the toe of the accretionary prism or by underplating at the base (Cloos and Shreve, 1988). Examples of accretionary subduction zones include Cascadia, Nankai, the Aleutians, and the Lesser Antilles. These subduction zones are characterised by shallow (<3°) slopes built of landward-dipping thrust faults and often exhibit mud diapirs and volcanoes due to overpressure within the prism (Clift and Vannucchi, 2004).

The process of subduction accretion does not preserve the majority of sediment that enters the subduction system. Indeed, only 7 – 37% of sediment entering the trench is accreted to the forearc (Clift and Vannucchi 2004). In fossil accretionary complexes, terrigenous turbiditic sediment is significantly more

common than pelagic and hemi-pelagic abyssal sediment, which is ubiquitous on the incoming plate. This suggests that the sediment pile is bifurcated into the material that will be off-scraped and the material that will be underthrust on the basis of lithology. This division is made by the décollement – the plate boundary fault proper – which is a major structural discontinuity and separates the high stress conditions in the off-scraped package from the low stress conditions on the downgoing slab. The décollement effectively separates the coarser, turbiditic trench sediment from the finer abyssal sediment, and therefore is not located at the top of the oceanic basement (Moore, 1989; Clift and Vannucchi, 2004). The décollement localises within a layer with low strength and a low coefficient of friction; typically the hemi-pelagic mudstones and carbonates deposited close to the upper plate but prior to arrival in the trench (e.g. Moore, 1989; Kurzwski *et al.*, 2016).

Frontal accretion is a primarily compressive process, producing structures such as thrust faults and buckle-folds with the maximum principal stress axis oriented sub-horizontally and perpendicular to the trench axis. Steeply dipping foliation indicating near-horizontal compression is typical in these rock units. Off-scraped sequences are typically characterised by imbricate thrust faults and tight – isoclinal folding with the intensity of deformation increasing landwards until fold hinges are sheared out and tectonic dismemberment into broken formation and tectonic *mélange* occurs (Vannucchi and Bettelli, 2002).

In addition to material accreted by frontal off-scraping at the toe of the margin, material may also be accreted by underplating. This process involves the down-stepping of the décollement below a section of underthrust material (Cloos and Schreve, 1988b). Several mechanisms have been proposed to explain the movement of the décollement, including lithification and strain-hardening of the existing décollement plane, necessitating migration to a new, weaker level structurally below the existing surface (e.g. Cloos and Schreve, 1988b; Buchs *et al.*, 2009), the propagation of accretionary prism thrusts below the décollement surface, offsetting the décollement and forcing downwards migration of the décollement on landwards wall (McCarthy and Scholl, 1985), and buoyancy-driven opposition to further subduction (e.g. Sutherland *et al.*,

2009; Scherwath *et al.*, 2010). Where the decollement migrates into the basement of the downgoing slab, ophiolite obduction may occur (Plunder *et al.*, 2015). Underplating allows the thickening and uplift of the accretionary prism without shortening of the prism width. Underplating of material below the forearc may be significant, even if no frontal accretion occurs and the forearc is undergoing long-term subsidence (Sutherland *et al.*, 2009). As such, the errors involved in estimates of material flux (e.g. Clift and Vannucchi, 2004) may be difficult to quantify (Sutherland *et al.*, 2009).

Material that has been underplated is typically spared the compressive deformation that occurs above the décollement, and is instead subjected to simple shear, resulting in structures such as asymmetric grains (e.g. sigma and delta structures) and scaly fabric (Cloos and Shreve, 1988b). Additionally, the presence of unconformably overlying slope sediments has been used by Vannucchi and Bettelli (2002) as a discriminator between underplated and frontally accreted packages.

Sutherland *et al.* (2009) proposed that forearc uplift due to underplating and subsequent collapse – including mass wasting to the trench – to reattain the critical taper angle may result in cycles of subduction, accretion, uplift, mass wasting to the trench, and re-subduction.

3.2.2. What is subduction erosion?

Subduction erosion is the removal of forearc material from the hanging wall of the subduction zone fault and its conveyance towards and into the mantle. This is primarily accomplished by fracturing of the base of the overriding plate and piecemeal incorporation of fragments into the subduction channel (von Huene *et al.*, 2004). Examples of erosive subduction zones are Izu-Bonin-Mariana, Middle America, and Tonga. These margins feature narrow and steep forearc slopes composed of volcanic, plutonic, metamorphic, or mantle rocks cut by normal faults. Clift and Vannucchi (2004) calculated that 52 – 88% of the material dragged to mantle depths in erosive subduction zones is derived from tectonic erosion of the upper plate. A small frontal prism of transient sedimentary material lies at the very toe of the forearc wedge and accommodates compressional deformation prior to

subduction (Clift and Vannucchi, 2004). This frontal prism is significantly smaller than accretionary prisms and also consists of landward dipping thrust faults. However, these prisms form by progressive disruption of the forearc basement towards the toe of the wedge, and so contact between the frontal prism and its backstop is gradational. This means that the frontal prism is composed predominantly of disrupted upper plate material, not off-scraped lower plate material (von Huene *et al.*, 2004). Study of erosive subduction zones is hindered by the process of tectonic erosion, by definition, consuming the rocks it creates, with only very rare examples of erosive subduction channels being preserved where dramatic perturbations in the subduction zone system occurred. Their location below the depths generally accessible to ocean drilling and sufficiently high resolution seismic further impedes study of these margins (von Huene *et al.*, 2004).

Coats (1962) first noted that, in contrast to other margins where broad accretionary prisms were being recognised, the Aleutian margin lacked such a prism. He therefore surmised that at some margins no accretion occurs and therefore all the material on the incoming plate is subducted. Despite this, accretion of sediment at subduction zones was generally considered typical of all margins (e.g. Karig, 1974) until it was recognised that some margins are significantly smaller than would be expected if accretion had occurred throughout the time subduction was known to have been active at that margin, that deep sea drilling had not recovered accreted oceanic deposits, and that pelagic abyssal sediment – ubiquitous on the ocean floor – is rare in exposed accretionary complexes (e.g. Scholl *et al.*, 1977). Aubouin *et al.* (1982) noticed that the Middle America Subduction Zone lacked evidence of recent accretion. Murauchi and Ludwig (1980) and Langseth *et al.* (1981) noted the long-term subsidence of the upper plate near the Japan Trench and interpreted that material is being actively eroded from the base of the forearc. Murauchi and Ludwig (1980) interpreted that subduction of sediment, along with hydrofracturing from the pressurised pore-fluid, lubricates the subduction interface and facilitates upwards migration of the plate boundary fault.

Hilde (1983) observed in seismic reflections the presence of horsts and grabens on the subducting plate prior to and shortly following subduction. He interpreted that these bend-faults mechanically abrade against the base of the forearc in a manner similar to a ‘chain-saw’, removing material by “rasping” (Hilde, 1983; Clift and Vannucchi 2004). However, improved seismic imaging by von Huene and Culotta (1989) showed that the horsts and grabens on the lower plate were blanketed by sediment – both abyssal sediment and slump material from the frontal prism – meaning that the decollement is located several 100 metres above the level of the horst basement (von Huene and Ranero, 2003). This suggests that mechanical “rasping” is not occurring. Tectonic abrasion by high friction on the plate interface – as modelled by Lallemand *et al.* (1994) – is not the dominant process governing subduction erosion and instead the high fluid pressures under the forearc reduce basal friction while promoting hydrofracturing of the overriding plate (von Huene *et al.*, 2004).

3.2.3. What controls accretionary or erosive behaviour?

Changes in erosive or accretionary behaviour in response to changing sediment supply is predicted by the subduction channel model of subduction zones (Shreve and Cloos, 1986; Cloos and Shreve, 1988b; Clift and Vannucchi, 2004). Subduction accretion is favoured where the convergence rate is >7.6 cm per year and sedimentary thickness at the trench is >1 km (Clift and Vannucchi, 2004). Exceeding the capacity of the inlet – the furthest extent of the overriding plate where underthrusting of the downgoing slab occurs – results in off-scraping of the sediment pile and accretion on the upper plate. Sediment supply is defined as the volume of sediment entering the trench multiplied by the convergence rate at the subduction zone, compensated for compaction due to deformation within the trench (Cloos and Shreve, 1988b). The thickness of sediment in the trench is strongly influenced by the rate of convergence, as the majority of sediment deposition on the oceanic plate occurs within the trench and therefore the longer a given section of the incoming plate spends in the trench prior to being subducted, the greater the thickness of sediment it will carry (Clift and Vannucchi, 2004).

THE SUBDUCTION ZONE PLATE BOUNDARY INTERFACE

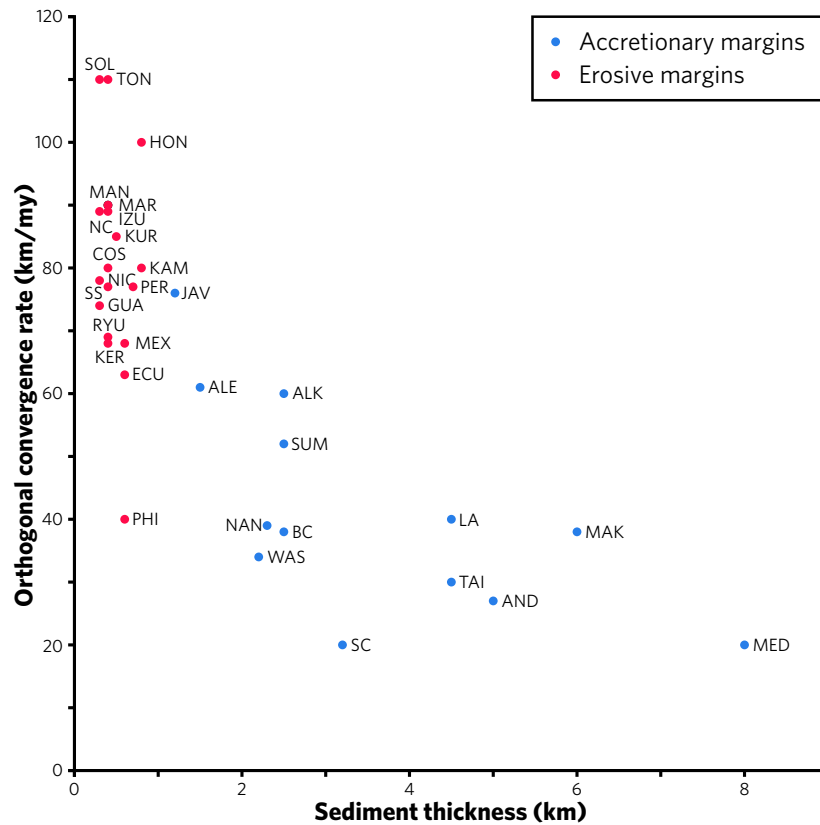


FIG. 3.5. Graph of sediment thickness at the trench vs plate convergence rate (modified from Clift and Vannucchi, 2004). NC, North Chile; PER, Peru; ECU, Ecuador-Columbia; COS, Costa Rica; NIC, Nicaragua; GUA, Guatemala; MEX, Mexico; KUR, Kurile; KAM, Kamchatka; HON, NE Japan; MAR, Mariana; IZU, Izu-Bonin; RYU, Ryukyo; MAN, South Luzon; PHI, Philippine; TON, Tonga; KER, Kermadec; SOL, Solomons; SS, South Sandwich; SC, South Chile; LA, Lesser Antilles; WAS, Oregon-Washington; BC, British Columbia; ALE, Aleutians; ALK, Alaska; TAI, Taiwan-north Luzon; SUM, Sumatra; JAV, Java; AND, Burma-Andaman; MAK, Makran; MED, Aegean.

As convergence rate does not vary significantly over short distances along an active margin, both subduction erosion and subduction accretion can occur concurrently on the same margin because of variations in the sediment thickness at the trench. Accretionary subduction zones accreted more material when the convergence rate is low, however, the rate of subduction erosion at erosive subduction zones is not correlated with

convergence rates (Clift and Vannucchi, 2004). The rate at which material is subducted is not systematically higher at erosive subduction zones than it is at accretionary subduction zones (Clift and Vannucchi, 2004), suggesting that subduction channels may have a defined capacity and accretion occurs when the sediment supply is in excess of this capacity, while upper-plate erosion occurs when this capacity is not met by incoming-plate sources. The rate of tectonic erosion is controlled by the subduction of major bathymetric highs on the oceanic plate, such as seamounts and aseismic ridges. Smaller examples of seafloor roughness, like small seamounts or bend-faults, do not provide a sufficient perturbation to noticeably alter rates of subduction erosion (Clift and Vannucchi, 2004).

3.2.4. Implications of accretionary and erosive behaviour for forearc morphology

The processes of subduction accretion and erosion have a primary influence on the morphology and internal structure of the entire forearc region. Forearcs typically operate as wedges at their critical taper (Dahlen, 1990; Clift and Vannucchi, 2004). Critical taper refers to the angle between the slope and the décollement at equilibrium where the wedge overrides the lower surface. This angle depends on the friction at the base of the wedge and the internal friction and cohesion of the wedge materials (Davies, 1983). Within natural systems, the critical angle is considered to be the sum of the forearc slope angle and the angle of subduction. As such, the angle of the forearc slope is strongly controlled by the friction on the décollement (Dahlen, 1990).

Clift and Vannucchi (2004) established that accretionary margins typically have forearc slopes of $<3^\circ$, while erosive margins have slopes of $>2.7^\circ$, and that convergence rate is a major control on slope angles. Slope and taper angles in accretionary subduction zones are inversely correlated to the thickness of trench-fill sediment (Clift and Vannucchi, 2004). This is because sediment is capable of storing and releasing more fluid during the early stages of subduction. This fluid drives up fluid pressure at the base of the forearc wedge and drives down basal friction. High fluid pressures promote shallow angles as they reduce the stress that can accumulate to promote compression in the wedge (Saffer and

THE SUBDUCTION ZONE PLATE BOUNDARY INTERFACE

Bekins, 2002). Slope and taper angles in erosive subduction zones are higher than those of accretionary subduction zones, likely because the lithified – often crystalline – rocks that compose the forearc basement are stronger and more cohesive, and therefore capable of maintaining a steeper slope angle. The consistently low permeability of these rocks means that fluid pressures at the base of the forearc are universally high. High fluid pressures have been suggested by von Huene *et al.* (2004) to cause fracturing at the base of the forearc wedge which facilitates material removal. It is therefore the rate of convergence that most strongly controls basal friction in erosive subduction zones. Indeed, taper angles in erosive subduction zones appear weakly correlated with convergence rate, with the fastest subduction zones exhibiting the steepest slopes (Clift and Vannucchi, 2004).

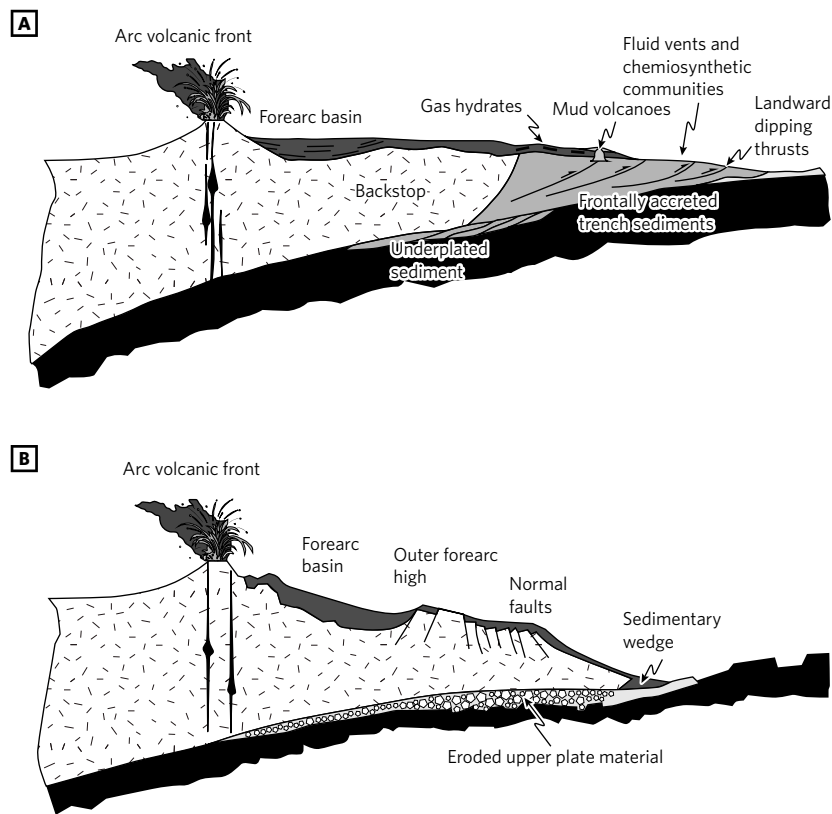


FIG. 3.6. Diagram showing cross sections of idealised accretionary and erosive margins showing common features in the forearcs of each margin type (from Clift and Vannucchi, 2004). **A:** Cross section of accretionary margin. **B:** Cross section of erosive margin.

Normal faults are common in the forearcs of erosive subduction zones due to collapse-related extension, with density of faulting increasing trench-ward. Because of this, seismic velocity decreases trench-ward (von Huene *et al.*, 2004). Faulting and disruption of the upper plate produce a gradational contact between the frontal prism and its backstop. Fluid derived from the plate interface has been observed to vent along these normal faults (e.g. Hensen *et al.*, 2004). At long-lived erosive margins punctuated by rapid erosive intervals, the entire thickness of forearc basement near the trench may be removed, leaving only the overlying terrigenous slope sediments as a “depositionary forearc” (Vannucchi *et al.*, 2016).

While these structures are typical of accretionary and erosive margins, they are not indicative of margin type. Due to the high degree of complexity and variability between subduction margins worldwide, the morphology of an active margin alone cannot be used to distinguish between an erosive and an accretionary subduction zone (Scherwath *et al.*, 2010). Similarly, stress states of compression or extension are not reliable indicators of accretion or erosion as accretionary forearcs may either grow by internal faulting or collapse due to over-steepening by underplating (Sutherland *et al.*, 2009). Finally, as margin type can change with time, margin structures and morphology may not reflect current margin behaviour (Clift and Vannucchi, 2004).

3.3. SLIP ON THE PLATE BOUNDARY

3.3.1. The Seismogenic Zone

Subduction zones are the dominant setting of the Earth’s major earthquakes, accounting for over 80% of earthquakes larger than magnitude 8.0 (Kopp, 2013). However, earthquakes do not occur uniformly along the subduction zone plate interface. Instead, the plate interface is segmented along-dip into zones based on the dominant slip behaviour. The shallow portion of the subduction zone, previously thought to deform by purely stable aseismic creep (Hyndman *et al.*, 1997) is now recognised to host a complex variety of slip behaviours, including stable slip, slow transient slip and tremors, and mega-thrust rupture to the trench. The “seismogenic zone”, occurring between depths of ~10 km and ~40 km of

THE SUBDUCTION ZONE PLATE BOUNDARY INTERFACE

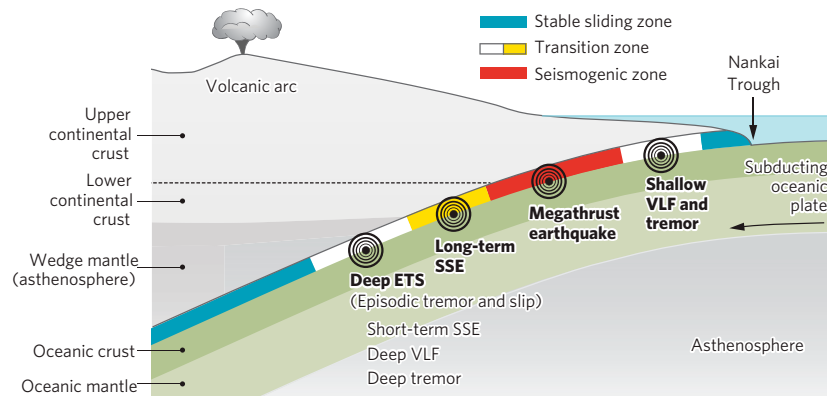


FIG. 3.7. Depths of different types of slip activity within the upper ~50 km of a subduction zone, showing that transient slip activity is not restricted to the “seismogenic zone” but that this zone hosts megathrust earthquakes (from Obara and Kato, 2016).

the subduction zone (Hyndman *et al.*, 1997), is characterised as a mostly locked zone which infrequently and unpredictably (Kagan, 1997) deforms by frictional dynamic slip producing mega-thrust earthquakes. The down-dip limit of the seismogenic zone transitions through a conditionally-stable, semi-frictional phase into a zone which hosts transient slow slip events with durations on the order of months (Angiboust *et al.*, 2015; Gao and Wang, 2017). In some subduction zones (e.g. Nankai and Mexico), a deeper zone exists which is characterised by episodic tremor and transient slow slip events with durations on the order of weeks. Below this, at depths typically >40 km, the subduction plate interface returns to stable sliding as the subducting slab moves through the mantle, and pressure and temperature conditions promote ductile flow in response to stress rather than brittle fracture (Gao and Wang, 2017). Even at this depth, the subduction zone plate interface is not aseismic and intermediate (50 – 300 km depth [Prieto *et al.*, 2013]) and deep (300 – 800 km depth [Hobbs and Ord, 1988]) earthquakes have been observed to occur, triggered either by dehydration embrittlement (see Jung *et al.*, 2004) or thermal runaway (see Prieto *et al.*, 2013; Thielmann *et al.*, 2015). Transient slip activity – including traditional earthquakes – are therefore not restricted to the “seismogenic zone” between ~10 – 40 km depth

and occur non-uniformly at a wide range of depths as a result of a variety of different slip mechanisms (Melgar *et al.*, 2016).

The marked occurrence of mega-thrust earthquakes at depths of 5 – 15 km, marking the up-dip limit of the “seismogenic zone”, has been traditionally associated with the temperature-dependant dehydration of clay minerals from smectite into illite around 100 – 150°C (Hyndman *et al.*, 1997; Vannucchi *et al.*, 2012). This mineral reaction is suggested to result in a transition from velocity-strengthening behaviour which prevents runaway slip and velocity-weakening behaviour, which promotes continuation of the rupture (the terms “velocity strengthening” and velocity weakening” are described in Chapter 3.3.3.2) (Hyndman *et al.*, 1997). However, experimental studies of clay-rich gouges show that illite proportion does not significantly affect frictional strength or induce velocity-weakening behaviour (Saffer and Marone, 2003; Ikari *et al.*, 2009; Saffer *et al.*, 2012). Indeed, Tembe *et al.* (2010) showed that increased illite proportion can accentuate the velocity-strengthening nature of the gouge. Alternatively, Collettini *et al.* (2009) proposed that the development of a shear fabric may be responsible for the change to unstable slip in subduction zones, while Ikari *et al.* (2007) and (Moore *et al.*, 2007 cited in Saffer *et al.*, 2012) suggested that lithification of the subducting plate sediments by silica cementation, consolidation, and the development of a fabric may also control this behaviour. However, experiments by Saffer *et al.* (2012) show that neither lithification nor the development of a fabric results in a change in frictional behaviour, and they propose that thermally activated processes such as pressure solution, precipitation of quartz and calcite veins, and localisation of slip into discrete plains may promote the velocity-weakening behaviour that is a prerequisite for seismic slip.

As occurred most notably during the 2011 Tōhoku-Oki earthquake in Japan, seismic rupture may propagate all the way up to the trench – previously thought unfeasible due to the plate interface at that depth consisting of unconsolidated muds – where it presents a significant tsunami hazard. During the Tōhoku-Oki earthquake, up to 50 metres of horizontal displacement occurred at the seafloor in the trench, inducing the devastating tsunami (Kodaira *et al.*, 2012). Rupture to the trench occurs at significantly

lower velocities than rupture at deeper levels, producing significantly lower frequency energy emissions that do not result in significant shaking (Melgar *et al.*, 2016). Slip solely within the traditional “seismogenic zone” produces strong shaking but does not trigger tsunamis (such as the 2015 Iquique earthquake in Chile [Hayes *et al.*, 2014; Melgar *et al.*, 2016]). Conversely, slip solely in the shallow portion may trigger a tsunami with little surface shaking (Lay *et al.*, 2012). However, earthquakes which rupture both portions of the plate interface (e.g. Tōhoku-Oki or the 2015 Illapel earthquake in Chile) present the greatest hazard as both phenomena are produced (Melgar *et al.*, 2016).

Slip in subduction zones is also not uniform along-strike and different segments move separately. Earthquakes nucleate at locked patches along the subduction zone plate interface — termed “asperities” (Byerlee and Brace, 1968 cited in Kopp, 2013; Cloos, 1992) — and propagate outwards until they terminate in a barrier which experiences no slip (Das and Watts, 2009). Asperities are typically thought to represent physical heterogeneities and high-relief features on the subducting slab — such as subducted seamounts (Abercrombie *et al.*, 2001) — which physically lock against the overriding plate until stresses on the plate interface exceed the high strength of the feature resulting in catastrophic failure (Cloos, 1992). However, seamounts may also act as barriers to seismic propagation (Bilek *et al.*, 2003), promoting the segmentation of slip along the plate interface and opposing the generation of large earthquakes (Sparkes *et al.*, 2010; Kopp, 2013). Asperities may also occur on smooth, well-sedimented plate interfaces, in which case the asperities are homogeneously distributed and are therefore unlikely to represent subducting plate morphology. Smooth, well-sedimented plate interfaces promote strong coupling between the two plates with few barriers to rupture propagation and therefore represent favourable conditions for large earthquakes (Kopp, 2013). Once ruptured, these asperities may lock again and accumulate stresses for the next earthquake (Cloos, 1992).

The amount of slip can vary across the rupture area, with ruptured asperities experiencing the greatest slip (Moreno *et al.*, 2012). The presence of these asperities and barrier segments

the subduction interface surface into regions that typically slip together. Earthquake events may rupture multiple segments and therefore areas that act as barriers to one earthquake may be overcome in a different earthquake. Rupturing across multiple segments of a subduction zone leads to a greater rupture area and therefore a greater energy release. The magnitude of the earthquake is dependant on the rupture area, as described in Equation 3.1 (Wells and Coppersmith, 1994). Some segments exhibit more seismic activity than others, with parts of the plate interface that are subducting aseismic ridges and plateaus experiencing less seismicity and therefore representing seismic gaps (Kellecher and McCann, 1976; Kopp, 2013).

$$M_o = \mu AD$$

M_o = Seismic moment

μ = Shear modulus

A = Rupture area

D = Displacement

EQUATION 3.1. Equation that relates rupture area to seismic energy release.

3.3.2. Spectrum of slip

Slip activity in subduction zones may be categorised into either earthquakes produced by dynamic frictional slip at high velocities, stable aseismic creep undergoing viscous deformation, or slow, transient slip that does not produce traditional earthquakes but which emits low and very low frequency acoustic signals and may be detected by geodetic monitoring (Ide *et al.*, 2007).

3.3.2.1. Traditional EQs

Mega-thrust earthquakes are the most obvious manifestation of slip along the plate boundary as they may be felt at the surface, cause catastrophic damage, and generate tsunamis. These earthquakes primarily occur within the seismogenic zone and represent high velocity dynamic/unstable slip (Wang *et al.*, 2012). Ruptures of mega-thrust earthquakes nucleate at asperities (Lay *et al.*, 1982; Cloos, 1992) and the energy they release is determined by their rupture area (Equation 3.1). These earthquakes occur as

THE SUBDUCTION ZONE PLATE BOUNDARY INTERFACE

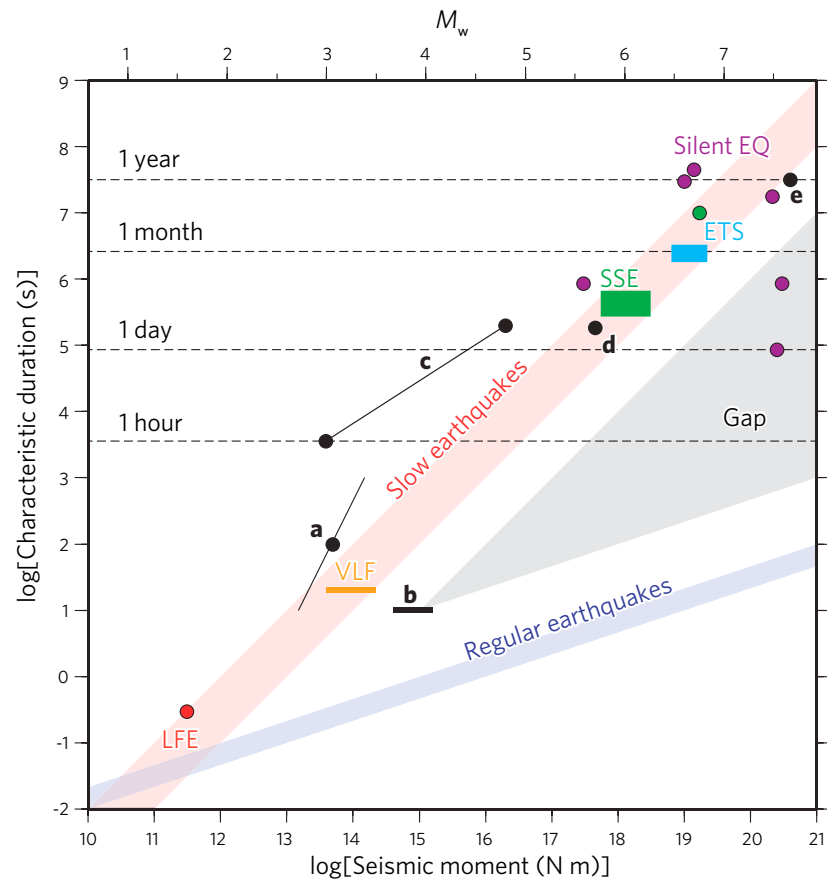


FIG. 3.8. Scaling laws showing the relationship between seismic moment and duration for regular earthquakes and slow earthquakes (from Ide *et al.*, 2007). This shows the scaling relationship between low and very low frequency earthquakes (LFE and VLF), slow slip events (SSE), episodic tremor and slip (ETS), and silent earthquakes.

shear fractures, likely supported by high fluid pressures which reduce the effective stress on the plate interface (Scholz, 1998).

3.3.2.2. Slow earthquakes

Seismic activity is not limited to traditional earthquakes that are typically destructive and cause very high energy release over a very short time. In addition to these, a category of slowly slipping ruptures, collectively termed “slow earthquakes” (Ide *et al.*, 2007) have been discovered since the installation of high-resolution GPS and seismic monitoring arrays in the 1990s (such as GEONET [Sagiya, 2004] and Hi-Net [Okada *et al.*, 2004] in Japan). These

phenomena have been shown to exist on a unified continuum of slip duration and energy release that is separate from the scaling relationship for regular earthquakes (Fig. 3.8) (Ide *et al.*, 2007). Events of this class have been termed “deep episodic tremor” (Obara, 2002), “low-frequency earthquakes” (1 – 8 Hz) (Katsumata and Kamaya, 2003), “very-low-frequency earthquakes” (0.02 – 0.05 Hz) (Ito *et al.*, 2007), “slow slip events” (Hirose and Obara, 2005), “silent earthquakes” (Kawasaki *et al.*, 1995, 2001; Ozawa *et al.*, 2002; Kostoglodov *et al.*, 2003), “episodic tremor and slip” (Obara and Kato, 2016), and “aseismic slip transients” (Skarbak *et al.*, 2012). While these terms refer to different slip durations, magnitudes and characters, they are all characterised by their transient nature, long event durations (minutes to years), slip distances ranging from millimetres to decimetres, and low energy release per unit of time. Slow earthquakes also typically reoccur at intervals from months to years, which is much shorter than megathrust earthquakes (Ide *et al.*, 2007). This slow slip activity has been documented along the Nankai, Cascadia, Hikurangi, Middle America, Ecuador, and Ryuko subduction zones and often different types of slow slip occur within the same portion of the

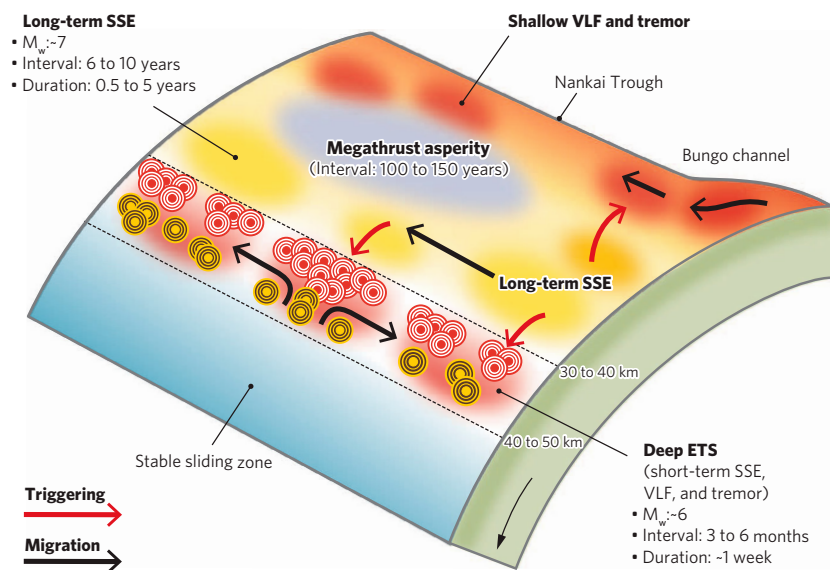


FIG. 3.9. Schematic diagram of the plate boundary surface showing the heterogeneous distribution of slip and the relationships between slipping packages (from Obara and Kato, 2016).

subduction zone (Ide *et al.*, 2007; Saffer and Wallace, 2015; Obara and Kato, 2016). Slow earthquakes have been observed to occur both shallower and deeper than the seismogenic zone and at depths previously thought to be dominated by stable aseismic slip (Obara and Kato, 2016).

Slow earthquakes are a form of fault slip that is intermediate between the fast rupture of traditional earthquakes and aseismic creep characterised by stable sliding (Obara and Kato, 2016). However, there is a gap between the scaling series (Fig. 3.8) of slow earthquakes and traditional earthquakes recognised by Ide *et al.* (2007). They proposed that this gap exists because these two types of seismic activity represent fundamentally different modes of slip propagation along the plate boundary, and that events which exist within this gap exhibit mixed-mode slip. Slow slip earthquakes have been observed to precede large megathrust earthquakes such as the Tohoku-Oki earthquake in 2011 (Obara and Kato, 2016) and the 2014 Iquique earthquake in northern Chile (Ruiz *et al.*, 2014), suggesting that slow earthquakes have the potential to sufficiently increase the stresses on megathrust asperities to prime the subduction interface for a mega-thrust rupture (Obara and Kato, 2016). Shallow slow earthquakes in the Boso region of the Nankai subduction zone have also been observed to trigger a swarm of small earthquakes at greater depths within the subduction zone (Obara and Kato, 2016).

Despite the underlying mechanisms responsible for slow earthquakes remaining unknown (Saffer and Wallace, 2015), they are thought to occur by the rupture of small asperities or locked regions, similar to traditional earthquakes, that produces low and very low frequency acoustic emissions detectable as low and very low frequency earthquakes (Ide *et al.*, 2007). These asperities interact as rupture at one locked patch transfers stress to its neighbouring patch, potentially inducing slip at that location (Obara and Kato, 2016). Slow earthquakes have been shown to be highly sensitive to small external changes in the stress field — including tidal forces (Rubinstein *et al.*, 2008) — suggesting these asperities are held dormant very close to their critical stress and that the subduction zone fault is therefore very weak at those locations (Obara and Kato, 2016).

Slow earthquakes have been observed not be restricted to any temperature window below $\sim 450^{\circ}\text{C}$, with the shallowest slow earthquakes observed to occur at $\sim 12^{\circ}\text{C}$ in Costa Rica (Saffer and Wallace, 2015). These shallow slow earthquakes are common close to – or even up to – the trench in regions previously thought to be dominated by stable sliding. Transitional frictional behaviour is interpreted to occur in this zone due to regions of fluid overpressure leading to low effective stress (Gao and Wang, 2017) and may also be promoted by the subduction of rough seafloor leading to a geometrically and compositionally heterogeneous subduction channel, causing a heterogeneous stress field which favours steady – episodic creep and small – moderate sized earthquakes (Saffer and Wallace, 2015).

3.3.3. The effect of different materials on seismic and aseismic slip in subduction zones

While the precise mechanisms promoting stable aseismic sliding, slow transient slip, and traditional earthquakes are not fully understood, comparative observations of highly seismic and less seismic subduction zones, along with frictional experiments and numerical modelling of the plate interface fault, allow the broad factors affecting seismicity to be determined (Ide *et al.*, 2007).

3.3.3.1. Sediment volume

Scholl *et al.* (2015) demonstrate that the subduction zones which host the largest earthquakes are thickly-sedimented, implying that smooth faults promote the greatest seismicity. Indeed, $\sim 75\%$ of magnitude >8.0 earthquakes and 100% of magnitude >9.1 earthquakes occur at thickly-sedimented subduction zones (Fig. 3.10). Where large earthquakes did occur on thinly-sedimented subduction zones, they occurred at locations where subduction erosion had contributed high volumes of debris which thickened the subduction channel and smoothed the plate interface fault. Conversely, rough, heterogeneous plate interfaces favour rupture termination and as such promote aseismic creep and generate smaller earthquakes (Skarbek *et al.*, 2012; Scholl *et al.*, 2015).

THE SUBDUCTION ZONE PLATE BOUNDARY INTERFACE

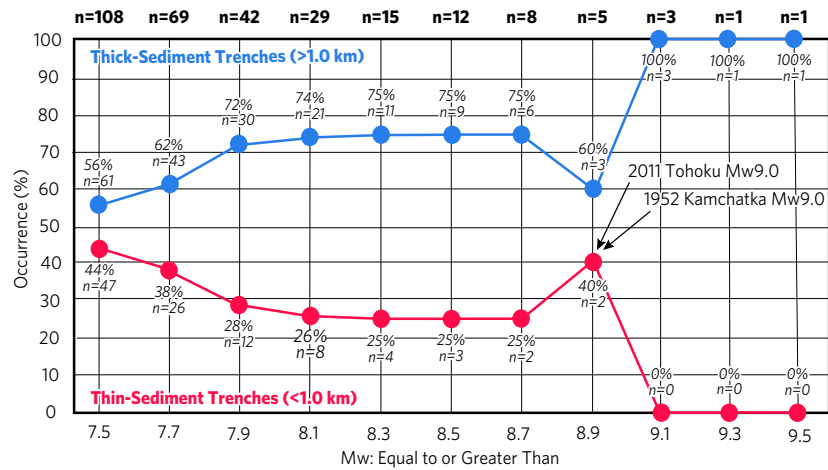


FIG. 3.10. Graph showing the relative occurrence of megathrust earthquakes (greater than Mw = 7.5) at thickly and thinly sedimented trenches, with values corrected for the greater occurrence of earthquakes at thickly sedimented trenches (modified from Scholl *et al.*, 2015).

3.3.3.2. Velocity-dependance

The coefficient of friction – which determines the energy required to initiate or maintain sliding – is often dependant on the velocity at which it is measured. The rate dependence of friction in geological materials is a fundamental control on the slip behaviour within a fault. Velocity-strengthening materials exhibit an increased coefficient of friction with higher velocities, meaning that with increased velocity, more strain energy is required to sustain the slippage. This acts a self-limiting factor which prevents the run-away slip seen in a seismic rupture. In contrast, velocity-weakening materials feature a reduced coefficient of friction when deformed at progressively higher velocities, potentially leading to acceleration of slip and seismic behaviour (Chen *et al.*, 2017). It is therefore frictional velocity dependance which controls slip behaviour, not the strength of the fault *in situ* (Chen *et al.*, 2017). The frictional properties of a material, including velocity dependence, varies with changes in the temperature, pressure, and fluid content (Chen *et al.*, 2017). While the application of this “rate-and-state friction” theory to slip on faults effectively explains sliding behaviour, it does not consider the underlying physical mechanisms by which this slip occurs – such as granular and cataclastic

flow, cracking and brittle micro-deformation, and crystal-plastic deformation – and so cannot be directly linked to field and structural analysis (Chen *et al.*, 2017).

The magnitude of velocity-strengthening or velocity-weakening behaviour is quantified by the property $(a - b)$, where “a” represents the difference between the stable coefficient of friction before velocity is experimentally increased and the maximum coefficient of friction achieved during the velocity stepping before the coefficient of friction decays to stability, and “b” represents the magnitude of this decay from the initial high friction behaviour during velocity stepping to the stable coefficient of friction at the new velocity (Fig. 3.11) (Woo *et al.*, 2015; Chen *et al.*, 2017). Therefore, positive values of $(a - b)$ indicate velocity-weakening behaviour and negative values indicate velocity-strengthening behaviour. The $(a - b)$ value also varies with velocity, with different velocity dependence regimes existing at different velocities (Shimamoto 1986). Typically, very low and high velocities feature high values of $(a - b)$ – meaning velocity strengthening behaviour – while moderate velocities feature lower values of $(a - b)$. However, very high velocities are typically accompanied by significant frictional heating which acts to weaken the slip surface (Chen *et al.*, 2017). As demonstrated by Skarbek *et al.* (2012), in a

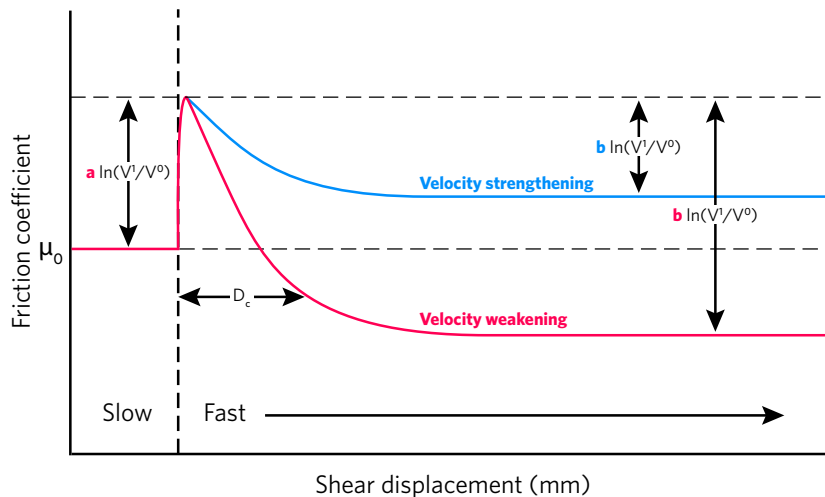


FIG. 3.11. Diagram demonstrating the principle of velocity weakening and velocity strengthening behaviour and deriving the property of $(a - b)$ (modified from Woo *et al.*, 2015 and Chen *et al.*, 2017).

heterogeneous, poly-rheological fault zone, bulk slip behaviour is determined by the dominant component, and velocity-weakening behaviour may still be exhibited even when the fault zone contains a significant fraction of velocity-strengthening material. Due to this complexity of velocity-dependant frictional properties and a lack of understanding of the underlying physical mechanism responsible for slip, experimental analysis of the $(a - b)$ value of fault materials offers only limited reliability for predicting slip behaviour (Chen *et al.*, 2017).

Despite the long-held association of illite with velocity-weakening behaviour, numerous studies (e.g. Saffer and Marone, 2003; Ikari *et al.*, 2009; Tembe *et al.*, 2010; Saffer *et al.*, 2012) have shown that both smectite and illite typically exhibit velocity-strengthening behaviour under the conditions expected within subduction zones. Quartz and calcite, however, have both been shown to exhibit velocity-weakening behaviour (e.g. Blanpied *et al.*, 1995; Saffer *et al.*, 2012) with chert-rich layers towards the base of the Ocean Plate Stratigraphy sequence (see Isozaki *et al.*, 1990) hypothesised to localise shear at the trench and decouple the down-going slab from its sedimentary cover in the subduction channel (Hayashi and Tsutsumi, 2010). Gouges produced from plagioclase and pyroxene (i.e. basaltic composition) mixtures have also been shown to exhibit velocity-weakening behaviour under moderate – high pressure and temperature, hydrous conditions (He *et al.*, 2013). The presence of talc and serpentinite significantly reduce the coefficient of friction on a fault and typically promote velocity-strengthening behaviour (Moore and Lockner, 2011).

3.3.3.3. *Heterogeneity*

In addition to the frictional properties of individual lithologies, physical heterogeneity of the subduction channel also plays a key role in controlling seismic nucleation and propagation. In subduction channel mélanges, the ratio between rigid blocks and compliant matrix has been shown by Fagereng and Sibson (2010) to influence the propensity for seismic or aseismic behaviour. High block-to-matrix ratios lead to greater interaction – potentially including physical contact – between the rigid blocks and the reduced proportion of matrix prevents significant strain from being accommodated by flow between the blocks. This may

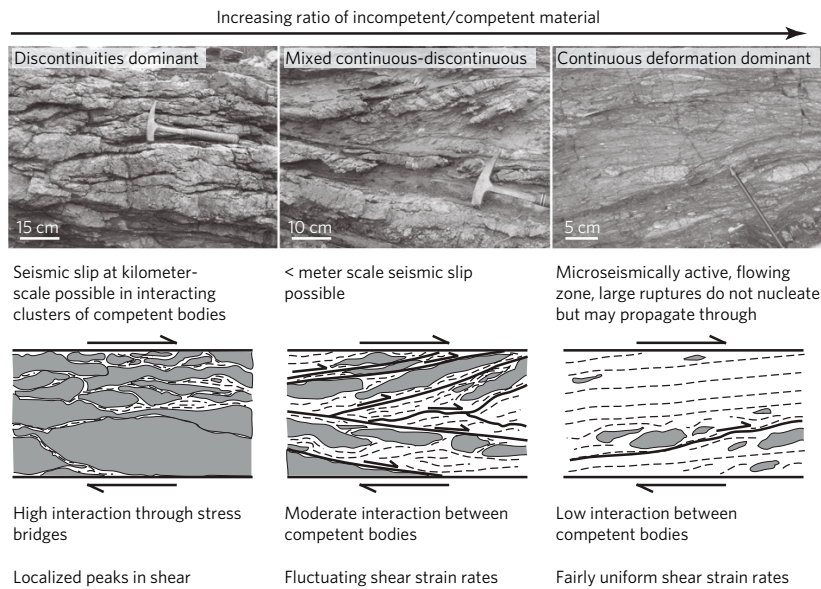


FIG. 3.12. Inferred relationship between block-to-matrix ratios and seismic style showing photographs and traces of end-member situations and an intermediate situation (from Fagereng and Sibson, 2010).

produce an asperity and create conditions favourable for the nucleation of seismic and microseismic slip, depending on the block size (Fagereng and Sibson, 2010). Conversely, low block-to-matrix ratios imply that the subduction channel is dominated by incompetent material which deforms by aseismic creep while the sparse blocks float freely within the matrix (Fagereng and Sibson, 2010). Despite high block-to-matrix ratios promoting the nucleation of seismic slip, highly heterogeneous plate interfaces produce highly complex stress fields which can impede the propagation of a rupture and lead to the earthquake's arrest. Similarly, the mixture of different frictional properties along a rupture surface also create conditions unfavourable for large earthquake (Skarbek *et al.*, 2012). Therefore high block-to-matrix ratios may promote greater numbers of small earthquakes.

3.4. SUMMARY OF SUBDUCTION ZONE BACKGROUND

The plate interface in subduction zones is a shear zone with a finite thickness, termed the "subduction channel". This subduction channel is a crustal-scale shear zone that modulates the tectonic processes of subduction accretion and subduction erosion by

promoting accretion if the incoming plate sediments are too thick, or tectonic erosion if subducting sediments are undersupplied (Clift and Vannucchi, 2004). Once subducted to sufficient depths, blocks suspended within the subduction channel may migrate against the shear direction due to their own buoyancy if their buoyant force exceeds the shear traction between the downgoing slab and the overriding plate. This can result in mixing of material of different metamorphic grade within the same mélange (e.g. Warren *et al.*, 2008).

The subduction channel also hosts slip along the plate interface to accommodate plate motion. This slip may produce an earthquake or it may produce stable aseismic creep or slow transient slip. While earthquakes are not entirely confined to depths between ~10 – 40 km as previously believed, the majority of high-velocity, mega-thrust earthquakes occur within the “seismogenic zone” (Hyndman *et al.*, 1997). The cause of this change in slip behaviour remains unknown. However, factors such as the sediment thickness within the subduction channel, the presence of velocity-weakening materials under favourable temperature, pressure, and velocity conditions, and high block-to-matrix ratios in subduction channel mélanges promote seismicity (e.g. Fagereng and Sibson, 2010; Scholl *et al.*, 2015).

Chapter 6 expands upon existing theories of subduction accretion (e.g. Clift and Vannucchi, 2004) to present a new setting where subduction accretion can occur. Chapters 7 and 8 address processes occurring within the subduction channel which control the nucleation of seismic slip, and Chapter 8 presents a fine-scale mechanism for subduction erosion of pre-deformed, highly heterogeneous upper plate.

CHAPTER 4. MÉLANGES

Definition and history

Mélanges are rock units consisting of blocks of one or more lithologies contained within a variable amount of “matrix”. The matrix can either have a sedimentological meaning — as in a sedimentary breccia — or it can be a mechanically weaker, finer-grained material, such as pelite or serpentinite, sheared to the point of surrounding the blocks. Blocks may be of a range of scales, but generally regularly exceed 10 centimetres in diameter and may reach hundreds of metres in length. Block-in-matrix rock units are typically considered a “mélange” if their exposed extent is at a scale mappable on a 1:25,000 or smaller scale map.

Mélanges are found throughout the world, and are typically associated with subduction convergent margins (Wakabayashi and Dilek; 2011). However, they have also been reported associated with extensional regimes (e.g. Cecca *et al.*, 1981), passive margins (e.g. Robertson and Pickett, 2000), continental and oceanic transform faults (e.g. Saleeby, 2011), and within orogens (e.g. Vollmer and Bosworth, 1984).

Mélanges that have a tectonic origin are of interest to workers as they are often “fossil” analogues to material found within large-scale fault zones active at present. In fact, large crustal-scale faults are not discrete planes or homogenous shear zones but complex, polyrheological features (Fagereng and Sibson, 2010). The structures and rheological relationships recorded in tectonic mélanges may inform as to the processes operating in these zones which are often too deep to be directly observed through drilling and too complex to be resolved through geophysical observations.

This section outlines in detail the meaning of the term “mélange” and provides historical context to the terms used in their study. Terms crucial to the study of mélanges and used liberally throughout this thesis are defined here. This section also provides the background to the later discussion of whether the Osa Mélange can be considered a mélange *sensu stricto* (Chapter 10.2).

4.1. HISTORY OF THE TERM

4.1.1. Coining the term and its early usages (1919 to 1950)

The term “mélange” was first coined by Edward Greenly in 1919 in his comprehensive survey of the geology of Anglesey, NW Wales (Wood, 2012), conducted with notable input from his wife, Annie Greenly (Williams, 2007). He coined this term to describe the broken, blocky nature of the Gwna Mélange, which had previously been recognised and described by Matley (1889; 1890 cited in Greenly, 1919) who termed it “crush breccia.” Greenly (1919) described the Gwna Mélange as consisting predominantly of “sigmoidal overlapping lenticles” of quartzite, limestone, pillow basalt and chert within a schistose matrix with a sheared texture (Fig. 4.1). Greenly’s (1919) discussion of the setting of mélange formation – published prior to the acceptance of plate tectonics – presaged the concept of subduction zones by suggesting mechanical, “autoclastic” breakup of previously stratified units during burial beneath a nappe. He defined this mélange as such:

“The essential characters of an autoclastic mélange may be said to be the general destruction of original junctions, whether igneous or sedimentary, especially of bedding, and the shearing-down of the more tractable material until it functions as schistose matrix in which the fragments of the more obdurate rocks float as isolated lenticles or phacoids.”

This was not the first published description of block-in-matrix rock units, as rocks exhibiting this fabric had previously been described in the Alps and termed “wildflysch” (Kaufmann, 1886 [German] cited by Festa, 2010). These were recognised to contain exotic blocks and interpreted to form by sedimentary sliding and later (Beck, 1912 [German] cited by Festa, 2010) as the result of tectonism ahead of an advancing nappe.

Prior to Greenly’s (1919) detailed application of the term “mélange” to describe the block-in-matrix texture of the Gwna Mélange, the term was used generically by workers to describe varied rock units consisting of multiple lithologies in complex field relationships (e.g. Goodchild, 1892; Callaway, 1905). After 1919, application of the term narrowed to generally refer to rock

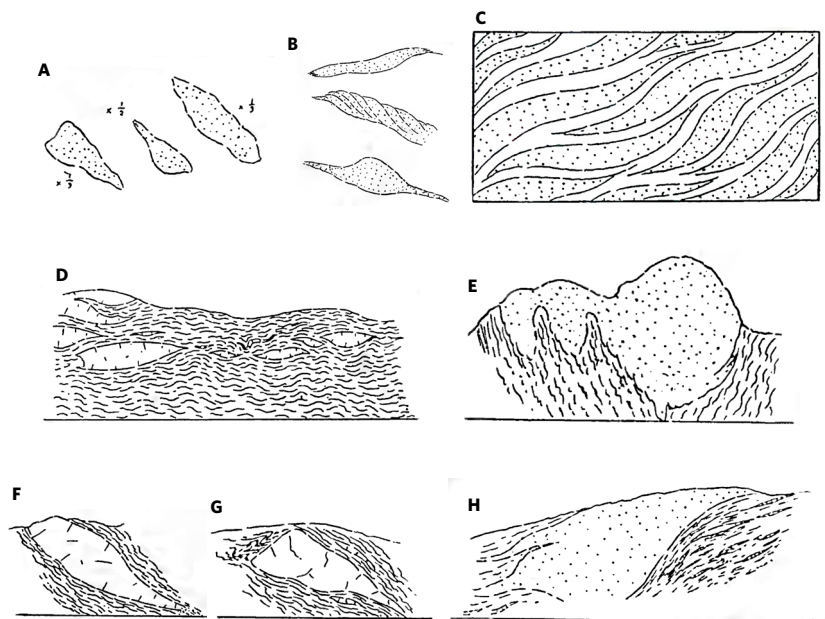


FIG. 4.1. Selection of Greenly's (1919) sketches of the block-in-matrix texture of the Gwna Mélange with his original descriptions included below. **A:** "Phacoids of grit in Gwna Mélange north of Glyn-afon." **B:** "Phacoids of grit, Aethwy region." **C:** "Diagram of Autoclastic Mélange." **D:** "Limestones in Gwna Green-schist ... Height about 15 feet". **E:** "Large quartzite in Gwna Mélange. (Several yards high.) 300 yards north-west of Porth Cadwaladr." **F & G:** "Limestones in Gwna Green-schist. About four feet and three feet thick." **H:** "Lenticular quartzite. Three and a half feet long. In Gwna Mélange, Llansadwrn."

units where one lithology is encased in another, including igneous bodies containing xenoliths (e.g. Taylor, 1934; Wilson, 1938; McMath, 1947).

4.1.2. Revival and early proliferation (1950 – 1970)

In 1950, Bailey and McCallien revived Greenly's definition of "mélange" when describing the rocks of Ankara, Turkey. Building upon the unpublished work of Oguz Erol who first recognised the "broken, block structure", they drew comparisons with Greenly's (1919) description of the Gwna Mélange and termed this rock unit the "Ankara Mélange" (Bailey and McCallien, 1950, 1954). They described this mélange as consisting of blocks of greywacke,

limestone, radiolarite, serpentinite and pillow basalt within a sheared matrix and ascribed the breakup and mixing to subsurface tectonic processes. Following the application of the term to the Coloured Mélange in Iran by Gansser (1955), use of the term “mélange” to describe block-in-matrix rock units became favoured (e.g. Naha, 1961; Bailey and McCallien, 1962) over other terms such as “crush breccia” (Reynolds, 1928), “chaos breccia” (Katz, 1968), or wildflysche (Eardley and White, 1947; Trechmann, 1948). This solidified the definition of *mélange* to apply to block-in-matrix rock units where the matrix is composed of a more compliant, solid material (e.g. pelite or serpentinite), typically mixed under low-grade metamorphic conditions.

Use of the term “*mélange*” proliferated during the 1960s with both the recognition of new block-in-matrix rock units and the reclassification of previously recognised rock units under the unified term. At this time, the term was used by workers to describe highly varied rock units bearing block-in-matrix textures irrespective of scale, mechanism of mixing, and tectonic setting (e.g. Naha, 1961; Ridd, 1964; Ernst, 1965; Kear and Waterhouse, 1967; Ward *et al.*, 1968). During this time, community attention began to focus on the Franciscan Complex in California, USA – especially among North American workers – as it was recognised to be a large *mélange* containing a great range of lithologies in confusing associations (e.g. Dott, 1965; Hsü 1965 cited in Hsü, 1968; Hsü 1966 cited in Hsü, 1968; Ernst and Seki, 1967). Extensive study of the chaotic complexes of *argille scagliose* in the Apennines of Italy – in light of the advancements made elsewhere in the world – also began at this time (e.g. Merla, 1951 [Italian] cited in Gallitelli, 1955; Merla, 1952 [Italian] cited in Bailey and McCallien, 1963; Gallitelli, 1955; Bailey and McCallien, 1963; Page, 1963; Abbate and Sagri, 1970). At this time, both tectonic and sedimentary processes were considered to have produced these Italian *mélanges* (e.g. Gallitelli, 1955; Ernst and Seki, 1967), and Horne (1969) proposed that a combination of processes (sedimentary mixing followed by tectonic shearing) produced the Dunnage Mélange of the Dildo Sequence in Newfoundland. Meanwhile, Shackleton (1954) reinterpreted the Gwna Mélange and found significant evidence that parts of this *mélange* were produced by sedimentary processes.

4.1.2.1. *Olistostromes*

Independent of the term “mélange”, Flores (1955) coined the term “olistostrome” to describe large-scale sedimentary deposits formed by “sliding” of a sediment mass. In his original definition, paraphrased by Raymond (1984):

“An olistostrome is a mappable sedimentary slide deposit, within a normal geological sequence, which is characterised by lithologically or petrographically heterogenous bodies of harder rock mixed and dispersed in a matrix of prevalent pelitic, heterogenous material.”

The definition of this term was later modified by Jacobacci (1965 [Italian] cited in Abbate *et al.*, 1970), Merla *et al.* (1964 [Italian] cited in Abbate *et al.*, 1970), and Abbate *et al.* (1970) to include all sedimentary slide deposits containing blocks of harder rock – termed “olistoliths” – within a matrix. Elter and Raggi (1965 [Italian] cited in Raymond, 1984) recognised that some olistoliths are sourced from within the same sedimentary basin as their surrounding matrix, while others are sourced from another sedimentary environment or the basement. They termed rock units consisting exclusively of the former “endolistostromes”, while rock units including the latter are termed “allolistostromes.” Recognising the similarity between olistostromes and mélanges, Rigo de Righi and Cortesini (1964) described the chaotic rock unit of the Taurus Mountains, in SE Turkey as both a mélange and an olistostrome. As it became clear that such chaotic rock units could be formed by both tectonic and sedimentary processes, Passerini (1965 [Italian] cited in Abbate *et al.*, 1970) was the first to define criteria for distinguishing between these two different processes – with vastly different geological implications – based on field data.

4.1.3. A stricter definition

In his highly influential paper, Hsü (1968) – conscious of the varied and inconsistent application of the term – attempted to formally define ‘mélange’ as:

MÉLANGES

“...Mappable bodies of deformed rocks characterized by the inclusion of tectonically mixed fragments or blocks, which may range up to several miles long, in a pervasively sheared, fine-grained, and commonly pelitic matrix. Each mélange includes both exotic and native blocks and a matrix.”

He further defined native blocks as “disrupted brittle layers which were once interbedded with the ductilely deformed matrix” and exotic blocks as “tectonic inclusions detached from some rock-stratigraphic units foreign to the main body of the mélange.” The inclusion of this requirement that mélanges possess “exotic” blocks initiated an as-yet not fully resolved controversy regarding the definition of the term “mélange.” Hsü’s (1968) definition was made to fit the Franciscan Mélange as described by Hsü (1965; 1966 cited in Hsü’s 1968) and the Gwna Mélange (Greenly, 1919) but excluded several rock units previously defined as ‘mélange’ on the basis of a sedimentary interpretation of origin, lack of exotic blocks, or insufficient scale. Chaotic rock units that lacked exotic blocks were instead termed “broken formations”. As an aid to future mélange workers, Hsü (1968) also defined five “rules for mélanges”:

1. “The Making of a Geologic Map of a Melange Terrane Cannot Be Based Upon a Presumption of Stratal Continuity”
2. “The Stratigraphy of a Melange Sequence Cannot Be Established on a Presumption of Normal Superposition.”
3. “The Assignment of a Time-Range of Deposition to all the Rocks in a Melange on the Basis of the Oldest and Youngest Fossils Found in Such a Melange Is Wrong.”
4. “The Contact Between a Rock-Stratigraphic Unit and a Subjacent or Superjacent Melange May Be a Depositional Contact or a Dislocation Contact.”
5. “The Rock-Stratigraphic Unit Overlying a Melange Can Be Autochthonous in One Place and Allochthonous Elsewhere.”

Despite Hsü’s (1968) assertion that tectonically-formed mélanges should be distinguishable from sedimentary olistostromes “on the basis of their deformational styles” as “Melanges resulted from the deformation of consolidated rocks under an overburden” while “Olistostromes ... resulted from the submarine

sliding of unconsolidated sediments”. This distinction proved difficult for workers in the field, especially where originally sedimentary units are later tectonised. As several rock units regarded as *mélanges* were interpreted as forming by sedimentary processes, and sedimentary origins had been proposed for both the Franciscan (Ernst, 1965) and the Gwna *mélanges* (Shackleton, 1954), many workers chose to ignore this requirement of Hsü’s (1968) definition. Additionally, some workers (e.g. James, 1972; 1973; 1975) continued to apply the term “*mélange*” to small rock units at the scale of individual beds consisting of lithologically and genetically similar blocks and matrix.

4.1.4. Proliferation and controversy (1970 – 1980)

Research into *mélanges* proliferated after Hsü’s (1968) paper popularised the concept (Raymond, 1984). However, Hsü’s (1968) stricter definition of the term “*mélange*” caused significant controversy as rock units previously termed *mélanges* were now excluded from the *sensu stricto* definition. In particular, the requirements that *mélanges* contain exotic blocks and have undergone break-up and mixing by tectonic processes caused the most debate. Even among workers who accepted Hsü’s (1968) definition, disagreement existed about how to determine whether blocks are exotic to the *mélange* and how to discern the processes of *mélange* formation (Raymond, 1984). Zhang and Jin, (1979) asserted the matrix lithology should define whether a chaotic rock unit is a *mélange* or an olistostrome, with rock units that have a serpentinite matrix being termed “*mélange*” while those with a pelitic matrix are termed “olistostromes”; assuming *a priori* that chaotic rock units consisting of sedimentary material are dismembered and mixed by sedimentary processes while those with a serpentinite matrix are mixed by tectonic processes. While they argue that the tectonic processes involved in dismembering and mixing a chaotic rock unit differ significantly between those with a serpentinite matrix and those with a pelitic matrix, this definition excludes most recognised *mélanges* and ignores the pelitic matrix *mélanges* interpreted to have formed by tectonic processes. Similarly, Gansser (1974) coined the modified term “ophiolitic

mélanges” to describe chaotic rock units consisting of a mixture of sedimentary and non-sedimentary ophiolitic materials.

Whether the term *mélange* should be applied to rock units interpreted to have been formed by sedimentary processes became a topic of significant debate, with some workers arguing that the difference in processes between sedimentary sliding and tectonic dismemberment and mixing justified different terms (e.g. Cowan, 1974), while others argued that the similarity in appearance between the products of these two processes made distinguishing between them difficult and the distinction unworkable (Berkland *et al.*, 1972; Raymond, 1975). While the requirement that *mélanges* be formed tectonically concurred with Greenly’s (1919) interpretation of Gwna *Mélange*, it did not account for subsequent reinterpretations by the Gwna *Mélange* as forming due to sedimentary processes (Shackleton, 1954; Maltman, 1975), therefore any definition which requires *mélanges* be formed by tectonic processes excludes the type locality of the term (Raymond, 1985). Both Hsü (1974) and Cowan (1978) abandoned their earlier stipulations that *mélanges* be formed by tectonic processes in favour of purely descriptive definitions.

The requirement that *mélanges* contain “exotic” blocks also proved divisive, with proponents (e.g. Berkand *et al.*, [1972], Raymond [1975, 1984]) arguing that the presence of exotic blocks is evidence of extensive mixing, whereas other workers (e.g. DeJong, 1974; Cowan, 1974; Beutner, 1975) argue that exotic blocks are difficult to identify, especially in the field, and that identification of exotic blocks is ultimately interpretive. They also argue that the process of incorporating exotic blocks is accidental and that not all parts of an exotic rock unit may contain them. It was also noted by Beutner (1975) that in Greenly’s (1919) original usage, he referred to both a “phyllite-and-grit *mélange*” which did not contain exotic blocks and an “autoclastic general *mélange*” that did contain exotic blocks. Disagreement also existed on the definition of “exotic” blocks, with Hsü’s (1968) definition being “tectonic inclusions detached from some rock-stratigraphic units foreign to the main body of the *mélange*” whereas Beutner (1975) narrowed their definition to blocks that are “far removed from the site where they underwent metamorphism” and not “time-equivalent” with their surrounding rock unit.

As the theory of plate tectonics became widely accepted, mélanges — which had previously been attributed to deposition or tectonism during the filling or uplift of eugeosyncinal basins — became recognised as a common component of fossil subduction zones and the product of oceanic trench processes (first by Ernst [1970] and later by Dickinson [1970], Moore [1970], Ernst [1971], Cowan [1974], Coleman [1975]). The interpretation that the Duck Creek mélange in the Hoh assemblage on the Olympic Peninsula, Washington USA, formed as part of a mud diapir (Rau and Grocock, 1974) expanded the debate surrounding the setting and processes of mélange formation, introducing the term “diapiric mélange” which was contrasted with “tectonic mélanges” and olistostromes as a major category of mélange (Lash, 1987).

4.1.5. The Penrose definition

In an attempt to resolve the discord regarding the definition of the term “mélange”, a Penrose conference was convened in 1978. While this conference did not reach a consensus on the definition — and could not even agree that mélanges consist of blocks in a matrix due to the recognition of a “block-on-block” texture in mélanges in Japan — but generally agreed that any definition should be descriptive, rather than genetic (Silver and Beutner, 1980). Based on the outcomes of these discussions, Silver and Beutner (1980) defined mélanges as such:

“Mélange’ is a general term describing a mappable (at 1:25,000 or smaller scale), internally fragmented and mixed rock body containing a variety of blocks, commonly in a pervasively deformed matrix.”

This definition deliberately and explicitly does not exclude any mixing process and does not imply any setting of genesis. Silver and Beutner (1980) also recognised many mélanges — including the Gwna, Franciscan, Dunnage and some Apennine mélanges — exhibit sedimentary histories before being later tectonised.

MÉLANGES

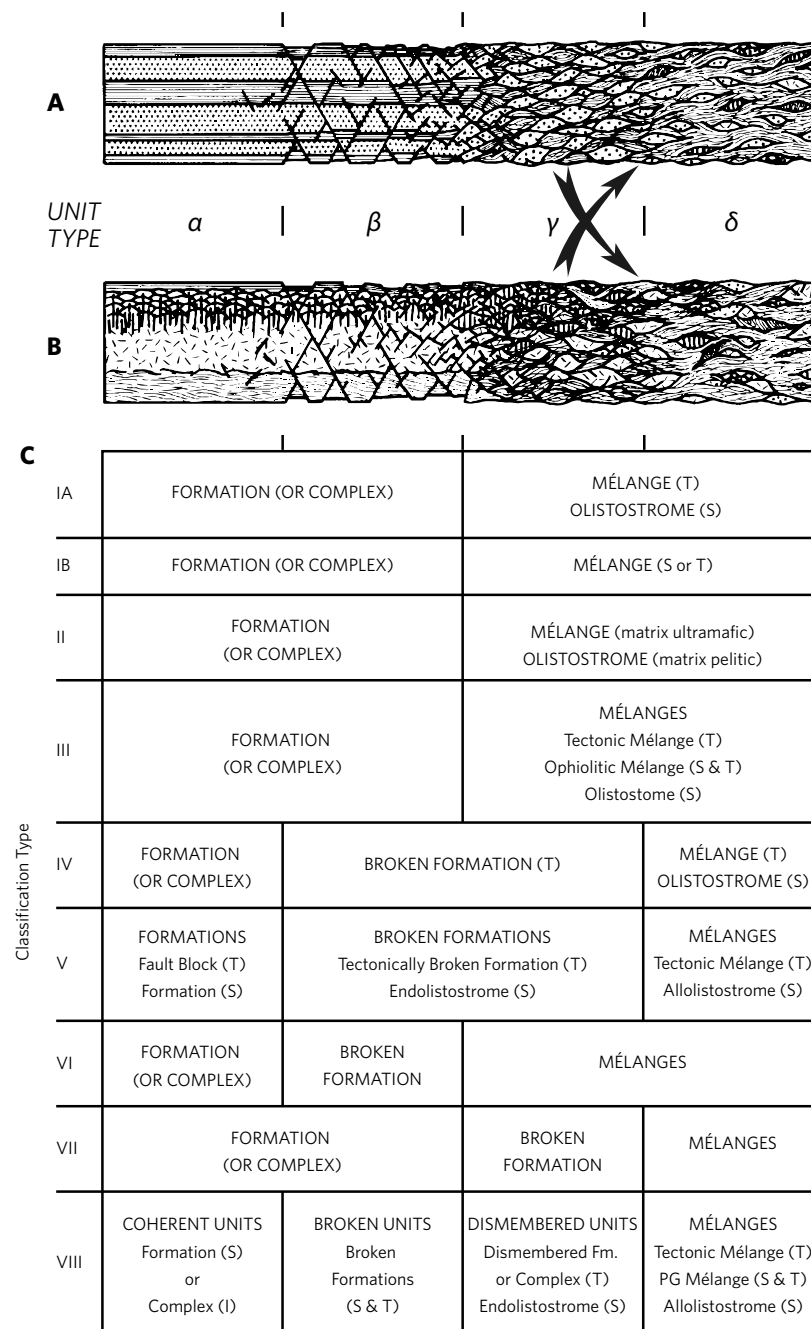


FIG. 4.2. Systems for classifying mélangé units from Raymond (1984). Unit types of α , β , γ , and δ indicate progressively greater degrees of stratal disruption, with α indicating undeformed bedded/layered units, β indicating faulted and disrupted bedded/layered rock units that retain stratal continuity, γ indicating block-in-matrix rock units that lack exotic blocks, and δ indicating block-in-matrix rock units with exotic blocks. **A**: Progressive disruption of a shale-and-sandstone protolith mélangé. (Caption continued on opposite page.)

4.1.6. Developing understanding (1980 – 2010)

In response to Silver and Beutner (1980) and the outcome of the 1978 Penrose conference, Raymond (1984) – in his GSA Special Paper – conceptualised the various contrasting and contradictory definitions and classification systems used by *mélange* workers as different ways of subdividing a continuum of deformation from intact formations to entirely dismembered and extensively mixed *mélanges* containing exotic blocks (reproduced as Fig. 4.2). Raymond (1984) and Raymond and Terranova (1984) agreed with Silver and Beutner’s (1980) definition that the term “*mélange*” be used in a descriptive manner based on observed criteria rather than interpretations of origin, but revived the requirement from Hsü (1968) that they contain exotic blocks. They defined *mélanges* as such:

*“A *mélange* is a body of rock mappable at a scale of 1:24,000 or smaller and characterised both by lack of internal continuity of contacts or strata and by the inclusion of fragments and blocks of all sizes, both exotic and native, embedded in a fragmented matrix of finer grained material.”*

While *mélanges* were closely associated with deformation in subduction zones, this was typically envisaged to occur by offscraping at the trench (e.g. Moore and Byrne, 1987). Cloos (1982) proposed that the extreme deformation observed in *mélanges* was produced as a result of flow within the rock unit at depth within a subduction zone, explaining the visual similarity between tectonic *mélanges* and olistostromes formed by surface flow. This idea was developed into the subduction channel hypothesis by Shreve and Cloos (1986) and Cloos and Shreve (1988a, b) (described in detail in Chapter 3.1) which provided the location within the subduction zone system where the extremely high shear deformation observed in many *mélanges* could be

FIG. 4.2 (CONTINUED) **B:** Progressive disruption of an ophiolitic protolith *mélange*. **C:** Graphical representation of alternative definitions of “*mélange*” and related terms used in literature (see Raymond [1984] for which workers advocated which classification system).

MÉLANGES

accomplished, and the return-flow mechanism provided an explanation of the presence of blueschist blocks within a lower-metamorphic-grade matrix. It also conceptualised mélanges as a form of intra-plate fault rock.

As the general processes of mélange formation were recognised to frequently involve a combination of sedimentary and tectonic processes, study of mélange formation advanced to consider in detail the mechanisms by which rock units can be dismembered and mixed and what the implications of these are for the tectonics of their region. Cowan (1985) described 10 processes that can give rise to the stratal disruption seen in mélanges:

- Excessive pinch-and-swell/boudinage of bedded rock units *in situ* facilitated by the ductility contrast between the layers.
- Layer-parallel extensional minor faulting of the competent layers of a bedded rock unit occurring *in situ*.
- Layer-parallel shearing accommodated by compliant layers which in turn disrupts more competent layers into ellipsoidal blocks.
- “Gravity driven downslope stretching” during mass wasting.
- “Heterogenous bulk deformation” where the matrix flows ductilely in response to shear and some blocks are formed and flattened while others retain their shape.
- Brecciation and cataclasis during shearing.
- Break-up or plucking of blocks from larger bodies.
- Emplacement of a disrupted, block-in-matrix rock unit by a mass wasting deposit mixed by the processes within the flow.
- Mud diapirism entraining fragments of other lithologies and mixing during flow.
- Segmentation of previously intact rock masses by a dense network of anastomosing sub-parallel faults, producing lensoidal phacoids, sometimes within a matrix of gouge or compliant rock.

The importance of high fluid pressures to many processes of mélange formation was recognised by Moore and Byrne (1987) and Talbot and von Brunn (1989) as it reduces the effective stress within the rock system, fluidises granular materials, and leads to hydrofracturing of competent materials.

Lindquist and Goodman (1994) were among the first workers to conduct analogue modelling experiments on mélanges based on the premise that the mélange blocks are stiffer and stronger

than their surrounding matrix and concluded higher proportions of blocks leads to decreased cohesion and reduced ability to accommodate strain without failure than mélanges with lower proportions of blocks. Fagereng and Sibson (2009) later linked block proportion to subduction zone seismicity. Various workers (e.g. Polat and Casey 1995; Kusky and Bradley 1999; Jongens *et al.*, 2003; Federico *et al.*, 2007; Ujiie *et al.*, 2007) began to consider the material properties of the various mélange constituents and how their rheologies at different temperatures and pressures control the deformation seen.

Additionally, Hibbard and Karig (1987) recognised that intense sheath folding, including parasitic folding along the fold limbs, can disrupt previously bedded rock units and produce highly complicated geological structures in the Shimanto belt in Japan. Needham (1987) recognised Reidel shear structures in mélanges of the Shimanto belt in Japan and the Southern Uplands of Scotland and proposed them as a mechanism of stratal disruption (later expanded upon in Needham [1995]). Kano *et al.* (1991) suggested that the sense of motion recorded by these Reidel structures was related to the plate convergence direction, which was later used by Onishi and Kimura (1995) to determine a change in oblique convergence direction in the western Pacific in the early Palaeogene. They thereby utilised the complicated systematics of the mélange fabric; recognising that it is not truly chaotic. Increased understanding of the processes of mélange formation led to comprehension of the structures within mélanges allowing for interpretations of the tectonic implications of these processes. Cowan (1990) estimated the magnitude of shear strain by analysing the rotation of rigid blocks, while Kimura and Mukai (1991) used deformed radiolarian microfossils to determine the magnitude of strain. Vannucchi and Bettelli (2002) and Bettelli and Vannucchi (2003) expanded upon the work of Hibbard and Karig (1987) and described how the extensive folding of interlayered competent and compliant rock units produces stratal breakup and highly complex block shapes that can be reconstructed using careful structural analysis.

Despite the earlier recognition of diapiric mélanges (Rau and Grocock, 1974; Lash, 1987), only limited study was conducted on

MÉLANGES

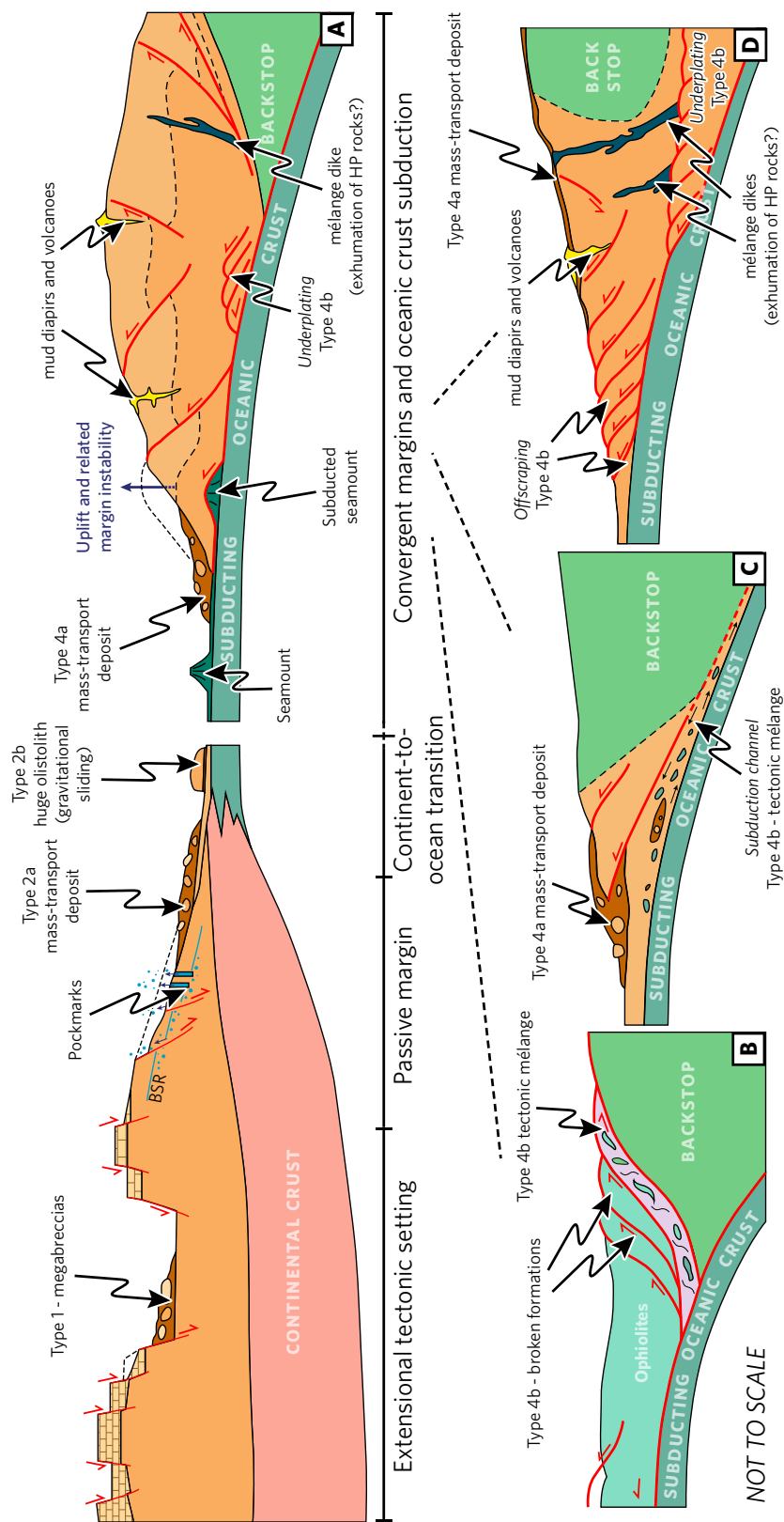
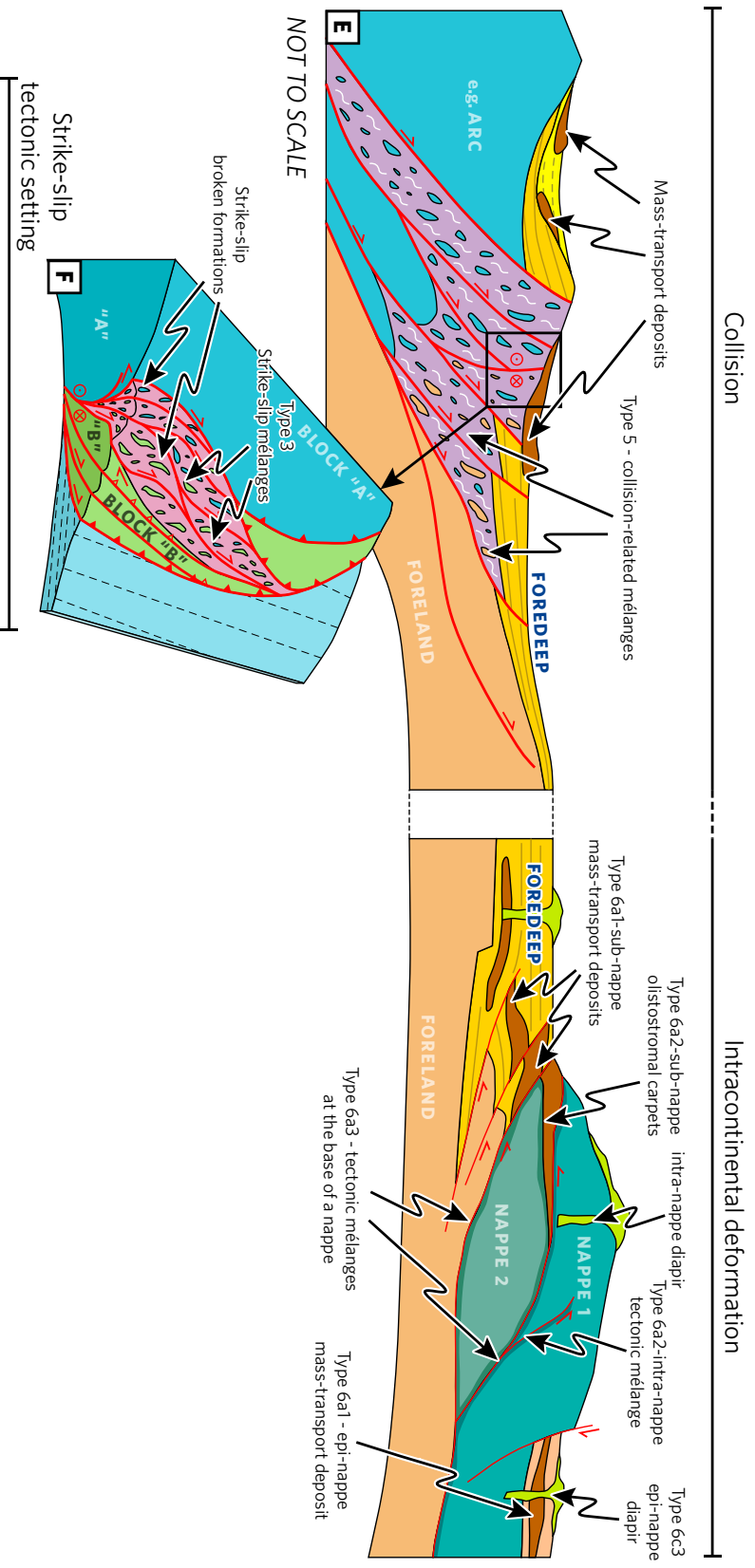


FIG. 4.3. (Caption overleaf.)



MÉLANGES

FIG. 4.3 (CONTINUED) Genetic classification system of mélanges formed in different tectonic settings (from Festa *et al.*, 2012) showing the diversity of mélange forming processes acting in a wide range of tectonic settings. **A:** “Type 1” mélanges formed in extensional settings, “Type 2a” mélanges formed in passive margin settings, “Type 2b” mélanges formed in ocean-continent transition zone settings, and “Type 4” mélanges formed in convergent margins. **B:** Mélanges formed during the obduction of ophiolites. **C:** Mélanges formed within the subduction channel. **D:** Mélanges formed in an accretionary wedge where the backstop is located high above underplated sediments. **E:** “Type 5” mélanges related to continental collision and “Type 6” mélanges formed by orogenic processes within continents. **F:** “Type 3” mélanges formed in strike-slip settings.

their processes of formation until recent years (e.g. Dela Pierre *et al.*, 2007; Festa *et al.*, 2010, 2012; Festa, 2011; Barber, 2013). Orange (1990) recognised that diapiric mélanges can be distinguished from mélanges formed by other processes based on the following criteria:

- Foliation that is radial in map view and which is most strongly developed at the margins of the mélange.
- Blocks that are strongly aligned at the margins and show poor alignment in the centre.
- Increasing size and angularity of blocks towards the centre of the mélange.

Festa (2011) added to these criteria that diapiric mélanges feature opposing shear sense on opposite mélange contacts.

4.1.7. Recent advances (2010 – recent)

The diversity of mélange-forming processes and settings now recognised was highlighted by Wakabayashi and Dilek (2011) in their GSA Special Paper, as mélanges formed at oceanic fracture zones, incipient subduction zones, ocean trenches, subduction accretionary complexes and post-collisional basins. In contrast to previous workers, Wakabayashi and Dilek (2011) assert that – in their view – attempts to develop a universally applicable classification scheme for mélanges would be inappropriate given the diversity of these rock units. Wakabayashi and Dilek (2011) defined mélanges as:

“...Mappable geological units consisting of blocks of different ages and origin, commonly embedded in an argillitic, sandy, or serpentinite matrix showing high stratal disruption and a chaotic internal structure.”

Festa *et al.* (2010, 2012) reviewed the development of the term “*mélange*” since the Penrose conference (Silver and Beutner, 1980) and collated recent and established hypotheses of *mélange* formation around the world and developed a general classification scheme for tectonic settings of *mélange* formation (Fig. 4.3). Barber (2013) reinterpreted the *mélanges* in the Banda and Sunda arcs in South East Asia – long regarded as tectonic or olistostromal *mélanges* – as forming and being emplaced due to diapiric processes, and advises other workers to avoid overlooking diapiric processes in their interpretations.

In their papers proposing melting of *mélange* rocks as the source for arc magmas, Marschall and Schumacher (2012) and Nielsen and Marschall (2017) describe a rock unit consisting of physically mixed hydrated mantle peridotite, subducted sedimentary material, altered oceanic crust, and slab dehydration-derived fluids. This mixed material is then inferred to rise through the mantle wedge as a diapir before melting (Nielsen and Marschall 2017; Liu *et al.*, 2017; Cruz-Uribe *et al.*, 2018). They propose that these components are mixed and homogenised in the solid state at mantle depths prior to melting. They apply the term “*mélange*” to what other workers refer to as the matrix of the *mélange* as they describe *mélanges* as containing “fragments of their precursor materials” rather than being a composite rock unit consisting of both blocks and matrix. They attribute this homogenisation to both chemical (both fluid-assisted and solid-state metamorphic diffusion) and mechanical (comminution and mixing of component particles) processes. Description of *mélanges* as “homogenised” is a departure from previous workers who had hitherto regarded heterogeneity as a component of their definition.

4.2. DIFFERENT DEFINITIONS PROPOSED

4.2.1. Block in Matrix

In Greenly's (1919) original definition, blocks are defined as "more obdurate rocks [which] float as isolated lenticles or phacoids" in a matrix of "more tractable material." This term is now used simply to describe fragments of one lithology entirely encased within another lithology (Medley and Zekkos, 2011). This texture is the defining characteristic of mélanges (Cowan, 1974), although rock units with a very small matrix proportion where the texture could be more accurately described as "block-on-block" are still classified as mélanges if they have undergone sufficient mixing (Silver and Beutner, 1980). Blocks are typically described as >64 mm in size (Raymond, 1984), but as mélanges typically contain fragments at a wide range of scales, if a rock unit contains abundant >64 mm fragments, typically all >20 mm are considered blocks *sensu lato*. A wide variety of tectonic, sedimentary, and diapiric processes have been proposed to describe the extensive breakup and mixing required to produce a block-in-matrix fabric (Lash, 1987; Festa *et al.*, 2012).

4.2.2. Mappable Scale

The requirement that a block-in-matrix rock unit be of "mappable scale" to be classified as a mélange is typically interpreted as meaning that the outcropping area of a mélange must be large enough to appear on a 1:25,000 or smaller scale map (Silver and Beutner 1980; Raymond, 1984). Block-in-matrix units occupying a single bed are typically excluded from the term "mélange".

The choice of 1:25,000 scale map in this definition has historical precedent but is arbitrary. Rock units which are mostly buried or eroded, or which are formed by mélange-forming processes at a smaller scale, may be excluded because their outcropping area is insufficiently large to satisfy the "mappable scale" requirement. Whether a unit is deemed "mappable" is also subjective, as practitioners may not agree on the minimum feature size of the map. It may also be difficult for the practitioner to assess if mapping at a scale other than 1:25,000.

The "mappable scale" requirement introduces the question of what a block-in-matrix rock unit too small to be termed "mélange"

should be called. Rock units with a sedimentary origin may be given the term “olistostrome” which does not have a minimum unit size requirement. However, rock units with a tectonic or ambiguous origin lack such an alternative term as the terms “tectosome” (Pini, 1999) and “bimrock” (Medley, 1994) have not been widely adopted. The term breccia or mega-breccia is sometimes used to describe such rock units, although it is typically assumed to refer to a sedimentary deposit unless prefixed as a “tectonic breccia”. As such, no widely used, unambiguously descriptive term exists to describe rock units with a block-in-matrix texture that do not, or may not, satisfy the definition of “mélange”.

4.2.3. Exotic Blocks

Exotic blocks are defined by Raymond (1984) as:

“...a fragment of rock greater than 64 mm in diameter that was not interbedded or intimately associated with the dominant formation(s) that give rise to the matrix ± blocks of a chaotic unit.”

The requirement for exotic blocks was proposed and advocated as it implied significant, “extra-formational,” mixing which was regarded as the key characteristic of mélanges (Raymond, 1984). The minimum particle size requirement for exotic material is of significant importance, as siliciclastic grains — either single-crystal grains or lithic clasts — are *sensu strictissimo* exotic to their environment of deposition. These grains are not considered to constitute exotic blocks in the definitions of mélange.

Determining whether a block is exotic or native to the mélange may be significantly difficult. Without age constraints on the blocks and the matrix, whether a block is exotic to the mélange may be ambiguous. While discrepancies in metamorphic grade may reveal exotic blocks, and metamorphosed blocks within an unmetamorphosed matrix are unambiguously exotic, blocks of sedimentary rocks or lavas cannot *a priori* be categorised as either exotic or native. An olistostrome sourced from interbedded lavas and sediments may produce a rock unit consisting of native igneous blocks within a sedimentary matrix. Without age constraints,

MÉLANGES

this may be indistinguishable from an olistostrome sourced from a sedimentary unit and its igneous basement or another source external to the sediment pile; a scenario in which the igneous blocks may be considered exotic. Similarly, incorporation of sedimentary basement lithologies into a sedimentary mélangé may be indistinguishable from intraformational mixing without sufficiently precise age constraints. As such, many workers (e.g. Festa *et al.*, 2010) now disregard requirements for exotic blocks.

4.3. USE OF THE TERM “MÉLANGE” IN THIS THESIS

Despite the highly varied processes and settings of formation, mélanges can be recognised by their block-in-matrix texture and mappable scale. For this doctoral thesis, I adopt the Penrose definition of mélanges (Silver and Beutner 1980):

“Mélange’ is a general term describing a mappable (at 1:25,000 or smaller scale), internally fragmented and mixed rock body containing a variety of blocks, commonly in a pervasively deformed matrix.”

However, I recognise the significance of extra-formational mixing to the geological history of a mélangé unit and as such describe block-in-matrix rocks which lack exotic blocks as “dis-membered formations” as a sub-category of the term “mélangé”. I also utilise the term “broken formation” to describe bedded/layered rock units which have been intensely tectonised but not to the point of stratal breakup. Rock units which would not themselves be classified as “mélangé” are included within a larger rock

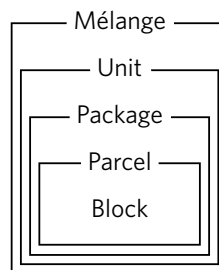


FIG. 4.4. Hierarchical subdivision of mélangé units used in this thesis, adapted from Leslie *et al.* (2012).

unit that mostly consists of *mélange sensu stricto*. To describe sections or areas exhibiting block-in-matrix fabric which cannot themselves be termed *mélange* – such as individual packages or blocks within the *mélange* – I favour the term “bimrock” (Medley, 1994). For the process of subdividing *mélanges*, I adapt the litho-demic subdivision scheme for tectono-metamorphic units from Leslie *et al.* (2012) (Fig. 4.3).

MÉLANGES

THIS PAGE INTENTIONALLY LEFT BLANK.

CHAPTER 5. METHODOLOGY

This chapter details the methodologies employed in this thesis, categorised into field methods, light microscopy methods, rock mechanics methods, numerical modelling methods, geochemical methods, and image analysis methods. These methodologies are integrated in Chapters 6, 7, and 8, which allows for holistic and novel analyses of the studied rock unit. The field, light microscopy, rock mechanics and geochemical techniques used are mostly based on the routine methods for this type of study. These techniques are developed upon to facilitate study of this highly complex rock unit and answer the specific research questions of this study. Where this routine analysis is not well known outside of its specific discipline, this is explained in detail. The specific setup of rock mechanics and numerical modelling experiments are explained here and in Chapter 7. The image analysis technique presented in this chapter are novel and have been developed to aid characterisation and quantification of block-in-matrix fabrics in the absence of a strong planar foliation. This is justified and explained in detail in Chapter 5.6 which is written in the format of a paper and intended for publication pending additional data collection not within the scope of this doctoral project.

5.1. FIELD METHODS

5.1.1. Rationale

Mapping of the Osa Mélange was conducted to clarify the proportions of basalt and sediment after some workers (Meschede *et al.*, 1999; Vannucchi *et al.*, 2006) described the mélange as consisting mostly of highly deformed basalt with a low proportion of sediment, while others (Di Marco *et al.*, 1995; Buchs *et al.*, 2009) described it as consisting predominantly of sediment containing basalt blocks. Preexisting geological maps by Vannucchi *et al.* (2006) and Buchs *et al.* (2009) do not discriminate between significant differences in lithology and fabric within mélange units and, where structural analysis was done (Vannucchi *et al.*, 2006), the descriptions of the variations in these structures is limited to planar features (e.g. foliation and bedding) and does not

METHODOLOGY

include shape, size, and orientation of the blocks. Descriptions of the variance of the block-in-matrix fabric throughout the mélange were not available from previous studies. Additional sampling was necessary as previous studies lacked samples from areas key to our study and no previously collected sample was suitable for triaxial strength experiments due to their small size and method of collection (see Chapter 5.3).

5.1.2. Technique

5.1.2.1. Mapping strategy

Two study areas on the Osa Peninsula were mapped onto a 1:5000 scale base-map of the topography and major geographical features of the Osa Peninsula. This base-map was an enlargement and digital re-render of the Government of Costa Rica (1965) map of the Osa Peninsula. Re-rendering was accomplished using Adobe Photoshop to produce a two-tone image of the scanned map and remove artefacts from the scanning process. The “Live Trace” feature of Adobe Illustrator was then used to create a vector image of the map so that lines on the map would remain acceptably sharp when enlarged to 1:5000. Artefacts and inconsistencies between the original map and the vector map were identified and corrected manually. This map was then imported into ArcGIS and geo-referenced using the grid lines on the original map. Finer grid lines were added at one second intervals and the map sheets were printed for use in the field.

A length of coastline 15 km long from Bahia Drake to Punta San Pedrillo was mapped to represent the San Pedrillo Unit. Likewise, the Cabo Matapalo Unit was mapped from Punta Carbonera to Cabo Matapalo; a coastline length of 5 km. Very good exposure along the coast allowed for near continuous observations, data collection, and sample collection. This mapping and sampling were conducted over two field campaigns, one 2-week-long campaign in February 2015 and one 5-week-long campaign in January – February 2016. A Garmin GPSmap 62 GPS was used to accurately identify location, occasionally supplemented by the satellite imagery (Google Maps) and onboard GPS of an iPhone 6s where necessary.

Geological mapping was conducted using the widely-recognised standard approach with modifications suited to the study of a highly complex block-in-matrix rock unit. Due to the near-continuous outcrop and the high density of mappable geological features, localities were recorded as precise latitude and longitude locations and key observations were recorded directly onto the map. Distinguishing between major lithologies and structural associations (block or matrix) was made difficult due to the monotonous dark grey colour and very fine grain/crystal size of most lithologies. Where available, proxies such as fracture density and tortuosity, and the texture of the weathered surface, were used to distinguish between similar-appearing lithologies. Where lithology could not be confidently identified, samples were collected for further petrographical analysis. A highly descriptive approach was adopted for the field observations in order to limit subjectivity and allow for reinterpretation in light of new evidence from lab-based analysis.

Mapping of the *mélange* was conducted in accordance with the methodology described by Hsü (1968) (see Chapter 4.1) for mapping *mélanges*. Specifically, that:

- A. Stratal continuity was nowhere presumed and even the outcrop pattern of apparently planar features was extensively investigated where possible. The irregular shape of blocks was acknowledged while mapping, and every attempt was made to represent this.
- B. Superposition of *mélange* packages or other layers carries no stratigraphical significance and all contacts were assumed tectonic unless evidence of a depositional contact was observed.
- C. Biostratigraphic or chronostratigraphic ages of the *mélange* components – derived from literature (e.g. Hauff *et al.*, 2000 G3; Buchs *et al.*, 2009) – were not used to establish the timing of *mélange* formation
- D. The observed contact between the Osa *Mélange* and the La Vaca Member of the cover sediments was recognised to be a depositional contact.

Due to the highly chaotic nature of *mélanges* and the near-zero inland exposure in the Osa Peninsula, projections of geological features inland, below ground, and above ground were not possible. These features can only be confidently extended

METHODOLOGY

for a maximum of 50 m in any direction and the presence of blocks or structures not exposed — as illustrated in Fig. DR3H and Fig. DR4D in Chapter 6 — are hypothetical. Finalisation of mapped units was decided following petrographic analysis of collected samples. The map shown in Fig. 1 and Fig. DR1 of Chapter 6, Fig. 7.1, and Fig. 8.1 was drawn in Adobe Illustrator and the inland extent is significantly exaggerated to allow the features of the map to be visible. At most, 20 m of exposure perpendicular to the coastline was available and this would occupy less width than the outline at the scale presented.

5.1.2.2. Sampling strategy

Samples for microstructural, petrographical, and geochemical analysis were collected in the field during geological mapping in 2015 and 2016. Most samples were extracted from outcrop using a hammer and chisel, however, where possible, samples were pulled from outcrop with unaided manual force. Where possible, samples of both block and matrix were collected at each locality. Attempts were made to always select the least weathered material at each outcrop.

Samples for mechanical testing were collected in the field during geological mapping in 2016. Samples for triaxial strength testing were chosen as large (>30 cm average diameter) boulders whose lithology most closely matched the lithology in outcrop. The lack of any mechanical lifting equipment and the fact that these samples required carrying by hand over rough terrain for several kilometres placed an upper limit on the size of the samples that could be collected. Such large samples were required to produce a sufficient number of machined cylinders to complete the experiments. These samples were collected from float so as to avoid introducing artificial fractures due to hammering.

Samples for point load analysis were collected from localities across the mapped area, and these were extracted using a hammer and chisel as the presence of artificial fractures is negated by the sample preparation and the repeated experiments. These samples were >10 cm average diameter and were chosen as representative of the lithologies in the *mélange*. Some samples tested by point load analysis were collected by Paola Vannucchi in 2012 as cobbles in float, mostly near rivers.

5.2. LIGHT MICROSCOPY METHODS

5.2.1. Rationale

Given the extraordinary similarity in colour and texture between the varied lithologies in the mélange, analysis of these rocks under a microscope is necessary to distinguish between and identify lithologies. Petrographic study of these rocks also allows the relative proportions of clast types and mineralogy to be identified. Microstructural analysis of these same thin sections allows cross-cutting relationships to be established and allows further characterisation of the complex fabric at a scale smaller than can be observed in hand specimen.

5.2.2. Technique

Thin section slides were produced from selected samples following the standard procedure. Thin sections were ground to 30 µm in thickness, polished, and were left uncovered to allow for the possibility of further analysis.

The thin, partially transparent thin section slide is often sufficient to reveal the detailed texture of these rocks without being viewed through a microscope. The scale of these structures may be more conducive to study at low magnification. As such, initial analysis of these rocks was conducted by viewing the thin sections on a lightbox and describing the major structural features. Photographs were taken of each thin section slide mounted atop a photographic polariser on a lightbox to simulate light within a petrological microscope. A second photo was taken of each thin section with a second polariser oriented at 90° to the first lying between the slide and the camera, to simulate cross polarised light within a petrological microscope.

A standard polarising petrological microscope (Vickers Instruments M722836) was used to view the thin sections in transmitted light. Primarily, the 10× objective was used for analysis of structural details; however, the 20× and 40× objectives were used for mineralogical and palaeontological identification. Photographs of thin sections were taken using a Nikon Microphot-FX trinocular petrological microscope and a Nikon DS-SM digital camera.

METHODOLOGY

Due to the highly altered and/or weathered nature of most of the samples, original mineralogy had to be inferred from pseudomorphs now composed of clay, silica, or carbonate. As such, detailed mineralogical analysis of these rocks was not possible. Order of deformation events was inferred by cross-cutting relationships, and shear and dilatational fractures were discriminated based on the presence of significant offset of markers.

5.3. ROCK MECHANICS METHODS

5.3.1. Rationale

In order to more fully characterise the material within the Osa Melange, rock mechanics experiments were conducted on samples of all lithologies to quantify their strength, Young’s modulus, porosity, and density. This allows assessment of the impact of previous deformation on the materials within the melange and allows prediction of the style of future deformation within this rock unit.

Two techniques for testing rock strength were used. Triaxial experiments were conducted on samples of basalt and volcanoclastic matrix as these are common lithologies with complex microstructures. Triaxial experiments were used to assess how the physical properties of these two materials, and their relationships to each other, varied with increased depth of burial. Triaxial experiments provide detailed data on stress-strain curves, yield strength, Young’s modulus, and Poisson’s ratio. However, these tests are time-consuming, expensive and require large volumes of material. In order to characterise the strength of the full range of lithologies in the melange, point load tests were conducted. These provide only the yield strength of the material, but can be conducted on a large number of samples quickly and with a minimum of sample preparation. Porosity and density experiments were conducted separately on all samples.

5.3.2. Technique

5.3.2.1. Porosity and Density Experiments

The porosity and density of each subsample used for mechanical testing were measured non-destructively using the saturation and buoyancy technique (ISRM [2014], see also Franklin *et al.* [1977]).

Subsamples were first weighed air dry using a pan balance, before being placed in an ~100°C oven overnight to oven dry; the oven dry samples were again weighed using a pan balance. These subsamples were then placed in a vacuum chamber filled with deaerated water and subjected to a vacuum until no more bubbles were visible in the chamber. Two experimental setups were used, one at the British Geological Survey which used deaerated water as an input into the vacuum chamber and one at Royal Holloway which took tap water as an input and deaerated it during the vacuum process by agitating the water using a magnetic stirrer (Fig. 5.1). The subsamples were then left overnight to saturate before being weighed submerged in water and suspended in air by a hanging balance.

W_a = Air dry weight

W_o = Oven dry weight

W_s = saturated weight

W_w = saturated underwater weight

These four measurements were then used in the following equations to calculate density and porosity for each subsample.

$$\rho_d = \frac{W_o}{(W_s - W_w)}$$

EQUATION 5.1. Equation to calculate dry density (ρ_d) from oven dry weight (W_o), saturated weight (W_s), and saturated underwater weight (W_w).

$$\rho_s = \frac{W_s}{(W_s - W_w)}$$

EQUATION 5.2. Equation to calculate saturated density (ρ_s) from saturated weight (W_s), and saturated underwater weight (W_w).

$$\rho_p = \frac{W_o}{(W_o - W_w)}$$

EQUATION 5.3. Equation to calculate particle density (ρ_p) from oven dry weight (W_o) and saturated underwater weight (W_w).

METHODOLOGY

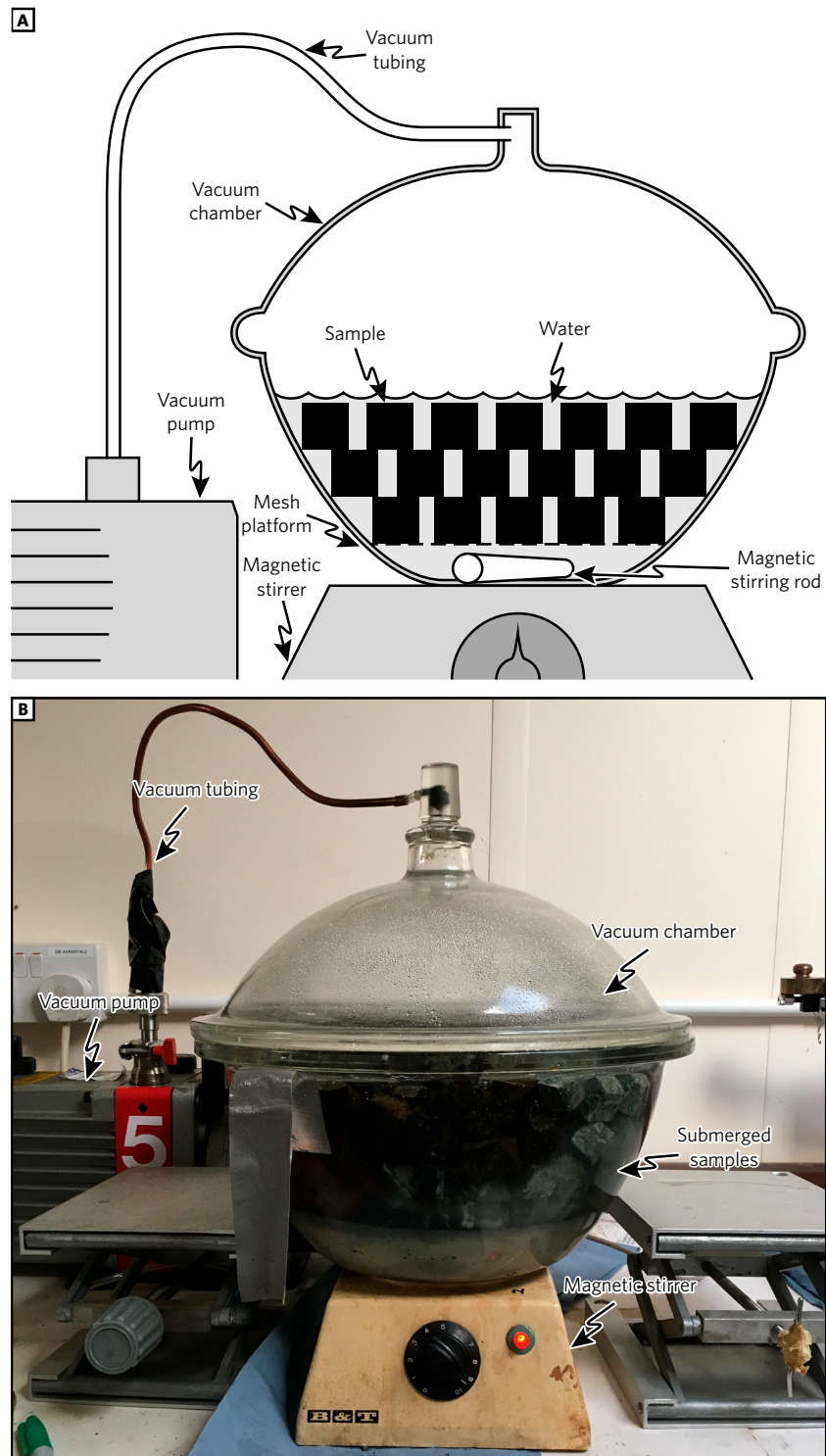


FIG. 5.1. Experimental setup to measure density and porosity using the saturation buoyancy test at Royal Holloway, showing **A**: Schematic representation of the apparatus, and **B**: Photograph of the setup in use.

$$\phi = 100 \times (\rho_s - \rho_d)$$

EQUATION 5.4. Equation to calculate porosity (ϕ) from saturated density (ρ_s) and particle density (ρ_p).

Unless otherwise specified, the density referred to in this thesis is particle density.

5.3.2.2. *Triaxial Experiments*

Out of the 6 large samples recovered from the Osa Melange, only two samples were suitable for triaxial deformation experiments. The remaining samples failed during sample preparation and were therefore deemed unsuitable for further study. The two samples were of the altered basalt and the indurated volcanoclastic matrix at the Punta Marengo package. One sample of vesicular basalt derived from the Cocos Ridge – recovered by IODP Exp. 344 (Harris *et al.*, 2013) – was also analysed to compare with the altered basalt. None of these samples displayed orientated fabrics and were therefore tested in a single orientation.

These samples were initially cut into ~20 cm cubes using a large diamond-tipped saw, from which 54 mm diameter cylindrical subsamples were cut using a radial drilling machine with a hollow barrel tripped with a diamond cutting piece. These cylinders were then cut to a length/diameter ratio of approximately 2:1 using a diamond-tipped saw and each end surface was ground to a roughness of <20 μm using a surface grinding machine. Where significant surface defects existed on the sample, they were filled by plaster to limit stress concentration at these locations. Samples were placed between two hardened steel platens and jacketed by a heat-shrink Polytetrafluoroethylene (PTFE) membrane. A good seal between the jacket and the section of the platens was ensured using a latex gasket and locking wires.

Axial strain was measured by two axial extensometers (MTS 632.90F-12, accurate to $\pm 0.01\%$) located at 180° to each other around the sample, while circumferential strain was measured by a single circumferential chain extensometer (MTS 632.92H-03, accurate to $\pm 0.01\%$) located around the centre of the sample. A third platen with a spherical seat – used to prevent eccentric loading of the sample – was then attached to a 2.6 MN capacity

METHODOLOGY

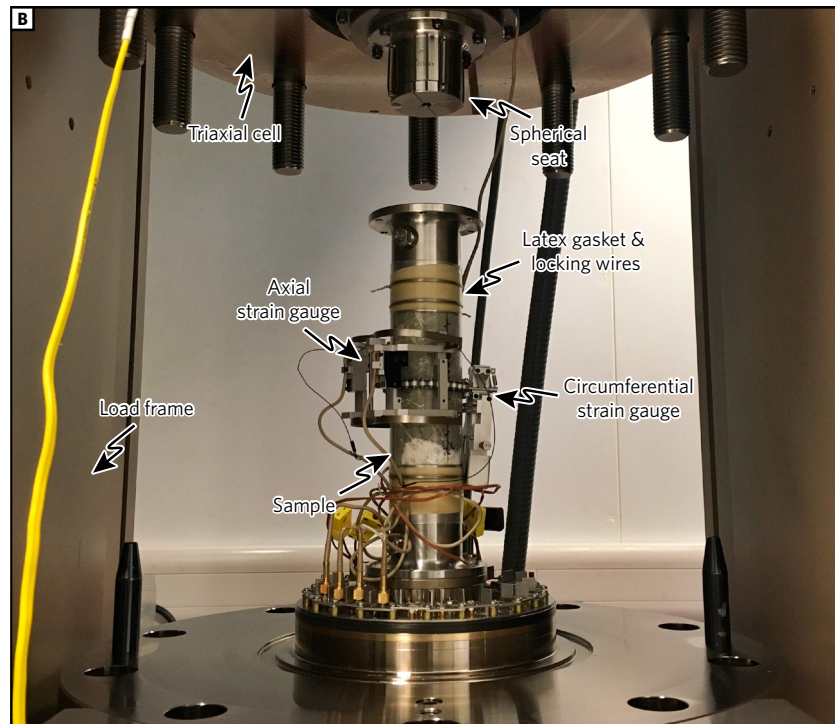
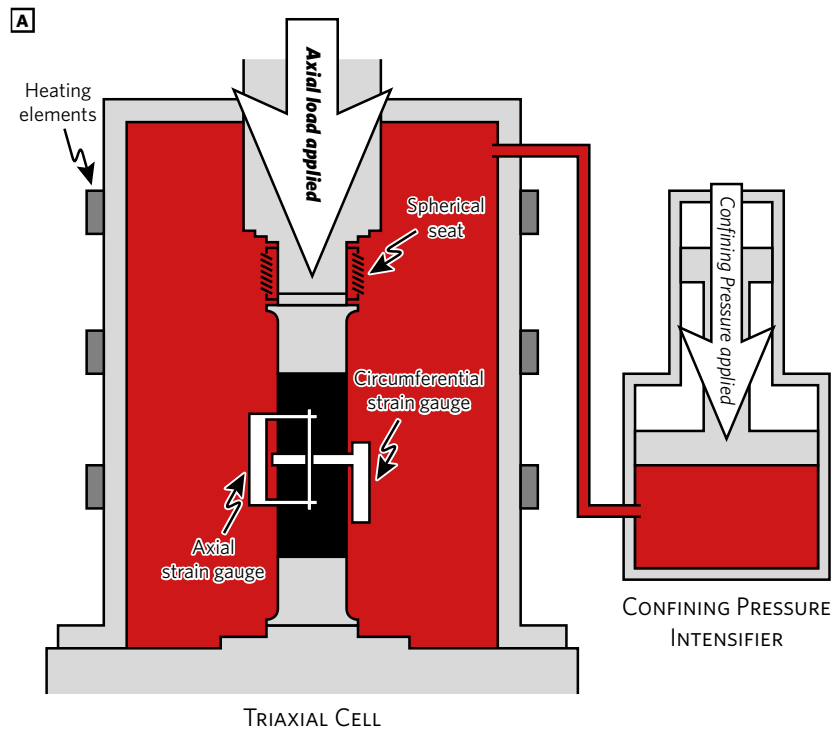


Fig. 5.2. Setup for the cell for triaxial strength test at the British Geological Survey, showing **A**: Schematic representation of the apparatus, and **B**: Photograph of the setup immediately prior to use.



FIG. 5.3. Photograph of the full setup for triaxial strength tests at the British Geological Survey showing the cell in use, the pressure intensifier, and the computer control system.

METHODOLOGY

force transducer (MTS 661.98B.01, accurate to $\pm 0.32\%$ of load) to measure the applied load on the sample (Fig. 5.2).

These experiments were conducted at the Rock Mechanics and Physics Laboratory at the British Geological Survey in Keyworth, UK (Fig. 5.3) following the ISRM suggested methods for determining the strength of rock materials in triaxial compression (ISRM, 1983). The machine used for the triaxial tests is an MTS 815 servo-controlled stiff frame containing a vessel capable of a maximum confining pressure of 140 MPa. Samples were tested in oven-dried conditions and no pore fluid was applied as part of these experiments. The cell is heated by external heater bands and controlled by internal and external thermocouples accurate to $\pm 0.5^\circ\text{C}$. An initial axial load of 2.3 kN was applied to the samples to maintain contact between the sample and the platens. Confining pressure was then applied using mineral oil as a confining fluid which was pressurised using a pressure intensifier (MTS model number). Axial loading was applied at a constant rate of $5.0 \times 10^{-6} \text{ s}^{-1}$ until macroscopic strain occurred or peak stress was exceeded. The axial load, displacement, axial stress, differential stress, confining pressure, axial strain, circumferential strain, and temperature were measured throughout the experiments and were sampled every 1 second and 250 N.

Experiments were conducted at pressure and temperature conditions of $60^\circ\text{C}/60 \text{ MPa}$ and $60^\circ\text{C}/120 \text{ MPa}$. One test was conducted at $120^\circ\text{C}/120 \text{ MPa}$ and the result was within 2.5% of sample strength at 60°C , which is below the expected sample-to-sample variability. These conditions were chosen as they approximately bracket the conditions expected at the updip limit of the seismogenic zone at 2 – 4 km depth (Arroyo *et al.*, 2014). Fluid pressure was not applied in these experiments to simplify the procedure. Detailed background and justification for these experiments are included in Chapter 7.

At some point, while the sample was in the triaxial cell, the polytetrafluoroethylene jacket was punctured allowing infiltration of confining fluid into the sample causing it to become saturated. To ensure this infiltration did not occur due to failure of the gasket, one sample was loaded to experimental P/T conditions and removed with no axial load applied; this sample was not infiltrated with confining fluid. As such, it was concluded that infiltration

occurred by puncturing the jacket during rock failure. As this is at the end of the experiment, this is not considered to have influenced the results.

Samples were desaturated by passive soaking in isopropanol to preserve the delicate gouge textures and keep the polytetrafluoroethylene jacket intact. These samples were later cut into thin sections for light microscopy analysis. However, damage during transport resulted in the destruction of one sample and damage to the gouge textures in other samples.

5.3.2.3. Point Load Experiments

Point load tests were carried out using an HMA Geotechnical Systems Point Load Tester Model 6500 provided by the Rock Mechanics and Physics Laboratory at the British Geological Survey according to the methodology of Franklin (1985). At least 10 subsamples of each lithology were tested and the two highest and lowest values were discarded to ensure statistical significance of the results. Samples were first measured along their height and their width by a Vernier calliper accurate to $\frac{1}{10}$ mm. Samples tested were cut into irregular pieces with a diamond-tipped saw and many of the intensely pre-deformed samples broke along preexisting fractures ahead of the saw tip. As such, many samples can be classified as “irregular lumps” for the purpose of this test. While size and shape of these samples varied, all samples had a width (W) to height (H) ratio greater than 1 and were loaded along their shortest axis with the load applied close to the centre of the sample.

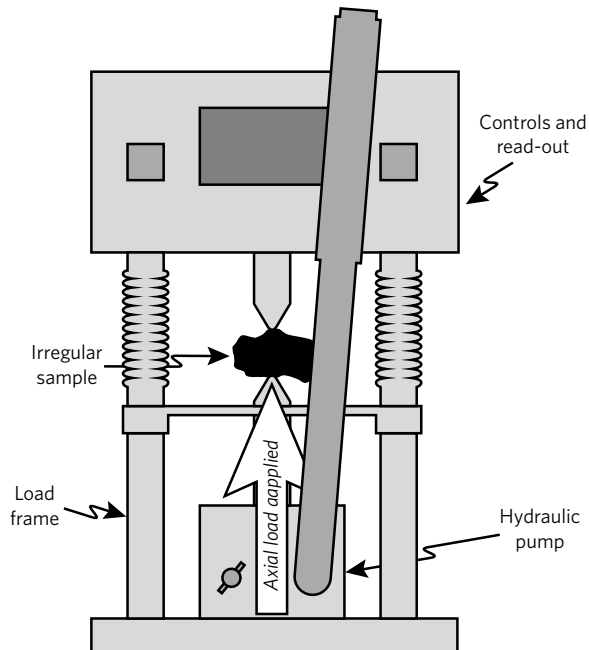
Load was applied by hydraulic press as part of the point load tester and delivered by two opposing spherically truncated conical platens (Fig. 5.4). Load was increased slowly (within 10 – 60 seconds) until sample failure and the maximum force (P) applied was recorded by the point load tester. The “uncorrected point load strength” (I_s) is calculated as:

$$I_s = \frac{\pi P}{(4WH)}$$

EQUATION 5.5. Equation to calculate uncorrected point load strength from the force applied to break the sample and the size of the sample.

METHODOLOGY

A



B

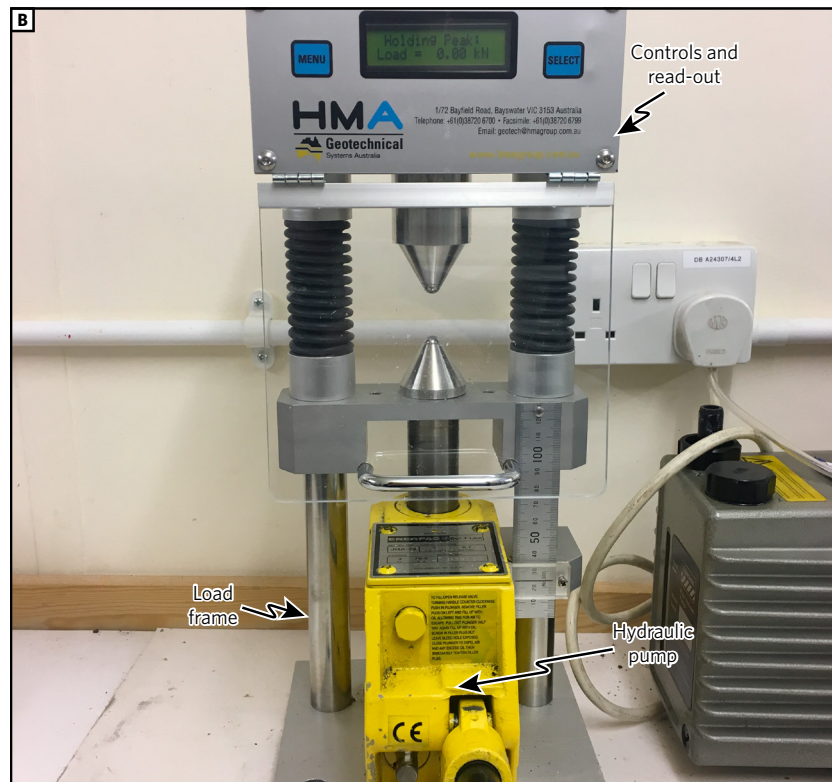


Fig. 5.4. Setup for the point load strength test **A**: Schematic representation of the apparatus, and **B**: Photograph of the setup prior to use.

This is corrected for the size of the sample to produce the “size-corrected point load strength” by:

$$I_{s(50)} = F \times I_s$$

EQUATION 5.6. Equation to calculate size-corrected point load strength from the uncorrected point load strength and a function of the size of the sample (F, given in Equation 5.7).

$$F = \left(\frac{\sqrt{4WH}}{50 \sqrt{\pi}} \right)^{0.45}$$

EQUATION 5.7. Equation to calculate the size correction factor needed to relate the uncorrected point load strength with the size-corrected point load strength.

$I_{s(50)}$ is the measurement of rock strength as measured by point load experiments. It represents a linear extrapolation from the size of the sample (which varies for each sample) to a uniform size of $H = 50$ mm. Due to this extrapolation, the strengths of samples of different sizes can be compared. The mean $I_{s(50)}$ of all subsamples is taken to represent the strength of the material. This, in turn, can be converted to an equivalent uniaxial compressive strength by multiplying the mean $I_{s(50)}$ by 24.

5.4. NUMERICAL MODELLING METHODS

5.4.1. Rationale

Numerical modelling allows visualisation of patterns of stress concentrations within geological structures undergoing deformation. This allows the occurrence and location of induced fractures to be inferred from where concentrated stresses exceed the independently-assessed strength of the material. Varying material properties, shape, or structure of the modelled rocks can be accomplished simply.

METHODOLOGY

5.4.2. Technique

The numerical modelling in this thesis uses the finite element modelling software COMSOL Multiphysics® (www.comsol.com) to model stress concentrations in a 2D linear elastic model. The results of these numerical experiments, as well as the rationale and background for the model setup, can be found in Chapter 7. As these models simulate deformation within a subduction channel, we measured shear (von Mises) stress accumulations in and around blocks in a matrix undergoing simple shear deformation. The Young's moduli of the blocks and the matrix was varied during these experiments to test the effect of differential Young's modulus on where fractures will occur.

The block is modelled as an elliptical inclusion with an aspect ratio of 2:1. All physical properties are assumed to be isotropic and

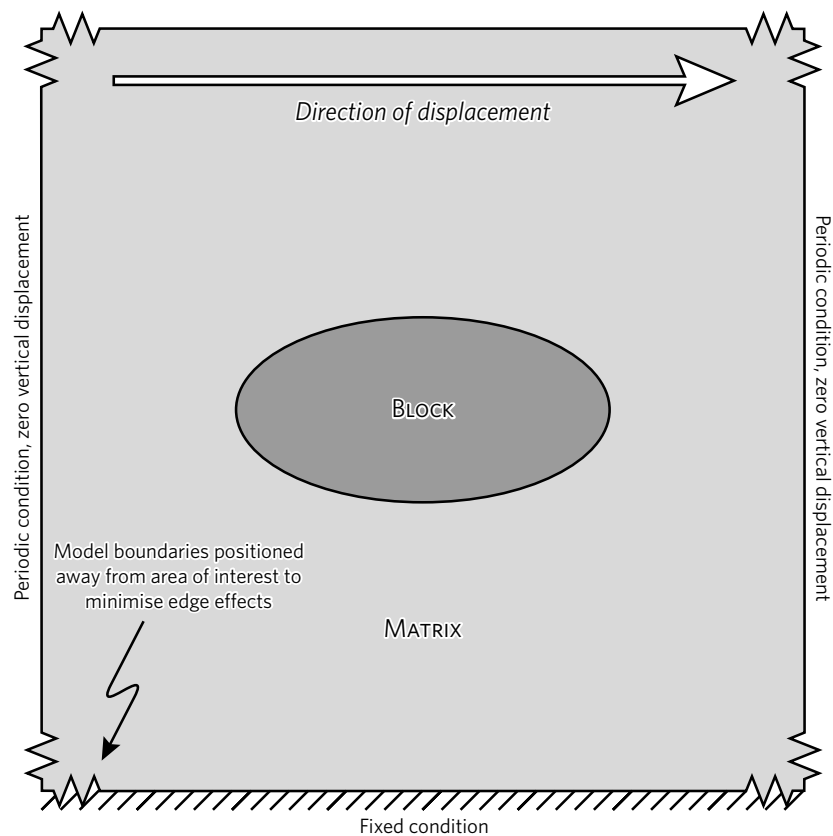


FIG. 5.5. Model geometry showing the elliptical block within its matrix and the boundary conditions at the edges of the model. Note that the image is zoomed in to show block and that the model boundaries are positioned away from the area of interest in order to minimise edge effects.

homogenous. The lower bounding surface of the model is fixed in place, while the vertical bounding surfaces are treated as a periodic condition with zero vertical displacement to ensure overall simple shear. The top surface is prescribed a shear displacement varying from zero to 10% of the model width to apply stress within the model.

The elastic properties of the blocks and the matrix were varied in these experiments, with most focus placed on varying Young's modulus. Single blocks and clusters of blocks at varying distances were both modelled. The effects of a fracture within the model was simulated by introducing an elliptical cavity with an aspect ratio of 1000:1. The specific uses of this model and the input parameters used are detailed in Chapter 7.

5.5. GEOCHEMICAL METHODS

5.5.1. Rationale

Geochemical analysis of blocks from the Osa Mélange was conducted to discern the provenance of mélange material. While Hauff *et al.* (2000a) and Buchs *et al.* (2009) have analysed the igneous rocks, this study aimed to span the full range of lithologies by including serpentinite and sedimentary rocks. This study aimed to test the interpretation by Buchs *et al.* (2009) that the intermediate – felsic rocks are derived from the Central American arc while the basaltic blocks are derived from the same intra-oceanic source as the Osa Igneous Complex; the results of this study are detailed in Chapter 9. While more extensive geochemical analysis of these rocks was planned, due to the highly altered nature of these rocks (see Chapter 9), this line of investigation was discontinued after the pilot study.

5.5.2. Technique

Samples for geochemical analysis were chosen to span the range of lithologies present in the mélange, with a focus towards the igneous rocks. Lithologies tested consist of basalt, gabbro, dacite, granodiorite, serpentinite, volcanoclastic sediment, pelite, and chert. No carbonate rocks were analysed.

The least altered portions of the samples were selected to minimise the effects of weathering and alteration, but no attempt was

METHODOLOGY

made to chemically remove the most altered portions using acids. These samples were broken down to single-cm-sized fragments using a steel-tipped fly press and ground to a fine powder using a TEMA disk mill composed of tungsten carbide. These powdered samples were then prepared for XRF analysis by producing from them fusion beads for major element analysis and powder pellets for trace element analysis using the standard methodologies. Fusion beads were produced by mixing 0.7 g of oven-dried powdered sample with 0.42 g of Li-tetraborate flux and heating to produce a melt. Powder pellets were produced by thoroughly mixing 10 mg of powdered sample with 8 – 10 ml polyvinyl alcohol binding solution and compressing in a die with 10 tsi of pressure for approximately 20 seconds. Analysis was conducted on a 2010 PANalytical Axios XRF spectrometer at Royal Holloway, University of London.

5.6. IMAGE ANALYSIS METHODS

Image analysis was conducted using ImageJ (Schneider *et al.*, 2012) on traces of field photos of outcrops displaying block-in-matrix texture. These traces were performed using Adobe Illustrator. Image analysis data was then used to determine the structural anisotropy of the pictured rock unit using the methodology presented below.

Unless otherwise specified, all values of structural anisotropy in this thesis are read at the 95th percentile (SA_{95}).

QUANTITATIVE CHARACTERISATION OF MÉLANGE FABRICS USING IMAGE ANALYSIS:

A simple method for determining structural
anisotropy from field photos.

Alexander P. Clarke¹, Paola Vannucchi¹

1: Royal Holloway, Egham Hill, Egham, Surrey, TW20 0EX, UK

The following section is a co-authored manuscript intended for publication following additional research and redrafting. The methodology presented was conceived of and developed by Clarke, and all data was collected or synthesised by Clarke. The manuscript was authored by Clarke and modified following reviews by Vannucchi. Clarke illustrated all figures and took the field photographs.

5.6.1. Introduction

Mélanges are rock units defined by their block-in-matrix texture (Raymond and Terranova, 1984). These blocks, characterised by their shape, orientation, size, and proportion, are the principal component of a mélange fabric. These characteristics are the fundamental parameters for defining the fabric of a block-in-matrix rock unit, but are rarely described systematically. While mélanges commonly – but not universally – exhibit a sheared matrix, this foliation typically deflects around the blocks, producing a wide spread in the orientation of this foliation making it difficult to precisely characterise the orientation of the mélange fabric (e.g. Eden and Andrews, 1990; Shervais *et al.*, 2011).

Despite this reality, most structural analysis of mélanges is based chiefly on the orientation of this foliation, not on the shape and orientation of the blocks which define the mélange fabric (e.g. Kano *et al.*, 1991; Fuentes *et al.*, 2016; Singleton and Cloos, 2013). This technique is unusable in mélanges without a foliated matrix and is difficult in mélanges where the foliation

METHODOLOGY

shows a high degree of deflection or where multiple generations of foliation exist.

In response to this, we have developed a methodology to quantitatively analyse the shape and orientation of blocks using image analysis to characterise *mélange* fabrics. This methodology assesses the aggregated aspect ratios and orientations of a representative number of blocks to determine the generalised structural anisotropy of the fabric. Structural anisotropy refers to the difference between the proportions and the aspect ratios of blocks oriented parallel to and perpendicular to the orientation of the fabric.

The structure of a rock mass is a first-order control on its mechanical anisotropy (including strength and elastic anisotropies), as these structures control the location and orientation of flaws, concentrate stresses, and impede the propagation of seismic waves (Louis *et al.*, 2005). Therefore, structural anisotropy – defined by the shape and orientation of the structures in the rock mass – is a key indicator of other forms of material anisotropy and has been shown to influence the deformation style within the rock mass (e.g. Butler *et al.*, 2008). The shape and orientation of these structures also define the fabric of the rock, with higher aspect ratio features generally aligning parallel – sub-parallel with this fabric. As shape and orientation of structures both controls the physical properties of the rock unit and defines its fabric, characterisation of the rock's structure provides a proxy of the rock unit's mechanical anisotropy.

Typically, mechanical anisotropy is directly measured in laboratory conditions by either destructive deformation experiments (e.g. Broch, 1983) or by propagating acoustic waves through the material (e.g. Svitek *et al.*, 2014). Both methods typically require samples <10s of centimetres in size. Alternatively, *in situ* measurements of elastic anisotropy may be conducted at a macro- – mega-scale from the travel time of seismic waves through the rock mass (Savage, 1999; Tepp *et al.*, 2018). Using structural anisotropy as a proxy for mechanical anisotropy, the difference in strength between different orientations of the *mélange* fabric can be estimated, even in cases where traditional methods of determining mechanical anisotropy cannot be used, for example, due to the scale of the blocks.

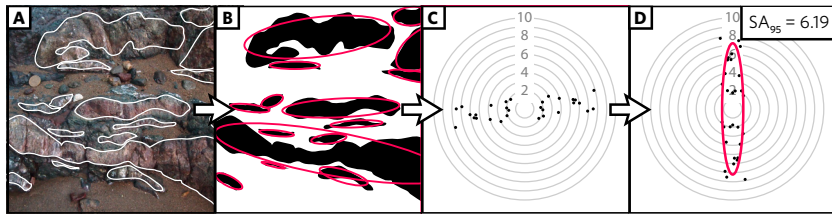


FIG. 5.6. Process of discerning structural anisotropy. **A:** First, block outlines are identified on a photograph. **B:** These outlines are analysed by image analysis software which fits ellipses to each block. **C:** Aspect ratio and orientation are plotted on a radar diagram to produce a cloud of data-point representing the general trend of the block-in-matrix fabric. **D:** Since no orientation marker is present in the photograph, the data cloud is detrended to remove the camera bias and an ellipse is plotted at the 95th percentile of the data cloud to produce the SA_{95} value.

While structural anisotropy of rocks has been explored (e.g. Louis *et al.*, 2005) it has not been used to characterise block-in-matrix rock units and no method to systematically quantify it has been proposed. Additionally, no graphical approach has been developed to show the structural anisotropy of a rock unit defined by the shape and orientation of its included fragments and no means of deriving a single value for such an anisotropy has been proposed. Crystallographic preferred orientation (CPO) is a well-established technique to characterise the structural anisotropy at the crystal scale (Lloyd *et al.*, 1991; Menegon *et al.*, 2008). However, it is not applicable to macro-scale structural anisotropy of mélangé units as its scale of observation differs wildly from the scale of the block-in-matrix fabric and it can only address a single lithology while mélangés are highly heterogeneous. Analysis of crystallographic preferred orientation also requires use of a specially fitted scanning electron microscope (Lloyd *et al.*, 1991) while measuring structural anisotropy by image analysis does not require any specialist equipment.

This paper details the methodology for determining structural anisotropy from field photos using image analysis, describes how interpretation of structural anisotropy can be applied to the study of mélangés and illustrates this with two examples, and discusses the strengths and limitations of this technique. This technique was developed to facilitate study of the Osa Mélangé, which lacks

METHODOLOGY

a well-developed foliation and displays a wide variety of block aspect ratios. The reproducibility of this method is tested by its application to the Gwna Mélange in north Wales. This mélange was chosen due to its strongly developed block-in-matrix texture, the presence of a strong foliation lacking in the Osa Mélange, and the diversity of block shapes and aspect ratios, in addition to its proximity to the study's authors and the presence of existing maps and photographs from Clarke (2014, unpublished masters thesis).

5.6.2. Proposed Methodology for Determining Structural Anisotropy

Determination of structural anisotropy requires as an input an image – typically a photograph – upon which image analysis can be performed. This image should clearly show the block-in-matrix texture and contain a sufficient number of blocks to show a representative range of aspect ratios and orientations. To avoid distortions, this photograph should ideally be taken orthogonal

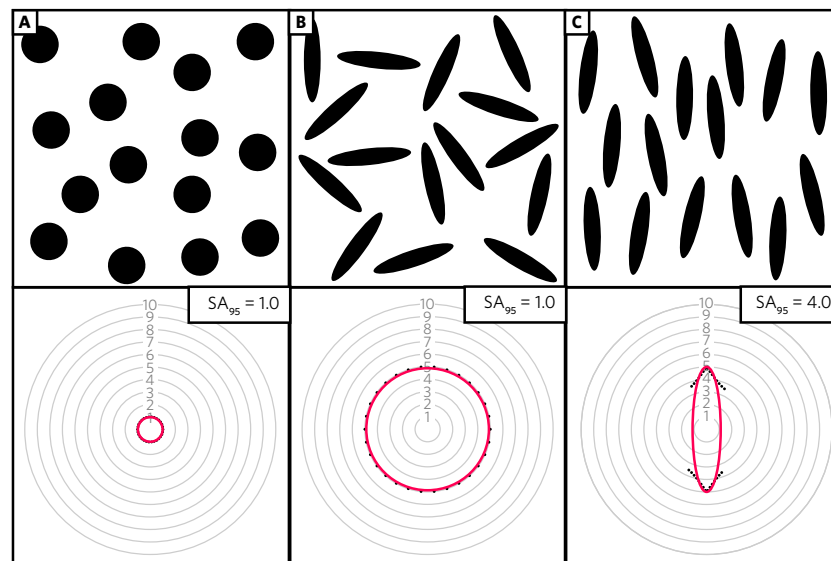


FIG. 5.7. Figure showing 3 examples of structural anisotropy for synthetic data. **A:** Circular blocks with an aspect ratio of 1:1 resulting in an SA_{95} value of 1.0. **B:** Elongate blocks with aspect ratios of 5:1 oriented so that no orientation is favoured, resulting in an SA_{95} value of 1.0. **C:** Elongate blocks with aspect ratios of up to 5:1 with a strong preferred orientation resulting in an SA_{95} value of 4.0.

to the rock surface being shown and care should be taken to avoid optical distortions within the camera, such as barrel distortion. Images that may have been digitally distorted, such as georeferenced satellite imagery or panoramas constructed from multiple photographs, should be avoided. Ideally, all photos should be taken in the same orientation (e.g. facing directly downwards) to enable accurate comparisons in the case when anisotropy varies in three dimensions. If this technique is being used to characterise variations in the block-in-matrix fabric over a mapped area, a compass should be visible in the frame of the photo to allow correct orientation of the image. The precision of this technique is limited by the quality of the input photograph and photographs showing a high degree of perspective may be unsuitable for this approach.

The outline of these blocks must then be carefully traced using graphics software (e.g. Adobe Illustrator) – with care given to ensure blocks do not touch – to produce a two-tone image showing the shape of the blocks. It is not necessary to trace every block contained within the frame of the photograph providing a representative portion of the image is covered. Care must be taken to faithfully reproduce the geometries of the blocks and not favour blocks in certain orientations. Image analysis software (e.g. ImageJ) should then be used to analyse the shape of these blocks. Blocks which are truncated by the frame of the photograph should be excluded from analysis.

The two parameters required to determine structural anisotropy are block aspect ratio and block orientation. This should be plotted on a radar plot with orientation on the radial axis and aspect ratio on the circumferential axis. The data should be duplicated with 180° added to the orientation data to represent the bi-directionality of this data. The plotted data will produce an elliptical cloud of data points representing the generalised shape and orientation of the blocks (Fig. 5.7). If the photograph is geographically oriented (e.g. there is a compass within the frame of the photograph), this data cloud should be rotated to match this orientation. If the image is not geographically oriented, this data cloud should be detrended to remove the artefact of the camera orientation relative to the rock fabric.

METHODOLOGY

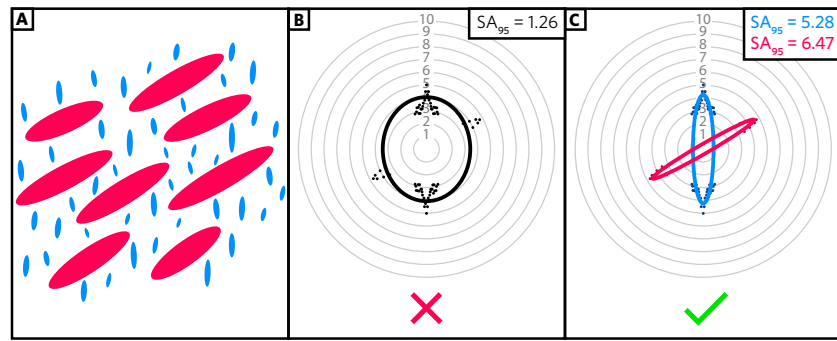


FIG. 5.8. Different domains within an image showing two distinct orientations and **A**: how not to characterise this using structural anisotropy, and **B**: how to correctly characterise it.

Detrending can be used to rotate the data cloud such that the maximum spread of data is in the plane of the Y-axis. This can be used to aid comparison between differently oriented fabrics and it should always be used where the orientation of the fabric is unknown. It is also necessary for quantification of structural anisotropy. Detrending is accomplished by rotating the orientation of the data until a minimum spread on the x-axis is reached. This is calculated as the difference between the sums of X-axis positions where X is negative and where X is positive, when only the pre-doubled data is considered.

To extract a single value for structural anisotropy from this cloud of data, an ellipse must be plotted which encloses the majority of the data cloud while excluding outliers. The semi-axes of this ellipse – referred to as the “structural anisotropy ellipse” – is defined by a percentile of the spread of data along the X and Y axes in a detrended diagram. The percentile chosen should reflect the number of data points and should be consistent between all images being compared; this percentile should be declared when reporting values from this technique, for example, if the 95th percentile is used, the value reported is the SA_{95} value, whereas if the 99th percentile is used, the value is the SA_{99} value. The 95th percentile is generally appropriate for images containing 10s of blocks, while the 99th percentile may be more appropriate where images contain 100s or 1000s of blocks. The aspect ratio of the resultant ellipse is taken as the “structural anisotropy value”. Where images are geographically oriented, the orientation of the

long-axis of the structural anisotropy ellipse should be reported alongside the structural anisotropy value.

5.6.3. The Structural Anisotropy Ellipse

The structural anisotropy diagram (Fig. 5.8) provides a highly visual means of representing block-in-matrix fabrics. Fig. 5.8 shows structural anisotropy in synthetic data to show how orientation and aspect ratio – two of the primary parameters in describing a block-in-matrix fabric – are presented in these diagrams. Fig. 5.7a shows circular blocks, i.e. without alignment, even though an orientation value is assigned to them by the image analysis software due to error inherent in representing a circular shape with square pixels. Since circles have an aspect ratio of 1:1, they plot at aspect ratio = 1 on the diagram, producing a structural anisotropy ellipse that is also circular, giving an SA_{95} value of 1. Fig. 5.7b shows elongate blocks (aspect ratio = 5:1) oriented such that no orientation is favoured. This produces a structural anisotropy diagram where all the blocks plot at aspect ratio = 5 and are evenly spaced around the diagram. Therefore, the structural anisotropy ellipse is once again circular, giving an SA_{95} value of 1. In both cases, the structural anisotropy value remains the same despite the differences in aspect ratios. This is because both cases lack a preferred orientation. The structural anisotropy value is therefore controlled not by the aspect ratios of the blocks directly, but the relationship between the aspect ratios of blocks in different orientations.

Fig. 5.7c shows elongate blocks (aspect ratio = 3.5:1 – 5:1) oriented with a moderate preferred orientation (N – S). In this case, the blocks plot around aspect ratio = 5 on the structural anisotropy diagram but are clustered towards the N and S of the diagram, therefore producing an elongated structural anisotropy ellipse and giving an SA_{95} value of 4.0.

The structural anisotropy ellipse is comparable to the ellipse of mechanical anisotropy (e.g. Osinowa *et al.*, 2017; Forbes Inskip *et al.*, 2018). The mechanical anisotropy ellipse represents the strength or seismic wave velocity at each orientation around the sample and is constructed by fitting an ellipse to this data. In contrast, the structural anisotropy ellipse encloses the cloud of

METHODOLOGY

datapoints, exclusive of outliers. This is done to account for the significantly greater degree of scatter in the structural data.

This method of determining structural anisotropy is entirely independent of scale. It also cannot distinguish between multiple domains with different orientations. In this case, the practitioner must discriminate these zones and analyse each separately (Fig. 5.8). This approach also only applies in two dimensions in the plane of the photograph, whereas true anisotropy varies in three dimensions. Only multiple photographs of surfaces cut at varying angles to the fabric can overcome this limitation, and this may not be possible at a given outcrop.

5.6.4. Examples

5.6.4.1. Example 1: Osa Mélange, Costa Rica

The Osa Mélange, located in southwest Costa Rica, is an accreted unit of oceanic olistostromes, debris flows, and turbidites that has undergone intense deformation at a shallow depth within the Middle America Subduction Zone in the Eocene – Miocene (Vannucchi *et al.*, 2006). This mélange was formed from mass wasting of a seamount complex into its surrounding flexural moat basin followed by frontal accretion and shallow underplating to the forearc (Clarke *et al.*, 2018). It consists of blocks of basalt, chert and carbonate within a volcanoclastic pelitic matrix and blocks generally range in size from 10^{-2} – 10^2 m, although megablocks up to a few hundred metres are present. This mélange consists of: a) chert-rich packages containing high aspect ratio (up to 11:1) blocks with a strong preferred orientation and visible folding, b) pelite-rich packages with low – moderate aspect ratio (generally up to 4:1 with outliers up to 8.5:1) blocks of many lithologies with very weak preferred orientation, and c) basalt-rich packages containing brecciated blocks and megablocks with low – moderate aspect ratios (generally up to 4:1 with outliers up to 7:1).

Much of the Osa Mélange lacks a defined foliation and, where present, any foliation is weakly developed. The presence, orientation, and aspect ratio of the blocks are the overwhelmingly dominant feature in this mélange and as such, traditional methods of characterising the fabric of a rock unit – such as measurement of planar/linear structures using a compass and representation

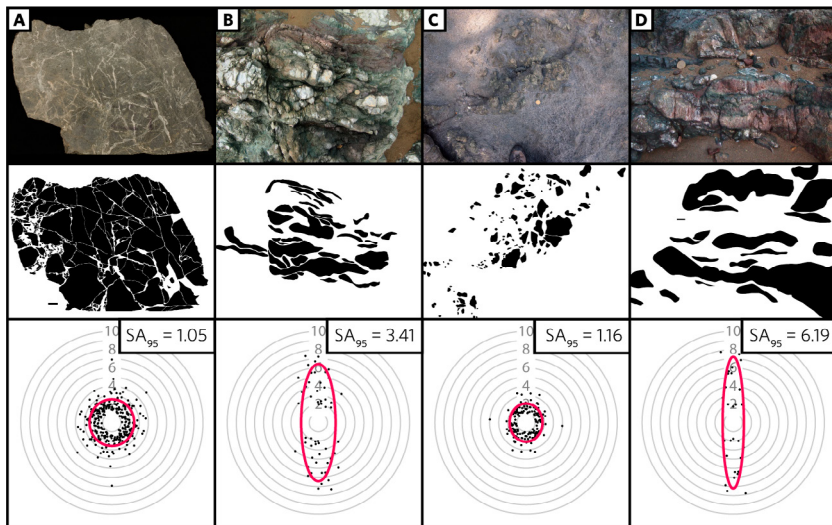


FIG. 5.9. Examples of structural anisotropy analysis performed on photos from the Osa Mélange. The structural anisotropy diagrams are shown detrended as no orientation data is available for these photographs.

A: This process is applied to a cut surface, allowing for 100% coverage of the image and producing high quality data. **B:** The process is applied to a challenging outcrop photo where care is taken to avoid exaggerating block shape due to perspective. **C:** Complex block-in-matrix structure represented using this method. **D:** High aspect ratio aligned blocks represented using this method.

of this data using a stereonet — are inadequate and inappropriate. While these structures — where they're present — may still be used to determine the deformation history (e.g. Vannucchi *et al.*, 2006), they cannot be used to comprehensively characterise the fabric. Aspect ratio and orientation of the blocks are more useful descriptors of the fabric than dip and strike of foliation. The structural anisotropy diagram therefore represents this mélange fabric more effectively and makes structural characterisation possible in areas where no planar structures exist. Using structural anisotropy, the weak preferred alignment of Fig. 5.9a and Fig. 5.9c can be detected. Identification and quantification of weak fabrics in block-in-matrix textures is a key strength of this methodology. This method can also quantify the true preferred orientation in rock units with moderate – strong preferred orientation (e.g. Fig. 5.9b and Fig. 5.9d) at a higher precision than measuring block margins or estimating block axes in the field can accomplish.

METHODOLOGY

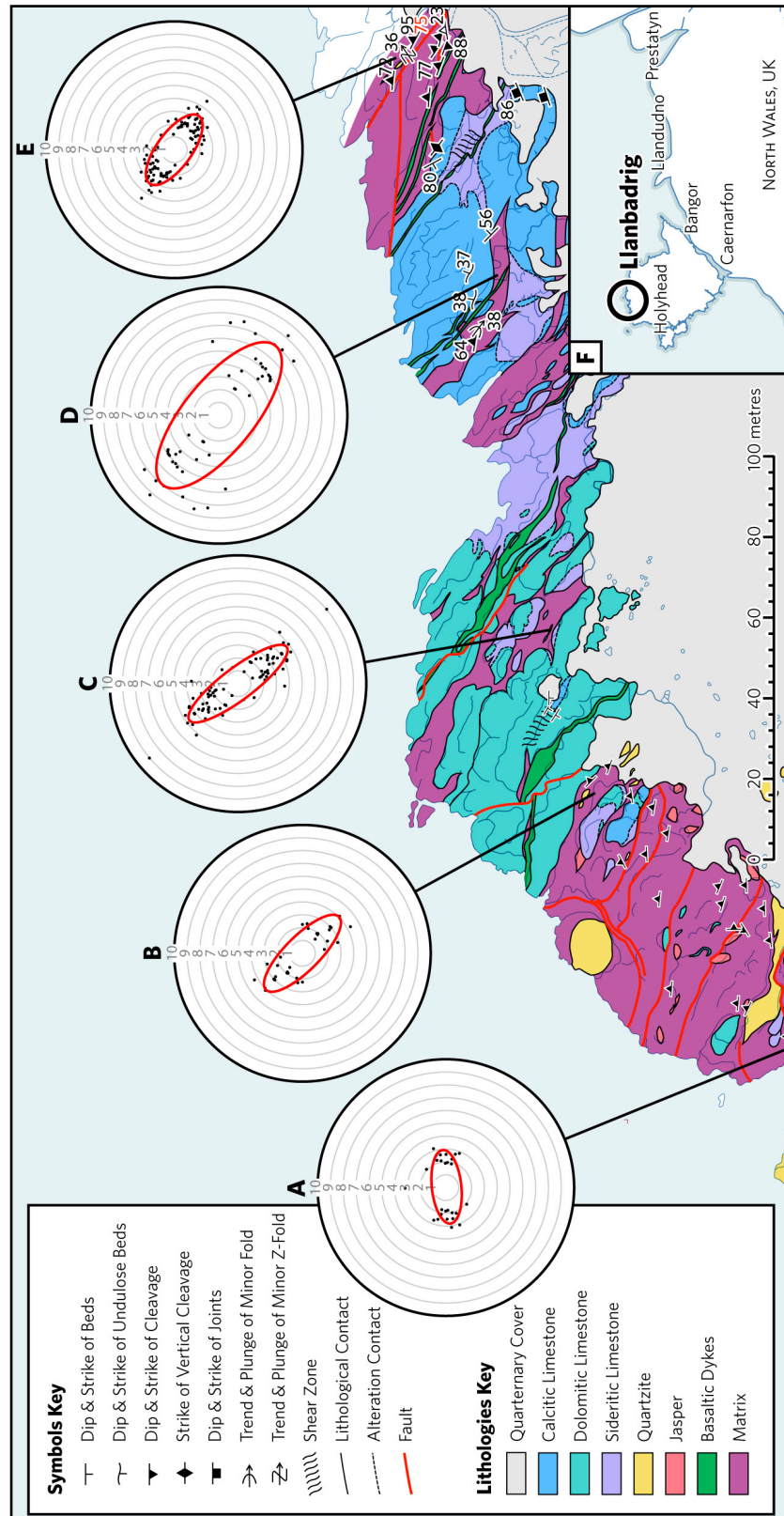


FIG. 5.10. (Caption on opposite page.)

5.6.4.2. Example 2: Gwna Mélange, Wales

The Gwna Mélange — located on Anglesey and the Llŷn Peninsula in north Wales, UK — is a late Neoproterozoic – early Cambrian accreted package consisting of tectonically dismembered sections of oceanic crust (Kawai *et al.*, 2008) and olistostromes (Wood, 2012). The area of Llanbadrig, on the northern coast of Anglesey, contains a deformed olistostrome displaying remarkable block-in-matrix texture and consisting of blocks of variably sideritised limestone, red chert, and quartzite in a pelitic matrix (Wood, 2012). The region displays a strong NW – SE structural trend consistent with the closure of the Iapetus Ocean (Gibbon and McCarroll, 1993). The strong foliation which cuts the matrix here sinuously deflects around blocks, sometimes rotating as much as 90° in the space of a metre. This foliation is largely absent from the limestone, chert and quartzite blocks, although occasional shear zones in this orientation cut the limestone blocks (Clarke, 2014).

Despite the matrix of the Gwna Mélange possessing a strong pervasive planar foliation, the greatest variation in the fabric of the matrix — varying on the scale of ~10 m — is block aspect ratio and the degree of preferred alignment. The Gwna Mélange therefore provides an ideal test of the broader applicability of the structural anisotropy method beyond the Osa Mélange. Structural anisotropy effectively represents this variation in block shape and orientation (Fig. 5.10) and, when the structural anisotropy diagrams are oriented to reflect the cardinal orientations of the blocks, provides an intuitive visualisation of the fabric.

Figures 5.10a, 5.10b and 5.10e represent areas with low block proportions and where blocks exhibit low – moderate aspect ratios; however, the alignment of these blocks remains strong. Fig. 5.10c represents an area between several mega-blocks where the matrix features highly elongate blocks showing strong

FIG. 5.10: (CONTINUED) Detailed geological map of the Gwna Mélange at Llanbadrig, northern Anglesey (Clarke, 2014, unpublished masters thesis) with structural anisotropy diagrams showing the variation in the block-in-matrix texture within this small area.

alignment. Fig. 5.10d shows high proportions of blocks with high aspect ratios and moderate – strong alignment.

5.6.5. Discussion & Conclusions

Structural anisotropy diagrams represent an effective way to visually represent the fabric of block-in-matrix rocks units such as *mélanges*. They also provide a simple means of quantifying this fabric for comparison to other areas with a block-in-matrix fabric. The dominant structure in a *mélange* unit is its blocks, and not planar or linear features as is typical of other rock units. Indeed, such features are commonly observed to bend around blocks or be deflected by blocks, and the orientation of block margins may not necessarily represent the orientation of the block as a whole. Foliations may also represent later overprints and not match the orientation of the blocks' structural anisotropy. Despite this, stereonet are commonly used to represent a *mélange's* fabric. We propose the structural anisotropy diagrams are a superior means of visually representing the fabric of a block-in-matrix rock unit and should supplant their use (see Fig. 5.10).

This methodology is limited to only two-dimensional sections of the rock mass, as true three-dimensional images cannot be obtained by photograph. The accuracy and precision of this method are strongly dependent on the interpretation of the practitioner, as the precise location of blocks and block boundaries may be difficult to determine due to weathering or visual similarities between the block and matrix lithologies. Therefore care must be taken to fairly represent all block sizes, orientations and aspect ratios within the frame of the photograph. This method does not consider the proportions of blocks and matrix, which – in addition to the shape and orientation of the blocks – also represent a key first-order control on material anisotropy. While image analysis has the capacity to quantify the area of the image covered by blocks and the area covered by matrix, this would require that all blocks within the frame of the photograph be traced; it is not practical to expect that all blocks will be recognised and traced with sufficient accuracy to allow this analysis. In many cases, there may be significantly more blocks than can practically be traced, and often sections of the photograph are obscured. There is also a tendency for the practitioner to be biased towards tracing the

larger blocks or blocks whose visual characteristics allow easier recognition of the block boundaries.

In addition to visually representing the fabric of a block-in-matrix rock unit, structural anisotropy may also represent an effective proxy for material anisotropy that may be used in scenarios where material anisotropy cannot be measured experimentally due to the scale of observation, logistical difficulties, or expense. This is possible because the material properties of a block-in-matrix rock unit are strongly influenced by the shape and orientations of their included blocks.

This technique allows quantification of *mélange* fabrics from field photos. Image analysis of these field photos can be used to determine the orientation and aspect ratios of each of the blocks, from which a structural anisotropy diagram can be constructed which visually represents the block-in-matrix nature of the *mélange* fabric. As *mélange* fabrics are characterised by their blocks, not by any planar or linear structures that may cut the *mélange*, this structural anisotropy diagram represents this fabric in a manner which is superior to stereonet. This method also provides a proxy for mechanical anisotropy, the measurement of which typically requires costly experiments using specialist equipment and which is limited to only small samples.

METHODOLOGY

THIS PAGE INTENTIONALLY LEFT BLANK.

CHAPTER 6. SEAMOUNT CHAIN – SUBDUCTION ZONE INTERACTIONS:

Implications for accretionary and erosive subduction zone behavior

Alexander P. Clarke¹, Paola Vannucchi¹, Jason Morgan¹

1: Royal Holloway, Egham Hill, Egham, Surrey, TW20 0EX, UK

2: Department of Earth Science, University of Florence, Via la Pira, 4, 50121
Florence, Italy

The following chapter is a co-authored manuscript published in Geology. Clarke and Vannucchi were responsible for planning the mapping and sample collection strategy. Geological mapping, sample collection and petrological analysis were conducted by Clarke. Seamount moats as a potential depositional environment was proposed by Morgan and developed by Clarke, Vannucchi and Morgan. The manuscript was authored by Clarke, modified following reviews by Vannucchi and Morgan. Clarke illustrated all figures and took the field and microscopic photographs. An expanded discussion of the ideas presented in this chapter is found in Chapter 10.

Seamount chain–subduction zone interactions: Implications for accretionary and erosive subduction zone behavior

Alexander P. Clarke¹, Paola Vannucchi^{1,2}, and Jason Morgan¹

¹Department of Earth Science, Royal Holloway, University of London, Egham Hill, Egham, Surrey TW20 0EX, UK

²Department of Earth Science, University of Florence, Via la Pira, 4, 50121 Florence, Italy

ABSTRACT

Sediment volume at the trench and topographic highs on the incoming plate are two of the main factors controlling whether a forearc will undergo subduction erosion or accretion. On oceanic plates, topographic highs such as large seamount complexes are commonly associated with significant volumes of flanking volcanoclastic sediments in the form of >100-km-wide debris aprons, with the largest deposits found in flexural moat basins. We propose that subduction of these sediment accumulations promotes localized frontal accretion, even in otherwise non-accretionary margins. The Osa mélangé in southwestern Costa Rica is a field example that provides new insights into the nature and occurrence of this interaction. The southwestern margin of Central America is punctuated by accreted Late Cretaceous–middle Eocene seamounts that formed at the Galápagos hotspot and accreted throughout the late Miocene. In contrast to most accreted seamounts along this margin, which retained their overall structure, the Osa mélangé is a chaotic mixture of seamount lithologies. It consists of basalt, chert, and carbonate blocks in a fine-grained pelitic matrix composed predominantly of feldspar and pyroxene grains with rare quartz. This lithology is consistent with sediment from a seamount chain's debris apron, such as the Hawaiian moat sampled during Ocean Drilling Program (ODP) Leg 136 and the Canary Islands moat sampled by ODP Leg 157. Subduction of seamounts and their debris aprons promotes concurrent accretion and erosion over short distances along the trench. This introduces heterogeneity into the subduction channel, with implications for deformation within the subduction zone plate interface.

INTRODUCTION

Subduction of bathymetric highs has traditionally been thought to be associated with tectonic erosion of the overriding forearc. Scars left on the forearc slope in the wake of subducting seamounts were the first convincing observations of material removal from the upper plate (Ranero and von Huene, 2000). However, seamount systems extend beyond the bathymetric high of the volcanic edifice to include broad sedimentary debris aprons, with the largest-volume deposits confined in flexural moat basins. Seamount flexural moats were first recognized by gravity measurements of the Hawaiian Islands (e.g., Vening Meinesz, 1941). These are several-hundred-kilometer-wide bathymetric depressions surrounding seamount chains (Fig. 1) that are caused by bending of the oceanic plate to flexurally compensate for the mass of the growing seamounts (e.g., Watts, 1994). Moat basins can accommodate the deposition of a thickness of up to 3 km of sediment from the adjacent seamounts through mass wasting of the igneous rocks and sedimentary cover (ten Brink and Watts, 1985). Even when a flexural moat is not obvious, major islands are typically surrounded by sedimentary debris aprons with up to 520-m-thick deposits extending >100 km

away from the island (e.g., de Voogd et al., 1999). The subduction of a seamount chain's debris apron and/or moat sediments (hereafter referred to as “moat”) offers a hitherto unconsidered opportunity for accretion of oceanic sediments at an otherwise “erosive” subduction margin. By this process, geologically significant volumes of volcanoclastic marine sediment may be transferred from the oceanic to the overriding plate.

Our recent work in southwest Costa Rica (Fig. 2) suggests that the subduction of a seamount chain can lead to the formation of a local frontal accretionary prism composed of sediments and igneous blocks initially deposited in the moat. Additional forearc material can be incorporated as the moat enters the trench. Accretion is prompted and/or enhanced by the local oversupply of thick, weak moat sediments to the trench.

GEOLOGY OF THE OSA MÉLANGE

The Osa mélangé constitutes up to 24.6×10^3 km³ of the Costa Rican forearc and contains 10^2 – 10^2 -m-scale blocks of carbonate, chert, and basalt, with rare blocks of gabbro, serpentinite, and granodiorite. The isotope geochemical character of the basalt in the Osa mélangé has

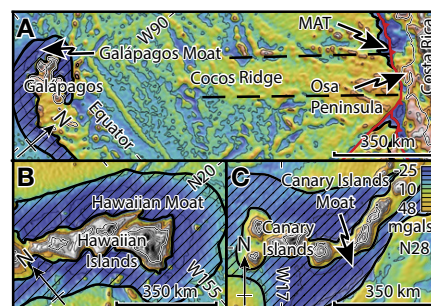


Figure 1. Gravity maps showing scale of seamount flexural moats (hachured areas) as low-gravity anomalies surrounding seamounts (Sandwell et al., 2014). A: Gravity map of Costa Rica, Galápagos Islands, and Cocos Ridge, showing Galápagos Moat as gravity low surrounding Galápagos Islands, Cocos Ridge as northeast-southwest-trending gravity high, and Middle America Trench (MAT) as gravity low along edge of Caribbean plate. B: Gravity map showing Hawaiian moat as gravity low surrounding Hawaiian chain. C: Gravity map showing Canary Islands moat as gravity low surrounding Canary Island chain.

been used to interpret a Galápagos ocean island basalt (OIB) geochemical affinity like that of the Osa Igneous Complex (Hauff et al., 2000; Vannucchi et al., 2006). Rare dacitic blocks, instead, have an ambiguous geochemical signature resembling that of the early stages of a volcanic arc (Buchs et al., 2009). The matrix consists of clay minerals (smectite and illite) and angular to subrounded grains of feldspar and clinopyroxene; quartz grain content varies from 0% to $5\% \pm 2\%$. This mélangé exhibits notable variation of the matrix and block populations and their relative proportions; the matrix to block ratio is high throughout. The general structure is layered, with alternating packages containing high proportions of clastic debris intercalated with those dominated by pelagic sediment (Fig. 2). Clastic-dominated units contain meter- to hundred-meter-sized blocks of carbonate, chert, basalt, and gabbro with low aspect ratios, whereas pelagic-dominated units exhibit a tectonic block-in-matrix fabric consisting of high-aspect-ratio centimeter- to meter-sized blocks of chert and carbonate with

DISCUSSION OF FORMATION MODELS AND COMPARISON TO VOLCANICLASTIC SEDIMENTS FLANKING SEAMOUNT CHAINS

High-resolution mapping, and geochemical and petrological analyses, reveal that the Osa mélange is mostly composed of igneous rocks and sediments typical of oceanic seamounts and their flanking debris aprons, but also contains rare blocks of granodiorite and dacite with an arc signature (Buchs et al., 2009). Deformation and metamorphic pressure-temperature (P - T) conditions of the Osa mélange are consistent with accretion in a frontal accretionary prism. The prevalence of OIB-affinity basalt and ubiquitous volcanoclastic sediment preclude an origin of the Osa mélange by tectonic dismemberment of the lower plate during subduction, or the upper plate by tectonic erosion, as suggested by Meschede et al. (1999). Vannucchi et al. (2006) interpreted the Osa mélange, together with the Osa Igneous Complex landward of the mélange, as an accreted seamount chain that preceded the arrival of the Cocos Ridge at ca. 6.5–8 Ma (Vannucchi et al., 2006, and references therein). In this model, the Osa mélange would have formed by tectonization of the seamount flanks during direct accretion while the tops of these seamounts were off-scraped to form the Osa Igneous Complex. This hypothesis requires that the composition of the Osa mélange resemble the composition of seamount flanks, which are dominantly zones of sediment bypass with low sediment proportions (cf. Morgan et al., 2007). This condition contrasts with the large (75%–90%) amount of sediment forming the Osa mélange. Alternatively, Buchs et al. (2009) interpreted that the Osa mélange formed by mass wasting of a previously accreted Osa Igneous Complex into the Middle America Trench combined with normal terrigenous sediment input. They attributed the source of rare felsic blocks to gravitational transport from the arc. However, arc-derived clasts are absent in the Eocene–Pliocene forearc basin—now exhumed in the Fila Costeña fold-and-thrust belt (Fisher et al., 2004)—and arc-derived plutonic rocks are absent from the Late Cretaceous–Eocene forearc rocks of the Golfito Complex (Buchs, 2008), adjacent to the Osa Igneous Complex. Minor input from the forearc as the seamount's moat met the trench would be anticipated due to surface transport and tectonic erosion above the adjacent subducting seamounts. Such tectonic erosion beneath the Golfito Complex may have supplied the granodiorite blocks found in the mélange.

Here we propose that the Osa mélange in southwestern Costa Rica is the first-recognized example where the flexural moat–debris apron package typically flanking an island chain has been accreted to the upper plate. Sedimentation into island moats consists of debris-avalanche

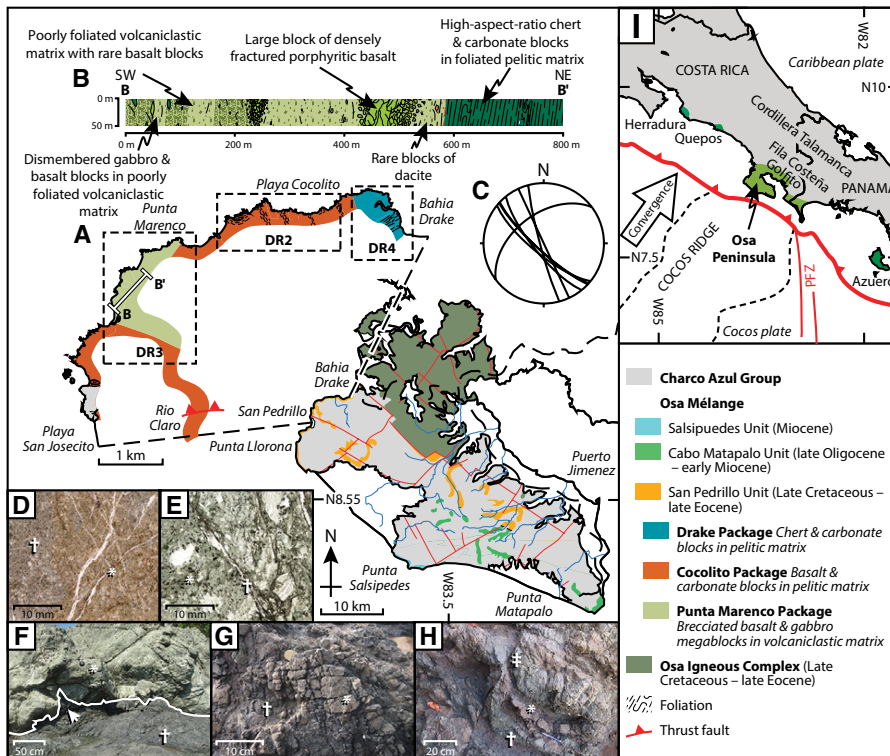


Figure 2. A: Geological map of Osa mélange from Bahia Drake (as shown in the figure) to Playa San Josecito (Costa Rica) (thrust fault from Vannucchi et al. [2006], and inland mapping of Rio Claro valley from Buchs et al. [2009]). Location of this map segment is shown on geological map of Osa Peninsula (lower right). (Modified from Vannucchi et al., 2006, and references therein.) B: Schematic cross-section from B to B' (see A) showing megablocks and block-in-matrix texture. Lithological variation shown in cross section is mapped in the Data Repository (see footnote 1). C: Stereonet of dominant foliation in Punta Marengo package. D: Photomicrograph of altered basalt showing “fresh” cores (*) containing unaltered feldspars and altered matrix (†) predominantly composed of clays. E: Photomicrograph of deformed volcanoclastic matrix showing phacoids (*) and localized shear zones (†). F: Gabbro megablock (*) in volcanoclastic matrix (†) with matrix injections into fractures (indicated by arrow) (8°40'50.5"N, 83°42'43"W). Line indicates boundary of block. G: Brecciated basalt megablock displaying brick-like geometric regularity (*) with “matrix” of comminuted basalt gouge (†) (8°41'22.7"N, 83°42'13.3"W). H: Dismembered chert and pelite with high-aspect ratio-blocks (*) in pelitic matrix (†) cut by minor fault (‡) (8°41'30.8"N, 83°40'18.0"W). I: Map of southern Central America showing location of Osa Peninsula in tectonic context and proximity to Middle America Subduction Zone, Cocos Ridge, and Panama Fracture Zone (PFZ).

a strongly developed lenticular fabric (see the GSA Data Repository¹; Fig. 2).

The Osa mélange experienced significant deformation during and subsequent to accretion, which overprinted any preexisting sedimentary structures. Thrust faults are present within the mélange (Fig. 2). Mapped thrusts are separated by ~5–10 km, but poor exposure limits our ability to detect all of them. The chaotic nature of the mélange prevents us from estimating their offsets

¹GSA Data Repository item 2018109, Item DR1 (detailed geological map of the San Pedrillo Unit), Items DR2–DR4 (photographs, thin sections, cross sections, and lithological descriptions of the Cocolito, Punta Marengo, and Drake packages, respectively), and Item DR5 (comparative Scale of the Osa Mélange and seamount moats/debris aprons), is available online at <http://www.geosociety.org/datarepository/2018/> or on request from editing@geosociety.org.

(Vannucchi et al., 2006). However, it appears that most deformation is accommodated by distributed shear within the matrix, which appears as a pervasively well-developed lenticular fabric with abundant anastomosing shear bands. Clastic-dominated units feature a chaotic fabric with discrete bands displaying moderate foliation, while pelitic layers are strongly foliated and feature high-aspect-ratio chert blocks formed by tectonic dismemberment of bedding. Basalt and gabbro olistoliths are densely fractured and feature pervasive matrix injection at their margins (see Fig. 2F), resulting in their dismemberment. The Osa mélange lacks pervasive recrystallization or greenschist facies minerals and contains abundant veins with calcite showing twinning types indicating the maximum experienced temperature was ~200–250 °C (Burkhard, 1993; Meschede et al., 1999).

deposits caused by mass wasting from unstable island flanks and pelagic sedimentary deposits derived from background pelagic sedimentation (Leslie et al., 2002; Morgan et al., 2007). Large-scale flank collapse can transport 100-m- to kilometer-scale megablocks into the moats (e.g., Moore et al., 1994). The moat has a maximum of 3 km thickness by up to 160 km width at Hawaii (e.g., ten Brink and Watts, 1985; Moore et al., 1994), a maximum of 455 m thickness by up to 250 km width at the Canary Islands (Collier and Watts, 2001; Gee et al., 2001), and a maximum of 520 m thickness by up to 130 km width at La Réunion island (southwestern Indian Ocean; de Voogd et al., 1999; Oehler et al., 2008) (widths as measured from Figure 1 and from Oehler et al. [2008]). Relatively little sediment is deposited on the flanks of the actual seamounts; these are dominated by sediment erosion and bypass into the moat (Leslie et al., 2002). Deepwater flexural moats are the dominant depositional environment for seamount-derived sediments. These deposits consist predominantly of mafic igneous clasts, carbonate clasts, highly immature grains of pyroxene and feldspar, and clays interbedded with pelagic sediment deposited during periods of quiescence (Leslie et al., 2002). Scientific drilling of the moat of the Hawaiian chain during Ocean Drilling Program (ODP) Leg 136 (Tribble et al., 1993) and the Canary Islands during ODP Leg 157 (Carey et al., 1998), as well as submersible surveys of the Hawaiian flank (Morgan et al., 2007), all reveal clay-dominated sediment containing high proportions of plagioclase and clinopyroxene clasts and lithic volcanic debris, with low proportions of quartz. Detailed sea-floor mapping at Hawaii finds that late slump-related tectonics during the intrusive growth of islands can tectonically stack the debris apron sediment package, a mode analogous to accretionary stacking at a subduction frontal toe (cf. Morgan et al., 2007).

Moat sediments contrast with ocean trench sediments, where sediments are mostly compositionally mature with high volumes of quartz and lithic clasts from the adjacent arc and forearc (Underwood and Bachman, 1982). Trenches starved of typical terrigenous sediment are still subject to mass wasting from the forearc and typically have a small frontal prism of disrupted forearc material (von Huene et al., 2004). In the Osa mélange, the dominance of plagioclase, clinopyroxene, and volcanoclastic grains over quartz argues against its source material being typical ocean trench sediments; instead, it is diagnostic of a moat deposit.

ACCRETION OF MOAT SEDIMENTS

At a subduction zone, marine sediment is typically accreted by the development of imbricate thrusts at the toe of the wedge and underplating of subducted sediment above the décollement

(Silver et al., 1985). Given sufficient volumes of its flanking moat sediments, the arrival of a seamount chain to the trench may therefore result in net accretion to the margin, even when the subducting seamounts themselves are associated with local subduction erosion (Ranero and von Huene, 2000; Dominguez et al., 2000).

Incorporation of oceanic igneous material from the incoming plate within accretionary complexes has previously been attributed to tectonic dismemberment of high-bathymetry features such as seamounts within the subduction channel (Cloos and Shreve, 1996) or back-stepping of subduction resulting in accretion of intact sections of oceanic crust (Wakabayashi and Dilek, 2003). However, incorporation of large blocks of oceanic material within accreted moat sediments must also be considered. Such a model effectively explains the hundreds-of-meters-thick blocks of basalt found within the predominantly fine-grained Osa mélange. Moreover, in the case of Osa, previously intact igneous material from the seamounts themselves was also accreted, now forming a geologically distinct Osa Igneous Complex on the landward side of the mélange (Buchs et al., 2016). The data at Osa cannot discriminate whether sedimentary apron stacking occurred during island growth (e.g., Morgan et al., 2007) or during forearc off-scraping and accretion. All thrusts mapped in the Osa mélange have an WNW–ESE

to ENE–WSW trend (Vannucchi et al., 2006; see the Data Repository) consistent with the direction of long-term plate convergence in this region and an origin linked to an accretionary subduction system.

CONCLUSIONS AND IMPLICATIONS

The moats that flank seamount chains can provide a significant local volume of sediment to the trench when subducted. Mass wasting and large-scale flank collapse from growing islands provide volcanoclastic material that includes very large igneous blocks. Accretion of flanking moat deposits appears favorable even at otherwise non-accretionary margins. This provides a simple means to transfer large volumes of seamount-derived volcanoclastic material to the upper plate. Here we recognize the Osa mélange to be a fossil example of an accreted moat deposit, explaining why it contains hundreds-of-meters-scale igneous blocks within a fine-grained quartz-poor matrix.

Unlike sediment accretion at typically accretionary margins, accretion of moat fill may occur concurrently with adjacent forearc erosion caused by subduction of the seamount chain (Fig. 3). This lateral heterogeneity of tectonic processes affecting the forearc would also influence the composition of the plate boundary shear zone at depth. In regions where seamounts are subducted, subduction erosion would be active

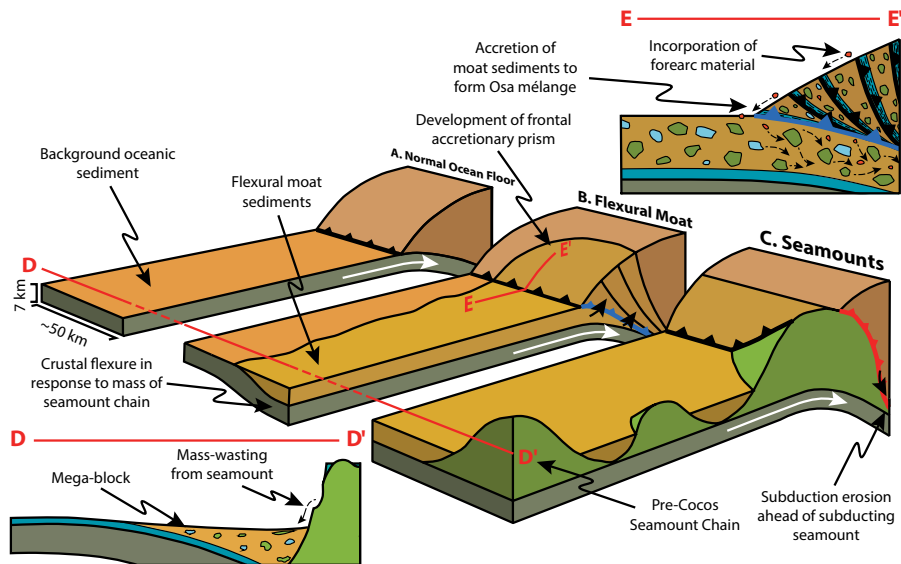


Figure 3. Conceptual model of frontal accretion of seamount moat sediments adjacent to subduction erosion by subduction of seamount. White arrows indicate convergence direction. A: Subduction of oceanic plate under conditions normal for this margin. B: Subduction of moat leading to increased accretion and development of frontal accretionary prism, even in otherwise non-accretionary subduction zones. This is the setting in which Osa mélange formed. Blue ticked line shows subduction accretion. C: Subduction of seamount (green) leading to localized subduction erosion of upper plate (e.g., Ranero and von Huene, 2000; Vannucchi et al., 2016). Material eroded from base of forearc may be mixed with subducted moat sediments and reaccruted. Red ticked line shows subduction erosion. Insets show cross-sections beneath lines D-D' and E-E'; D-D' shows mass wasting from volcanic edifice into moat; E-E' shows accretion of flexural moat into localized accretionary prism (see B) and mixing with upper-plate blocks.

and the plate boundary shear zone would be localized within material coming from the upper plate. Adjacent subduction accretion would drive localization of the plate boundary within former moat sediments. In this scenario, forearc material tectonically eroded above subducting seamounts may be mixed with subducted moat sediments within the plate boundary shear zone, accounting for the incorporation of exotic blocks from both settings, such as the rare upper-plate granodiorite blocks mixed into the moat-derived sediments of the Osa mélange.

Seamounts and aseismic ridges are common features of oceanic plates. They interact with subduction zones—e.g., where the Louisville Ridge subducts at the Tonga-Kermadec trench—and it has been estimated that ~17% of the total length of modern subduction systems are subducting major high-relief features (Vannucchi et al., 2016). Raymond's (1984) map of global distribution of mélanges shows good correlation between mélanges and modern subducting seamount chains. The above evidence suggests that the accretion of seamount flexural moats is a previously unrecognized and globally significant mechanism for transferring seamount-derived sediments to the upper plate.

ACKNOWLEDGMENTS

We thank S. Dominguez, M. Cloos, N. Kukowski, J. Morgan, and two anonymous reviewers for their reviews, which greatly improved the manuscript. This research was funded by a UK International Ocean Discovery Program Rapid Response Grant to Vannucchi, and by the Geological Society of London.

REFERENCES CITED

- Buchs, D.M., 2008, Late Cretaceous to Eocene geology of the South Central American forearc area (southern Costa Rica and western Panama): Initiation and evolution of an intra-oceanic convergent margin [Ph.D. thesis]: Lausanne, Switzerland, Université de Lausanne, 230 p.
- Buchs, D.M., Baumgartner, P.O., Baumgartner-Mora, C., Bandini, A.N., Jackett, S.-J., Diserens, M.-O., and Stucki, J., 2009, Late Cretaceous to Miocene seamount accretion and mélange formation in the Osa and Burica Peninsulas (Southern Costa Rica): Episodic growth of a convergent margin, in James, K.H., et al., eds., *The Origin and Evolution of the Caribbean Plate*: Geological Society of London Special Publication 328, p. 411–456, <https://doi.org/10.1144/SP328.17>.
- Buchs, D.M., Hoernle, K., Hauff, F., and Baumgartner, P.O., 2016, Evidence from accreted seamounts for a depleted component in the early Galapagos plume: *Geology*, v. 44, p. 383–386, <https://doi.org/10.1130/G37618.1>.
- Burkhard, M., 1993, Calcite twins, their geometry, appearance and significance as stress-strain markers and indicators of tectonic regime: A review: *Journal of Structural Geology*, v. 15, p. 351–368, [https://doi.org/10.1016/0191-8141\(93\)90132-T](https://doi.org/10.1016/0191-8141(93)90132-T).
- Carey, S., Maria, T., and Cornell, W., 1998, Processes of volcanoclastic sedimentation during the early growth stages of Gran Canaria based on sediments from Site 953, in Weaver, P.P.E., et al., eds., *Proceedings of the Ocean Drilling Program, Scientific Results, Volume 157*: College Station, Texas, Ocean Drilling Program, p. 183–200, <https://doi.org/10.2973/odp.proc.sr.157.119.1998>.
- Cloos, M., and Shreve, R.L., 1996, Shear-zone thickness and the seismicity of Chilean- and Marianas-type subduction zones: *Geology*, v. 24, p. 107–110, [https://doi.org/10.1130/0091-7613\(1996\)024<0107:SZTATS>2.3.CO;2](https://doi.org/10.1130/0091-7613(1996)024<0107:SZTATS>2.3.CO;2).
- Collier, J.S., and Watts, A.B., 2001, Lithospheric response to volcanic loading by the Canary Islands: Constraints from seismic reflection data in their flexural moat: *Geophysical Journal International*, v. 147, p. 660–676, <https://doi.org/10.1046/j.0956-540x.2001.01506.x>.
- de Voogd, B., Palomé, S.P., Hirn, A., Charvis, P., Gallart, J., Rousset, D., Dafiobeitia, J., and Perroud, H., 1999, Vertical movements and material transport during hotspot activity: Seismic reflection profiling offshore: *Journal of Geophysical Research*, v. 104, p. 2855–2874, <https://doi.org/10.1029/98JB02842>.
- Dominguez, S., Malavieille, J., and Lallemand, S.E., 2000, Deformation of accretionary wedges in response to seamount subduction: Insights from sandbox experiments: *Tectonics*, v. 19, p. 182–196, <https://doi.org/10.1029/1999TC900055>.
- Fisher, D.M., Gardner, T.W., Sak, P.B., Sanchez, J.D., Murphy, K., and Vannucchi, P., 2004, Active thrusting in the inner forearc of an erosive convergent margin, Pacific coast, Costa Rica: *Tectonics*, v. 23, TC2007, <https://doi.org/10.1029/2002TC001464>.
- Ge, M.J.R., Watts, A.B., Masson, D.G., and Mitchell, N.C., 2001, Landslides and the evolution of El Hierro in the Canary Islands: *Marine Geology*, v. 177, p. 271–293, [https://doi.org/10.1016/S0025-3227\(01\)00153-0](https://doi.org/10.1016/S0025-3227(01)00153-0).
- Hauff, F., Hoernle, K., Tilton, G., Graham, D.W., and Kerr, A.C., 2000, Large volume recycling of oceanic lithosphere over short time scales: Geochemical constraints from the Caribbean Large Igneous Province: *Earth and Planetary Science Letters*, v. 174, p. 247–263, [https://doi.org/10.1016/S0012-821X\(99\)00272-1](https://doi.org/10.1016/S0012-821X(99)00272-1).
- Leslie, S.C., Moore, G.F., Morgan, J.K., and Hills, D.J., 2002, Seismic stratigraphy of the Frontal Hawaiian Moat: Implications for sedimentary processes at the leading edge of an oceanic hotspot trace: *Marine Geology*, v. 184, p. 143–162, [https://doi.org/10.1016/S0025-3227\(01\)00284-5](https://doi.org/10.1016/S0025-3227(01)00284-5).
- Meschede, M., Zweigel, P., Frisch, W., and Völker, D., 1999, Mélange formation by subduction erosion: The case of the Osa mélange in southern Costa Rica: *Terra Nova*, v. 11, p. 141–148, <https://doi.org/10.1046/j.1365-3121.1999.00237.x>.
- Moore, J.G., Normark, W.R., and Holcomb, R.T., 1994, Giant Hawaiian landslides: *Annual Review of Earth and Planetary Sciences*, v. 22, p. 119–144, <https://doi.org/10.1146/annurev.earth.22.050194.001003>.
- Morgan, J.K., Clague, D.A., Borchers, D.C., Davis, A.S., and Milliken, K.L., 2007, Mauna Loa's submarine western flank: Landsliding, deep volcanic spreading, and hydrothermal alteration: *Geochemistry Geophysics Geosystems*, v. 8, Q05002, <https://doi.org/10.1029/2006GC001420>.
- Oehler, J.F., Lénat, J.F., and Labazuy, P., 2008, Growth and collapse of the Reunion Island volcanoes: *Bulletin of Volcanology*, v. 70, p. 717–742, <https://doi.org/10.1007/s00445-007-0163-0>.
- Ranero, C.R., and von Huene, R., 2000, Subduction erosion along the Middle America convergent margin: *Nature*, v. 404, p. 748–752, <https://doi.org/10.1038/35008046>.
- Raymond, L.A., 1984, Prologue: The melange problem—A review, in Raymond, L.A. ed., *Mélanges: Their Nature, Origin, and Significance*: Geological Society of America Special Paper 198, p. 1–5, <https://doi.org/10.1130/SPE198-p1>.
- Sandwell, D.T., Müller, R.D., Smith, W.H.F., Garcia, E., and Francis, R., 2014, New global marine gravity model from CryoSat-2 and Jason-1 reveals buried tectonic structure: *Science*, v. 346, p. 65–67, <https://doi.org/10.1126/science.1258213>.
- Silver, E.A., Ellis, M.J., Breen, N.A., and Shipley, T.H., 1985, Comments on the growth of accretionary wedges: *Geology*, v. 13, p. 6–9, [https://doi.org/10.1130/0091-7613\(1985\)13<6:COTGOA>2.0.CO;2](https://doi.org/10.1130/0091-7613(1985)13<6:COTGOA>2.0.CO;2).
- ten Brink, U.S., and Watts, A.B., 1985, Seismic stratigraphy of the flexural moat flanking the Hawaiian Islands: *Nature*, v. 317, p. 421–424, <https://doi.org/10.1038/317421a0>.
- Tribble, J.S., Wilkens, R., Arvidson, R.S., and Busing, C.J., 1993, Sediments of the Hawaiian Arch: X-ray mineralogy and microfabric, in Wilkens, R.H., et al., eds., *Proceedings of the Ocean Drilling Program, Scientific Results, Volume 136*: College Station, Texas, Ocean Drilling Program, p. 65–76, <https://doi.org/10.2973/odp.proc.sr.136.205.1993>.
- Underwood, M.B., and Bachman, S.B., 1982, Sedimentary facies association within subduction complexes, in Leggett, J.K., ed., *Trench-Forearc Geology: Sedimentation and Tectonics on Modern and Ancient Active Plate Margins*: Geological Society of London Special Publication 10, p. 537–550, <https://doi.org/10.1144/GSL.SP.1982.010.01.35>.
- Vannucchi, P., Fisher, D.M., Bier, S., and Gardner, T.W., 2006, From seamount accretion to tectonic erosion: Formation of Osa Mélange and the effects of Cocos Ridge subduction in southern Costa Rica: *Tectonics*, v. 25, TC2004, <https://doi.org/10.1029/2005TC001855>.
- Vannucchi, P., Morgan, J.P., Silver, E.A., and Kluesner, J.W., 2016, Origin and dynamics of depositional subduction margins: *Geochemistry Geophysics Geosystems*, v. 17, p. 1966–1974, <https://doi.org/10.1002/2016GC006259>.
- Vening Meinesz, F.A., 1941, Gravity over the Hawaiian Archipelago and over the Madeira area: Conclusions about the Earth's crust: *Proceedings of the Royal Netherlands Academy of Arts and Science*, v. 44, <http://www.dwc.knaw.nl/DL/publications/PU00017532.pdf>.
- von Huene, R., Ranero, C.R., and Vannucchi, P., 2004, Generic model of subduction erosion: *Geology*, v. 32, p. 913–916, <https://doi.org/10.1130/G20563.1>.
- Wakabayashi, J., and Dilek, Y., 2003, What constitutes “emplacement” of an ophiolite?: Mechanisms and relationship to subduction initiation and formation of metamorphic soles, in Dilek, Y., and Robinson, P.T., eds., *Ophiolites in Earth History*: Geological Society of London Special Publication 218, p. 427–447, <https://doi.org/10.1144/GSL.SP.2003.218.01.22>.
- Watts, A.B., 1994, Crustal structure, gravity anomalies and flexure of the lithosphere in the vicinity of the Canary Islands: *Geophysical Journal International*, v. 119, p. 648–666, <https://doi.org/10.1111/j.1365-246X.1994.tb00147.x>.

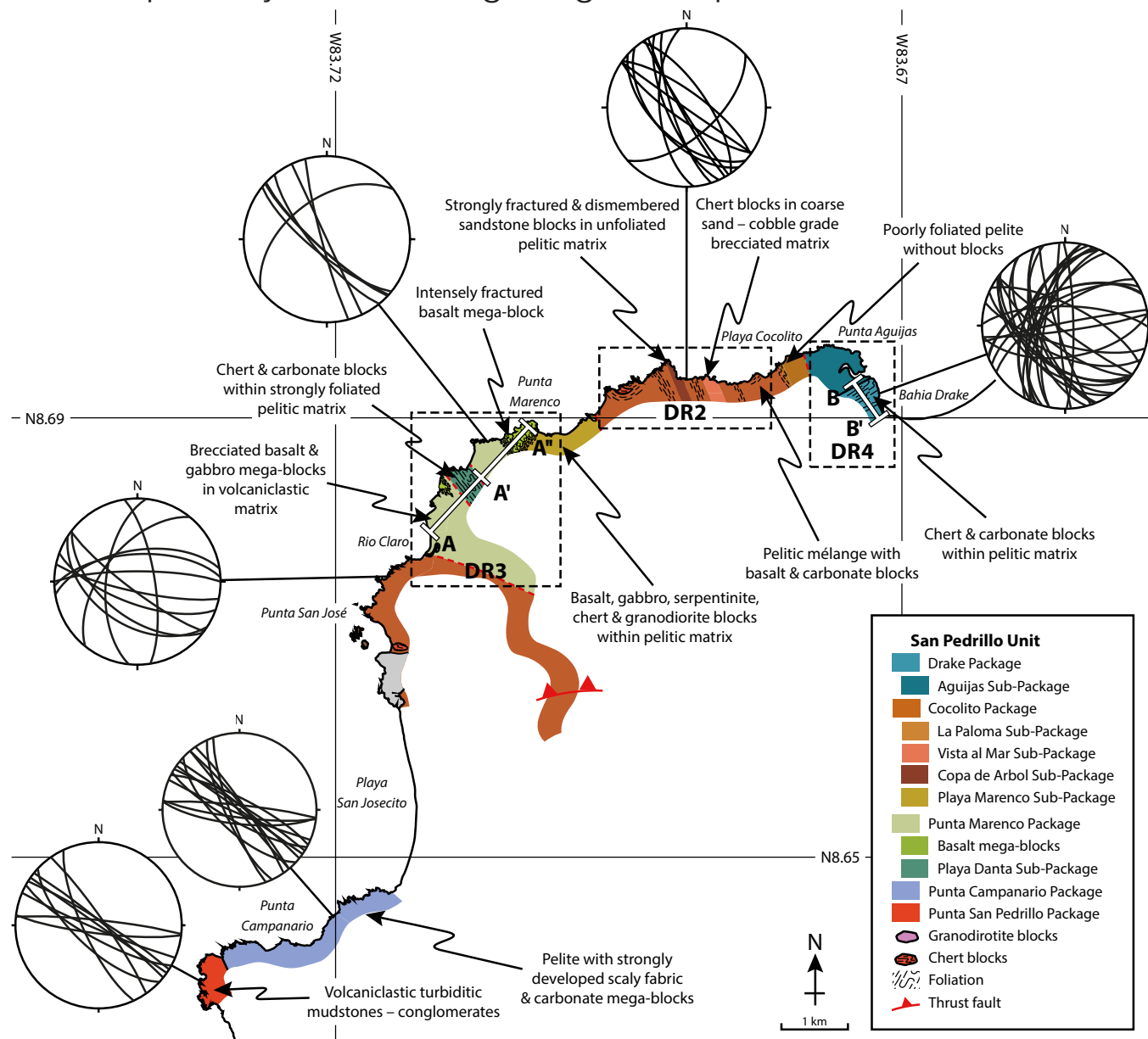
Manuscript received 2 March 2017

Revised manuscript received 15 January 2018

Manuscript accepted 18 January 2018

Printed in USA

Data Repository 1: Detailed geological map of the San Pedrillo Unit



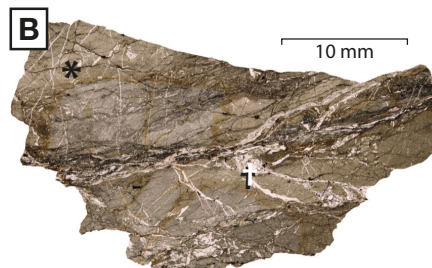
Geological map of the San Pedrillo Unit of the Osa mélangé from Bahia Drake to Punta San Pedrillo showing lithological and structural variation. Inset stereoplots show dominant foliation in each area.

Data Repository 2: Cocolito Package

The Cocolito package consists of low – moderate aspect ratio blocks of mudstone, sandstone, chert, carbonate, and basalt within a predominantly pelitic matrix (A). This matrix lacks a consistent foliation but possesses a strongly developed scaly fabric (B) with pervasive anastomosing slip surfaces and localised shear bands (B†). Some blocks are brecciated leading to progressive dismemberment towards the block margins. The La Paloma sub-package is a ~400 m thick pelite unit containing no blocks. The Vista al Mar sub-package has a coarse sand – cobble grade matrix consisting

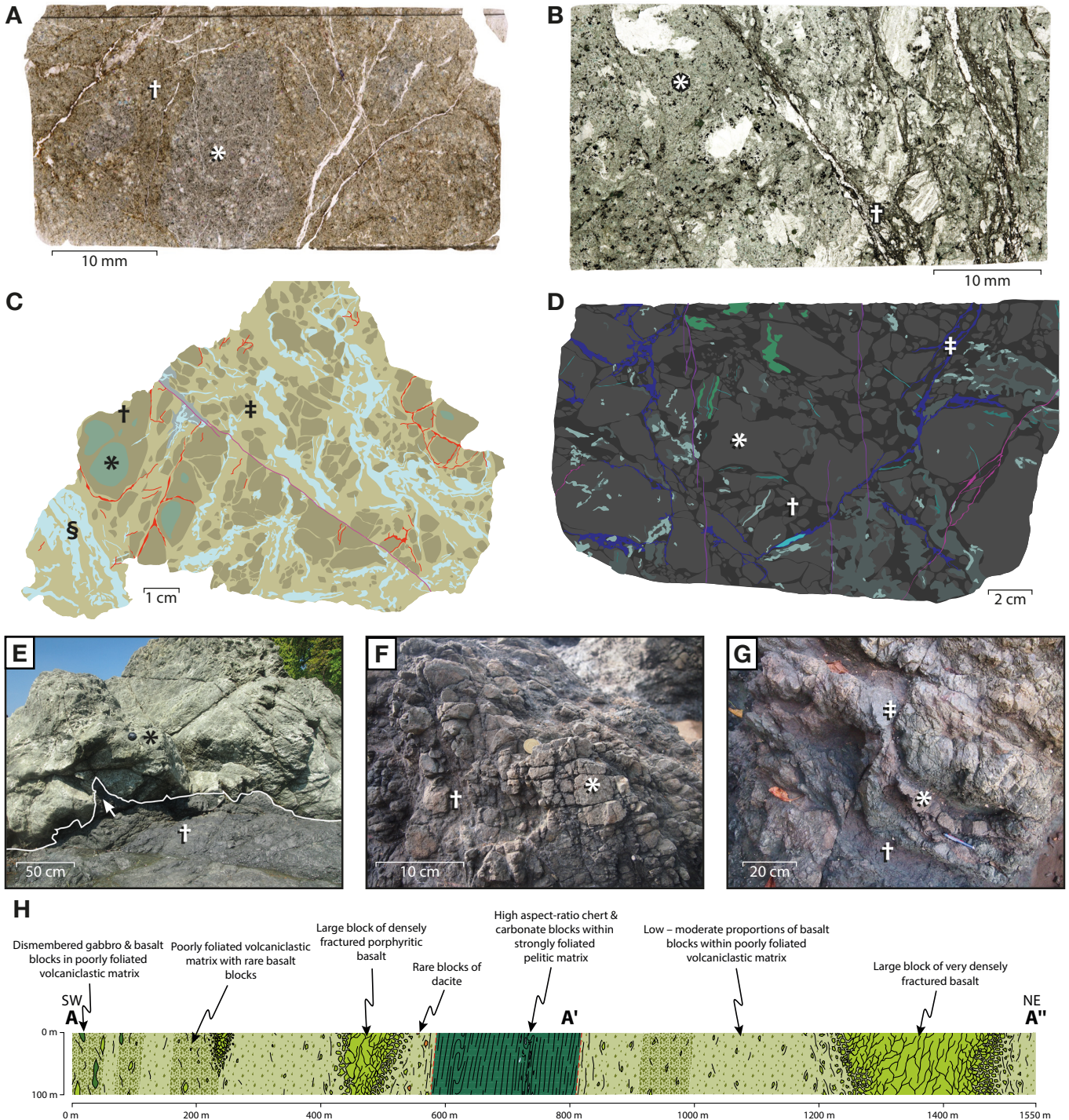
of red and teal chert with rare blocks of high aspect-ratio chert that display no preferred orientation. The Copa de Arbol sub-package features mudstone and sandstone blocks that are pervasively brecciated, and the Playa Marenco sub-package contains 10s of cm – 10s of m-scale blocks of basalt, gabbro, serpentinite and granodiorite.

A: Typical outcrop appearance of Cocolito package showing varied blocks (*) in unfoliated matrix (†) (N 8° 41' 39.5", W 83° 41' 31.2"). B: Pelitic matrix with scaly fabric (*) and localised shear bands (†) with veining concentrated along shear bands.



Data Repository 3: Punta Marengo Package

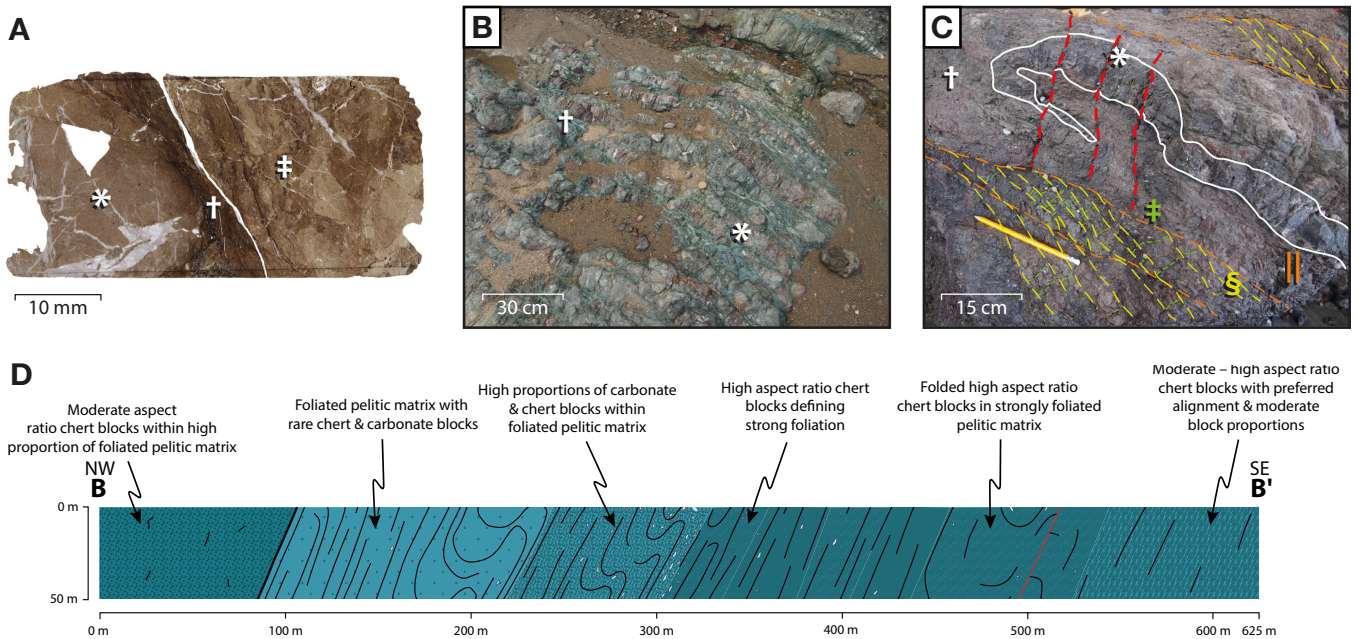
The Punta Marengo package consists of 100 m-scale mega-blocks of basalt within a volcanoclastic matrix. cm – 10s of m scale blocks of basalt, gabbros, chert and rare dacite are also present. Block aspect ratios are low – moderate and display no preferred orientation. Basalt mega-blocks are strongly brecciated with injections of matrix into the fractures leading to progressive dismemberment towards the block margins. This brecciation, combined with pervasive alteration of the basalt by through-going fluids, has led to the development a block-in-matrix texture within the basalt mega-blocks (A, C & F) Within this unit is the Playa Danta sub-package, a ~400 m-thick unit of dismembered chert and pelite displaying a strong foliation defined by block alignment.



A: Photomicrograph of altered basalt block showing “fresh” cores (*) containing unaltered feldspars and altered matrix (†) predominantly composed of clays. **B:** Photomicrograph of deformed volcaniclastic matrix showing phacoids (*) and localised shear zones (†). **C:** Illustrated interpretation of cut surface of altered basalt blocks showing “fresh” cores (*), partially altered core rims (†) and sheared matrix (‡) cut by folded calcite veins (§). **D:** Illustrated interpretation of cut surface of volcaniclastic matrix showing brecciated phacoids (*) in sheared matrix (†) with dark gouge-filled fractures (‡). **E:** Gabbro mega-block (*) in volcanoclastic matrix (†) with matrix injections into fractures (arrow) (N 8° 40' 50.5", W 83° 42' 43"). **F:** Brecciated basalt mega-block displaying brick-like geometric regularity (*) with “matrix” of comminuted basalt fracture fill (†) (N 8° 41' 22.7", W 83° 42' 13.3"). **G:** Dismembered chert & pelite with aligned high aspect ratio blocks (*) in pelitic matrix (†) cut by minor fault (‡) (N 8° 41' 30.8", W 83° 40' 18.0"). **H:** Cross-section from A to A'' in DR1 (A and A' in this figure corresponds to B and B' in Fig. 2).

Data Repository 4: Drake Package

The Drake package consists of strongly dismembered interbedded chert and pelite with minor blocks of carbonate and a strong foliation defined by block alignment. Chert blocks are typically cm – m-scale with moderate to ultra-high aspect ratios and occasional isoclinal folding. Carbonate blocks are m – 10s of m-scale lenticular blocks displaying pinch and swell structures. The Punta Aguijas sub-package to the north of Bahia Drake contains higher proportions of chert and lacks foliation.



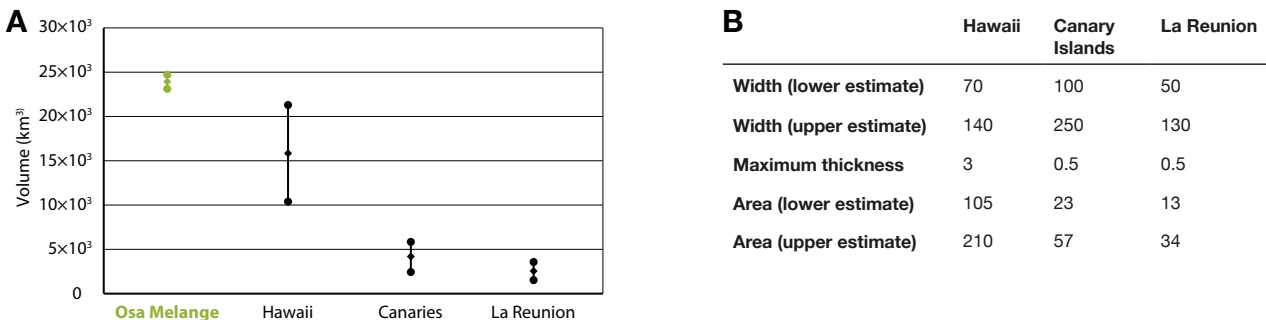
A: Photomicrograph showing fractured and veined pelite block (*) within sheared pelitic matrix displaying scaly fabric (†). Partially brecciated pelitic block (‡) also present. **B**: Aligned red chert blocks (*) within matrix of green pelite (†) (N 8° 41' 35.1", W 83° 40' 18.5"). **C**: Isoclinally folded chert block (*) within pelitic matrix (†) showing D₁ extensional fractures (‡, green), D₂ S surfaces (§, yellow) and D₂ C surfaces (||, orange) (N 8° 41' 26.6", W 83° 40' 17.4"). **D**: Cross-section from B to B' in DR1.

Data Repository 5: Comparative Scale of the Osa Mélangé and seamount moats/debris aprons

The cross-sectional area of Osa mélangé is derived by subtracting the estimated area of frontal prism from the estimated area of forearc wedge up to the landwards extent of the Osa mélangé (45 km); at this point, the thickness is estimated to be 10 km. The frontal prism extends from the trench to the seaward limit of the Osa mélangé (10 – 15 km) and the thickness at this point is calculated to be 2.2 – 3.3 km. This yields an Osa mélangé cross-sectional area estimate of 200 – 214 km². The volume of the Osa mélangé is estimated as the product of its cross-sectional area and its trench-parallel length (115 km), yielding an Osa mélangé volume estimate of 23.0 – 24.6 × 10³ km³.

The cross-sectional area of the Hawaiian, Canary Islands and La Reunion moat/debris apron deposits was calculated following the method described in ten Brink & Watts (1985), where the geometry of these basins is considered as a wedge and the thickness is calculated from the difference between the two-way-travel-time to the top of the sedimentary package and the basement and the p-wave velocity is considered to be 3.5 km/s.

Fig. A shows the estimated volumes of the Hawaiian, Canary Islands and La Reunion moat/debris apron deposits over an arbitrary length of 100 km in comparison to the volume of the Osa mélangé. This shows that the volume of the Osa mélangé is comparable (within 2 orders of magnitude) with the volume of modern moat/debris apron deposits.



A: Graph showing the estimated volume of the Osa mélangé and Hawaiian, Canary Islands and La Reunion moats, calculated as described in DR 5. Volumes for the Hawaiian, Canary Islands and La Reunion moats are calculated by multiplying the cross-sectional areas (B) by an arbitrary length of 100 km. **B**: Table showing values of width and thickness used to calculate estimated cross-sectional areas of Hawaiian, Canary Islands and La Reunion moats/debris aprons.

CHAPTER 7. WEAK BLOCKS IN A STRONG MATRIX:

The effects of rheological inversion on subduction zone seismicity

*Alexander P. Clarke¹, Paola Vannucchi^{1,2},
Audrey Ougier-Simonin³, Jason Morgan¹*

1: Royal Holloway, Egham Hill, Egham, Surrey, TW20 0EX, UK

2: Department of Earth Science, University of Florence, Via la Pira, 4, 50121 Florence, Italy

3: British Geological Survey, Keyworth, Nottingham, NG12 5GG, UK

The following chapter is a co-authored manuscript submitted to the Journal of Geophysical Research. Clarke, Vannucchi, and Ougier-Simonin were responsible for the initial study design; including sampling strategy and plans for the experiments. Geological mapping, sample collection and petrological analysis were conducted by Clarke. Rock mechanics experiments were performed by Clarke and Ougier-Simonin, and the resultant data was analysed by Clarke under guidance from Ougier-Simonin. Numerical modelling was undertaken by Clarke with input from Morgan. Ideas regarding the implications of rheological inversion on subduction zone seismicity were developed by Clarke, Vannucchi, and Morgan. The manuscript was authored by Clarke, modified following reviews by Vannucchi, Morgan, and Ougier-Simonin. The testing methodology (supplement) was part-written by Ougier-Simonin. Clarke illustrated all figures and took the field and microscopic photographs.

Mélanges are block-in-matrix rock units typically envisaged to consist of mechanically strong blocks within a relatively weak matrix. Triaxial deformation experiments on blocks and matrix from the Osa Mélange in southern Costa Rica reveal that this mélangé features blocks which are mechanically weaker than their surrounding matrix. Analysis of blocks and matrix in the Osa Mélange reveal that the basalt blocks have been weakened by mechanical brecciation and hydrothermal alteration while their

surrounding volcanoclastic matrix has been significantly indurated by compaction, diagenesis, and the development of mechanically strong lenticular fabric. As the Osa Mélange was frontally accreted and not subducted to significant depth, this inversion of the rheological relationship must occur early in the subduction process. With the rheological relationship inverted, our data show that low block to matrix ratios do not create conditions favourable to aseismic creep, as typically predicted, and high block to matrix ratios promote brittle failure regardless of the rheological relationships. Whether fractures form in the blocks or the matrix is dependent on the interplay between the difference in strength and the difference in Young's modulus of the two materials; while greater stress will concentrate in the stiffer and stronger material, as illustrated in our models, the lesser stress concentrating in the more compliant and weaker material may be sufficient to break it before the stronger material fails. Failure in one block promotes failure in its neighbouring blocks and in the surrounding matrix, which primes the subduction interface for a larger, through-going rupture. Failure of these blocks may be detectable as micro-seismic events analogous to tremors, and would precede the larger seismic rupture when the matrix fails.

7.1. INTRODUCTION

The plate boundary interfaces in subduction zones host Earth's biggest and most destructive earthquakes, as well as episodic tremors and slip (Rogers and Dragert, 2003; Ide *et al.*, 2007). A key element to investigate how megathrust slip nucleates and propagates is the study of the rock units within the plate boundary interface. Its structure is often conceptualised in detail as either a homogenous layer undergoing viscous deformation (e.g. Cohen, 1999) or a heterogeneous shear zone, also known as the subduction channel (Cloos and Shreve, 1988a; Vannucchi *et al.*, 2012), consisting of lenses of competent material within a strongly sheared matrix, analogous to the exhumed mélanges found in fossil subduction systems around the world (e.g. Fisher and Byrne, 1987; Cloos and Shreve, 1988a; Federico *et al.*, 2007).

Blocks are commonly conceived as being more competent than their surrounding matrix, so they act as rigid inclusions (e.g. Raymond, 1984a; Medley, 1997; Fagereng and Sibson, 2010).

WEAK BLOCKS IN A STRONG MATRIX

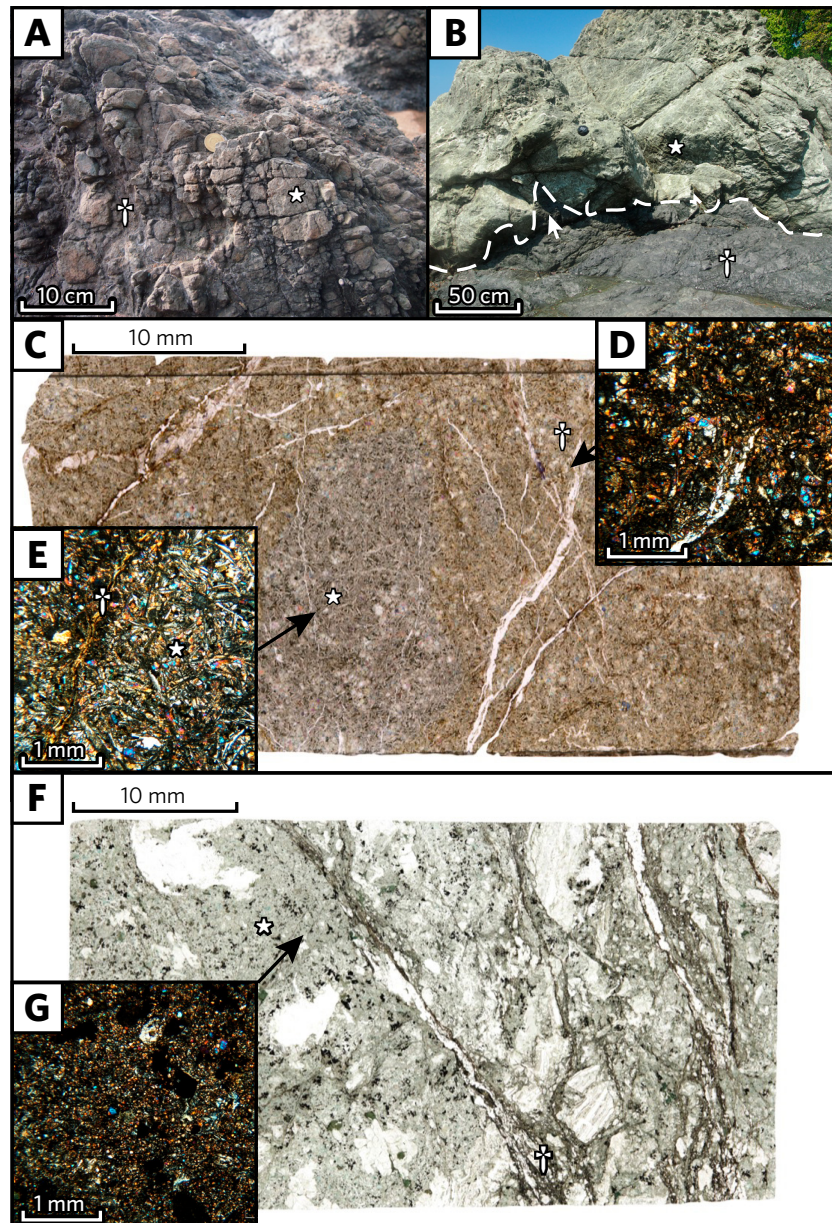


FIG. 7.2. Field photos and photomicrographs of blocks and matrix in the Punta Marengo Package. **A:** Brick-like brecciation at the edge of an altered basalt mega-block (*) with a "matrix" of comminuted basalt gouge (†). **B:** Gabbro mega-block featuring matrix injections at its margins (arrow) within a volcanoclastic matrix (†). **C:** Photograph of thin section of altered basalt showing relict cores (*) surrounded by altered material cut by zeolite veins (†). **D:** Photomicrograph of altered basalt with feldspars altered to dark brown clay and pyroxenes remaining. **E:** Photomicrograph of relict core showing intact feldspars (*) in groundmass and fracture with thin alteration rim (†). (Caption continued on opposite page.)

of the overall deformation through aseismic creep. Conversely, low block-to-matrix ratios are inferred to increase propensity for creep. In this case, creep refers to ductile flow, not aseismic slip along an existing brittle fracture (Sleep and Blanpied, 1992; Fagereng and Sibson, 2010). Even low block proportions are sufficient to act as flaws that weaken the subduction interface as a whole to promote creeping, whereas laterally homogenous subduction interfaces can concentrate more stress leading to greater ruptures (Scholl *et al.*, 2015). The potential for mega-thrust earthquakes can, therefore, be anticipated from the structure and rheological properties of the subduction channel (e.g. Kodaira *et al.*, 2002; Scholl *et al.*, 2015).

This paper reports findings that challenge the paradigm of mélanges as necessarily consisting of strong blocks within a weak matrix. Our recent work on the Osa Mélange in southwestern Costa Rica (Fig. 7.1) reveals that chemical alteration and mechanical brecciation of blocks in the shallow portion of the subduction zone (Fig. 7.2) coupled with diagenetic induration of the surrounding matrix may cause this rheological relationship to invert. Using a simple shear numerical model to simulate the subduction channel, we show that rheological inversion (weak and compliant blocks within a strong and stiff matrix) significantly impacts the seismic potential of a subduction zone.

7.2. GEOLOGY OF THE OSA MÉLANGE

The Osa Mélange is predominantly composed of blocks of basalt, chert and carbonate within a pelitic matrix. It has an overall low block-to-matrix ratio, and blocks are typically 10^{-2} – 10^2 m in size (Fig. 7.2). This mélange originated on the incoming plate by mass wasting from a seamount complex into its surrounding debris apron (Clarke *et al.*, 2018), accounting for the predominance of seamount lithologies within large volumes of quartz-poor sediment. The seamount complex was subducted ca. 50 – 10 Ma (Vannucchi *et al.*, 2006, and references therein) and its surrounding

FIG. 7.2. (CONTINUED) **F**: Photograph of thin section of volcanoclastic matrix (*) showing abundant micro-scale shear zones filled with dark clay gouge (†). **G**: Photomicrograph of volcanoclastic matrix showing fine-grained clasts of pyroxene within a matrix of dark brown clay.

WEAK BLOCKS IN A STRONG MATRIX

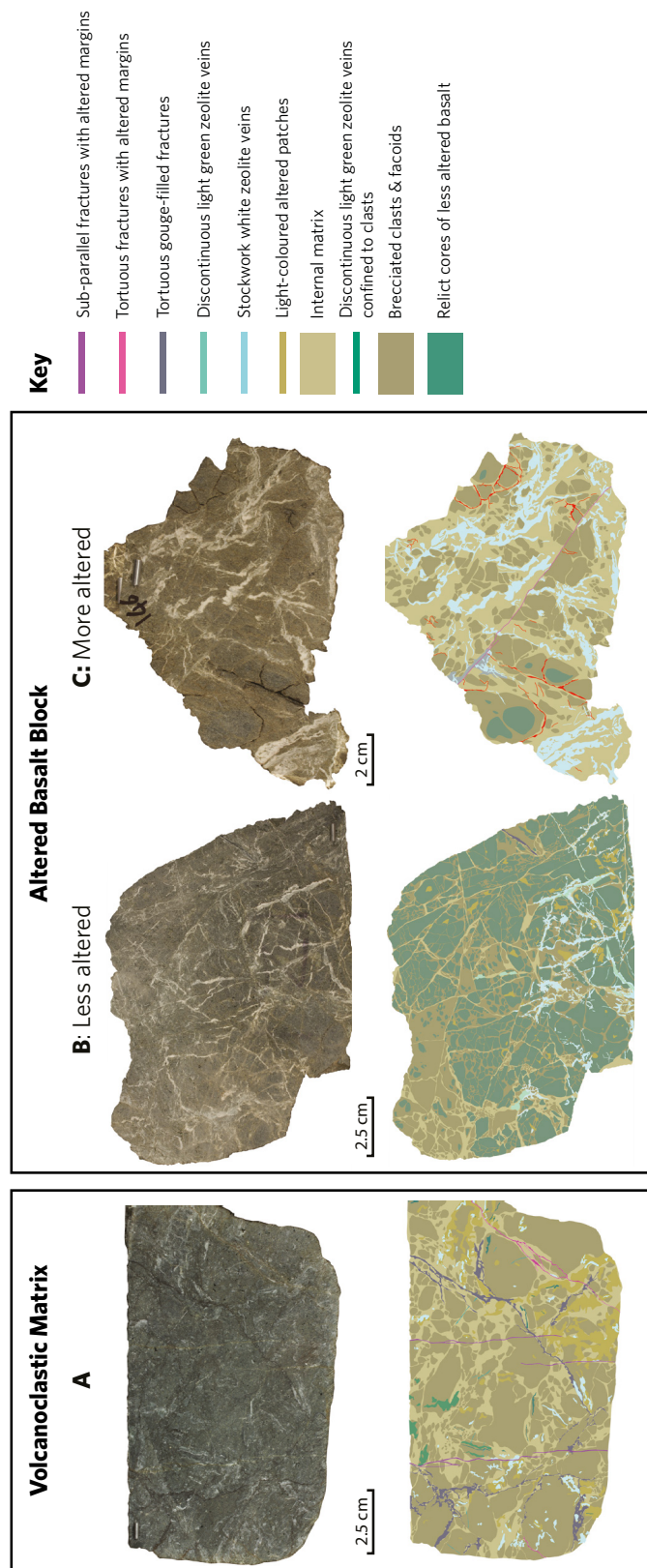


FIG. 7.3. Photographs (top) and schematic illustrations (bottom) of cut surfaces of the volcanoclastic matrix and two samples of altered basalt. **A:** Matrix composed of low aspect-ratio lenticular phacoids and cut by dark gouge-rich tortuous fractures and discontinuous veins. **B:** Less altered basalt is predominantly composed of relict basalt and brecciated clasts with little internal matrix of clay-rich gouge. **C:** More altered basalt is pre-dominantly composed of clay-rich gouge internal matrix with relict basalt cores. Matrix is extensively veined with zeolite.

debris apron was accreted to the Costa Rican margin in a localised frontal accretionary prism formed due to the local oversupply of sediment to the trench (Clarke *et al.*, 2018). This material was not subducted deeply, as evidenced by its lack of greenschist minerals or pervasive recrystallisation and by abundant calcite veins displaying twinning patterns typical of formation at ~200 – 250°C (Burkhard, 1993; Meschede *et al.*, 1999).

The largest blocks in this mélange are >100-m-scale megablocks of basalt which are surrounded by a clast-rich volcanoclastic matrix (Fig. 7.1). These blocks feature extensive fracturing and matrix injections with brick-like geometric regularity at their margins which has led to progressive dismemberment towards the edges of the blocks (Fig. 7.2a, b). The basalt blocks are intensely brecciated, veined and altered to clay. These ubiquitous clay alteration products (determined petrographically) fill feldspar pseudomorphs and dominate the groundmass, while fractured subhedral pyroxenes remain and olivines are rare (Fig. 7.2d). The basalts contain variable proportions of less altered basalt preserving intact feldspars; relict basalt is confined to the cores of brecciated clasts. Altered basalts are pervasively cut by zeolite veins. This altered basalt has a relatively high average porosity (measured using the saturation and buoyancy technique [ISRM, 2014]) of 5.7% and is pervasively cut by <1 mm wide unfilled fractures, although no vesicles or macro-scale inter-grain pore spaces are visible. The brecciated fabric of these basalt blocks is the product of 2 stages of brecciation followed by chemical alteration (Fig. 7.3b, c). Following the first phase of brecciation, passive chemical alteration of the margins of the clasts produces the distinction between the altered basalt in the outer portions of the clasts and the relict cores. Re-cementation followed by subsequent brecciation and further alteration of the clasts results in the observed texture with multiple relict cores per clast and cores located close to the margins of the clasts (Fig. 7.3b). Subsequent veining and fracturing preferentially cuts through the more altered basalt and reactivates pre-existing fractures (Fig. 7.3c).

The volcanoclastic matrix is mostly composed of clay, rounded silt-sized pyroxene grains, and basalt lithic clasts; as determined petrographically. This is pervasively cut by micro-scale anastomosing shear bands producing phacoids with a lenticular fabric

WEAK BLOCKS IN A STRONG MATRIX

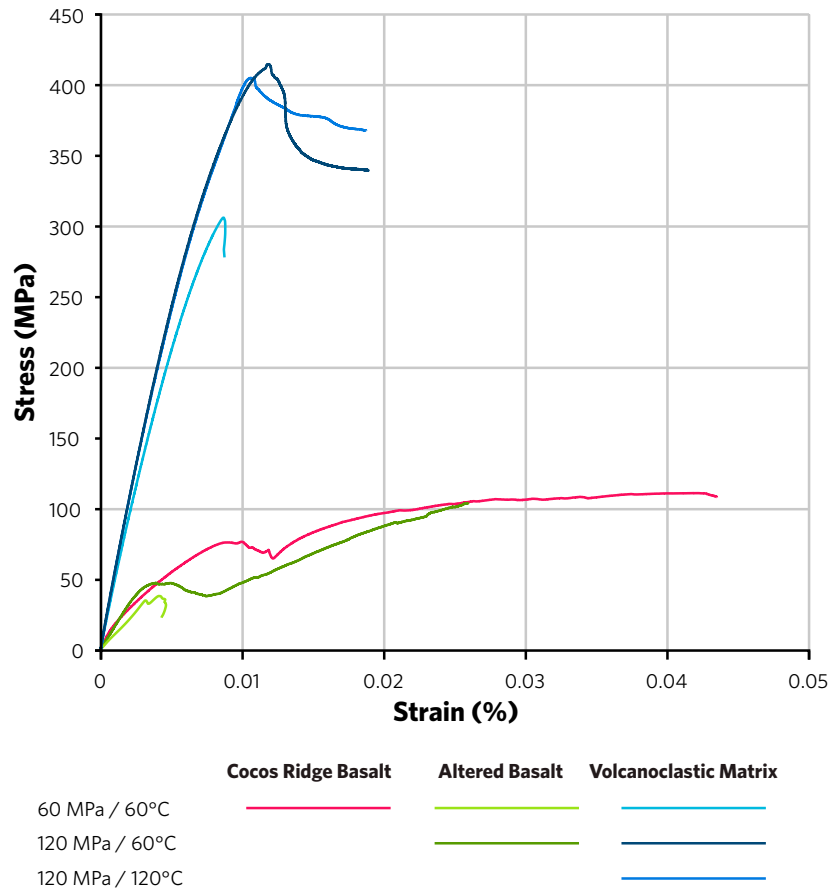


FIG. 7.4. Stress - strain graph showing the results of triaxial deformation experiments. Blocks (greens) exhibit lower yield stress, lower Young's modulus, and multi-stage failure, whereas the matrix (blues) exhibits high yield stress and higher Young's modulus. Cocos Ridge basalt (red) exhibits higher yield stress than the basalt blocks in the mélangé, but it has a similar Young's modulus. Failure of the altered basalt and Cocos Ridge basalt samples occurred catastrophically and no data is recorded post-failure.

similar in geometry to a scaly fabric but lacking the characteristic polished surfaces. This matrix is cut by anastomosing tortuous fractures filled with dark clay-rich gouge which preferentially reactivates shear bands between phacoids. The matrix contains a minor proportion of discontinuous veins but lacks the extensive veining seen in the basalt blocks (Fig. 7.3). This volcanoclastic pelite has a low average porosity of 1.0% and features no macroscopic intergranular pore spaces and minimal unfilled fractures.

7.3. EXPERIMENTAL DEFORMATION OF BLOCKS AND MATRIX

Triaxial deformation experiments were conducted at the Rock Mechanics and Physics Laboratory, British Geological Survey, UK, on the altered basalt and volcanoclastic matrix collected from the same locality. The complete description of the sample preparation and testing methodology is given in Supplementary Material. These experiments reveal that the matrix is approximately an order of magnitude stronger than the basalt under the same pressure and temperature conditions (Fig. 7.4; see also Table S1). At $P_c = 60$ MPa and $T = 60^\circ\text{C}$, the altered basalt has a strength (σ_1) of 38.5 MPa and a Young's modulus (E) of 12.2 GPa, while the volcanoclastic matrix has $\sigma_1 = 305.8$ MPa and $E = 40.6$ GPa. At higher pressure conditions of $P_c = 120$ MPa and $T = 60^\circ\text{C}$, the altered basalt has $\sigma_1 = 104.8$ MPa and $E = 4.2$ GPa, while the volcanoclastic matrix has $\sigma_1 = 414.8$ MPa and $E = 46.1$ GPa. The altered basalt exhibits a multi-stage failure mode with an initial stress drop at 45 – 92% of peak stress; this early failure may be attributed to initial cataclastic flow into a stronger configuration which can once again accumulate stress.

For comparison, we also analysed basalt recovered from the Cocos Ridge by IODP Exp. 344 (Harris *et al.*, 2013) as the closest analogue to the Osa Melange basalts prior to their subduction. This basalt is moderately altered and vesicular, with an average porosity of 4.9%. It is predominantly composed of plagioclase lathes in a groundmass altered to brown clay and exhibits low proportions of clinopyroxene; no glassy material is present. No crystallographic preferred orientation is exhibited. Vesicles are <1 mm in size, rounded, and equant and are uniformly distributed throughout the sample. The Cocos Ridge basalt at $T = 60^\circ\text{C}$ and $P_c = 60$ MPa has $\sigma_1 = 111.2$ MPa and $E = 7.6$ GPa. This is approximately three times as strong as the altered basalt from the melange, but is weaker than would be expected for a fresh, sub-aerially erupted basalt whose strength is well defined – e.g. Etna basalt: $\sigma_1 = 140$ MPa (Heap *et al.*, 2009) – and commonly considered to typify the strength of this lithology. The Cocos Basalt is also significantly weaker than the indurated volcanoclastic matrix that surrounds the blocks of altered basalt in the Osa Melange.

WEAK BLOCKS IN A STRONG MATRIX

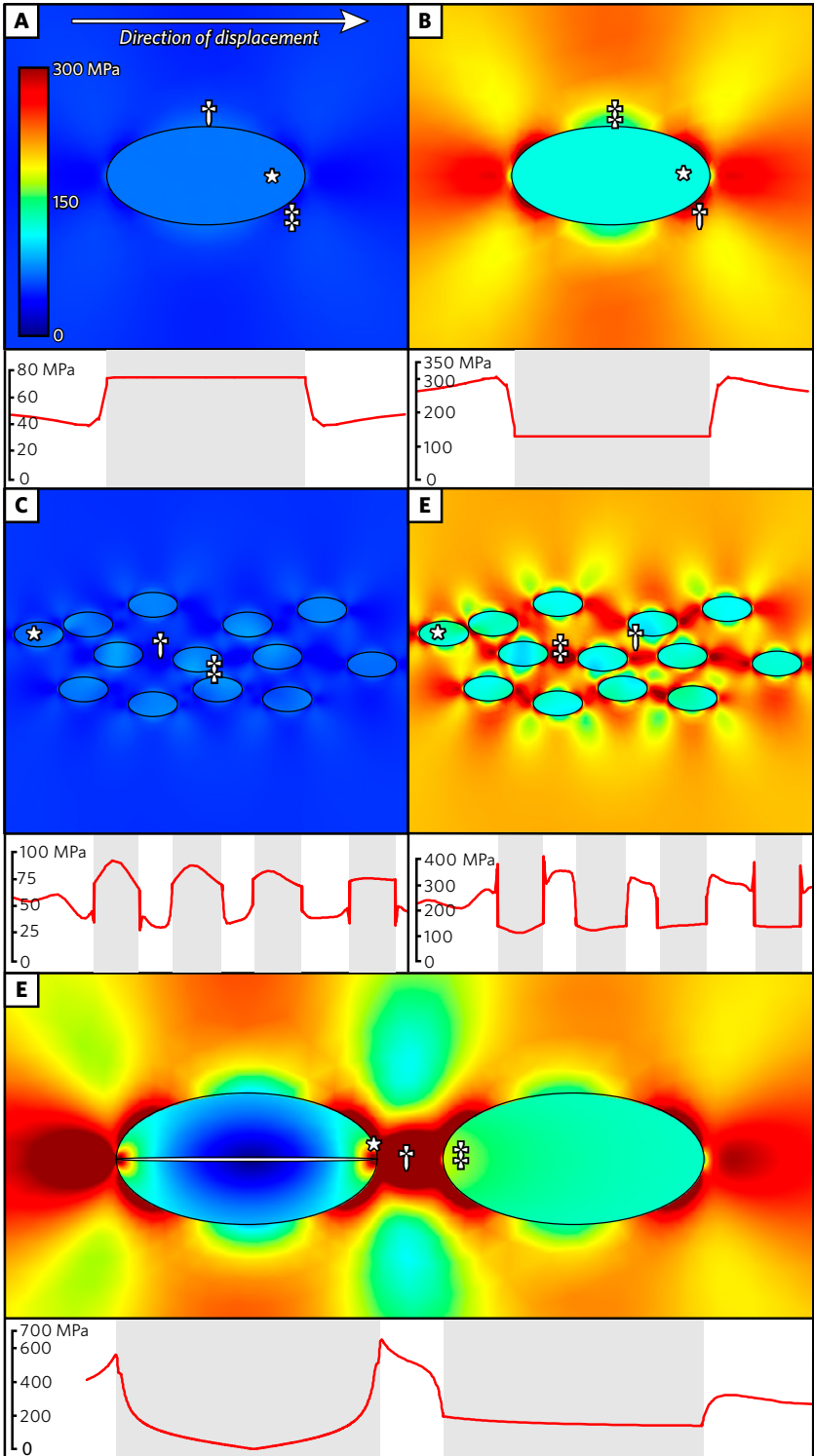


FIG. 7.5. (caption on opposite page.)

7.4. NUMERICAL MODELLING

To investigate the effects of this rheological inversion (blocks both weaker and more compliant than the matrix) on deformation within a subduction zone, we numerically modelled shear stress concentrations within a simple shear model as an analogy to deformation within a subduction channel. To study the elastic effects of different strengths and Young's moduli of the blocks and matrix on deformation within the subduction channel, we used the finite element modelling software Comsol Multiphysics® (www.comsol.com). In particular, we investigated shear (von Mises) stress concentrations in and around blocks within a rheologically distinct matrix during simple shearing. We modelled the blocks as elliptical inclusions within an otherwise homogenous matrix and varied the physical properties of the blocks and matrix.

FIG. 7.5. (CONTINUED) **A:** Von Mises stress concentrations around a single block in the normal rheological relationship (i.e. stiff blocks in a compliant matrix) showing uniform high stress within the block (*), stress maxima in the matrix around the block both parallel to and perpendicular to the direction of shearing (†) with stress minima oblique to the direction of shearing (‡). **B:** Stress concentrations around a single block in the inverted rheological relationship showing uniform low stress within the block (*), stress maxima in the matrix around the block oblique to the direction of shearing (†) and stress minima both parallel to and perpendicular to the direction of shearing (‡). **C:** Stress concentrations around multiple blocks in the normal rheological relationship showing increased stress in the blocks nearest their neighbours (*), stress minima between blocks in the direction of shearing (†) and stress maxima between blocks in the direction perpendicular to the direction of shearing (‡). **D:** Stress concentrations around multiple blocks in the inverted rheological relationship showing increased stress in the blocks nearest their neighbours (*), stress minima between blocks perpendicular to the direction of shearing (†) and stress maxima between blocks in the direction of shearing (‡). **E:** Stress concentrations around two blocks in the inverted rheological relationship, one of which has a fracture. Significant stress concentrates in block at the tip of the fracture (*), significant stress maxima between the two blocks in the direction of shearing with greatest stress adjacent to the fracture in the block (†), elevated stress in the adjacent block next to the fractured block (‡).

In these experiments, all physical properties were assumed to be isotropic. Stress was applied by sequentially increasing the prescribed shear displacement of the top surface from 0 to 10% of the model width and height while keeping the bottom surface fixed. Vertical bounding surfaces were treated as a periodic boundary condition and given a prescribed vertical displacement of zero to ensure overall simple shear. We modelled stress concentrations around a single block and clusters of blocks at varying distances from each other. To model the influence of a fracture within a failed block, an elliptical cavity was introduced; fractures within blocks and within the matrix were both modelled.

We used our experimentally derived strengths, Young's moduli and Poisson ratios for the altered basalt blocks and indurated volcanoclastic matrix at $P_c = 60$ MPa and $T = 60^\circ\text{C}$ as inputs into our models. For comparison, we also switched these experimentally derived properties to the opposite components to explore the stress distributions around blocks with a normal rheological relationship (i.e. the conventionally assumed stronger and stiffer blocks within a weak and compliant matrix).

To characterise the conditions where rheological inversion between blocks and matrix occurs within the parameter space of the difference in Young's modulus and the difference in strength (between the blocks and the matrix), we systematically varied the Young's modulus of the blocks and matrix to produce different values of the difference in Young's modulus and maximum Young's modulus (Fig. 7.6). We then compared the maximum stress concentrated within each component of the model with systematically varied strengths for both the blocks and the matrix. Failure in this model is inferred by stress concentrations exceeding the threshold of yield stress of the material, which is assessed separately during post-processing. Whether the matrix or blocks fail first (at lower values of displacement) is recorded and the difference in strength at which both components fail simultaneously is regarded as the point of rheological inversion.

Our models show greatest stress accumulation within the stiffer material. The maximum stress throughout the model is higher for the same displacement when the matrix has a higher Young's modulus than the blocks. Stress in the matrix

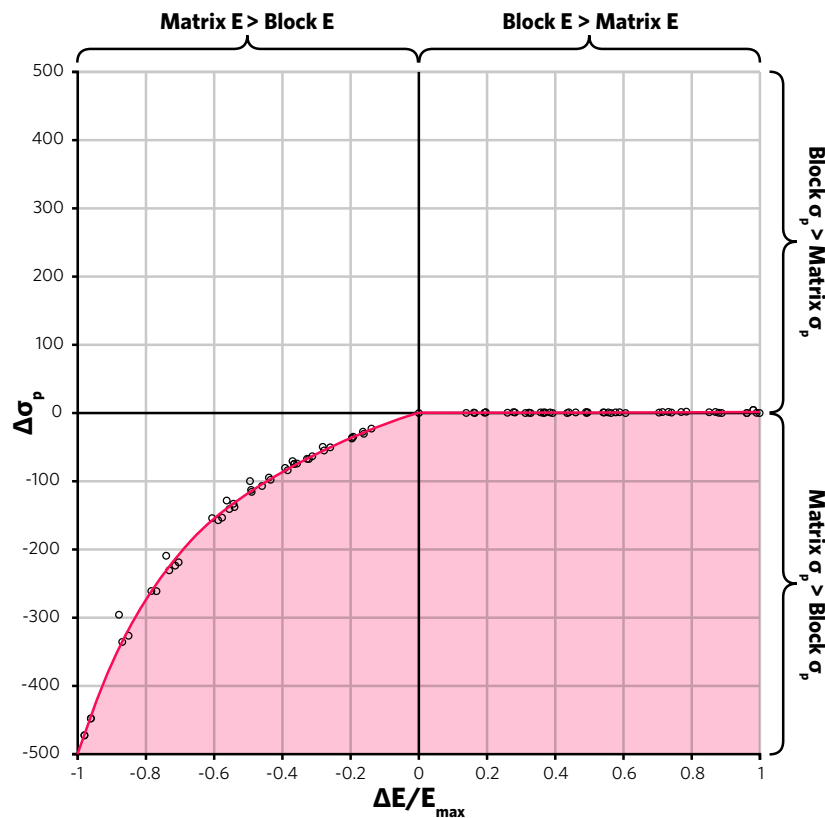


FIG. 7.6. Graph showing which component (block or matrix) will fail first with different rheological properties. In the area under the line (shaded in red), the blocks will fail preferentially to the matrix. Points plotted represent coincident failure of both components, used to connote the point of rheological inversion. The x-axis shows the difference in Young's modulus normalised to the Young's modulus of the stiffest material, where negative values indicate that the matrix has a higher Young's modulus than the blocks. The y-axis shows the difference in strength where negative values indicate that the blocks are weaker than the matrix. The top right quadrant denotes the conventional rheological relationship (e.g. Fagereng and Sibson, 2010), while the lower left quadrant denotes an inverted rheological relationship (this paper).

surrounding the furthest point of the block in both the orientation parallel to and perpendicular to the direction of shearing always approaches the stress level in the block. Where the block has a relatively high Young's modulus, the greatest stresses in the matrix are found at these points; where the block has a relatively low Young's modulus, the minimum stresses in the matrix are at these points. Conversely, when the block has a relatively high

WEAK BLOCKS IN A STRONG MATRIX

Young's modulus, the lowest stresses in the matrix are found at an angle from the direction of shearing that is a function of the block's aspect ratio; when the block has a relatively low Young's modulus, the peak stress in the matrix can be found at the same angle. Where blocks do not interact, stress concentrations in the blocks remain effectively uniform.

7.5. INTERPRETATION & IMPLICATIONS

Weakening of the basalt begins prior to subduction by seawater and seamount hydrothermal alteration — as evidenced by the already altered nature of the Cocos Ridge basalt found on the incoming plate. Additional early fracturing is linked to mass wasting and incorporation within the seamount's debris apron sediments. Circulating fluids within the sediment pile continue to progressively weaken the basalt blocks. The volcanoclastic matrix is weak, unconsolidated sediment at the surface at the time of initial mixing with the basalt blocks, but undergoes diagenesis and progressive strengthening during burial.

As this sediment package is subducted, the alteration and weakening of the blocks and induration of the matrix are enhanced by circulating fluids in the subduction zone, compression, and shearing. The increased fluid pressure leads to fracturing of the blocks and injections of the matrix into those fractures. The presence of these matrix injections demonstrates that, at this time, the blocks were the more competent material, and the matrix was still able to flow. Shear in the matrix leads to the development of the pervasive lenticular fabric which acts as a mechanically strong configuration. Induration of the matrix occurs during compaction associated with the rapidly increasing burial and the occurrence of low-temperature diagenetic mineral reactions. The measured high strength and Young's modulus of this material are likely to be the product of its mechanically strong texture, as geochemical and petrological analyses reveal no abnormalities to which the high strength and stiffness can be attributed. As the strength of the blocks decreases, so too does the block's Young's modulus. Similarly, the Young's modulus of the matrix increases as its strength increases.

The decreasing strength and Young's modulus of the blocks combined with the increasing strength and Young's modulus of the matrix eventually lead to the inversion of the original rheological relationship consistent with the present-day mechanical properties of the matrix relative to the basalt. Our experiments also imply that the difference in Young's modulus of the blocks and matrix will increase with increasing pressure and temperature conditions.

We conceive that stress within the subduction channel will accumulate until the deformation of one component accommodates that stress. After the rheological inversion has occurred, stresses within the blocks will exceed the block strength first, causing the blocks to fail before the greater stress concentrations within the matrix exceed the matrix strength.

Which component of the subduction interface — blocks or matrix — is the first to fail will depend on the interplay between the strength and Young's modulus of the materials (Fig. 7.6). While the Young's modulus of the blocks remains higher than the Young's modulus of the matrix, the magnitude of stress concentrations in the matrix around the block will approach that of the block itself (Fig. 7.5a). At this point, failure will occur in the weaker of the two materials; usually in the matrix. If the Young's modulus of the matrix exceeds that of the blocks, then the matrix will concentrate the greatest stress; however, this stress may be insufficient to fracture this material. At the same point, the lesser stress concentrated in the blocks may already be sufficient to break that material (Fig. 7.6). Due to these geometric effects on stress concentrations, failure need not always occur in the weaker or the higher Young's modulus material, and the point where rheological inversion occurs may not exactly coincide with inversion of strength or Young's modulus.

Fagereng and Sibson (2010) predict that, in the conventional rheological relationship, when the matrix volume fraction is higher, more strain will be accommodated through aseismic creep, while with a greater block fraction, there will be a greater propensity for seismic slip. Our numerical experiments (Fig. 7.5) indicate that after the inversion of the Young's modulus relationship, the matrix will become the least compliant component and higher proportions of matrix would not make aseismic creep

more favourable. However, higher block proportions would imply a reduced distance between blocks that would lead to increased stress concentrations between the blocks regardless of the contrast in elastic properties between the two materials. This means that higher block to matrix ratios will still increase the propensity for seismic slip, even when the rheological relationship between the two materials is inverted. The highest stress concentrations are observed in scenarios in which the matrix has a high Young's modulus and the blocks have a low Young's modulus. These high stress concentrations imply that the whole rock unit is at its weakest in these scenarios, meaning it will fail under lower regional stresses.

In the conventional rheological relationship, blocks will generate stress shadows in the matrix in the direction of shearing and stress concentrations perpendicular to the direction of shearing. When the rheological relationship is inverted, stress in the matrix will concentrate between blocks in the direction of shearing, increasing the likelihood of a through-going fracture (Fig. 7.5c, d). Blocks in the inverted scenario will also exhibit greater stress concentrations with increasing proximity to their neighbours, further reinforcing the relationship between higher block proportions and a greater propensity for large-scale seismic failure.

Once a fracture forms within a block, it will further concentrate stress near its tips (e.g. Griffith, 1920). When the fracture tip is in contact with the matrix, this additional concentration of stress may be enough to exceed the strength of the matrix, thereby propagating the fracture into the matrix (Fig. 7.5e). The presence of a fracture in one block will also increase stress concentrations in neighbouring blocks, meaning that a fracture in one block will tend to promote further deformation of its neighbouring weak blocks, even prior to failure of the intervening matrix. If stress concentrations are exceeding the yield stress of the material (assessed separately), fractures will also develop in these neighbouring weak blocks. As the mechanical and chemical weakening of the blocks is most active at the block margins, fractures in the blocks may follow these margins.

If a fracture already exists within the matrix, stress concentrating near the tip of that fracture will far exceed the stress

concentrated around or within the block, irrespective of its physical properties. However, if the matrix is deforming by distributed viscoelastic shear throughout the subduction channel, then ductile strain may accommodate the stress before it reaches the brittle yield stress of the material. Furthermore, fractures in the matrix that have arrested may heal during subsequent creep.

We suggest that failure of a larger block may be detectable as a micro-seismic event, with the rupture area, and energy release, limited by the size of the block (Wells and Coppersmith, 1994). As failure of one block will lead to further stress concentrations that promote failure of its neighbours, progressive block failure may be observable as a swarm of tremor-like micro-seismic events. A block fracturing event will weaken the plate boundary interface as a whole, as it will reduce the amount of intact material that can resist further displacement while increasing stress concentrations within the surrounding still-intact matrix. As such, failure of weaker blocks will prime the subduction interface for a major through-going rupture. If stress concentrations within the matrix adjacent to a failed block become sufficiently high to overcome the strength of this material, then the fracture may propagate into the matrix, triggering a through-going rupture event. Precursor swarms of micro-seismic events prior to major seismic ruptures have been observed in subduction zones around the world (e.g. Liu *et al.*, 2007). Accommodating deformation by failure of weak blocks promotes a higher frequency of smaller ruptures as no one failure event has a sufficient rupture area or accumulates sufficient stress to produce a large earthquake. However, in this scenario, tremor events do not relieve the overall stress on the plate interface. Instead, they represent increased loading on the stronger links within the fault and — if the surrounding matrix cannot be induced to creep — could lead to an earthquake at the exact same location.

7.6. CONCLUSIONS

Despite the common conception of a *mélange* as consisting of strong blocks within a weak matrix (Raymond, 1984; Fagereng and Sibson, 2010; Wakabayashi and Dilek, 2011), we report on a case in the Osa *Mélange*, SW Costa Rica, in which blocks of basalt have been weakened by progressive alternation as their

surrounding volcanoclastic matrix has been indurated to the point that the commonly conceived rheological relationship is inverted. This rheological inversion has occurred by the geochemical alteration and mechanical brecciation of the blocks with concurrent induration of the matrix through compaction, diagenesis and the development of a lenticular shear fabric.

In places where this strength inversion has occurred, the relationship between lower block to matrix ratios and more aseismic creep predicted by Fagereng and Sibson (2010) does not apply, as the matrix is now the least compliant component. *Mélanges* previously considered to have a low propensity for seismic slip due to their low block-to-matrix ratios may actually have a high propensity of seismic slip when the matrix acts as the more competent material. However, high block to matrix ratios will continue to promote brittle failure linked to the presence of local mechanical heterogeneity, independent of the rheological relationship. Where the Young's modulus of the matrix is higher than the Young's modulus of the blocks, whether fractures preferentially form in the matrix or in the block will depend on the interplay between the difference in Young's modulus and difference in strength of the two materials. Once a fracture forms in a block, this will lead to stress concentrations that promote failure in its neighbours and in the surrounding matrix. This effect could lead to a swarm of micro-seismic events analogous to tremors that may prime the subduction interface for a later through-going fracture associated with matrix rupture.

This process likely requires volcanoclastic sediment as inputs into the subduction zone plate interface as it requires a matrix with the potential for significant induration. This degree of induration without metamorphic recrystallization is likely to be unique to subduction zone settings as they provide a mechanism to rapidly increase overpressure during pervasive shearing. Basalt is highly abundant at the Earth's surface and readily alters in the presence of fluids to form clays. Incorporation of blocks of basalt into the subduction channel may occur by mass wasting (e.g. Osozawa *et al.*, 2009) onto the oceanic plate or by tectonic incorporation following subduction (e.g. Ikesawa *et al.*, 2005). Basalt blocks are commonly found in exhumed melanges — e.g. the Gwna

Mélange (e.g. Maruyama *et al.*, 2010), the Franciscan Mélange (e.g. Ogawa *et al.*, 2014), and the Mugi Mélange in the Shimanto Belt (e.g. Ikesawa *et al.*, 2005) – and as such the conditions necessary for rheological inversion may be common. Therefore, this process of rheological inversion during subduction is likely to be globally significant.

7.7. REFERENCES

- Arroyo, I.G., Grevemeyer, I., Ranero, C.R., and Huene, R. von, 2014, Interplate seismicity at the CRISP drilling site: The 2002Mw 6.4 Osa Earthquake at the southeastern end of the Middle America Trench: *Geochemistry, Geophysics, Geosystems*, v. 15, p. 3035 – 3050, doi: 10.1002/2014GC005359.
- Burkhard, M., 1993, Calcite twins, their geometry, appearance and significance as stress-strain markers and indicators of tectonic regime: a review: *Journal of Structural Geology*, v. 15, no. 3 – 5, p. 351 – 368, doi: 10.1016/0191-8141(93)90132-T.
- Clarke, A.P., Vannucchi, P., and Morgan, J., 2018, Seamount chain – subduction zone interactions : Implications for accretionary and erosive subduction zone behavior: *Geology*, v. 46, no. 4, p. 367 – 370, doi: 10.1130/G40063.1.
- Cloos, M., and Shreve, R.L., 1988a, Subduction-channel model of prism accretion, melange formation, sediment subduction, and subduction erosion at convergent plate margins: 1. Background and description: *Pure and Applied Geophysics*, v. 128, no. 3 – 4, p. 455 – 500, doi: 10.1007/BF00874548.
- Cloos, M., and Shreve, R.L., 1988b, Subduction-channel model of prism accretion, melange formation, sediment subduction, and subduction erosion at convergent plate margins: 2. Implications and discussion: *Pure and Applied Geophysics*, v. 128, no. 3 – 4, p. 501 – 545, doi: 10.1007/BF00874549.
- Cohen, S.C., 1999, Numerical models of crustal deformation in seismic zones: *Advances in Geophysics*, v. 41, p. 133 – 231.
- Fagereng, A., and Sibson, R.H., 2010, Melange rheology and seismic style: *Geology*, v. 38, no. 8, p. 751 – 754, doi: 10.1130/G30868.1.
- Federico, L., Crispini, L., Scambelluri, M., and Capponi, G., 2007, Ophiolite mélangé zone records exhumation in a fossil subduction channel: *Geology*, v. 35, no. 6, p. 499 – 502, doi: 10.1130/G23190A.1.
- Fisher, D., and Byrne, T., 1987, Structural Evolution of Underthrust Sediments, Kodiak Islands, Alaska: *Tectonics*, v. 6, no. 6, p. 775 – 793.

WEAK BLOCKS IN A STRONG MATRIX

- Griffith, A.A., 1920, VI. The phenomena of rupture and flow in solids: *Philosophical Transactions of the Royal Society of London. Series A, Containing Papers of a Mathematical or Physical Character*, v. 221, no. 582 – 593, p. 163 LP-198.
- Heap, M.J., Vinciguerra, S., and Meredith, P.G., 2009, The evolution of elastic moduli with increasing crack damage during cyclic stressing of a basalt from Mt. Etna volcano: *Tectonophysics*, v. 471, no. 1 – 2, p. 153 – 160, doi: 10.1016/j.tecto.2008.10.004.
- Ide, S., Beroza, G.C., Shelly, D.R., and Uchide, T., 2007, A scaling law for slow earthquakes: *Nature*, v. 447, no. 7140, p. 76 – 79, doi: 10.1038/nature05780.
- Ikesawa, E., Kimura, G., Sato, K., Ikehara-Ohmori, K., Kitamura, Y., Yamaguchi, A., Ujiie, K., and Hashimoto, Y., 2005, Tectonic incorporation of the upper part of oceanic crust to overriding plate of a convergent margin: An example from the Cretaceous-early Tertiary Mugi Mélange, the Shimanto Belt, Japan: *Tectonophysics*, v. 401, no. 3 – 4, p. 217 – 230, doi: 10.1016/j.tecto.2005.01.005.
- ISRM, 1983, Suggested methods for determining the strength of rock materials in triaxial compression: Revised version: *International Journal of Rock Mechanics and Mining Sciences & Geomechanics Abstracts*, v. 20, no. 6, p. 285 – 290, doi: [https://doi.org/10.1016/0148-9062\(83\)90598-3](https://doi.org/10.1016/0148-9062(83)90598-3).
- ISRM, 2014, *The ISRM Suggested Methods for Rock Characterization, Testing and Monitoring: 2007-2014* (R. Ulusay, Ed.): Springer International Publishing.
- Kodaira, S., Kurashimo, E., Park, J.O., Takahashi, N., Nakanishi, A., Miura, S., Iwasaki, T., Hirata, N., Ito, K., and Kaneda, Y., 2002, Structural factors controlling the rupture process of a megathrust earthquake at the Nankai trough seismogenic zone: *Geophysical Journal International*, v. 149, no. 3, p. 815 – 835, doi: 10.1046/j.1365-246X.2002.01691.x.
- Liu, Y., Rice, J.R., and Larson, K.M., 2007, Seismicity variations associated with aseismic transients in Guerrero, Mexico, 1995-2006: *Earth and Planetary Science Letters*, v. 262, no. 3 – 4, p. 493 – 504, doi: 10.1016/j.epsl.2007.08.018.
- Maruyama, S., Kawai, T., and Windley, B.F., 2010, *Ocean plate stratigraphy and its imbrication in an accretionary orogen: the Mona Complex, Anglesey-Lleyn, Wales, UK*: Geological Society, London, Special Publications, v. 338, no. 1, p. 55 – 75, doi: 10.1144/SP338.4.

- Medley, E., 1997, Uncertainty in estimates of block volumetric proportions in melange bimocks, in Marinos, P.G., Koukis, G.C., Tsiambaos, G.C., and Stournaras, G.C. eds., *Engineering Geology and the Environment, International symposium on Engineering Geology and The Environment*, Athens, Greece, p. 267 – 272.
- Meschede, M., Zweigel, P., Frisch, W., and Völker, D., 1999, Mélange formation by subduction erosion: the case of the Osa Mélange in southern Costa Rica: *Terra Nova*, v. 11, no. 4, p. 141 – 148.
- Ogawa, Y., Mori, R., Tsunogae, T., Dilek, Y., and Harris, R., 2014, New interpretation of the Franciscan mélange at San Simeon coast, California: tectonic intrusion into an accretionary prism: , no. April 2015, p. 37 – 41, doi: 10.1080/00206814.2014.968813.
- Osozawa, S., Morimoto, J., and Flower, M.F.J., 2009, “Block-in-matrix” fabrics that lack shearing but possess composite cleavage planes: A sedimentary mélange origin for the Yuwan accretionary complex in the Ryukyu island arc, Japan: *Bulletin of the Geological Society of America*, v. 121, no. 7 – 8, p. 1190 – 1203, doi: 10.1130/B26038.1.
- Raymond, L.A., 1984, Classification of melanges, in Raymond, L.A. ed., *Melanges: Their Nature, Origin, and Significance*, Geological Society of America.
- Rogers, G., and Dragert, H., 2003, Episodic Tremor and Slip on the Cascadia Subduction Zone: The Chatter of Silent Slip: *Science*, v. 300, no. 5627, p. 1942 – 1943.
- Scholl, D.W., Kirby, S.H., von Huene, R., Ryan, H., Wells, R.E., and Geist, E.L., 2015, Great (\geq Mw8.0) megathrust earthquakes and the subduction of excess sediment and bathymetrically smooth seafloor: *Geosphere*, v. 11, no. 2, p. 236 – 265, doi: 10.1130/GES01079.1.
- Sleep, N.H., and Blanpied, M.L., 1992, Creep, compaction and the weak rheology of major faults: *Nature*, v. 359, p. 139 – 141.
- Vannucchi, P., Fisher, D.M., Bier, S., and Gardner, T.W., 2006, From seamount accretion to tectonic erosion: Formation of Osa Mélange and the effects of Cocos Ridge subduction in southern Costa Rica: *Tectonics*, v. 25, no. 2, p. TC2004, doi: 10.1029/2005TC001855.
- Vannucchi, P., Sage, F., Phipps Morgan, J., Remitti, F., and Collot, J.-Y., 2012, Toward a dynamic concept of the subduction channel at erosive convergent margins with implications for interplate material transfer: *Geochemistry, Geophysics, Geosystems*, v. 13, no. 2, p. 1 – 24, doi: 10.1029/2011GC003846.

WEAK BLOCKS IN A STRONG MATRIX

- Wakabayashi, J., and Dilek, Y., 2011, Introduction: Characteristics and tectonic settings of mélanges, and their significance for societal and engineering problems, in Wakabayashi, J. and Dilek, Y. eds., *Mélanges: Processes of Formation and Societal Significance*, Geological Society of America.
- Wells, D.L., and Coppersmith, K.J., 1994, New Empirical Relationships among Magnitude, Rupture Length, Rupture Width, Rupture Area, and Surface Displacement: *Bulletin of the Seismological Society of America*, v. 84, no. 4, p. 974 – 1002.

7.8. SUPPLEMENTARY MATERIAL

7.8.1. Testing Methodology

The compressive strength and static elastic moduli of six samples under three different confining pressure and temperature conditions were determined using the ISRM suggested methods for determining the strength of rock materials in triaxial compression (ISRM, 1983). In total, we tested two altered basalt samples, three volcanoclastic matrix samples from the Marengo package, and one vesicular basalt sample recovered from the Cocos Ridge by IODP Exp. 344 (Harris *et al.*, 2013). The samples were all intact and tested in oven-dried conditions with no pore-fluid pressure applied. The samples did not present regularly oriented fabrics and were tested in a single orientation.

Cylindrical samples of 54 mm diameter were cut using a radial drilling machine tool equipped with a diamond-tipped hollow barrel. The cylinders were then trimmed with a diamond-tipped rock saw so that the length: diameter ratio was approximately 2:1; the end surfaces were ground to a flatness of <20 μm using a surface grinding machine tool. We placed all samples between two hardened steel platens and then encased them in a heat-shrink Polytetrafluoroethylene (PTFE) membrane to prevent ingress of confining fluid into the rocks. The samples were then instrumented with two axial extensometers (MTS 632.90F-12, accurate to $\pm 0.01\%$), positioned diametrically opposite each other over the central 50 mm of the sample, and a circumferential chain extensometer (MTS 632.92H-03, accurate to $\pm 0.01\%$) positioned at mid-length. A third platen, not part of the aforementioned specimen assembly, was spherically seated to prevent eccentric loading. This

	60 MPa / 60°C			120 MPa / 60°C			120 MPa / 120°C		
	Peak Stress (MPa)	Young's Modulus (GPa)	Poisson's ratio	Peak Stress (MPa)	Young's Modulus (GPa)	Poisson's ratio	Peak Stress (MPa)	Young's Modulus (GPa)	Poisson's ratio
ALTERED BASALT	38.5	12.2	0.39	104.8	4.2	0.93			
VOLCANOCLASTIC MATRIX	305.8	40.6	0.10	414.8	46.1	0.21	404.9	41.1	0.11
COCOS RIDGE BASALT	111.2	7.6	0.29						

Table Supplement 1: Summary of mechanical results, showing peak stress, static Young's modulus, and Poisson's ratio values for altered basalt, volcanoclastic matrix and Cocos Ridge basalt under 60 MPa/60°C, 120 MPa/60°C, and 120 MPa/120°C conditions. Grey cells indicate no data.

WEAK BLOCKS IN A STRONG MATRIX

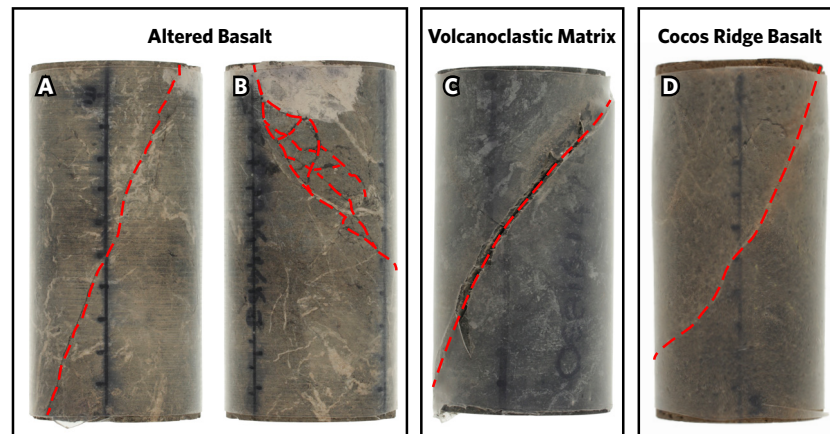


Fig. Supplement 1: Photographs of samples after experimental deformation. All samples experienced a through-going shear fracture forming an acute angle with the vertical maximum principle stress σ_1 . **A & B** show different deformation in the same cylinder of altered basalt as failure is accommodated by a single tortuous fracture where no relict cores are present (A) whereas fractures exploit and reactivate pre-existing fractures around and between the cores where present (B). **C**: Volcanoclastic matrix failed by a single fracture with visible displacement and a loss of cohesion. **D**: Cocos Ridge basalt failed by a single curved fracture with visibly negligible displacement and mild tortuosity.

spherically seated platen was in turn fixed to a 2.6 MN capacity force transducer (MTS 661.98B.01, accurate to $\pm 0.32\%$ of load) to measure the load applied to the sample.

Triaxial testing was undertaken at the Rock Mechanics and Physics Laboratory, British Geological Survey, UK, in an MTS 815 servo-controlled stiff frame inside a vessel capable of a confining pressure up to 140 MPa. The confining cell is fitted with external heater bands and utilizes cascade control from internal and external thermocouples (accurate to $\pm 0.5^\circ\text{C}$). An initial axial pre-load of 2.3 kN was applied, to ensure a stable contact and alignment of the platens. The confining pressure vessel was then closed and filled with mineral oil confining fluid. The axial pre-load was maintained while the confining pressure was applied at 2 MPa/min to 60 or 120 MPa; these values were chosen to approximately bracket the pressures at the up-dip limit of seismic nucleation, corresponding to 2 – 4 km depth (Arroyo *et al.*, 2014). At this

point, whilst held in axial force and confining pressure control, the rig was heated at 2°C/min to 60°C to approximate the average temperature conditions at the depth of the up-dip limit of seismic nucleation (Harris and Spinelli, 2010). The samples were then left for approximately 1 hour allowing thermal equilibrium to be reached throughout the confining fluid and the samples. Once stable, axial loading was initiated in constant axial strain rate control at a rate of $5.0 \times 10^{-6} \text{ s}^{-1}$ until macroscopic failure occurred or a significant amount of post-peak-stress axial strain was recorded (between 2% and 5%). We note that one test was conducted at the higher temperature of $T = 120^\circ\text{C}$ with a result within 2.5% of the strength at $T = 60^\circ\text{C}$ (Table 1). As this is below the expected sample-to-sample variability, no further temperature studies were conducted. The axial load, axial load actuator displacement, axial stress (σ_1), differential stress ($Q = \sigma_1 - \sigma_3$), confining pressure P_c ($= \sigma_2 = \sigma_3$), confining pressure actuator displacement, axial strain (ϵ_{ax}), circumferential strain (ϵ_{circ}) and temperature were monitored throughout at sampling frequencies of 1 s and 250 N.

Young's modulus was calculated as the tangent modulus for the linear elastic portion of the deformation curve. Poisson's ratio was calculated as the ratio between axial and circumferential strain.

7.8.2. Rock Mechanics Results

At P_c (confining stress) = 60 MPa and $T = 60^\circ\text{C}$, the volcanoclastic matrix has a strength of $\sigma_1 = 305.8$ MPa, which is about an order of magnitude higher than of the altered basalt blocks which is $\sigma_1 = 38.5$ MPa. The Cocos ridge basalt is nearly 3 times stronger with $\sigma_1 = 111.2$ MPa than the altered Osa Melange basalt, but about 3 times weaker than the volcanoclastic matrix. At $P_c = 120$ MPa ($T = 60^\circ\text{C}$) the altered basalt is considerably stronger, as could be expected, with $\sigma_1 = 104.8$ MPa, but still remains weaker than the volcanoclastic matrix which increased in strength to $\sigma_1 = 414.8$ MPa. The confining pressure increase has significantly reduced the strength difference between the altered basalt and the volcanoclastic matrix. At $P_c = 120$ MPa and $T = 120^\circ\text{C}$, we were only able to measure the strength of the volcanoclastic matrix and observed that it did not differ significantly from its value at $T = 60^\circ\text{C}$: $\sigma_1 = 404.9$ MPa and $\sigma_1 = 418.8$ MPa respectively. The

altered basalt exhibits a multi-stage failure with an initial stress drop at 45 – 92% of peak stress (as seen in Fig. 7.4).

All sample deformation resulted in a through-going shear fracture propagating through the sample forming an acute angle with the vertical maximum principal stress, σ_1 (all subsequent orientations are with respect to the vertical σ_1) (Fig. Supplement 1a, b and c). Whilst all other samples exhibit a single dominant fracture, the altered basalt deformed at $P_c = 60$ MPa exhibits an anastomosing fracture. The deformation was accommodated by a composite fracture formed by a straight slip surface in the most altered material oriented at 20° , and an anastomosing fracture network in the unaltered cores of the basalt clasts, where it reactivates pre-existing fractures at a range of angles from 0 to 80° either side of vertical (Fig. Supplement 1d). The volcanoclastic matrix deformed at $P_c = 60$ MPa failed developing a single curved fracture with orientation between 24° and 41° . This is the only sample with measurable slip of ~ 13 mm. All the other samples developed fractures with displacements so small that they were not measurable. At $P_c = 120$ MPa, the altered basalt developed a single curved fracture with orientation varying between 8° and 17° that did not cut through any unaltered basalt clast cores. The volcanoclastic matrix failed along a curved slip surface with a maximum angle of 56° and a minimum of 8° towards the edge of the sample; this also shows a secondary slip surface at 21° . The Cocos Ridge basalt failed by a single curved fracture with a varying orientation between 18° and 37° .

CHAPTER 8. DEFORMATION HISTORY OF THE OSA MÉLANGE, SW COSTA RICA, AND THE INFLUENCE OF ITS RHEOLOGY AND COMPLEX FABRIC ON SUBDUCTION EROSION IN CENTRAL AMERICA

*Alexander P. Clarke*¹, *Paola Vannucchi*^{1,2},
*Audrey Ougier-Simonin*³, *Jason Morgan*¹

1: Royal Holloway, Egham Hill, Egham, Surrey, TW20 0EX, UK

2: Department of Earth Science, University of Florence, Via la Pira, 4, 50121 Florence, Italy

3: British Geological Survey, Keyworth, Nottingham, NG12 5GG, UK

The following chapter is a co-authored manuscript intended for submission to Tectonics. Clarke, Vannucchi, and Ougier-Simonin were responsible for the initial study design; including sampling strategy and plans for the experiments. Geological mapping, sample collection and petrological analysis were conducted by Clarke. Rock mechanics experiments were performed by Clarke and Ougier-Simonin, and the resultant data was analysed by Clarke under guidance from Ougier-Simonin. Image analysis, along with the development of the structural anisotropy technique (Chapter 5.6), was conducted by Clarke. The manuscript was authored by Clarke, modified following reviews by Vannucchi and Morgan. Clarke illustrated all figures and took the field and microscopic photographs.

In southwestern Costa Rica, the Middle America Subduction Zone is tectonically eroding into the Osa Mélangé. This mélangé exhibits a complex preexisting fabric and consists predominantly of blocks of chert, carbonate, and basalt in a matrix of volcanoclastic pelite. This mélangé initially formed by mass wasting from a Galapagos-hotspot-related seamount complex onto the oceanic plate and was later accreted to the Caribbean Plate. Deformation and chemical alteration of the blocks and matrix strongly affected their mechanical properties, in some places causing an inversion of the common rheological relationship to produce weak blocks

within a strong matrix. Deformation associated with accretion also produced both a strong fabric in some areas and a chaotic fabric in others. The incorporation of the Osa Mélangé into the erosive plate boundary shear zone is controlled by the nature and orientation of its fabric and the rheology of its constituents. Weaker material is more readily comminuted while stronger material forms blocks within the subduction channel. Where the block-to-matrix aspect ratios are high, the orientation of the fabric controls the relative size and internal structure of the new blocks in the subduction channel. As the block-to-matrix ratios and frictional properties of the subduction channel influence seismic style, the fabric and rheology of the material entering the plate boundary interface from the upper plate influence the probability of earthquakes.

8.1. INTRODUCTION

The subduction erosion tectonic process removes material from the base of the forearc and accounts for approximately half of global subduction zones (Clift and Vannucchi, 2004; von Huene *et al.*, 2004). Tectonic erosion means that material of the upper plate – which is possibly already deformed – can be incorporated into the plate boundary shear zone, i.e. subduction channel (*sensu* Cloos and Shreve, 1988a, b; Vannucchi *et al.*, 2012), by way of hydrofracturing due to upwards migrating fluids (von Huene *et al.*, 2004). The effects of pre-existing rock fabrics on the incorporation of material into the subduction channel and its implications for plate boundary processes have so far been neglected. Study of the processes of subduction erosion is complicated by the paucity of erosive products preserved in the rock record (Vannucchi *et al.*, 2008), as these products are mostly consumed by the subduction zone. For this reason, previous studies of the lithologies and physical properties of the subduction zone plate interface have focused on accretionary environments where incoming plate sediments are the input material to the plate boundary interface and assume that plate boundary zones deform these materials to progressively higher pressure and temperature conditions (e.g. Brown *et al.*, 2003; Kurzwski *et al.*, 2016).

In erosive systems the upper plate input into the subduction channel can be composed of lithified – often crystalline – rocks

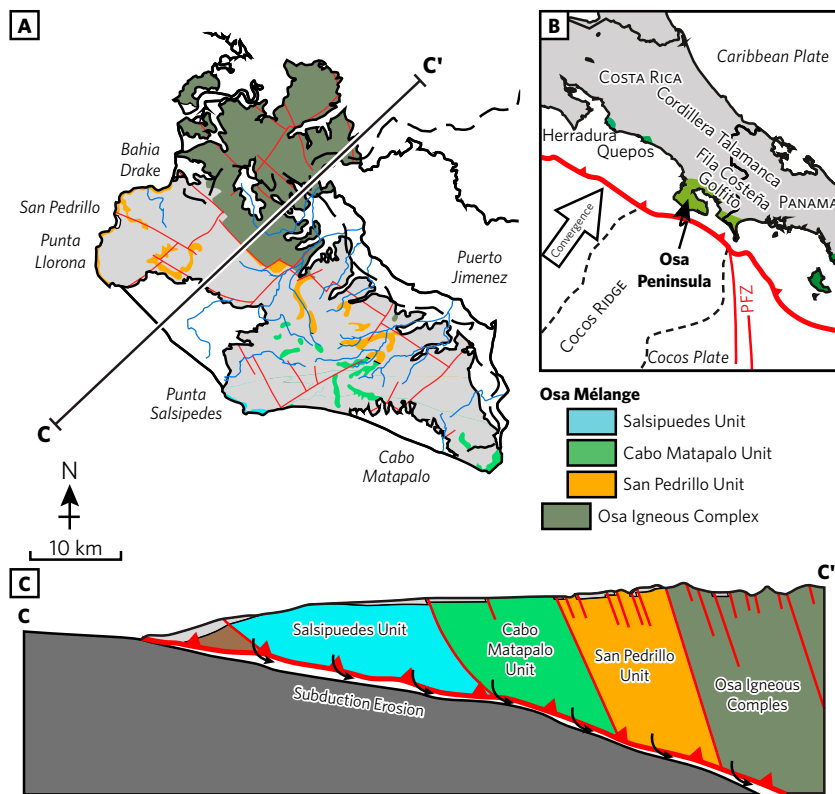


FIG. 8.1. **A:** Geological map of the Osa Peninsula (modified from Vannucchi *et al.*, 2006 and Clarke *et al.*, 2018) showing the outcrop distribution of the Osa Mélangé and the adjacent Osa Igneous Complex. **B:** Map of southern Central America showing the location of the Osa Peninsula and nearby features. **C:** Generalized cross section SW to NE through the Middle America forearc at the Osa Peninsula from C to C' on Fig. 8.1a (modified from Buchs *et al.*, 2009).

that commonly feature a highly structurally complex fabric produced by previous tectonic events (Clift and Vannucchi, 2004). Further complexity can result from the three-dimensional structure of the subduction system: Clarke *et al.*, (2018), for example, show that even in otherwise erosive subduction zones, locally thick accumulations of sediment – such as found in the debris aprons of seamount chains – can induce localized subduction accretion. The mechanical properties of this accreted material may also be significantly modified during the subduction/accretion process, causing weakening of some lithologies and dramatic induration of others (Chapter 7). In some cases, this process can lead to an inversion in the conventional rheological relationship

(Chapter 7). Although complex, these heterogeneous upper plates offer the possibility to look at specific processes within a limited portion of the subduction system.

Here we investigate the structure and the physical properties of the rock complex forming the forearc of the southern part of the Middle America Subduction Zone offshore Costa Rica: the Osa Mélangé (Fig. 8.1) (Stavnhagen *et al.*, 1998). The Middle America Subduction Zone is arguably the best studied erosive margin in the world (e.g. Ranero and von Huene 2000; Vannucchi *et al.*, 2001, 2003, 2013; Kinoshita *et al.*, 2006; Ranero *et al.*, 2008). Subduction erosion in southern Costa Rica is locally enhanced by the subduction of the Cocos Ridge (Vannucchi *et al.*, 2006), an aseismic ridge representing the trace of the Galapagos hotspot (Hoernle *et al.*, 2002). Recent IODP Exp. 334 and 344 results revealed that $1.2 \times 10^6 \text{ km}^3$ of forearc material, possibly Osa Mélangé-like rock complexes, was removed in $\sim 0.3 \text{ Ma}$ corresponding to an upward migration of 5.8 km of the plate boundary interface (Vannucchi *et al.*, 2013). Here we combine detailed field observations, microstructural analysis, and rock mechanics experiments on the poly-deformed Osa Mélangé to characterize the fabric and rheology of this material at present and to better understand how this material is incorporated in the subduction channel.

8.2. METHODS

This study incorporates field-based mapping, microstructural analysis, image analysis, and deformation experiments to holistically characterize the Osa Mélangé (see Supplement for detailed methodology). Field mapping focused on quantifying block-to-matrix proportions, describing block shape and orientation, characterizing the overall mélangé fabric, and detailing evidence of past rheological relationships. Due to vegetation cover inland, mapping was restricted to the coasts. Samples collected for further analysis included both blocks and matrix and care was taken to avoid introducing new fractures during the sampling process.

Aspect ratio and orientation of blocks were analyzed by image analysis of field photos following the methodology of Chapter 5.6. This was then plotted on a radar diagram with aspect ratio on the radial axis and orientation on the circumferential axis to produce an elliptical cloud of data points representative of the mélangé

fabric. An ellipse was fitted to the 95th percentile of this data cloud, the aspect ratio of which defines the “structural anisotropy value.” This structural anisotropy is regarded as a proxy for the mechanical anisotropy of the rock unit (Chapter 5.6).

Three types of rock mechanics experiments were conducted. Triaxial deformation experiments were conducted on samples of basalt blocks and volcanoclastic matrix under P-T conditions of confining pressure (P_c) = 60 MPa and temperature (T) = 60°C, P_c = 120 MPa and T = 60°C, and one sample of volcanoclastic matrix was tested at P_c = 120 MPa and T = 120°C; the results of this analysis are described in (Chapter 7). Strength analysis of a broad range of lithologies in the Osa Mélange was accomplished using the point load strength test (Franklin, 1985) on irregularly shaped samples. Samples collected from float or from outside the mapped area are attributed to their most similar unit within the mapped area. This technique produces the $Is_{(50)}$ value of strength, corresponding to the extrapolated strength of a sample 50 mm in size, and from which an estimated “equivalent unconfined compressive strength” can be derived. Porosity and density analysis were conducted using the non-destructive “saturation and buoyancy technique” (Franklin *et al.*, 1977; ISRM 2014). Unless otherwise specified, the density referred to in this article is particle density. The variation in porosity within a sample – measured as the standard deviation of the subsamples used to calculate the mean porosity for that sample – is here used as a proxy for material heterogeneity. Due to the size of the samples, the scale of heterogeneity we are measuring is on the centimetre scale.

8.3. GEOLOGY OF THE OSA MÉLANGE

The Osa Mélange is an intensely tectonised seamount-derived sediment package accreted to the Caribbean Plate in the Eocene – Miocene (Vannucchi *et al.*, 2006; Clarke *et al.*, 2018). This mélangé is predominantly composed of blocks of basalt, carbonate and chert within a fine-grained pelitic matrix, with approximately 75 – 90% sedimentary material. Basalt blocks have been partially altered to clay and are intensely fractured with volcanoclastic pelite derived from the matrix filling the fractures (Clarke *et al.*, 2018).

DEFORMATION HISTORY OF THE OSA MÉLANGE, SW COSTA RICA

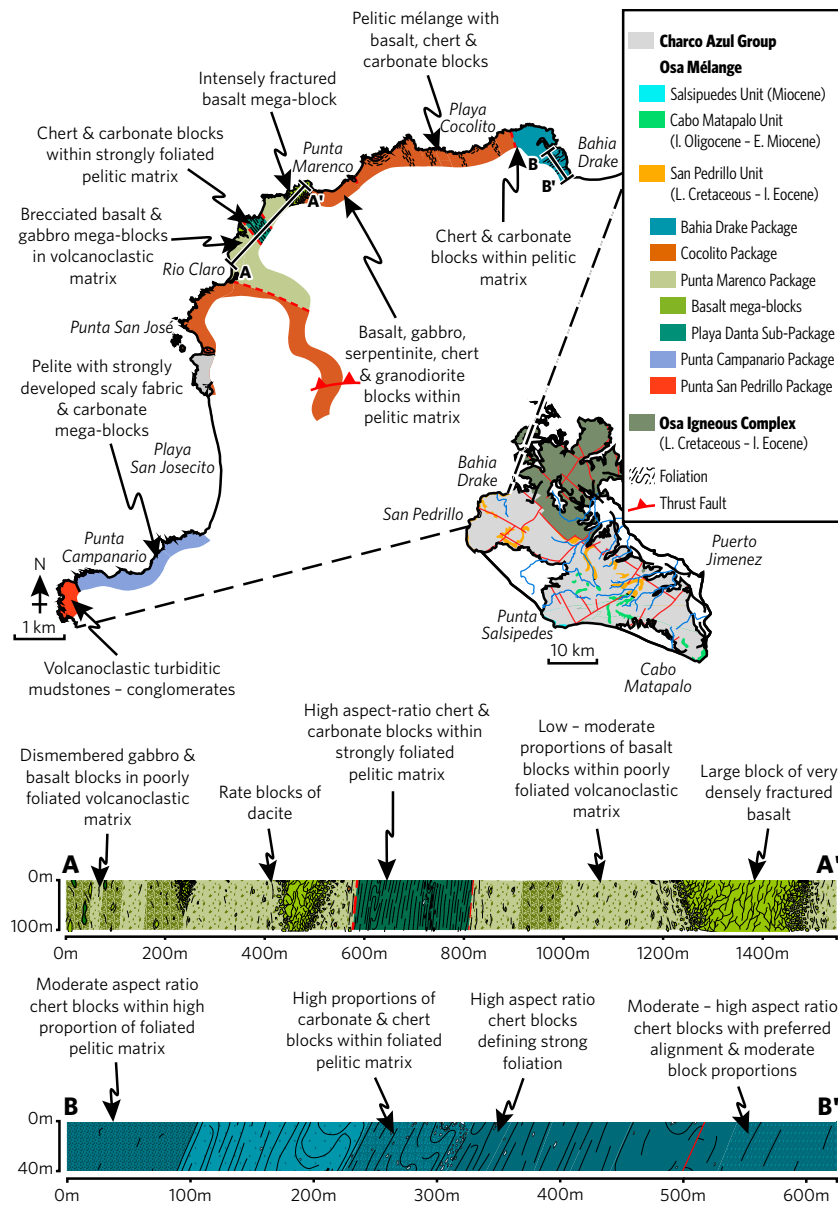


FIG. 8.2. **A:** Geological map of the San Pedrillo Unit (modified from Clarke *et al.*, 2018) showing the outcrop distribution and the mapped packages and sub-packages and the location of the mapped area on the Osa Peninsula. **B:** Schematic cross section of the Punta Marenco Package from A to A', showing dismembered basalt mega-blocks and the chert-rich Playa Danta Sub-Package. **C:** Schematic cross section of the Drake Package from B to B', showing folding in the chert and carbonate block-dominated unit.

The Osa Mélange consists of three main structural units defined by Di Marco *et al.* (1995); the San Pedrillo Unit, the Cabo Matapalo Unit, and the Salsipuedes Unit (Fig. 8.1). The San Pedrillo Unit – the oldest and largest unit of the Osa Mélange – consists predominantly of siliceous and volcanoclastic sandstones and pelites with blocks of basalts and carbonates. The Cabo Matapalo Unit contains blocks of recrystallized pelagic carbonates and basalts, whereas the Salsipuedes Unit is predominantly composed of carbonate blocks (Buchs *et al.*, 2009).

The San Pedrillo Unit – the primary focus of this study – is the largest unit in the Osa Mélange and the best exposed. Clarke *et al.*, (2018) subdivided the San Pedrillo Unit into five major packages exposed between Bahia Drake and Punta San Pedrillo (Fig. 8.2) on the basis of dominant block lithology and fabric.

1. Punta Marengo Package: Blocks and megablocks of basalt and gabbro in a volcanoclastic matrix (see Chapter 7).
2. Cocolito Package: Low aspect ratio blocks of chert, carbonate and basalt – with minor components of serpentinite and granodiorite – within high proportions of pelitic matrix.
3. Bahia Drake Package: Strongly dismembered and high aspect ratio chert blocks in a pelitic matrix with minor blocks of carbonate.
4. Campanario Package: Foliated and strongly deformed pelite displaying a lenticular fabric.
5. Punta San Pedrillo Package: Densely faulted interbedded conglomerate, sandstone, and mudstone broken formation (Hsü, 1968).

8.3.1. Punta Marengo Package

The Punta Marengo Package (Fig. 8.1), exposed from Punta Marengo to Rio Claro, contains 10s – 100s of meter-scale megablocks of basalt and gabbro within a volcanoclastic matrix. Rare metre – 10s of metre scale blocks of dacite are also present in this package (Fig. 8.2g). These blocks feature extensive fracturing and brecciation with matrix injections at block margins (Fig. 8.3c), in places leading to progressive dismemberment towards the block margins. Block aspect ratios are low to moderate and display no preferred orientation (Fig. 8.3m – p).

DEFORMATION HISTORY OF THE OSA MÉLANGE, SW COSTA RICA

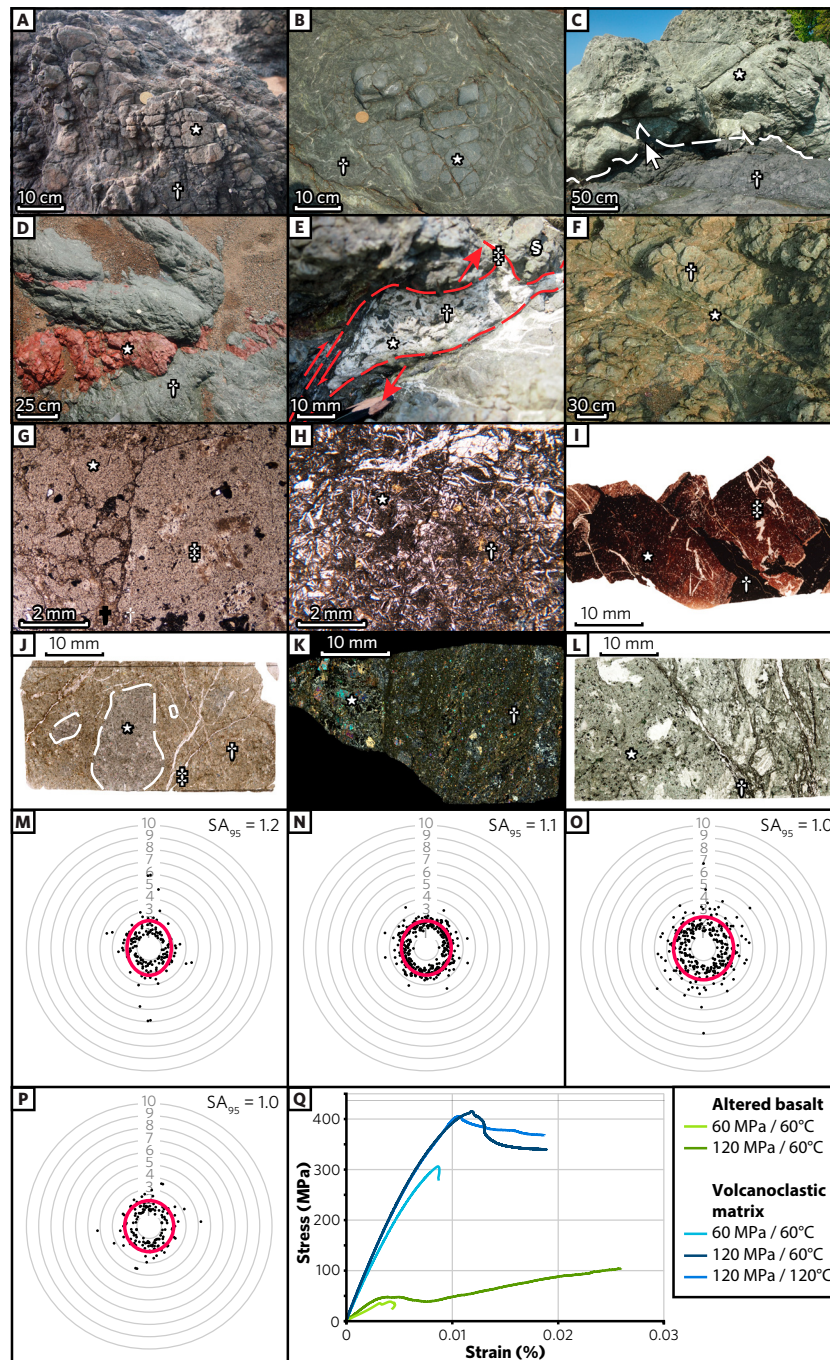


FIG. 8.3. Photographs and data for the Punta Marenco Package. **A:** Brecciated basalt block with brick-like geometric regularity of clasts (*) and interstitial gouge matrix (†). **B:** Dismembered gabbro block (*) within green, veined volcanoclastic matrix (†). **C:** Gabbro mega-block (*) in volcanoclastic matrix (†) with matrix injections into fractures (arrow). (Caption continued on opposite page.)

Basalt blocks in the Punta Marengo Package are typically fine-grained (50 – 400 μm), with abundant acicular plagioclase lathes and smaller olivine and clinopyroxene crystals with no alignment of crystals. The basalt is strongly brecciated into centimetre-scale clasts, with some showing brick-like geometric regularity and others displaying a high degree of irregularity (Fig. 8.3a). Brecciated clasts within these blocks typically feature aspect ratios of $AR = \leq 3:1$ – with a weak preferential orientation of the high aspect ratio clasts and the highest aspect ratio clasts (7:1) occurring parallel to this orientation – giving this material a weak average structural anisotropy value of $SA_{95} = 1.0 - 1.2$ (Fig. 8.3m – p) – although larger blocks were observed in the field to have higher aspect ratios. These blocks are pervasively altered to moderately Al-rich clay minerals and cut by abundant, randomly orientated,

Fig. 8.3. (CONTINUED) **D:** Internally dismembered red chert block (*) within volcanoclastic matrix (†). **E:** Dilational jog implosion breccia showing white zeolite vein fill (*) supporting highly angular clasts of basalt wall rock displaying jig-saw fit (†). Vein injects (‡) into fractures within brecciated basalt wall rock (§). **F:** Thick straight vein (*) cutting brecciated basalt block (†). **G:** Photomicrograph of brecciated basalt showing sub-rounded clasts (*) in matrix of comminuted gouge (†). Basalt is strongly altered and feldspar phenocrysts are pervasively altered to clay (‡). **H:** Photomicrograph of fractured and altered basalt showing pseudomorphs of plagioclase entirely replaced by clay (*) and growth of epidote within a dark clay groundmass (†). **I:** Photomicrograph of deformed red chert block showing cyclical grading in grain size and colour (*), showing injection structure of dark haematitic chert into coarser-grained bed (†) and folded and dismembered quartz veins (‡). **J:** Thin section of altered basalt showing less altered core (*) surrounded by pervasively altered basalt (†) and cut by zeolite veins (‡). **K:** Thin section showing the edge of an altered gabbro block (*) within a matrix of volcanoclastic pelite and comminuted gabbro (†). **L:** Thin section of volcanoclastic matrix (*) pervasively cut by anastomosing shear zones (†). **M – P:** Structural anisotropy diagrams produced by image analysis of photos of the Punta Marengo Package, showing overall low values of structural anisotropy. **Q:** Stress/strain graph showing results of triaxial deformation experiments (modified from Chapter 7). Altered basalt is shown to fail at a consistently lower peak stress than the volcanoclastic matrix.

folded zeolite veins within the internal matrix. The brecciated clasts commonly feature relatively less altered regions which are themselves brecciated, suggesting two phases of brecciation. In the most altered basalt, these regions correspond to the cores of the altered clasts, whereas less altered basalt contains less altered regions which are located at or near to the clast margins (Fig. 8.3j). Small-scale parallel shear fractures cut this brecciated and altered fabric, and minor extensional fractures cut the matrix surrounding clasts with relatively unaltered cores. One dilational jog containing brecciated clasts displaying jig-saw fit suspended entirely in vein material – interpreted as an implosion breccia – was observed in the field (Fig. 8.3e) within a brecciated basalt megablock. The fracture hosting this implosion breccia cuts the brecciated fabric and is not observed to be cut by later fractures. The altered basalt blocks are mechanically weak – as shown by Chapter 7 – with strengths of $I_{s(50)} = 1.4 - 1.5$, and feature moderate porosity of $\phi = 5.5$ and a low degree of heterogeneity at $H = 0.3 - 0.8$ (Fig. 8.4).

The volcanoclastic matrix in the Punta Marenco Package is a matrix-supported breccia containing a high proportion of basaltic lithic fragments ranging from millimetre to metre-scale, and plagioclase and clinopyroxene grains (Fig. 8.3l). This brecciation is tectonically enhanced with clasts of both basalt lithics and clasts of volcanoclastic sandstone displaying a weak planar elongation. Aspect ratios within the matrix are typically $\leq 4:1$ with weak preferred orientation resulting in structural anisotropy values of $SA_{95} = 1.0 - 1.1$ (Fig. 8.3m – p). This defines a weak anastomosing fabric featuring lenticular phacoids with the same geometry as in scaly fabric but typically lacking the polished surfaces characteristic of that texture. Short, randomly orientated, discontinuous zeolite veins up to 5 mm wide cut this fabric, but are often themselves cut by shear planes defining the foliation within the internal matrix. The degree of veining within the matrix is significantly lower than that within the blocks. The pervasive alteration of basalt lithics seen in the blocks is not seen in the matrix. Anastomosing, tortuous fractures filled with a dark gouge cut this fabric with little consistency in orientation, and these are themselves cut by two sets of later fractures surrounded by thin alteration rims at a high angle to the foliation. While the coarser

grained volcanoclastic breccia and sandstone has been significantly indurated ($Is_{(50)} = 3.1$, see also Fig. 8.3r and Chapter 7), the fine grained pelite in this unit is notably weak, with variable strengths of $Is_{(50)} = 0.6 - 1.4$. These volcanoclastic pelites feature highly variable porosity of $\phi = 1.7 - 13.1$ and also exhibit variable degrees of heterogeneity, ranging from $H = 0.4 - 19.2$. Chert blocks within the Punta Marengo Package feature moderate strength with $Is_{(50)} = 3.0$, low - moderate porosity of $\phi = 2.0$, and a low heterogeneity of $H = 0.5$ (Fig. 8.4).

Gabbro blocks at Rio Claro (N 8.680215°, W 83.711949°) display a significantly lower density of fractures than the basalt and they are less altered than the basalts, preserving some of their primary mineralogy. Some brecciation is present within the gabbro (Fig. 8.3b) and these blocks frequently feature matrix injection structures (Fig. 8.3c). These gabbro blocks are notably stronger than the altered basalt or the pelite, with a strength of $Is_{(50)} = 8.8$, porosity of $\phi = 0.7$ and a heterogeneity of 0.2 (Fig. 8.4).

The Punta Marengo Package — as well as the Cocolito Package — is cut by several-cm-thick, straight veins of pale green - white zeolite and calcite oriented sub-parallel to the plane of foliation, where present (Fig. 8.3f). At a micro scale, these veins are composed of multiple fracture events and contain lenticular phacoids of strongly sheared and altered wall rock.

The Punta Marengo Package blocks show distinctly different microstructure and mechanical strength than the matrix. The degree of structural anisotropy is notably higher in the matrix than in the blocks. The clays, ubiquitous in both blocks and matrix, are organized into a strong lenticular fabric in the matrix while in the altered basalt they fill feldspar pseudomorphs. Many blocks contain a greater proportion of zeolite veins than the matrix, certainly contributing to the lower mechanical strength. The blocks also feature two distinct phases of brecciation, while only one is evident in the matrix. The distribution of relatively unaltered material at the edges of clasts in the less altered basalt indicates an initial phase of fracturing with accompanied passive alteration of the wall rock, post-dated by an episode of further fracturing and brecciation which did not preferentially cut through the altered material.

DEFORMATION HISTORY OF THE OSA MÉLANGE, SW COSTA RICA

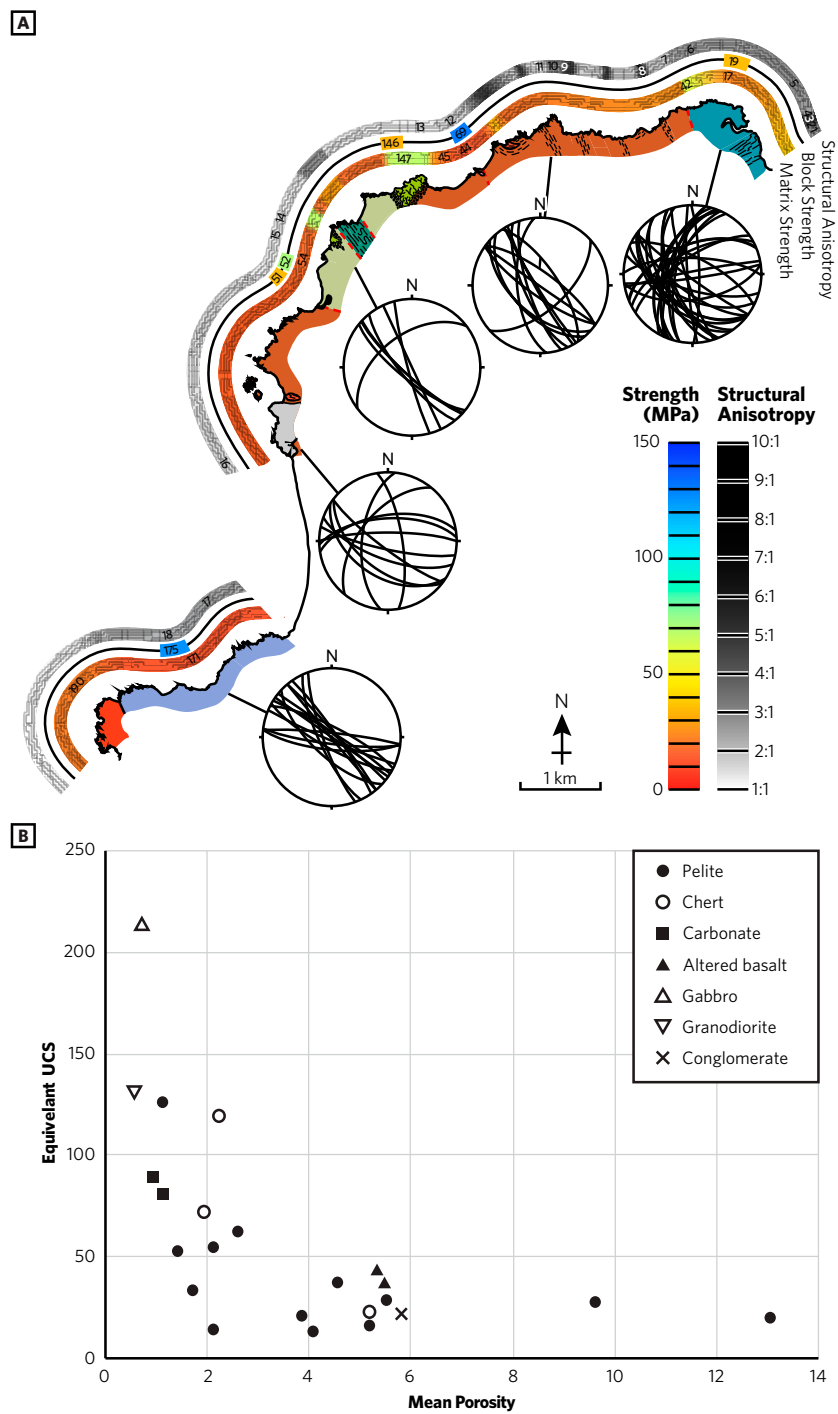


FIG. 8.4. **A:** Map of the San Pedrillo Unit shown in Fig. 8.2 showing the variation in matrix strength and the strength of the blocks as measured by point load tests and shown in Fig. 8.4b. Values of structural anisotropy (Figs. 8.3, 8.5, 8.6, 8.7, and 8.8) are also plotted on this map. (Caption continued on opposite page.)

The abundant folded veins in the matrix and injection structures into fractured blocks, as well as the well-developed lenticular fabric, indicate that the matrix initially deformed by viscous flow and had a weaker rheology relative to the basaltic blocks. The pervasive microscopic anastomosing shear planes defining the lenticular fabric show that deformation was distributed throughout the matrix. Multiple generations of veining and folding formed contemporaneously with movement on slip surfaces suggest variations in the material's viscosity and effective pressure in the system, likely controlled by cyclical changes in fluid pressures.

The later development of straight veins and fractures cutting the matrix lenticular fabric, in addition to the present high mechanical strength, indicates that the matrix underwent induration during the subduction process, likely due to compaction, diagenesis and dewatering, which increased the Young's modulus of the matrix beyond that of the blocks. The implosion breccia within a basalt block is clear evidence that fracturing at seismic velocities occurred within these blocks, while the fact that it cuts the brecciated fabric indicates that this seismic activity occurred at a late stage, after the weakening of the block.

8.3.2. Cocolito Package

The Cocolito Package (Fig. 8.1), exposed from Playa Cocolito to Playa Marengo and from Rio Claro to Playa San Josecito, consists predominantly of blocks of sandstone, mudstone, chert, carbonate and basalt within a largely pelitic matrix. These blocks exhibit low – moderate aspect ratios and no/weak preferred orientations. The macroscopic foliation in the matrix ranges from well-defined, to chaotic, to absent; this fabric typically contains blocks with aspect ratios $\leq 4:1$ with moderate preferred orientation, that

Fig. 8.4. (CONTINUED) **B:** Equivalent uniaxial compressive strength of samples measured by point load strength tests plotted against the mean porosity for each sample. Samples of pelite are mechanically weak and exhibit variable porosity, while samples of altered basalt are consistently weak with moderate porosity. Samples of gabbro and granodiorite exhibit the lowest porosity and the greatest strength. Chert, carbonate and conglomerate blocks exhibit moderate porosities and strengths.

DEFORMATION HISTORY OF THE OSA MÉLANGE, SW COSTA RICA

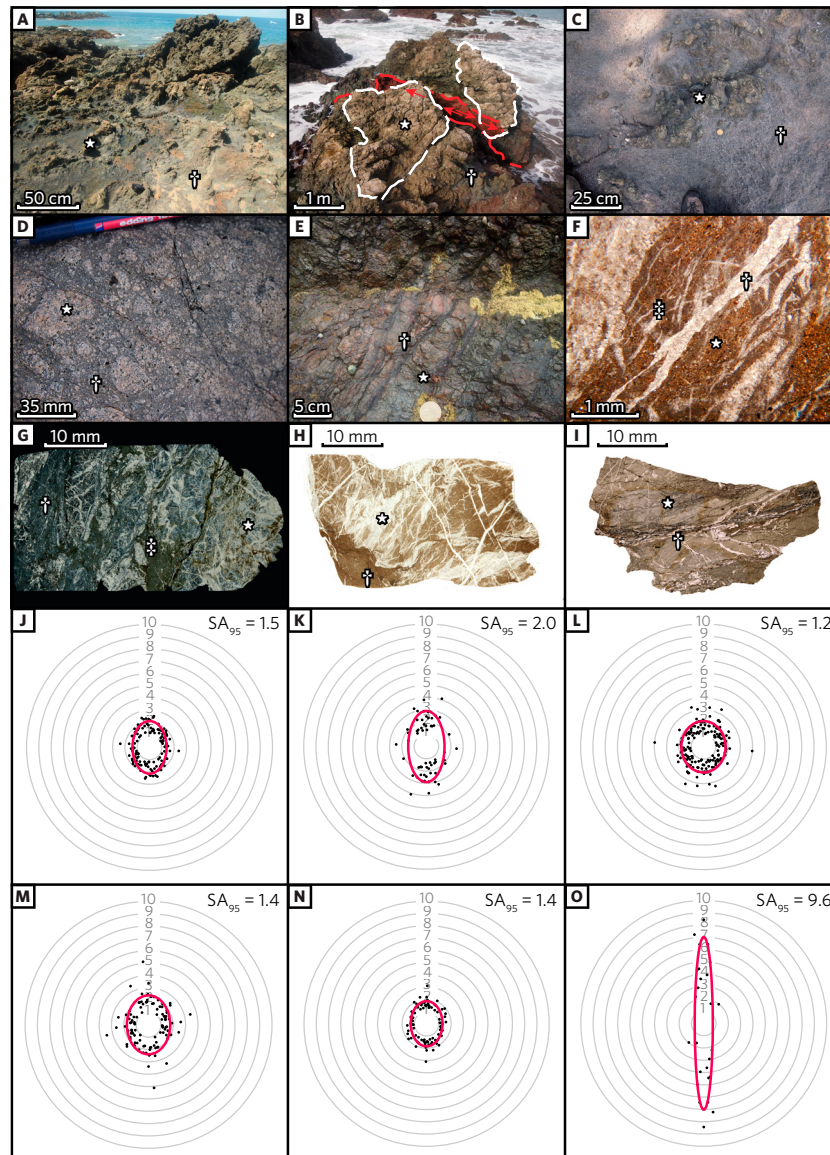


FIG. 8.5. Photographs and data for the Cocolito Package. **A:** Chaotic fabric containing brown carbonate blocks (*) within a grey pelitic matrix (†). **B:** Large block of chert (*) within pelitic matrix (†) cut by a sub-vertical dextral fault (red). **C:** Brecciated and dismembered block (*) within densely stockwork veined matrix (†). **D:** Brecciated granodiorite showing sub-rounded clasts (*) within a comminuted matrix (†). **E:** Shear zone within the Cocolito Package showing high aspect ratio pelitic phacoids (*) surrounded by anastomosing slip surfaces (†). **F:** Photomicrograph showing texture of pelite (*) cut by calcite veins (†) and discontinuous veinlets (‡). (Caption continued on opposite page.)

produced a low to moderate meso-scale structural anisotropy with a value of $SA_{95} = 1.2 - 2.0$ (Fig. 8.5j - n). However, shear zones present in this package exhibit strong block alignment and aspect ratios $\leq 8:1$ resulting in an average structural anisotropy value of $SA_{95} = 9.6$ (Fig. 8.5o). At the microscale samples of the matrix collected throughout this package have a strongly developed lenticular fabric with pervasive anastomosing shear bands. Some blocks are brecciated with pre-existing fractures enhanced by injections of matrix leading to progressive dismemberment at the edges of the blocks and the development of further block-in-matrix texture within the blocks (Fig. 8.5c).

The Cocolito Package displays a high proportion of clay-rich matrix which exhibits a lenticular fabric with more strongly veined, high aspect ratio phacoids within a finer-grained matrix. Veins in phacoids are typically sub-perpendicular to the major axis of the phacoid and terminate at the phacoid boundary (Fig. 8.5g, h). Veins in the matrix are discontinuous and are frequently cut by minor shear surfaces or localised within shear bands. This pelitic matrix is relatively strong compared to pelites in other packages, with $Is_{(50)} = 1.2 - 2.2$, while porosity is variable from $\phi = 1.5 - 5.5$, with heterogeneity for the lower porosity pelites at $H = 0.3 - 0.4$ while the high porosity pelite has a heterogeneity of $H = 1.9$ (Fig. 8.4).

In addition to the phacoids in the matrix, the blocks of the Cocolito Package also exhibit fracturing, veining, matrix injection and brecciation. The granodiorite block identified at $8.690574^\circ N$, $-83.697306^\circ W$ exhibits significant brecciation and comminution (Fig. 8.5d). This granodiorite block has a strength of $Is_{(50)} = 5.5$, a low porosity of $\phi = 0.6$, and a heterogeneity of $H = 4.0$ (Fig. 8.4).

Fig. 8.5. (CONTINUED) **G**: Strongly deformed carbonate-rich block (*) with attached sheared pelitic matrix (†) injecting into fractures (‡); carbonate is mostly reprecipitated in veins. **H**: Carbonate-rich block densely cut by carbonate veins (*) within less-veined sheared pelitic matrix (†). **I**: Sheared pelitic matrix (*) with shear zone (†) composed of anastomosing slip surfaces. **J - O**: Structural anisotropy diagrams produced by image analysis of photos of the Cocolito Package, showing overall low values of structural anisotropy, with the exception of the high anisotropy shear zone.

One microcrystalline calcite vein containing abundant suspended clasts of wall-rock is present oriented sub-perpendicular to the dominant vein orientation.

The blocks in the Cocolito Package – which feature low to moderate aspect ratios – were incorporated into this unit as olistoliths (Clarke *et al.*, 2018). The blocks are chaotically oriented and fractures filled by matrix injections and lacking displacement suggest initial deformation under high fluid pressure conditions. It is worth considering that some of the fractures could have been pre-existing fractures formed on the ocean floor as the effect of cooling, alteration or slope instability that further grew as a consequence of high pressure fluids. Injection of matrix into these fractures led to the progressive dismemberment of these blocks towards their margins. Anastomosing shear surfaces which accommodated distributed shear preferentially cut through the weaker pelite, shaping the more competent material as phacoids. Because of their higher Young's modulus, these phacoids were therefore more susceptible to brittle fracture and veining. If mineralized with a stronger material, the veins may locally indurate the phacoids, further increasing the rheological contrast between the phacoids and the anastomosing shear zones. The brecciated fragments of wall rock observed entirely suspended in veins in the granodiorite block in the Cocolito Package may also suggest instantaneous precipitation indicative of rapid – potentially seismic – processes (Sibson, 1986). The thick, straight veins cutting this package indicate that at least portions of the matrix here underwent sufficient induration to support a through-going fracture.

8.3.3. Bahia Drake Package

The Bahia Drake Package (Fig. 8.1), exposed in Bahia Drake, consists of boudinaged chert and carbonates blocks within a fine-grained, pelitic matrix. Block to matrix ratios are high and these blocks typically exhibit aspect ratios of $\leq 8:1$, strong preferred orientations, and average structural anisotropy values of $SA_{95} = 2.5 - 6.2$ (Fig. 8.6g - l). The matrix is moderately – strongly foliated and thin layers of pelitic matrix define the dominant slip surfaces. This pelite has a low strength of $Is_{(50)} = 0.6 - 1.5$, a variable porosity of $\phi = 2.1 - 9.7$, and a highly variable heterogeneity of

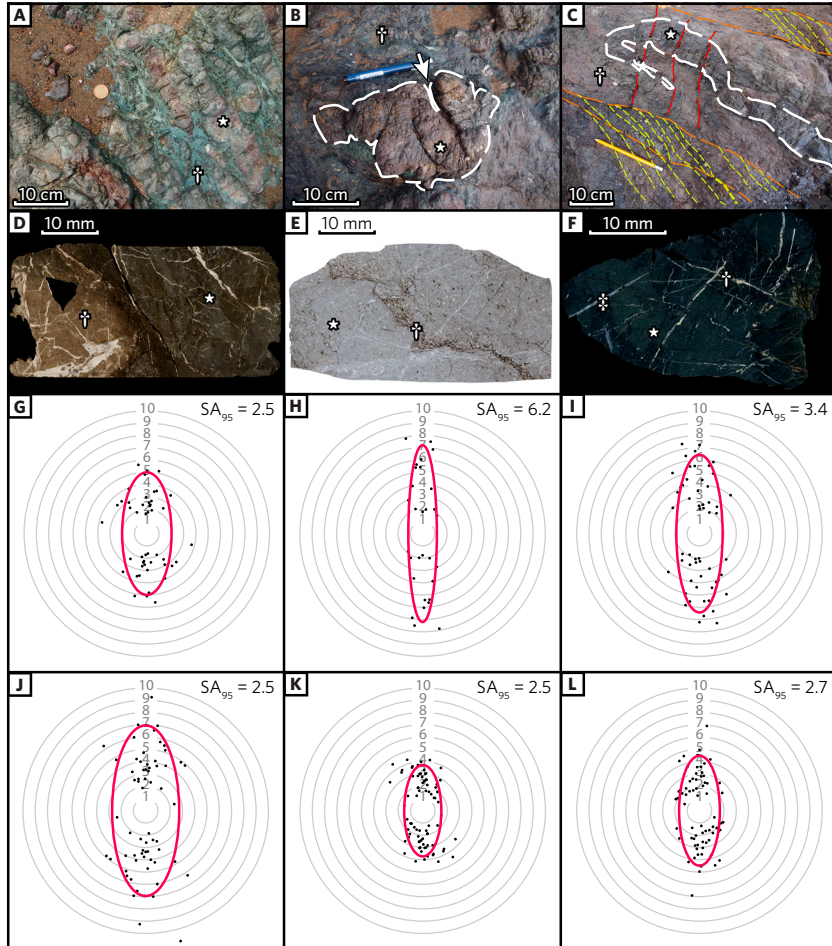


FIG. 8.6. Photographs and data from the Bahia Drake Package. **A:** High aspect ratio aligned red chert blocks (*) within a matrix of green pelite (†). **B:** Low aspect ratio fractured chert block (*) within a pelitic matrix (†) injecting into fractures in the block (white arrow). **C:** Recumbent folded chert block (*) in pelitic matrix (†) with C (orange) and S (yellow) structures and cut by fractures normal to C surfaces (red). **D:** Strongly fractured cherty pelite block with carbonate-rich zone (†) and abundant calcite veins. **E:** Carbonate block showing fossiliferous carbonate with siliciclastic grains (*) and highly contorted layer of dark clay and siliciclastic grains (†). **F:** Cherty pelite block (*) cut by carbonate (†) and zeolite (‡) veins. **G - L:** Structural anisotropy diagrams produced by image analysis of photos of the Bahia Drake Package, showing overall high values of structural anisotropy.

$H = 1.0 - 23.0$ (Fig. 8.4). Isolated, isoclinally folded chert blocks are present. Chert blocks frequently show dense networks of fractures – typically normal to the long axis of the blocks – as well as well-developed pinch and swell structures (Fig. 8.6a, c), while the matrix lacks these fractures and is observed to inject into fractures in the blocks. These chert blocks have low – moderate strengths of $Is_{(50)} = 0.9 - 4.9$, moderate porosities of $\phi = 2.6 - 5.2$, and low – moderate heterogeneities of $H = 0.4 - 3.5$ (Fig. 8.4).

Blocks are densely cut by 0.01 – 0.1 mm thick stockwork calcite and zeolite veins, with calcite veins typically cross-cutting the zeolite veins (Fig. 8.6d). Veins are predominantly oriented normal to the long axis of the blocks. The matrix features abundant anastomosing slip surfaces but lacks the well-developed microscopic lenticular fabric observed in the Cocolito Package. Rare basalt clasts and blocks are also present. Carbonate blocks contain an anastomosing network of fractures filled with dark clay, lithic fragments and clasts of the wall rock (Fig. 8.6e). These carbonate blocks have moderate strengths of $Is_{(50)} = 3.3 - 3.7$, low porosities of $\phi = 1.0 - 1.2$, and low heterogeneities of $H = 0.2 - 0.7$ (Fig. 8.4).

The high to ultra-high aspect ratio chert blocks in the Bahia Drake Package originated as interbedded chert and pelite beds which were intensely boudinaged and folded while the blocks behaved plastically until the necks of the boudins were pinched out to form disk-shaped blocks. However, the intense fracturing and veining normal to the long axis of the blocks indicate a later phase of brittle deformation in these blocks as further along-axis extension was accommodated by fracturing. Injections of pelitic matrix into these fractures, as well as the lack of such fractures in the matrix, indicate that the matrix was still weaker than the blocks at this point and was deforming by viscous creep.

8.3.4. Campanario Package

The Campanario Package (Fig. 8.1), exposed from Playa San Josecito to Punta Campanario, is mostly composed of strongly deformed pelite with a lenticular fabric. It consists of fine-grained pelite with rare serpentinite and lacks a major clastic component. Several blocks of carbonate with sizes ranging from metres to 10s of metres are present in this package. Some of these blocks exhibit brecciation and the development of a block-in-matrix

texture within the blocks. This package exhibits a strong lenticular fabric — with aspect ratios of $AR = \leq 7:1$ and preferred orientations producing an average structural anisotropy value of $SA_{95} = 2.1$ (Fig. 8.7g, h) — and contains a high abundance of discontinuous stockwork calcite veins; the larger of which form phacoids themselves. The phacoids of the Campanario Package display pinch and swell structures (Fig. 8.7a, f). This pelite-rich unit exhibits a variable strength of $Is_{(50)} = 0.5 - 5.2$, variable porosity of $\phi = 1.1 - 4.1$, and low degrees of heterogeneity at $H = 0.3 - 4.1$ (Fig. 8.4).

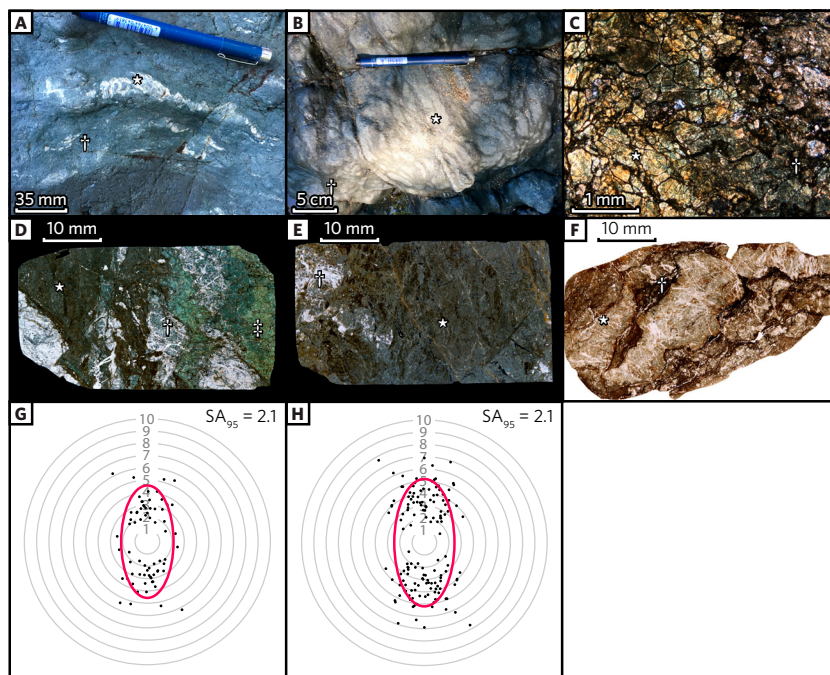


FIG. 8.7. Photographs and data from the Campanario Package.

A: Carbonate-rich phacoid (*) composed mostly of vein material within a pelitic matrix (†). **B:** High proportion of light grey sandstone phacoids (*) within matrix of darker grey pelite (†). **C:** Serpentinite partially replaced by silica and carbonate (*) and cut by dense, dark clay-rich fractures (†). **D:** Photomicrograph of pelitic matrix (*) containing recrystallised carbonate-rich phacoids (†) and an altered serpentinite phacoid (‡). **E:** Photomicrograph of densely fractured pelite matrix with carbonate veined region (†). **F:** Photomicrograph of lenticular fabric of pelitic matrix showing veined phacoids (*) within darker clay-rich shear zones. **G - H:** Structural anisotropy diagrams produced by image analysis of photos of the Campanario Package, showing moderately high values of structural anisotropy.

The Campanario Package, which lacks a significant volcanoclastic, basalt or chert content, continued to be deformed by viscous creep throughout the subduction and accretion process, as evidenced by the ubiquitous strongly folded veins, well developed lenticular fabric and the lack of any significant brittle fracturing besides the ubiquitous sub-vertical faults related to uplift (Vannucchi *et al.*, 2006).

8.3.5. Punta San Pedrillo Package

The Punta San Pedrillo Package (Fig. 8.1), exposed from Punta Campanario to Punta San Pedrillo, is composed of densely fractured interbedded conglomerate, coarse sandstone, and mudstone to the point of being broken formation (Fig. 8.8a – c) (*sensu* Raymond, 1984). The conglomerate has a low strength of $Is_{(50)} = 0.9$, a moderate porosity of $\phi = 5.8$, and a low heterogeneity of $H = 0.5$ (Fig. 8.4). Coarser units are strongly boudinaged with fractures and pinch-and-swell structures filled with mudstone. Some brick-like geometric regularity is seen in the coarser blocks (Fig. 8.8c).

The alternating layers of conglomerate, sandstone and mudstone in the Punta San Pedrillo Package suggest that this was originally deposited as turbidites. During deformation, the mudstone beds deformed viscously, with the conglomerate and sandstones

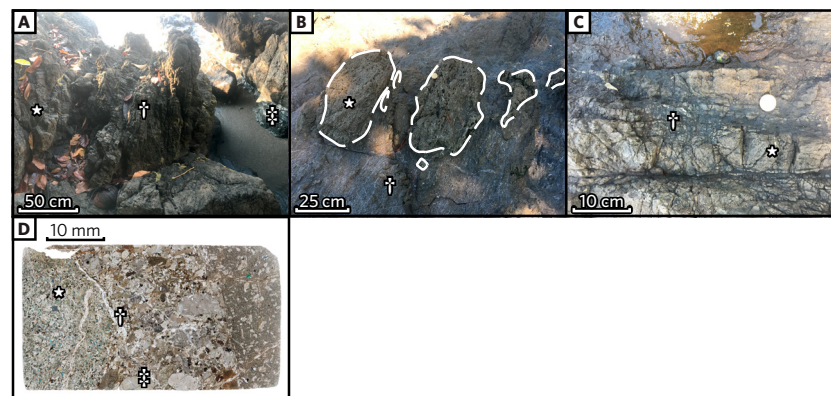


Fig. 8.8. Photographs of the Punta San Pedrillo Package. **A:** Broken formation of boudinaged conglomerate bed (*), bedded sandstone (†) and mudstone forming the matrix (‡). **B:** Low aspect ratio blocks of bedded sandstone (*) with consistent bedding between blocks within pelitic matrix (†). (Caption continued on opposite page.)

developing boudinage. With mudstone injecting into fractures in the coarser beds, the latter started to pinch out at the necks of boudins and accompanying minor faulting resulted in this package becoming broken formation (Hsü, 1968). This reveals that, at the time of initial *mélange* formation, the conglomerate and the sandstones behaved as the competent material while the mudstone became the weaker “mechanical” matrix.

8.4. MULTI-STAGE EVOLUTION OF THE OSA MÉLANGE

The heterogeneity and rheology of the Osa *Mélange* are the result of its polyphase history (Fig. 8.9), with distinct processes occurring prior to, during, and after accretion, ultimately resulting in a complex fabric and, in places, an inversion of the typical “strong blocks in weak matrix” rheological relationship. The integration of information coming from the modern seafloor characteristics surrounding seamount chains and forearc processes, together with the geological observations of the Osa *Mélange*, suggest the following evolution:

8.4.1. Stage 1: *Mélange* formation: sedimentary and tectonic processes in the paleo-Galapagos moat/debris apron.

The presence of block lithologies such as basalt, gabbro, ultramafics, granodiorite, and pelagic and shallow water carbonates (Vannucchi *et al.*, 2006; Buchs *et al.*, 2009; Clarke *et al.*, 2018) within a matrix of pelagic sediment suggests that the Osa *Mélange* was initially formed in an oceanic setting by mass wasting and gravitational sliding from a topographic high such as a seamount complex. Seamounts are favoured over other oceanic topographic features such as transform faults because of the relative paucity of ultramafic and serpentinitized blocks, and over continental margins because of the absence of continentally derived sediments. Furthermore, the Osa *Mélange* lies immediately adjacent to the Osa Igneous Complex, interpreted by Hauff

FIG. 8.8 (CONTINUED) **C:** Strongly fractured sandstone beds (*) with injections of pelite into fractures forming matrix around blocks (†). **D:** Photomicrograph of conglomerate showing dense, clast-supported texture, the presence of basalt and gabbro clasts (*), veins (†), and clasts containing veins formed prior to its incorporation in the conglomerate (‡).

DEFORMATION HISTORY OF THE OSA MÉLANGE, SW COSTA RICA

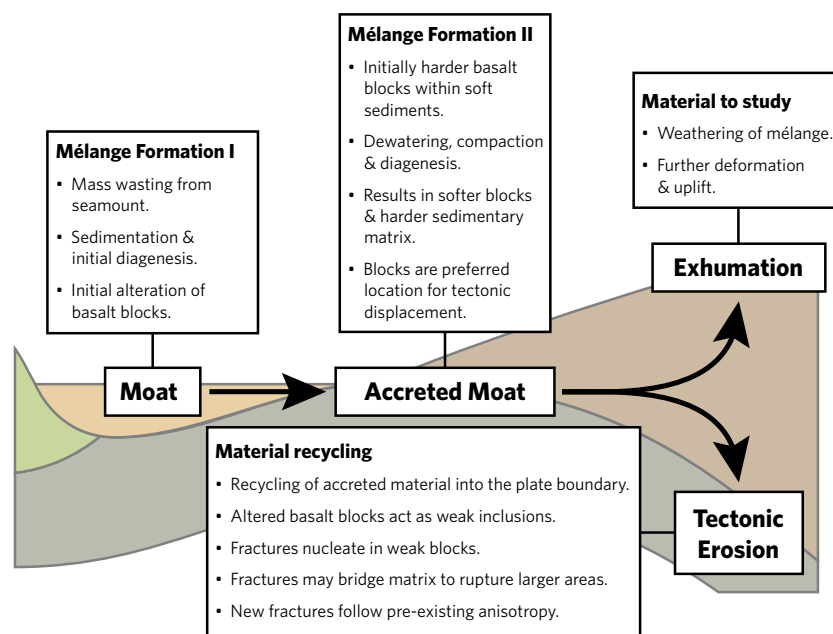


FIG. 8.9. Illustrative diagram showing the three phases of Osa Mélange evolution, from original deposition in the flexural moat/debris apron of Galapagos hotspot-derived seamounts, to accretion and deformation in the frontal portion of the subduction zone, to concurrent exhumation at the surface and tectonic erosion at depth.

et al., (2000) as an accreted seamount complex formed at the Galapagos hotspot. The presence of rare granodiorite and dacite blocks within the mélangé — two over the mapped ~15 km² — with an ambiguous geochemical signature resembling a proto-volcanic arc (Buchs *et al.*, 2009) can be related to later phases of deposition when the accreted moat/debris apron material interacted with the subduction zone.

In modern oceanic settings, thick debris aprons are developed surrounding seamount chain. The additional mass of these seamount complexes on the oceanic plate can cause flexural bending and the formation of a broad sediment basin: a flexural moat or debris apron. A moat/debris apron can accommodate the deposition of thick mass wasting deposits derived from the seamount complex in addition to background oceanic pelagic sediment. Debris aprons adjacent to seamounts can also develop in the absence of flexure, such as seen in La Reunion island (de Voogd *et al.*, 1999; Saint-Ange *et al.*, 2011), where the thickness of

the sediment can reach 1250 m (de Voogd *et al.*, 1999). Megablocks of basalt, 10s to 100s of meters in scale — similar to the sizes of megablocks occurring in the Osa Mélange — are described in modern seamount debris aprons such as the Hawaiian Moat, the Canaries Moat, and La Reunion fan (Moore *et al.*, 1994; Mitchell *et al.*, 2002; Oehler *et al.*, 2008). The Galapagos Islands also show a thin (up to ~500 m) debris apron (Feighner and Richards 1994).

The mass wasting process active in the moat/debris apron resulted in mechanically strong blocks of basalt and sedimentary rock being emplaced within beds of weak sedimentary and volcanoclastic material. The sedimentary rocks included as blocks in the mélange must have undergone some diagenesis prior to inclusion in the mélange in order to survive mass wasting without disaggregation; these include blocks of carbonate, chert, and sandstone. Pelagic chert and mudstone were also deposited during periods of quiescence between mass wasting events. The widespread seafloor alteration suggests fluid circulation which was also active during initial diagenesis with advective hydrothermal fluids, but also release of pore fluids through compaction. These percolating fluids promoted chemical alteration of the basalt blocks and reacted with the volcanoclastic sediment in the matrix, breaking down metastable components like volcanic glass and promoting the growth of new authigenic minerals, such as zeolites and clay minerals. Chapter 7 showed that the high degree of alteration and low mechanical strength of basalt derived from the Cocos Ridge indicates that basaltic material on the incoming plate is already weaker than fresh, subaerially erupted basalt.

8.4.2. Stage 2: Mélange Subduction and Deformation: the interaction of the Osa Mélange with the Middle America Trench.

The thick sediment pile of the seamount debris apron exceeded the volume capacity of the subduction channel, promoting localized subduction accretion in this otherwise erosive subduction zone (Clarke *et al.*, 2018). The Osa Mélange show prehnite-pumpellyite-facies metamorphism and penetrative shearing, but lacks greenschist-facies metamorphism or pervasive recrystallisation. The lack of superimposed higher-grade metamorphic phases indicates that the mélange was not subducted

to significant depth, but rather accreted to shallow levels of the Caribbean plate. Ocean-floor metamorphism is not easily distinguished from accretion-related metamorphism in these rocks; however, the high degree of alteration present in the Cocos Ridge basalt suggest that the Osa Mélangé experienced a high degree of alteration prior to being offscraped.

Subduction enhanced the diagenetic processes already occurring on the ocean plate. Ubiquitous matrix injection structures in blocks indicate that the sediments of the matrix were initially able to be mobilized into a relatively low viscosity fluid. We interpret the microscale anastomosing shear bands which define the lenticular fabric and chaotic foliation wrapping around the blocks as the effect of continuous shear focused in the matrix. Local variations in shear strain rate due to flow around obstacles or through heterogeneous material can promote chaotic (turbulent-like) flow (cf. Radjai and Roux 2002) leading to the development of the chaotic fabric seen in the Cocolito Package. In contrast, the highly structurally anisotropic fabric of the Bahia Drake Package — where the blocks formed by extensional tectonic processes — the aligned, high aspect ratio blocks partition flow in the matrix around and between themselves, preventing the meso-scale turbulence that would produce a chaotic fabric. In this aligned fabric, macro-scale folding that may occur to accommodate shortening may be more evident due to the change in orientation of the structurally anisotropic fabric.

Dewatering, compaction and diagenesis, combined with the development of a lenticular fabric, began to indurate the volcanoclastic matrix. Rotation, translation and internal deformation of the lithic fragments during shearing resulted in reorganization into a strong geometric configuration, contributing to the material's strength. Additionally, unknown mineral reactions — likely between components of the volcanoclastic sediment and circulating fluids — may have contributed to the strengthening of the matrix, accounting for its extraordinary mechanical strength. Where the pelitic matrix contained a higher proportion of fine-grained, pelitic material, this pervasive induration did not occur — likely due to insufficient volcanoclastic material and lithic fragments — producing a weak material which readily breaks along pre-existing fractures defining its lenticular fabric.

In contrast to the volcanoclastic matrix, the basaltic blocks underwent pervasive weakening during subduction by extensive brecciation and cataclastic comminution of the basalt blocks to produce the brecciated clasts, combined with hydrothermal alteration which replaces the original mineralogy with clays. Alteration processes began on the incoming plate and continued during subduction and accretion. The primary igneous mineralogy was altered to clays (mostly Na-rich smectites and illite) and zeolites, which is facilitated by percolating fluids. Dense fractures — both those inherent in the volcanic rock such as hyaloclastites, and those formed by dynamic processes — allowed the fluids to penetrate deep within the basaltic blocks. The reduced surface-area to volume ratio of the intact fragments accelerated the total alteration of the rock mass. These rock fragments frequently preserve a relict central core of less altered basalt. The extensive zeolite veining found in these basalt blocks further weakens these rocks. These processes weaken the basalt blocks such they become weaker than their surrounding volcanoclastic matrix (Chapter 7).

Other igneous blocks, such as the gabbro, dacite, and granodiorite blocks also underwent the alteration and brecciation experienced by the basalt blocks; however, these processes were less effective — likely because of the reduced permeability and more chemically resistant mineralogy of these lithologies — and do not appear to have resulted in rheological inversion. The granodiorite block, despite being extensively brecciated, has still retained much of its original strength, likely due to healing by further mineralization. Chert and carbonate blocks have been weakened by fracturing but remain stronger than their surrounding pelitic matrix.

As the rheological inversion in the Punta Marengo Package occurs, new fractures will preferentially nucleate within the weakened blocks, potentially triggering a micro-seismic event that may propagate into a through-going rupture (a process described in Chapter 7). As such, we suspect that the Punta Marengo Package would have hosted seismicity during subduction and accretion of the *mélange*, as corroborated by the presence of the dilational jog implosion breccia in the basalt block. Earthquakes would therefore nucleate within the rheologically inverted basalt and volcanoclastic layers, such as the Punta Marengo Package,

whereas the pelite-rich and chert-rich layers with the conventional rheological relationship — such as the Cocolito Package and the Bahia Drake Package respectively — would have deformed by aseismic creep.

8.4.3. Stage 3: Exhumation and Tectonic Erosion

The modern subduction system offshore southeast Costa Rica is described as tectonically erosive (Vannucchi *et al.*, 2013). Wide angle and reflection seismic models offshore Osa peninsula imply that the forearc basement is formed by the same material forming the basement of Osa Peninsula; i.e. the Osa mélangé (Fig. 8.1) (Stavenhagen *et al.*, 1998; Bangs *et al.*, 2016). Therefore the Osa Mélangé is both exhumed at its top, making it available for study, and subject to tectonic erosion at its base by the erosive Middle America Subduction Zone. Tectonic erosion is driven by hydrofracturing due to release of fluids within underthrust rocks (von Huene *et al.*, 2004). This recycles the accreted Osa Mélangé into the plate boundary interface, inputting this highly heterogeneous material, with its range of complex fabrics and rheological relationships, into the subduction channel. The highly variable mechanical strength, rheological relationships, and anisotropy within this mélangé will influence the distribution and style of deformation during active tectonic erosion, which in turn influences the properties and processes within the plate boundary interface.

As the Osa Mélangé is tectonically eroded into the subduction channel, the material with a largely chaotic fabric or a low structural anisotropy — like the Punta Marengo and Cocolito packages — will have the style of their incorporation controlled predominantly by their rheology (Fig. 8.10a). Where the mélangé has a “normal” rheological relationship (i.e. the blocks are stronger and have a higher Young’s modulus than their surrounding matrix), the matrix will be more readily comminuted, leaving the blocks temporarily protruding into the subduction channel (Fig. 8.10aI). This situation will increase the stress on the block until the block is either excised from the matrix and inherited into the subduction channel intact, or it is fractured and a fragment of the block is incorporated into the channel. In the specific case of the Cocolito Package, this process will result in the inheritance of the

sandstone, chert, carbonate, basalt and granodiorite blocks into the subduction channel as the mechanically weak pelitic matrix is more readily comminuted. Therefore the blocks and matrix

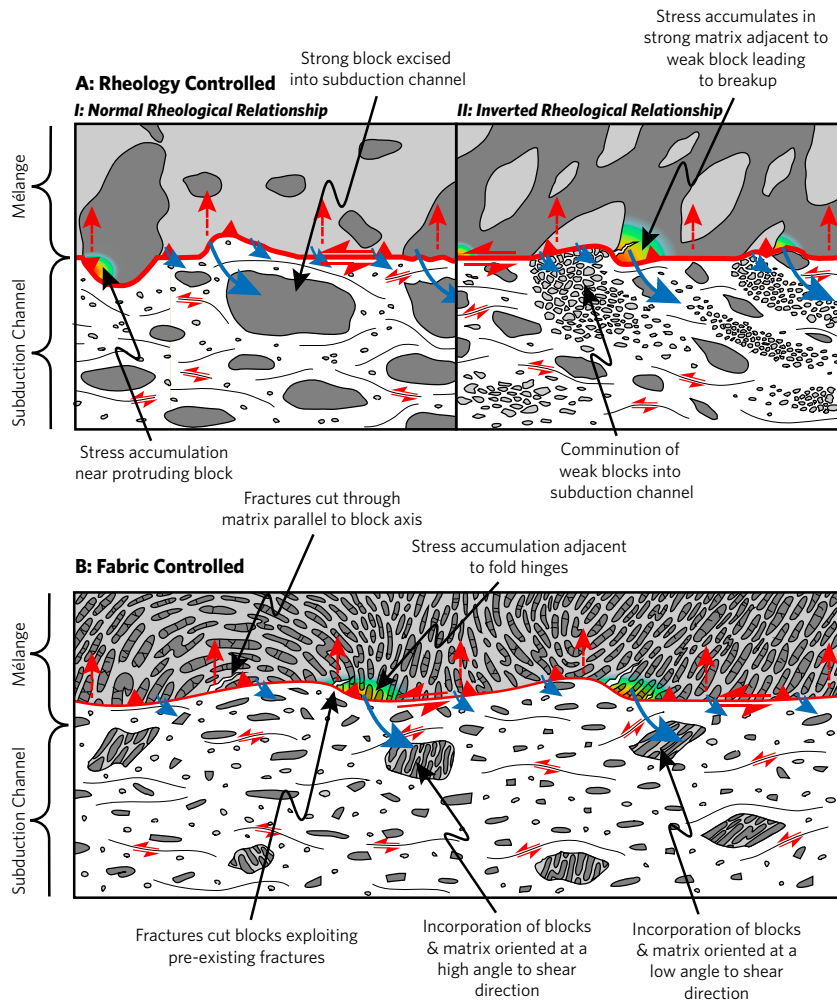


FIG. 8.10. Schematic illustration of different styles of incorporation into the subduction channel controlled by upper plate rheologies and fabrics. **A.i** shows how comminution of a weaker matrix leads to the temporary protrusion of strong blocks into the subduction channel before the block is either broken or excised into the channel. **A.ii** shows the converse situation, where weak blocks are readily comminuted resulting in temporary concavities in the base of the upper plate which increase stresses on the surrounding matrix promoting the breakup of the stronger matrix. **B** shows how the incorporation of highly anisotropic fabrics is controlled by the orientation of that fabric relative to the subduction zone.

retain their original relationship during inheritance from the Osa Mélangé into the subduction channel.

Where the mélangé has an “inverted” rheological relationship (Chapter 7) (i.e. the blocks are weaker and have a lower Young’s modulus than their surrounding matrix), it is the blocks that will be more readily comminuted, resulting in embayments in the roof of the subduction channel which will concentrate stresses on the side in the direction of shearing (Fig. 8.10aII). As a result, we predict that the indurated matrix will be incorporated into the subduction interface as blocks. In the case of the Punta Marengo Package, the altered basalt blocks will be comminuted into the subduction channel, while the indurated matrix, along with the gabbro and chert blocks which have retained their strength, will be incorporated as blocks into the channel.

Where the mélangé has a strongly structurally anisotropic fabric – such as Bahia Drake Package – the fabric becomes a dominant control on the style of incorporation into the subduction channel (Fig. 8.10b). Fractures preferentially propagate parallel to the fabric, and given the high block-to-matrix ratios in this package, fractures are likely to propagate between adjacent blocks. As such, the rheological relationship in this setting does not significantly change the outcome. The orientation of this fabric with respect to the subduction channel has a strong influence on the style of incorporation into the subduction channel. If sheared at a low angle to the fabric, the preexisting fractures normal to the long-axis of the blocks would facilitate extension and further dismemberment of the blocks. The matrix may also be sheared ductilely or host a through-going fracture if deformed in this orientation. In this case, blocks may be inherited into the subduction zone and matrix may be comminuted, or new blocks may be formed in the subduction channel consisting of both blocks and matrix from the mélangé oriented subparallel to the long axis of the new block. Conversely, if sheared at a high angle to the fabric – where the rock mass is strongest – new blocks formed in the subduction channel will consist of both blocks and matrix from the mélangé oriented at a high angle to the long axis of the new block, making them stronger in the direction of shearing than the block elongated parallel to their internal fabric.

Regions of the *mélange* with very low block proportions — such as the Campanario Package — will be readily comminuted into the subduction channel as the mechanically weak pelite is tectonically eroded. The anisotropy of this material may result in failure at different stresses depending on the orientation of the stress, but the overall weakness of this material in any orientation suggests it will readily yield to deformation. Conversely, regions of the *mélange* which have not undergone significant breakup — such as the broken formation of the Punta San Pedrillo Unit — will likely undergo full breakup of the rock unit when tectonically eroded. Deformation will likely continue to localize within the pelitic material and the relict layering will be further destroyed by mixing.

These differing styles of incorporation have a direct effect on the properties of the subduction zone plate interface. This is because they exert a strong control on the relative size of the blocks entering the subduction channel and what their physical properties are. Where structural anisotropy is low, blocks of the strong lithology being incorporated are accompanied by comminuted fragments of the weak lithology, reducing the proportion of new blocks and thereby resulting in a relatively low block-to-matrix ratio in the subduction channel. In contrast, where structural anisotropy is high, new blocks may consist of both the stronger and the weaker lithology, meaning less of the weak material is comminuted and the block-to-matrix ratio in the subduction channel is higher. High block-to-matrix ratios are shown by Fagereng and Sibson (2010) and Chapter 7 to promote seismicity, regardless of their rheological relationship with the matrix.

The style of incorporation also controls which lithologies from the *mélange* become blocks in the subduction channel, as blocks in the original *mélange* — if sufficiently weakened — may be comminuted into the matrix rather than inherited as a block. Once incorporated into the subduction channel, block rheologies will continue to evolve, with chemically unstable lithologies like basalt and gabbro continuing to weaken as they are subjected to increased fluid circulation and stresses. If these blocks weaken to the point of rheological inversion, they may promote seismicity, as described in Chapter 7. The materials comminuted into the matrix of the subduction channel may also have a significant

influence on the velocity dependent frictional properties of the plate interface, as incorporation of a significant proportion of velocity-weakening materials (such as carbonate minerals [Han *et al.*, 2010] and talc [Moore and Lockner, 2011]) may promote a velocity-weakening behavior of the subduction interface, significantly modifying the seismic potential for this plate boundary. Therefore, any analysis of upper plate material as an input into the subduction channel must consider how the present rheological and structural relationships will affect the style of its incorporation, as this will significantly affect how the added upper plate material impacts on plate boundary properties and processes.

In the case of the Osa Mélange, regions with both high and low structural anisotropy are present, as well as regions with the “normal” and “inverted” rheological relationship. The gabbro blocks in the Punta Marenco Package, as well as basalt blocks that have not yet undergone rheological inversion, will continue to weaken, potentially promoting seismicity by the mechanism described in Chapter 7. Meanwhile, indurated volcanoclastic blocks may also weaken as they are further fractured during shearing. Incorporation of material like the Bahia Drake Package will increase the block-to-matrix ratio in the subduction channel, promoting seismicity, while incorporation of material like the Campanario Package will add weaker, more comminutable material to the subduction channel, decreasing its block-to-matrix ratio and promoting aseismic slip.

8.5. CONCLUSIONS

The Osa Mélange is a highly structurally and mechanically diverse rock unit with: a) mechanically strong and structurally isotropic volcanoclastic *mélange* (e.g. Punta Marenco Package); b) mechanically moderately strong and structurally anisotropic chert-rich *mélange* (e.g. Bahia Drake Package); and c) mechanically weak and structurally isotropic pelite-rich *mélange* (e.g. Cocolito Package). This rock unit was initially formed by mass-wasting from a seamount complex onto the surrounding flexural moat/debris apron on the oceanic plate (Clarke *et al.*, 2018), and was accreted to the Caribbean Plate in the Eocene – Miocene (Vannucchi *et al.*, 2006 and references therein). During subduction and accretion, the structure and rheology of the *mélange* evolves, in places

leading to the inversion of the typical rheological relationship (Chapter 7). This *mélange* is currently in the hanging wall of the Middle America Subduction Zone and is being tectonically eroded into the subduction channel. We infer that the style of its incorporation is strongly controlled by the nature and orientation of its fabric and the rheology of its constituents. Inherited blocks influence the bulk rheology and seismic style of the subduction channel and determine the propensity for large-scale seismic slip (Fagereng and Sibson, 2010).

8.6. REFERENCES

- Bangs, N.L., McIntosh, K.D., Silver, E.A., Kluesner, J.W. and Ranero, C.R. 2016. A recent phase of accretion along the southern Costa Rican subduction zone. *Earth and Planetary Science Letters*, 443, 204 – 215, <https://doi.org/10.1016/j.epsl.2016.03.008>.
- Brown, K.M., Kopf, A., Underwood, M.B. and Weinberger, J.L. 2003. Compositional and fluid pressure controls on the state of stress on the Nankai subduction thrust: A weak plate boundary. *Earth and Planetary Science Letters*, 214, 589 – 603, [https://doi.org/10.1016/S0012-821X\(03\)00388-1](https://doi.org/10.1016/S0012-821X(03)00388-1).
- Buchs, D.M., Baumgartner, P.O., Baumgartner-mora, C. and Bandini, A.N. 2009. Late Cretaceous to Miocene seamount accretion and *mélange* formation in the Osa and Burica Peninsulas (Southern Costa Rica): episodic growth of a convergent margin. Geological Society, London, Special Publications, 328, 411 – 456.
- Chester, F.M., Rowe, C., *et al.*, 2013. Structure and Composition of the Plate-Boundary Slip Zone for the 2011 Tohoku-Oki Earthquake. *Science*, 1208 – 1212.
- Clarke, A.P., Vannucchi, P. and Morgan, J. 2018. Seamount chain – subduction zone interactions : Implications for accretionary and erosive subduction zone behavior. *Geology*, 46, 367 – 370, <https://doi.org/10.1130/G40063.1>.
- Clift, P.D. and Vannucchi, P. 2004. Controls on tectonic accretion versus erosion in subduction zones: Implications for the origin and recycling of the continental crust. *Review of Geophysics*, 42, <https://doi.org/10.1029/2003RG000127>.
- de Voogd, B., Palomé, S.P., *et al.*, 1999. Vertical movements and material transport during hotspot activity: Seismic reflection profiling offshore. *Journal of Geophysical Research*, 104, 2855 – 2874.
- Ernst, W.G. 1988. Tectonic history of subduction zones inferred from retrograde blueschist P-T paths. *Geology*, 16, 1081 – 1084.

DEFORMATION HISTORY OF THE OSA MÉLANGE, SW COSTA RICA

- Fagereng, A. and Sibson, R.H. 2010. Mélange rheology and seismic style. *Geology*, 38, 751 – 754, <https://doi.org/10.1130/G30868.1>.
- Feighner, M.A. and Richards, M.A. 1994. Lithospheric structure and compensation mechanisms of the Galápagos Archipelago. *Journal of Geophysical Research*, 99, 6711 – 6729.
- Fletcher, R.C. 2004. Anisotropic viscosity of a dispersion of aligned elliptical cylindrical clasts in viscous matrix. *Journal of Structural Geology*, 26, 1977 – 1987, <https://doi.org/10.1016/j.jsg.2004.04.004>.
- Franklin, J.A. 1985. Suggested method for determining point load strength. *International Journal of Rock Mechanics and Mining Sciences and Geomechanics Abstracts*, 22, 51 – 60, [https://doi.org/10.1016/0148-9062\(85\)92327-7](https://doi.org/10.1016/0148-9062(85)92327-7).
- Franklin, J.A., Vogler, U.W., Szlavin, J., Edmond, J.M. and Bieniawski, Z.T. 1977. Suggested Methods for Determining Water-Content, Porosity, Density, Absorption and Related Properties and Swelling and Slake-Durability Index Properties.
- Han, R., Hirose, T. and Shimamoto, T. 2010. Strong velocity weakening and powder lubrication of simulated carbonate faults at seismic slip rates. *Journal of Geophysical Research*, 115, <https://doi.org/10.1029/2008JB006136>.
- Harris, R.N. and Spinelli, G. 2010. Thermal regime of the Costa Rican convergent margin: 2. Thermal models of the shallow Middle America subduction zone offshore Costa Rica. *Geochemistry, Geophysics, Geosystems*, 11, 1 – 22, <https://doi.org/10.1029/2010GC003273>.
- Hauff, F., Hoernle, K., Bogaard, P. van den, Alvarado, G. and Garbe-schönberg, D. 2000. Age and geochemistry of basaltic complexes in western Costa Rica: Contributions to the geotectonic evolution of Central America. *Geochemistry, Geophysics, Geosystems*, 1, <https://doi.org/10.1029/1999GC000020>.
- Hoernle, K., Bogaard, P.V., Werner, R., Lissinna, B., Alvarado, G. and Garbe-Schönberg, D. 2002. Missing history (16 – 71 Ma) of the Galápagos hotspot: Implications for the tectonic and biological evolution of the Americas. *Geological Society of America Bulletin*, 30, 795 – 798, [https://doi.org/10.1130/0091-7613\(2002\)030<0795](https://doi.org/10.1130/0091-7613(2002)030<0795).
- Hsü, K.J. 1968. Principles of Mélanges and Their Bearing on the Franciscan-Knoxville Paradox. *Geological Society of America Bulletin*, 79, 1063 – 1074, [https://doi.org/10.1130/0016-7606\(1968\)79](https://doi.org/10.1130/0016-7606(1968)79).
- Ikari, M.J., Saffer, D.M. and Marone, C. 2007. Effect of hydration state on the frictional properties of montmorillonite-based fault gouge. *Journal of Geophysical Research*, 112, 1 – 12, <https://doi.org/10.1029/2006JB004748>.

- ISRM. 2014. The ISRM Suggested Methods for Rock Characterization, Testing and Monitoring: 2007-2014. R, U. (ed.). Springer International Publishing, SpringerLink : Bücher.
- Kinoshita, M., Moore, G., von Huene, R., Tobin, H. and Ranero, C. 2006. The Seismogenic Zone Experiment. *Oceanography*, 19, 28 – 38, <https://doi.org/10.5670/oceanog.2006.02>.
- Kurzwaski, R.M., Stipp, M., Niemeijer, A.R. and Behrmann, J.H. 2016. Earthquake nucleation in weak subducted carbonates. *Nature Geoscience*, <https://doi.org/10.1038/ngeo2774>.
- Di Marco, G., Baumgartner, P.O. and Channell, J.E.T. 1995. tectonostratigraphic subdivision of Costa Rica and western Panama.
- Mitchell, N., Watts, A.B. and Gee, M.J.R. 2002. The morphology of the flanks of volcanic ocean islands : A comparative study of the Canary and Hawaiian hotspot islands, [https://doi.org/10.1016/S0377-0273\(01\)00310-9](https://doi.org/10.1016/S0377-0273(01)00310-9).
- Moore, D.E. and Lockner, D.A. 2011. Frictional strengths of talc-serpentine and talc-quartz mixtures. *Journal of Geophysical Research*, 116, <https://doi.org/10.1029/2010JB007881>.
- Moore, J.G., Normark, W.R. and Holcomb, R.T. 1994. Giant Hawaiian Landslides. *Annual Review of Earth and Planetary Sciences*, 22, 119 – 144.
- Oehler, J., Lénat, J. and Labazuy, P. 2008. Growth and collapse of the Reunion Island volcanoes. *Bulletin of Volcanology*, 80, 717 – 742, <https://doi.org/10.1007/s00445-007-0163-0>.
- Radjai, F. and Roux, S. 2002. Turbulent-like fluctuations in quasistatic flow of granular media. *Physical Review Letters*, 89, <https://doi.org/10.1103/PhysRevLett.89.064302>.
- Ranero, C. and von Huene, R. 2000. Subduction erosion along the Middle America convergent margin. *Nature*, 404, 748 – 752, <https://doi.org/10.1038/35008046>.
- Ranero, C.R., Grevemeyer, I., *et al.*, 2008. Hydrogeological system of erosional convergent margins and its influence on tectonics and interplate seismogenesis. *Geochemistry, Geophysics, Geosystems*, 9, <https://doi.org/10.1029/2007GC001679>.
- Raymond, L.A. 1984. Classification of mélanges. In: Raymond, L. A. (ed.) *Mélanges: Their Nature, Origin, and Significance*. Geological Society of America.
- Saint-Ange, F., Savoye, B., *et al.*, 2011. A volcanoclastic deep-sea fan off La Réunion Island (Indian Ocean): Gradualism versus catastrophism. *Geology*, 39, 271 – 274, <https://doi.org/10.1130/G31478.1>.

DEFORMATION HISTORY OF THE OSA MÉLANGE, SW COSTA RICA

- Schneider, C.A., Rasband, W.S. and Eliceiri, K.W. 2012. NIH Image to ImageJ: 25 years of image analysis. *Nature Methods*, 9, 671 – 675, <https://doi.org/10.1038/nmeth.2089>.
- Sibson, R.H. 1986. Brecciation processes in fault zones: Inferences from earthquake rupturing. *Pure and Applied Geophysics PAGEOPH*, 124, 159 – 175, <https://doi.org/10.1007/BF00875724>.
- Stavenhagen, A.U., Flueh, E.R., *et al.*, 1998. Seismic wide-angle investigations in Costa Rica – a crustal velocity model from the Pacific to the Caribbean. *Zentralblatt für Geologie und Paläontologie, Teil I*, 1, 393 – 408.
- Vannucchi, P., Scholl, D.W., Meschede, M. and McDougall-Reid, K. 2001. Tectonic erosion and consequent collapse of the Pacific margin of Costa Rica: Combined implications from ODP leg 170, seismic offshore data, and regional geology of the Nicoya Peninsula. *Tectonics*, 20, 649 – 668, <https://doi.org/10.1029/2000TC001223>.
- Vannucchi, P., Ranero, C.R., Geleotti, S., Straub, S.M., Scholl, D.W. and McDougall-Ried, K. 2003. Fast rates of subduction erosion along the Costa Rica Pacific margin: Implications for nonsteady rates of crustal recycling at subduction zones. *Journal of Geophysical Research*, 108, 2511, <https://doi.org/10.1029/2002JB002207>.
- Vannucchi, P., Fisher, D.M., Bier, S. and Gardner, T.W. 2006. From seamount accretion to tectonic erosion: Formation of Osa Mélange and the effects of Cocos Ridge subduction in southern Costa Rica. *Tectonics*, 25, TC2004, <https://doi.org/10.1029/2005TC001855>.
- Vannucchi, P., Remitti, F. and Bettelli, G. 2008. Geological record of fluid flow and seismogenesis along an erosive subducting plate boundary. *Nature*, 451, 699 – 703, <https://doi.org/10.1038/nature06486>.
- Vannucchi, P., Sak, P.B., Morgan, J.P., Ohkushi, K. and Ujiie, K. 2013. Rapid pulses of uplift, subsidence, and subduction erosion offshore Central America: Implications for building the rock record of convergent margins. *Geology*, 41, 995 – 998, <https://doi.org/10.1130/G34355.1>.
- von Huene, R., Ranero, C.R. and Vannucchi, P. 2004. Generic model of subduction erosion. *Geology*, 32, 913 – 913, <https://doi.org/10.1130/G20563.1>.

8.7. SUPPLEMENTARY MATERIAL

8.7.1. Methodology

8.7.1.1. Field Methods

The San Pedrillo Unit of the Osa Mélange was mapped at a scale of 1:1000 to record the high degree of heterogeneity and structural complexity of this mélange (Fig. 8.2). Mapping focused on quantifying block and matrix proportions, characterizing structural anisotropy, and identifying structural indicators of past rheological relationships between blocks and matrix, such as matrix injections and fracture termination and propagation across lithological discontinuities. Samples of the outcropping rock were collected at a minimum of 50 m intervals, as permitted by outcrop, to characterize the variation in block and matrix properties throughout the San Pedrillo Unit. Representative samples of both blocks and matrix were collected where available. The samples used for point-load strength experiments and microstructural analysis were extracted from the outcrop with a hammer and chisel by exploiting pre-existing weaknesses to minimize the formation of new fractures. These samples are typically <20 cm in diameter. Samples selected for triaxial experiments (Chapter 7) were selected from >20 cm diameter boulders in float, with a lithology matched to that in outcrop at that location, so to entirely avoid the formation of new fractures during the sampling process.

8.7.1.2. Image Analysis Methods

The structural anisotropy of regions of the Osa Mélange was measured by image analysis of field photos. Blocks shown in field photos were manually traced in Adobe Illustrator and analyzed for orientation and aspect ratio using ImageJ (Schneider *et al.*, 2012). A radar plot was produced with aspect ratio on the radial axis and orientation on the circumferential axis and an ellipse fitted to the data with each semi-axis corresponding to the 95th percentile of the data on that axis. The aspect ratio of this ellipse is regarded as the structural anisotropy of the region in which the photo was taken. Elongation and alignment of constituent components (e.g. clasts or blocks) in a rock contribute to the mechanical anisotropy of the lithology (Fletcher, 2004). Analysis of the aspect

ratio and the orientation of blocks within regions of the Osa Mélangé using image analysis therefore provides a proxy for the mechanical anisotropy of the rock unit.

8.7.1.3. *Rock mechanics methods*

This study experimentally tested the current mechanical properties of materials spanning the range of block and matrix lithologies present in the mélangé, with two samples consisting of a basalt block and its surrounding volcanoclastic matrix selected for detailed analysis (see Chapter 7).

Porosity and density of the varied lithologies present in the Osa Mélangé were calculated from dry weights in air, water saturated weights in air, and water saturated weights in water using the saturation buoyancy technique (ISRM 2014). Water saturation was achieved by submersion in water and vacuum de-aeration for at least 1 hour, followed by continued submersion for at least 12 hours.

Point load strength of the varied lithologies present in the Osa Mélangé was measured by experiments conducted in accordance with Franklin's (1985) methodology. 10 irregular blocks of each sample were analyzed using an HMA Geotechnical Systems Point Load Tester Model 6500. Mean $Is_{(50)}$ – calculated by Franklin's (1985) methodology – is calculated for each sample. The samples used for both point load strength and porosity/density tests were at the approximate scale of 1 – 3 centimetres (see supplement for full table of this data).

Samples of altered basalt and volcanoclastic matrix were tested experimentally under triaxial conditions at the Rock Mechanics and Physics Laboratory, British Geological Society (see Chapter 7). Experimental conditions were chosen to bracket the up-dip limit of the seismogenic zone at 2 and 4 km depth: confining pressures (P_c) of 60 MPa and 120 MPa and temperatures of $T = 60^\circ\text{C}$ and $T = 120^\circ\text{C}$ were used (Harris and Spinelli 2010).

8.7.2. Rock Mechanics Results

	Area	Lithology	Mean Porosity	Standard deviation of Porosity	$I_{s(50)}$	Equivalent UCS (MPa)
Punta Marengo Package						
OSA12.21	Carbonera	Gabbro	0.7	0.2	8.8	211.9
OSA16.51	Rio Claro	Basalt	5.5	0.8	1.5	35.8
OSA16.52	Rio Claro	Chert	2	0.5	3	71.8
OSA16.54	Rio Claro	Pelite	13.1	19.2	0.8	19.9
OSA16.79	North Matapalo	Pelite	3.9	0.4	0.9	20.8
OSA16.83	North Matapalo	Pelite	5.2	1.4	0.6	15.3
OSA16.100	North Matapalo	Pelite	1.7	1.2	1.4	32.5
OSA16.146	Marengo	Basalt	5.5	0.3	1.4	32.7
Bahia Drake Package						
OSA12.20	Carbonera	Carbonate	1	0.2	3.7	88.5
OSA12.23	Carbonera	Chert	2.3	3.5	4.9	118.4
OSA12.24	Carbonera	Carbonate	1.2	0.7	3.3	79.7
OSA16.17	Drake bay	Chert	5.2	0.8	0.9	22.4
OSA16.19	Drake bay	Pelite	4.6	2.2	1.5	36.6
OSA16.42	Aguitas	Chert	2.6	0.4	2.6	61.6

	Area	Lithology	Mean Porosity	Standard deviation of Porosity	$I_{s(50)}$	Equivalent UCS (MPa)
OSA16.44	<i>Aguitas</i>	<i>Pelite</i>	2.1	23	0.6	13.2
OSA16.45	<i>Aguitas</i>	<i>Pelite</i>	9.7	1	1.1	27.5
Cocolito Package						
OSA12.15	<i>Carbonera</i>	<i>Pelite</i>	2.2	0.3	2.2	54
OSA12.22	<i>Carbonera</i>	<i>Pelite</i>	1.5	0.4	2.2	51.8
OSA16.69	<i>Caletas</i>	<i>Granodiorite</i>	0.6	4	5.5	130.8
OSA16.119	<i>Matapalo</i>	<i>Pelite</i>	5.5	1.9	1.2	28.6
Campanario Package						
OSA16.171	<i>Campanario</i>	<i>Pelite</i>	4.1	1.1	0.5	12.7
OSA16.175	<i>Campanario</i>	<i>Pelite</i>	1.1	0.3	5.2	125.1

CHAPTER 9. PROVENANCE OF THE OSA MÉLANGE BLOCKS

9.1. INTRODUCTION

This chapter details the results of a geochemical pilot study intended to identify the provenance of Osa Mélangé material. In particular, this study aimed to test the interpretation of Buchs *et al.* (2009) that the intermediate – felsic-composition blocks are derived from an arc and are not genetically related to the basalt blocks. Additionally, geochemical analysis of the volcanoclastic pelites and their associated interbedded cherts aimed to assess their geochemical similarity to the basalt blocks and therefore the proportion of seamount-derived basalt in the sediment. Analysis of the volcanoclastic pelites also provides a constraint on the alteration experienced by the basalt blocks, assuming that the sediment would have undergone maximum alteration. This is a first-order analysis concerned mostly with identifying the geochemical signature of the Osa Mélangé rocks and comparing that with their possible sources; determining the petrogenesis of these rocks is not an aim of this study. However, due to reasons discussed in this chapter, this pilot study was not investigated further as the results were inconclusive in regards to the intended research questions and would require additional sampling and analysis which is not within the scope of this doctoral project.

19 samples were analysed for major and trace elements, including 4 samples of basalt, 3 samples of gabbro, 4 samples of dacite, 3 samples of pelite, 2 samples of chert, 2 samples of serpentinite, and 1 sample of granodiorite. Samples of pelite and chert were collected from the Bahia Drake Package, samples of granodiorite and basalt from the Cocolito Package, and samples of basalt, dacite, and volcanoclastic matrix from the Punta Marengo Package. Additionally, samples of gabbro and serpentinite were collected from Punta Carbonera in the Cabo Matapalo Unit (Fig. 9.1). Equal numbers of basalt and dacite samples were analysed to ensure results were representative of each lithology and this does not reflect the relative abundance of these lithologies.

PROVENANCE OF THE OSA MÉLANGE BLOCKS

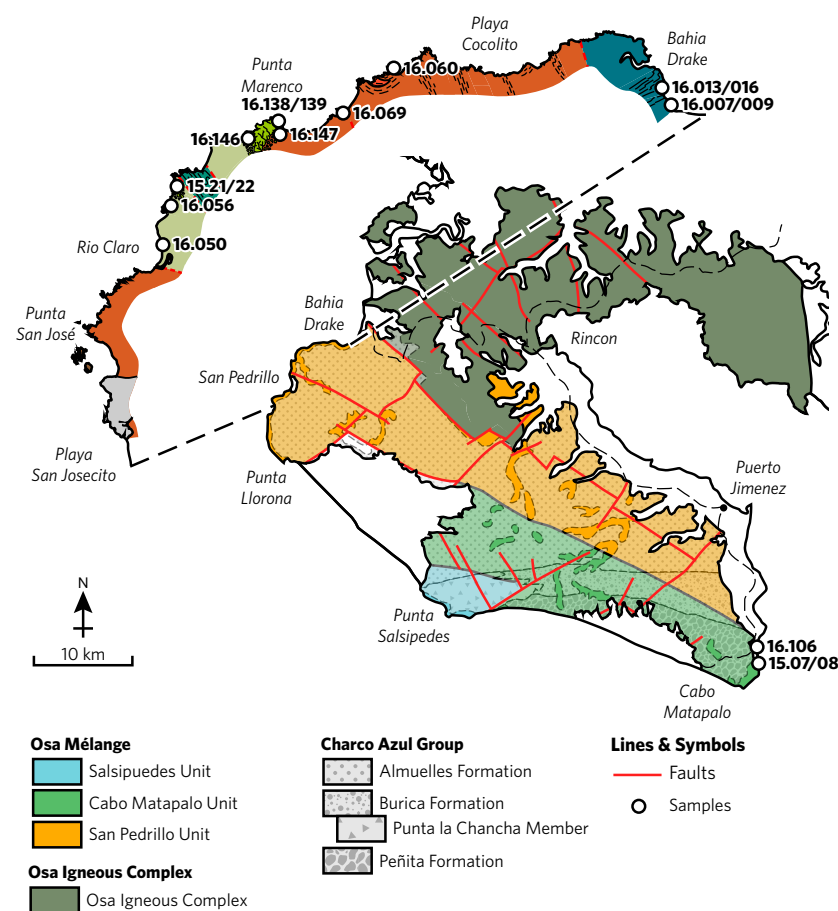


FIG. 9.1. Geological map of the Osa Peninsula showing the locations of the samples collected for this study. Outcrop distribution of the units of the Osa Mélange and their subdivisions are modified from Di Marco *et al.* (1995), Vannucchi *et al.* (2006) and Clarke *et al.* (2018).

As described in detail in Chapter 7, the basalt blocks in the Osa Mélange consist mostly of 0.2 – 0.8 mm plagioclase lathes and ~0.1 – 0.5 mm fractured clinopyroxene crystals within a ground-mass entirely altered to dark brown clay (Fig. 9.2a). The degree of alteration varies within these basalts and less-altered regions are present within the cores of some basalt clasts. The gabbros consist mostly of strongly altered plagioclase crystals within a serpentinised matrix with finely cleaved subhedral – anhedral clinopyroxene (Fig. 9.2b) and – in some samples – unserpentinised olivine crystals (Fig. 9.2c). While pervasive alteration has obscured the original texture, remaining crystals are ~1 – 3 mm in size. Serpentinite samples are composed of fine-grained serpentinite,

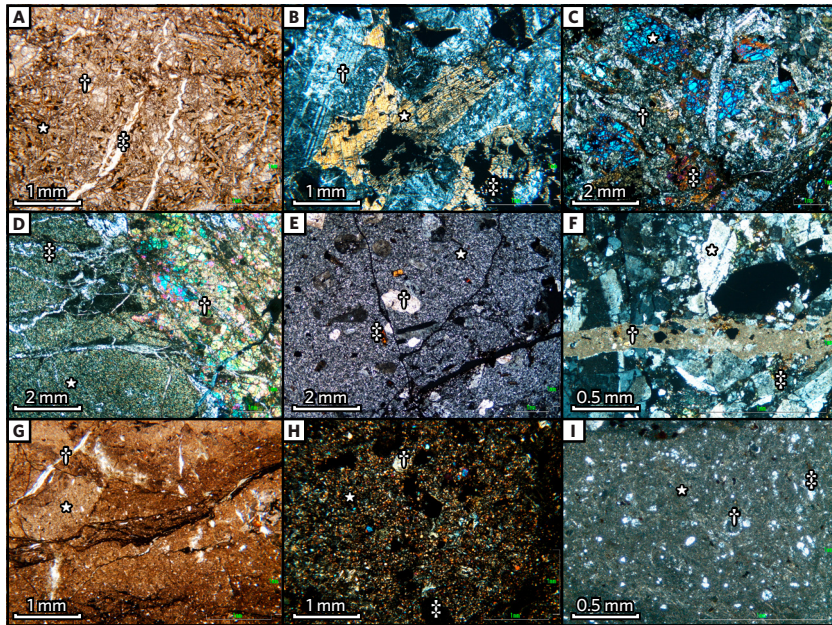


FIG. 9.2. Photomicrographs of the lithologies analysed in this geochemical pilot study. **A:** Altered basalt showing pseudomorphs of plagioclase lathes now replaced by clays (*), strongly altered and fractured olivine phenocrysts (†), and a zeolite vein (‡). **B:** Altered gabbro with twinned clinopyroxene phenocrysts (*), altered feldspar (†), and opaques (‡). **C:** Altered gabbro with fractured olivine (*), altered feldspar (†), and clinopyroxene (‡). **D:** Serpentinite containing fine grained serpentine and chlorite (*), zone of fractured fayalite (†), and quartz veins (‡). **E:** Fractured dacite with altered feldspar (*) and amphibole (†) phenocrysts within a fine-grained, clay-rich groundmass (‡). **F:** Brecciated granodiorite with altered feldspar phenocrysts with interstitial clay-rich material (†), cut by a microcrystalline calcite vein (‡). **G:** Deformed pelite containing phacoids of more cherty material (*) and cut by discontinuous zeolite veins (†). **H:** Volcanoclastic-rich pelite with abundant rounded silt-sized pyroxene clasts within a matrix of dark clay (*) with clasts of altered feldspar (†) and opaques (‡). **I:** Fossiliferous chert composed mostly of clays (*) with variably preserved silicious fossils (†) and amorphous silica (‡).

sometimes with chlorite, contain zones of fayalite, and are cut by calcite and quartz veins.

The dacites are identified as such by Buchs *et al.* (2009) on the basis of their geochemistry. These dacites are porphyritic with ~0.5 – 2 mm euhedral – subhedral phenocrysts of feldspar mostly altered to clays and ~0.2 – 0.5 mm subhedral phenocrysts

PROVENANCE OF THE OSA MÉLANGE BLOCKS

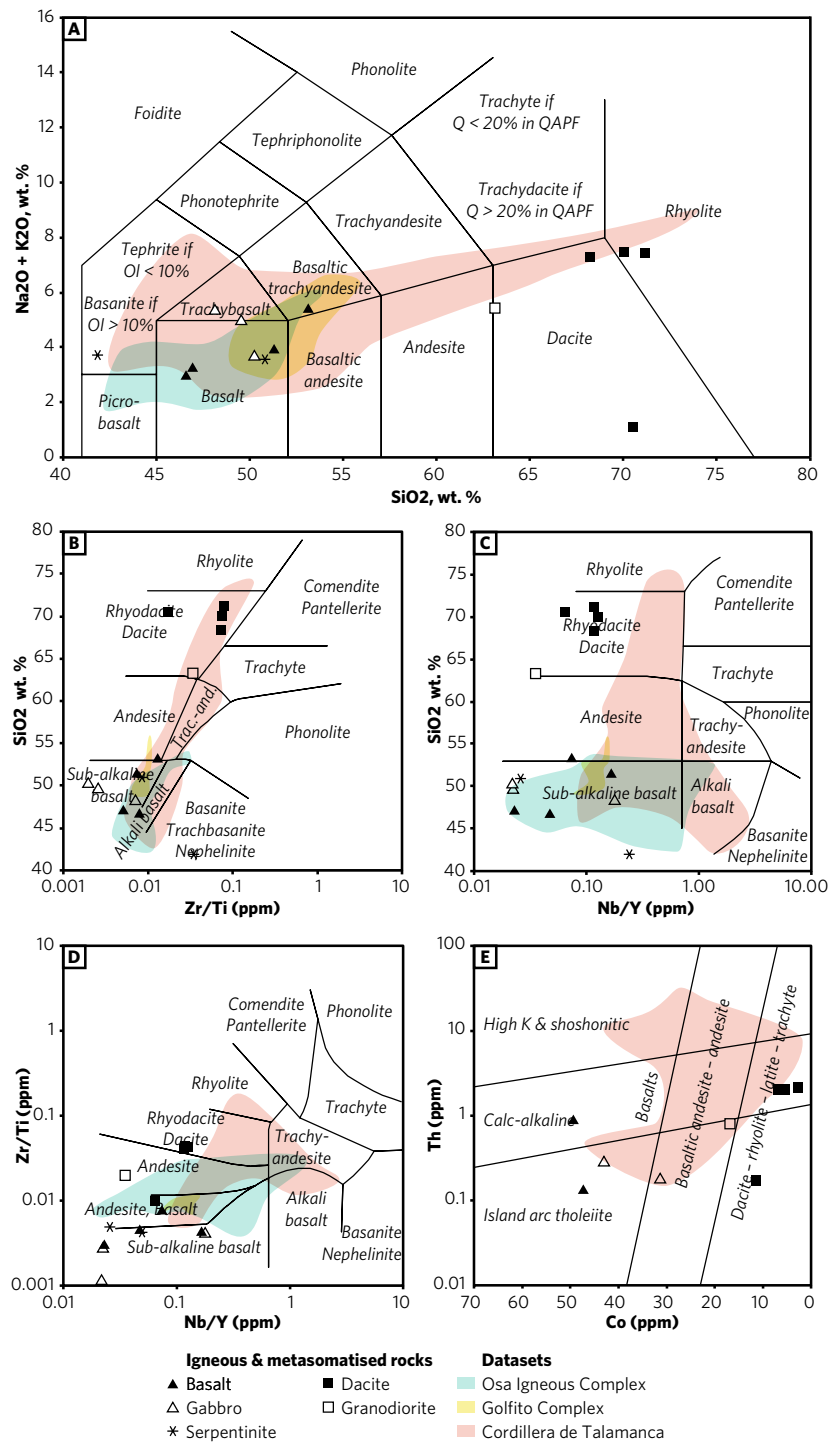


Fig. 9.3. Series discrimination diagrams showing samples of the Osa Mélangé over fields defined by the Osa Igneous Complex (Buchs et al., 2009), Golfito Complex (Buchs, 2008), and the Cordillera de Talamanca (Abratis, 1998). (Caption continued on opposite page.)

of amphibole in a fine-grained altered feldspathic groundmass. Despite being extensively brecciated, few veins cut this lithology (Fig. 9.2d). The granodiorite consists of ~0.5 – 2 mm subhedral quartz and feldspar crystals that have been pervasively brecciated with chlorite being present throughout. This brecciation includes cataclasis and comminution close to fractures zones, and fracturing within the more intact portions (Fig. 9.2e). The extensive alteration — especially of the feldspars — prevents accurate assessment of the mineralogical proportions in these rocks.

Pelite samples are composed of clays with varying contents of volcanoclastic material including basalt lithic clasts (Fig. 9.2f). Chert blocks also contain a high proportion of clay in addition to microfossil fragments and amorphous silica (Fig. 9.2g). Both pelite and chert blocks are pervasively cut by calcite and zeolite veins.

9.2. RESULTS

9.2.1. *Series discrimination*

These samples exhibit extensive alterations of the primary mineralogy — mostly to clays — which likely occurred throughout the geological history of the *mélange*, including during ocean floor metamorphism, subduction and deformation within the subduction channel (Chapter 7), by circulating fluids within the forearc, and by tropical weathering conditions at the surface. Additionally, several samples are cut by veins — mostly calcite and zeolite — which are too pervasive to exclude from the sample during preparation for geochemical analysis. As such, fluid-mobile elements — such as Ba, Cs, K, Na, Pb, Rb, Sr, U — were used with caution. Silica content of samples cut by quartz or zeolite veins is elevated from its photolith, while elevated Ca will be present in rocks containing

Fig. 9.3. (CONTINUED) **A:** Total alkalis over silica diagram (Le Bas *et al.*, 1986). **B – D:** Winchester and Floyd (1977). **E:** Hastie *et al.* (2007), Osa Igneous Complex and Golfito Complex datasets are not shown on this diagram as the Buchs (2008) and Buchs *et al.* (2009) datasets lack Co data. Serpentinite samples not shown as they lack sufficient concentrations of Co or Th to plot on the diagram.

PROVENANCE OF THE OSA MÉLANGE BLOCKS

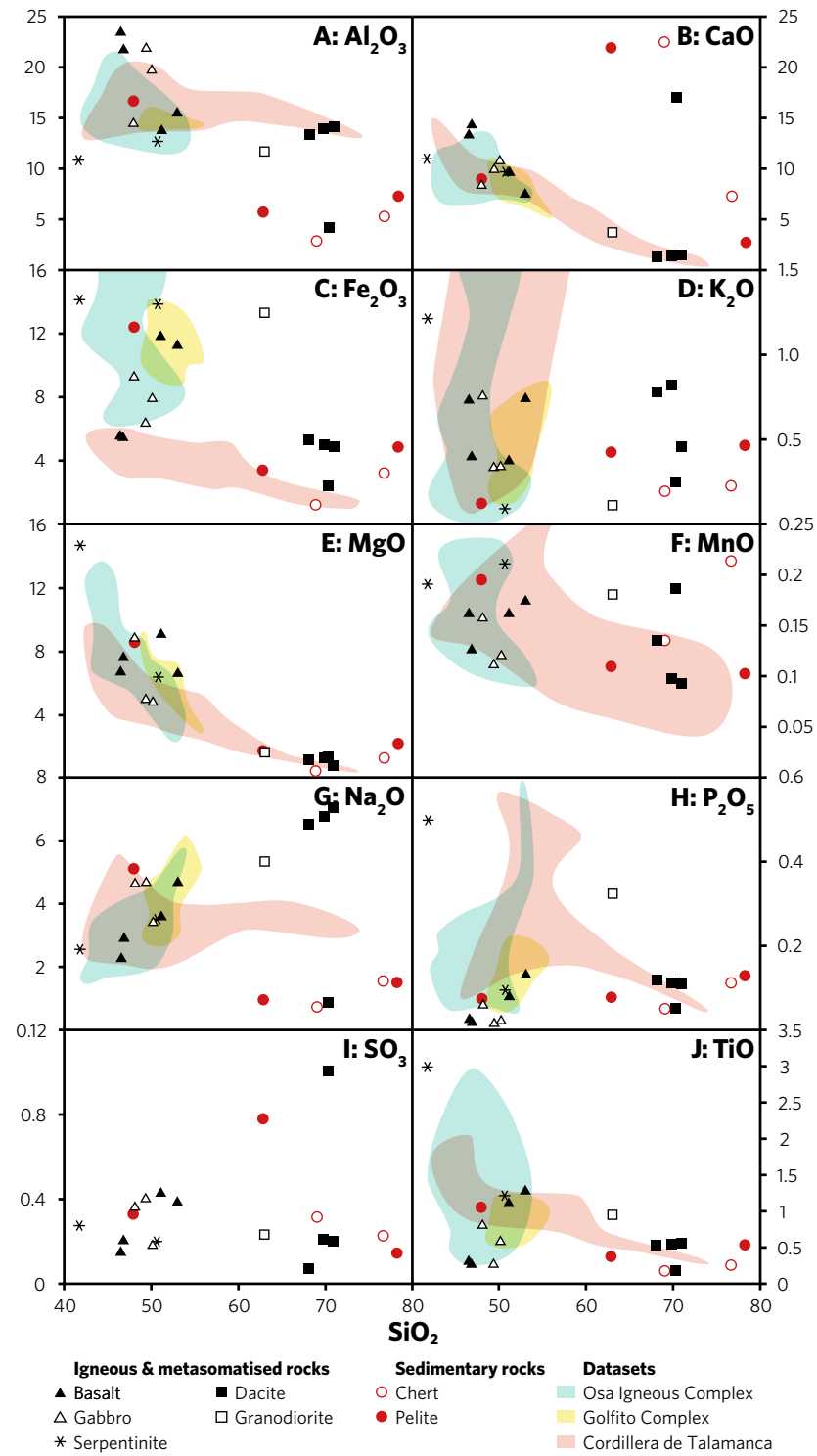


FIG. 9.4. Harker diagrams showing variation of major elements with silica. All oxides are in wt%. Diagrams show samples of Osa Mélange over fields demarcated by the Osa Igneous Complex (Buchs *et al.*, 2009), Golfito Complex (Buchs, 2008), and... (Caption continued on opposite page.)

calcite veins. High field strength elements (HFSEs) – such as Nb, Ta, Zr, and Y – are expected to more accurately reflect the primary composition of the rock. Due to the use of a tungsten-carbide mill in the sample preparation, contamination with Co and Ta is possible, therefore these elements are used with precautions.

Our geochemical results are in good agreement with other datasets produced from the Osa Mélange by Hauff *et al.* (2000a) and Buchs *et al.* (2009), although our study expands on these previous contributions by including analysis of sedimentary and metasomatised rocks.

The Total Alkali over Silica (TAS) diagram (Le Bas *et al.*, 1986) – as well as series discrimination diagrams from Winchester and Floyd (1977) and Hastie *et al.* (2007) – are in broad agreement about the lithological categorisation (Fig. 9.3). All samples display a sub-alkaline trend, as shown on a TAS diagram (Fig. 9.3), and samples cluster around the basalt and dacite/rhyodacite fields, with no samples intermediate between those compositions present in the mélange. Despite the extensive alteration, the agreement between the alkali content and the trace element ratios for most samples suggests that alteration was not sufficient to significantly change the mobile element concentrations at the scale of the sample.

Basalt samples exhibit a range of silica values from 46.6 to 53.2, placing them within the sub-alkaline basalt – basaltic trachyandesite fields. Gabbro samples exhibit silica values ranging from 48.2 – 50.2 and have generally higher alkali content than the basalts, although their HFSE ratios suggest less alkaline compositions than the basalts (Fig. 9.3). The serpentinite samples range in silica content from 41.9 to 50.9 with a narrow variation in alkali content from 3.5 to 3.7, giving it a mafic to ultramafic composition. Dacite samples straddle the dacite/rhyodacite/rhyolite fields of the TAS (Le Bas *et al.*, 1986) diagram and the Winchester and Floyd (1977) diagrams and exhibit silica contents ranging from

Fig. 9.4. (CONTINUED) ...the Cordillera de Talamanca (Abratis, 1998).

A: Al₂O₃. **B:** CaO. **C:** Fe₂O₃. **D:** K₂O. **E:** MgO. **F:** MnO, Golfito Complex not shown as Mn concentrations in this complex are significantly above those plotted. **G:** Na₂O. **H:** P₂O₅. **I:** SO₃, no comparative datasets shown as none of the datasets included SO₃. **J:** TiO.

68.3 to 71.2. The granodiorite sample has a less evolved composition than the dacites, plotting just within the dacitic field of the TAS diagram (Le Bas *et al.*, 1986) and Winchester and Floyd (1977) diagrams with a silica content of 63.2 (Fig. 9.3).

The mafic component of the Osa Mélange matches well with the Osa Igneous Complex (Buchs *et al.*, 2009). The intermediate – felsic component, however, is significantly more evolved than any rocks described from the Golfito Complex (Buchs, 2008) and is compatible only with the most evolved component in the Cordillera de Talamanca (Abratis, 1998).

9.2.2. Major elements

Most major elements – with the exception of sulphur – display very weak – moderate negative correlations with silica (Fig. 9.4). Basalt samples have highly variable major element compositions, most notably in the mobile elements (e.g. Al, K, and Na). These samples display no regular trend in Mg concentrations with silica, but exhibit a strongly positive correlation of Fe with silica. Positive correlations with silica also exist for Al, Na, P and Ti while Ca displays a negative correlation. Gabbros exhibit less variable major element compositions with a strong positive correlation of Ca with silica and moderate negative correlations of Mg with silica. Serpentine samples have similar Al, Ca, Fe, Mn, Na, and S concentrations but significant variations in K, Mg, P, and Ti contents. Dacite samples exhibit broadly similar concentrations of most elements with low Ca, Fe, Mg, P, S, and Ti, moderate Al, K, and Mn, and high Na; no elements display strong correlations with silica. With the exception of sample OSA 16.060 (which plots as an outlier on the Al, Ca, Fe, Na, S, and other diagrams), dacitic samples exhibit positive correlations in Al and Na against silica and negative correlations between Fe and silica. The granodiorite sample exhibits low Ca, K, Mg, S, and Ti, moderate Al, Mn, Na, and P, and high Fe, resulting in a high Fe/Mg ratio. Pelite samples display the most variable major element compositions, with silica contents ranging from 48.2 (OSA 16.147) – 78.5 (OSA 16.009); no major element exhibits strong correlation with silica. Chert samples display high (>69.2%) silica contents with broadly similar low concentrations of Al, Fe, K, Mg, Na, P, S, and Ti with elevated Ca (likely due to calcite veining) and Mn.

Mafic and ultramafic rocks exhibit major element concentrations consistent with the Osa Igneous Complex, with some minor variations outside of the ranges of this complex likely due to alteration. These samples also plot within or close to the fields defined by the Golfito Complex and mafic components of the Cordillera de Talamanca, although variability between these rocks and the datasets for these sources is greater than that between these rocks and the Osa Igneous Complex. While the dacite and granodiorite samples exhibit silica values consistent with the felsic end-member of the Cordillera de Talamanca – and significantly higher than any samples from the Osa Igneous Complex or Golfito Complex – their major element composition distinguishes them from the Cordillera de Talamanca rocks. Most notably they display lower K, higher Na, and higher Fe concentrations. Sample OSA 16.060 exhibits distinct chemistry from the other dacites and plots most like the pelite and chert samples; plotting most like the sedimentary rocks suggests a high degree of alteration. The sedimentary rocks generally plot distinct from the igneous rocks and do match the compositions of the Osa Igneous Complex, Golfito Complex, or Cordillera de Talamanca, however OSA 16.147 – a volcanoclastic-rich pelite containing basalt lithic clasts – consistently displays chemistry similar to the basalt blocks and to the Osa Igneous Complex (Fig. 9.4).

9.2.3. Trace elements

All lithologies display a broadly similar trace element pattern defined by moderately enriched large ion lithophile elements (LILEs) relative to mid-ocean ridge basalt (MORB) (Gale *et al.*, 2013) and MORB-like to slightly depleted high field strength elements (HFSEs) (Fig. 9.5). Maximum enrichments are two orders of magnitude above MORB while maximum depletions are one order of magnitude below MORB.

Basalt samples display elevated LILEs and MORB-like to depleted HFSEs. These samples show general depletion of Nb, Ta, and La but do not display a distinct negative Nb anomaly, and exhibit positive Pb and Sr anomalies. Gabbro samples display a similar trace element pattern to the basalts but display more pronounced anomalies; this includes Ta below detection in two samples, Pb below detection in all samples, a greater Sr anomaly, and

PROVENANCE OF THE OSA MÉLANGE BLOCKS

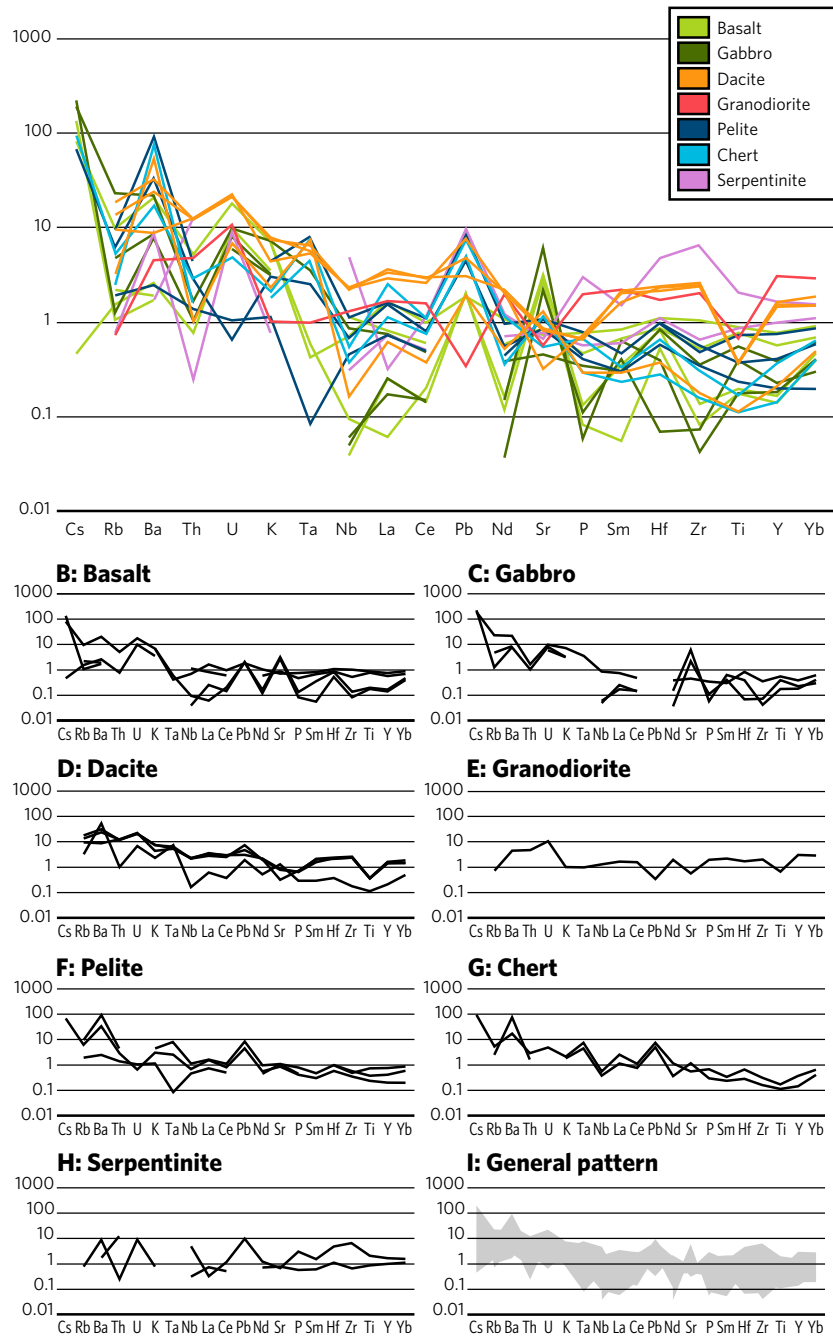


FIG. 9.5. Normalised multi-element (spider) diagrams for the Osa Mélangé normalised against MORB (Gale *et al.*, 2013). **A:** All samples plotted over each other to illustrate how each sample compares to and contributes to the general trend. **B:** Normalised multi-element diagram for basalt samples. **C:** Normalised multi-element diagram for gabbro samples. **D:** Normalised multi-element diagram for dacite samples. (Caption continued on opposite page.)

a mild negative Zr anomaly. No negative Nb anomaly is present in these samples. Dacite samples also display similar trace element patterns to the basalts and gabbros but exhibit less enrichment in LILEs. These rocks similarly exhibit mild negative Th, positive Pb, and negative Ti anomalies but these samples do display a mild negative Nb anomaly. The granodiorite sample does not display the typical trace element pattern and instead features slightly enriched HFSEs. Enrichments in Ba, Th and U are present, but Cs is below detection and Rb is depleted. This sample displays MORB-like Nb with no negative anomaly, while mild negative Pb, Sr and Ti anomalies are present. The serpentinite samples feature variable enrichments and depletions in LILEs with no overall enrichment. One sample exhibits a positive Pb anomaly while in the other sample Pb is below detection and in both samples Ta is below detection. Sedimentary samples display similar trace element patterns to the igneous rocks, with enriched LILEs and slightly depleted HFSEs. Two pelite samples exhibit enriched Ta and one sample exhibits a negative Ta anomaly, while Nb concentrations are MORB-like. Chert samples, however, feature positive Ta anomalies and negative Nb anomalies. It is notable that only the plutonic rocks have negative Pb anomalies, while all other lithologies — including the pelite and chert — feature positive Pb anomalies (Fig. 9.5).

The general pattern of Osa Mélange trace elements is consistent with both the Osa Igneous Complex and the Golfito Complex while overall trace element patterns in the mélange are less enriched than in the Cordillera de Talamanca (Fig. 9.6). The positive Pb anomaly present in the Osa Igneous Complex is less pronounced in the Osa Mélange, while depletions of HFSEs are greater in the Osa Mélange than in the Osa Igneous Complex. The Osa Mélange displays greater trace element variability than the

Fig. 9.5. (CONTINUED) **E:** Normalised multi-element diagram for granodiorite samples. **F:** Normalised multi-element diagram for pelite samples. **G:** Normalised multi-element diagram for chert samples. **H:** Normalised multi-element diagram for serpentinite samples. **I:** Normalised multi-element diagram showing the footprint of the general trace element pattern exhibited by the Osa Mélange samples.

PROVENANCE OF THE OSA MÉLANGE BLOCKS

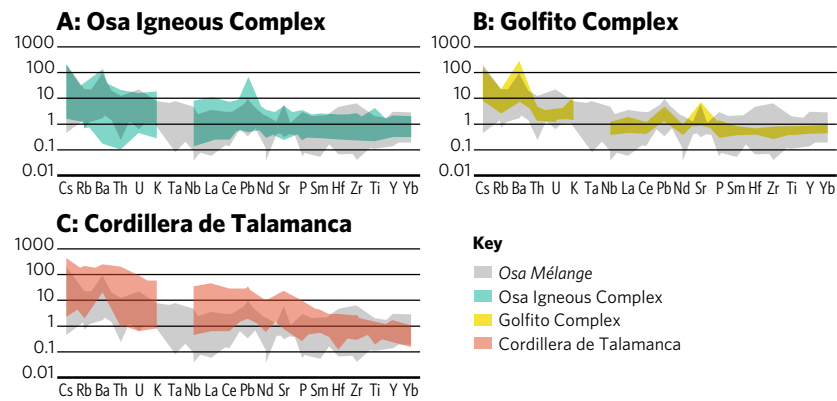


Fig. 9.6. Normalised multi-element (spider) diagrams showing the footprint of the general trace element pattern of the Osa Mélange against the footprint of the: **A:** Osa Igneous Complex (Buchs *et al.*, 2009) **B:** Golfito Complex (Buchs, 2008) **C:** Cordillera de Talamanca (Abratis, 1998).

Golfito Complex but similar overall trends, with a greater positive Ba anomaly than the Osa Mélange. Note that neither the Golfito Complex proto-arc nor the Cordillera de Talamanca arc display strong negative Nb anomalies, while the greatest positive Pb anomalies are present in the Osa Igneous Complex.

The tectonic discrimination diagrams (Fig. 9.7) are generally ineffective at discerning the origin of the mélange blocks due to their often-contradictory results. However, trace element ratios shown on these diagrams are useful for comparing the blocks to their possible sources. On the Fitton *et al.* (1997) diagram (Fig. 9.7a), the Osa Igneous Complex plots between MORB and the Icelandic plume array, while the Cordillera de Talamanca plots between the plume array and the arc field; the Golfito Complex plots entirely within the plume array. The majority of Osa Mélange samples plot below the lower tramline, within the MORB to arc field. The dacites – with the exception of OSA 16.060 which plots within the MORB field with the Osa Igneous Complex – plot at the periphery of the field demarcated by the Cordillera de Talamanca, while the granodiorite plots well within the MORB field. Two of the gabbro samples plot within the plume array but well outside of the Osa Igneous Complex field with Zr/Y ratios <1.

On the Pearce and Norry (1979) diagram (Fig. 9.7b) the Golfito Complex plots within the “island arc” field while both the Cordillera de Talamanca and Osa Igneous Complex span from

the “island arc” to the “within plate” fields, with the Osa Igneous Complex generally having higher Zr content than the Cordillera de Talamanca. Most Osa Mélange samples plot outside of the demarcated fields, however the basalt, gabbro, serpentinite and one dacite sample plot around and within the “island arc” field, while most of the dacites plot within the “within plate” field with Zr concentrations higher than any of the Cordillera de Talamanca samples, placing them within the Osa Igneous Complex field. The granodiorite sample also has Zr concentrations higher than the “island arc” field, placing it closest to the MORB field.

The Hollocher *et al.* (2012) diagrams (Fig. 9.7c, d) better discern the tectonic setting than the Fitton *et al.* (1997) or the Pearce and Norry (1979) diagrams. On these diagrams, the Osa Igneous Complex plots between the “major ocean”/“MORB” field and the “ocean island” field. The Golfito Complex plots within the “major ocean” field on Fig. 9.7c and the “oceanic arc” field on Fig. 9.7d. The Cordillera de Talamanca mostly plots within the “continental arc” to “alkaline arc” fields. The mafic blocks within the Osa Mélange generally plot between the “major ocean”/“MORB” field and the “oceanic arc” field with few samples plotting within the field demarcated by the Osa Igneous Complex. On Fig. 9.7e, the dacite blocks plot within the Golfito Complex field, within the “major ocean” field, and away from the Cordillera de Talamanca field. On Fig. 9.7d, the dacites plot away from the Golfito Complex and on the edge of the Cordillera de Talamanca field within the “oceanic arc” field. On all of these diagrams, the dacites plot away from or at the periphery of the Cordillera de Talamanca field, while the mafic blocks either plot within or close to the Osa Igneous Complex field.

9.3. DISCUSSION

The Osa Mélange basalts have been attributed — either directly (Vannucchi *et al.*, 2006; Clarke *et al.*, 2018) or indirectly (Buchs *et al.*, 2009) — to Galapagos-hotspot-derived seamounts on the basis of the similarity in trace element pattern with the better-studied Osa Igneous Complex; which has itself been shown by Hauff *et al.* (2000a) and Buchs *et al.* (2009; 2016) to derive from Galapagos-hotspot-derived seamounts and plateaus on the basis of its Pb

PROVENANCE OF THE OSA MÉLANGE BLOCKS

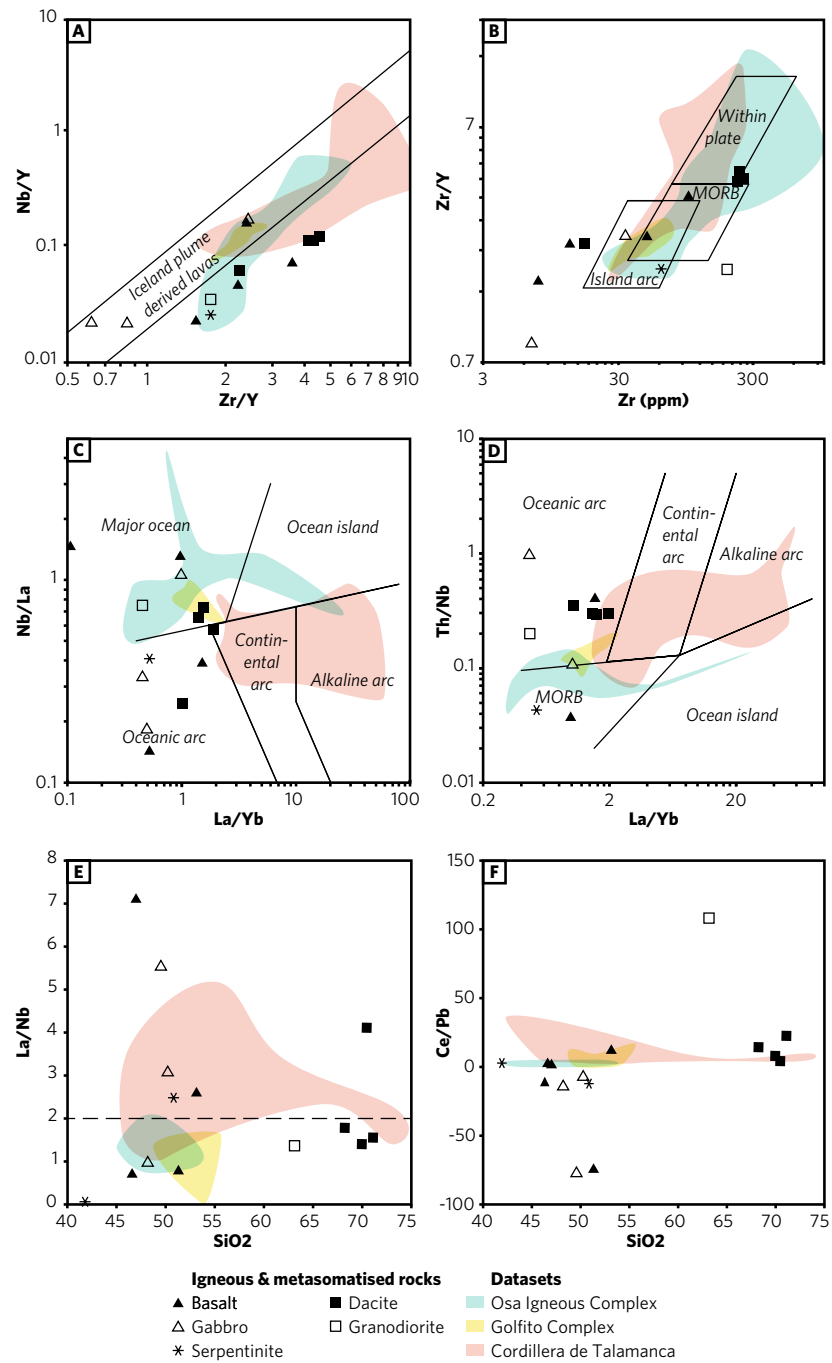


Fig. 9.7. Tectonic discrimination diagrams showing the Osa Mélange plotted over fields demarcated by the Osa Igneous Complex (Buchs et al., 2009), Golfito Complex (Buchs, 2008), and the Cordillera de Talamanca (Abratis, 1998). **A:** Nb/Y - Zr/Y diagram (Fitton et al., 1997). **B:** Zr/Y - Z (Pearce and Norry, 1979). **C:** Nb/La - La/Yb (Hollocher et al., 2012). **D:** Th/Nb - La/Yb (Hollocher et al., 2012). **E:** La/Nb - SiO₂. **F:** Ce/Pb - SiO₂.

and Nd isotope signature. The data presented in this chapter is in good agreement with that assessment.

Despite the enriched LILEs and slightly depleted HFSEs, the consistent plotted position of the Osa Mélange basalt within the field of the Osa Igneous Complex is convincing that they share a source. The plotted position of these basalts on the tectonic discrimination diagrams (Fig. 9.7) in the “MORB”/“ocean island” fields and away from the Golfito Complex and Cordillera de Talamanca arc suggests that these rocks did not form in a supra-subduction zone environment. No evidence is found for the presence of boninites or other high-silica mafic rocks associated with subduction zone magmatism.

Buchs *et al.* (2009) suggests that the intermediate – felsic rocks in the Osa Mélange are derived from the Central American arc. They make this interpretation on the basis of mild negative Nb anomalies, La/Nb and Ce/Pb ratios which they assert are representative of an arc-related origin, and a positive Pb anomaly also seen in the Cordillera de Talamanca (Abratis, 1998). The arc that sourced these blocks is inferred to be the Campanian – Eocene arc belt preserved in the Golfito Complex, as all recent models of Osa Mélange formation place mixing of the San Pedrillo Unit in the earliest Miocene or earlier, before the development of the Neogene – recent volcanic arc which the Cordillera de Talamanca is a part. While incorporation of arc material from the Golfito arc is possible due to its position in the frontal forearc at the time of Osa Mélange accretion, allowing both/either mass wasting at the surface and tectonic erosion at depth to contribute material to the mélange, incorporation of arc material from the Cordillera de Talamanca is improbable due to the presence of the Térraba forearc basin (from which the Fila Costeña fold and thrust belt was formed). The Fila Costeña does not contain blocks or substantial clasts of arc rocks and it is unfeasible for mega-blocks to be transported through this basin without depositing any similar material and without leaving a record of catastrophic flows within the stratigraphy of the Fila Costeña.

Despite the Osa Mélange dacites being interpreted by Buchs *et al.* (2009) as derived from the Golfito Complex arc, these rocks are compositionally distinct from any of the rocks found within the Golfito Complex. Notably, the highest silica rocks within the

Golfito Complex are basaltic trachyandesites (Fig. 9.3) and no rocks as evolved as the dacites and rhyodacites are present (Buchs, 2008). The most evolved end-members of the Cordillera de Talamanca arc display similar silica and alkali contents to the Osa Mélangé dacites; however, this arc also exhibits a broad range of magmatic lithologies from low-silica basalts through to rhyolites, but none of the more intermediate composition rocks are present in the Osa Mélangé. While the overall alkali content of the Cordillera de Talamanca and the Osa Mélangé dacites are similar, the Osa Mélangé dacites contain notably lower concentrations of K and notably higher concentrations of Na. The Osa Mélangé dacites have a slightly higher alkali content than the Golfito Complex, with similar K and high Na concentrations. Other major element concentrations are similar between the Cordillera de Talamanca and the Osa Mélangé dacites, while the Osa Mélangé dacites have lower Ca, Fe, Mg, and Ti, and higher Na than the Golfito Complex. The most notable major element characteristic of the Golfito Complex is high Mn concentrations >0.5 wt%, which is not present in the Osa Mélangé dacites which have Mn concentrations <0.2 wt%.

The trace element pattern of the Osa Mélangé dacites are most like the patterns of the Osa Igneous Complex and Golfito complex and are notably less enriched in LILEs than the Cordillera de Talamanca (Fig. 9.5 & 6). The trace element pattern of the Osa Mélangé granodiorite is notably distinct from the pattern of arc rocks – such as the Cordillera de Talamanca and the Golfito Complex – as it lacks significant enrichment of LILEs and exhibits enrichment of HFSEs. It is notable that the Osa Mélangé dacites and granodiorite exhibit less enrichment in LILEs than the Osa Mélangé basalts, despite arc rocks typically being characterised by LILE enrichment relative to MORB and ocean island rocks (Whattam and Stern, 2016). The Osa Mélangé dacites consistently plot outside or at the periphery of the Cordillera de Talamanca field on the tectonic discrimination diagrams and – with the exception of Fig. 9.7c – well outside of the Golfito Complex field (Fig. 9.7). This is not suggestive of a provenance from either location.

Neither the Golfito Complex nor the Cordillera de Talamanca feature noticeable negative Nb anomalies, and while negative Nb anomalies are present in the Osa Mélangé dacites, they are also

seen in some of the Osa Melange basalts, gabbros and sediments, and not seen in the granodiorite. In these cases, negative Nb anomalies are well within the range of the variable enrichments and depletions in trace elements. The La/Nb ratio (Fig. 9.7e) of the Osa Melange dacites — with the exception of OSA 16.060 — is <2; within the range of the all of the compared datasets, including the Osa Igneous Complex. This ratio is therefore not useful for discerning the origin of the Osa Melange dacites and is certainly not diagnostic of an arc origin in this case, as argued by Buchs *et al.* (2009). Similarly, the Ce/Pb ratio (Fig. 9.7f) of the Osa Melange rocks is highly variable, suggesting that the Pb content of these rocks has been affected by the pervasive alteration, despite the assertion from Buchs *et al.* (2009) that the Pb content in the Osa Melange rocks reflects their primary chemistry. Nonetheless, the Ce/Pb ratio of the Osa Melange dacites is higher than that of the Osa Igneous Complex and the Golfito Complex, but within the range of the Cordillera de Talamanca.

Therefore, the hypothesis that the dacites in the Osa Melange are derived from the Golfito arc has a significant problem in that

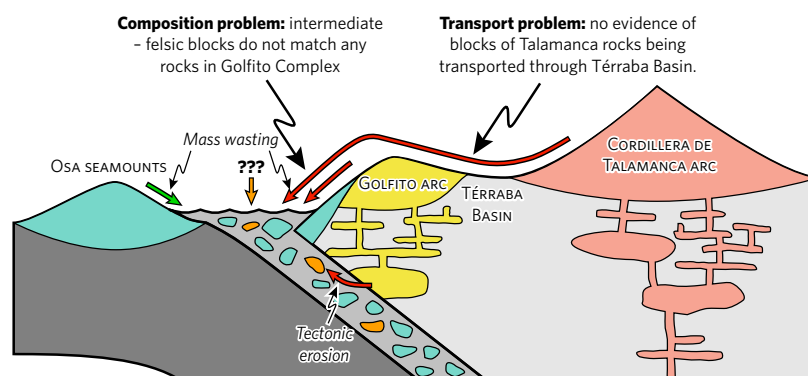


FIG. 9.8. Schematic diagram of the Costa Rican margin showing that Osa seamounts and the Golfito arc may be readily able to contribute material to the Osa Melange, but the Cordillera de Talamanca is — until the Quaternary — separated from the Middle America Trench by the Terraba basin in which the Fila Costena fold and thrust belt was deposited, which shows no evidence of input or transport of arc mega-blocks. The Golfito arc, while being positioned such that it may contribute blocks to the Osa Melange, lacks the high-silica rocks such as the Osa Melange dacites.

the rocks of the Golfito Complex arc are not compositionally resemblant of the Osa Mélangé dacites. These dacites are also highly unlikely to be derived from the Cordillera de Talamanca arc because this arc was not active at the time San Pedrillo Unit formation and because they lack a reasonable mechanism of transport. The attribution of the intermediate – felsic rocks in the Osa Mélangé to the Central American arc (Buchs *et al.*, 2009) is therefore challenged by this data. While it is conceivable that these intermediate – felsic blocks could be derived from a part of the Golfito arc that produced more evolved magmas and has now been entirely destroyed by tectonic erosion, alternative hypotheses, such as these dacites being derived from bimodal magmatism within the Osa seamount/plateau system itself, must therefore be considered.

Due to the similarity in the trace element chemistry between the Osa Igneous Complex, the Golfito Complex, and the Cordillera de Talamanca, definitively associating the Osa Mélangé intermediate – felsic rocks to one source cannot be done without further research. This is further complicated by the high degree of alteration experienced pervasively by these samples, meaning that fluid mobile elements cannot be reliably used in this analysis. Further analysis – likely including analysis of isotopes – is necessary to further discriminate between these datasets.

9.4. CONCLUSION

This study shows that the basalts, gabbro, and serpentinite samples are derived from the same Galapagos-hotspot-derived seamount system that produced the Osa Igneous Complex. Similarly, the sedimentary rocks are directly derived from decomposition of the basalts.

The provenance of the dacite and granodiorite blocks are ambiguous. To be sourced from the Golfito Complex arc, there must have been a compositionally distinct region with significantly more felsic rocks of which no remnants are exposed. However, there is no evidence that the Golfito arc ever produced dacites. While the Osa Mélangé dacites are compositionally similar to the felsic rocks of the Cordillera de Talamanca, any hypothesis that these dacites are derived from a proto-Cordillera de Talamanca arc faces a significant problem in the transport of these

>10s of metre blocks from the arc, through the Térraba forearc basin, and into the Middle America Trench where it was available for mixing into the Osa Mélange. It also faces a timing problem in that the San Pedrillo Unit – within which these blocks are found – was interpreted to have formed at the latest in the earliest Miocene, before the full development of the Neogene – recent volcanic arc which the Cordillera de Talamanca arc is a part. As such, this study suggests that the intermediate – felsic rocks within the Osa Mélange may not have been derived from the Central American arc as commonly assumed (e.g. Buchs *et al.*, 2009). Conceivable alternative sources for this intermediate – felsic material may be bimodal magmatism within the Osa seamount/plateau complex, although further analysis that is not within the scope of this doctoral project is needed to better constrain the provenance of these blocks.

THIS PAGE INTENTIONALLY LEFT BLANK.

CHAPTER 10. DISCUSSION

This thesis addresses how the input of a heterogeneous *mélange* from the upper plate affects the physical processes in the plate interface of an erosive subduction zone. Chapter 6 and Chapter 9 detail the origin of this *mélange* on the incoming plate and describes how significant volumes of volcanoclastic sediment containing blocks and megablocks of basalt and carbonate can accumulate on oceanic plates. Chapter 7 reports on the finding that these basalt blocks have been altered such that they are now weaker than their surrounding matrix and discusses the implications of this for the deformation that occurred in the subduction channel prior to accretion. Chapter 8 describes the varied complex fabrics present in the *mélange* and hypothesises how hydrofracturing-driven subduction erosion would occur in each of these varied rheologies and fabrics. In the following chapter, these ideas are synthesised, discussed and expanded upon in the answers to 4 key questions:

1. How and where did the Osa *Mélange* form?
2. What is the relationship between the Osa *Mélange* and the Caribbean Large Igneous Complex?
3. Is the Osa *Mélange* really a *mélange*?
4. What is the effect of *mélange* fabrics and rheology on slip at the plate boundary?

Sections 1, 2, and 3 of this discussion define the properties, structure, and deformation history of this heterogeneous material, while section 4 details how this material influences subduction erosion and slip within the subduction channel. These sections are followed by a critical evaluation of the processes and outcomes of this doctoral research.

10.1. HOW AND WHERE DID THE OSA MÉLANGE FORM?

As presented in Chapters 6 and 8, the Osa *Mélange* originated as an olistostrome within the flexural moat basin of a chain of Galapagos-hotspot-derived seamounts. This section compiles evidence and interpretations from Chapters 6, 7, 8, and 9 with relevant pre-existing literature (detailed in Chapter 2) to:

DISCUSSION

- Evaluate the relative merits of this hypothesis in comparison to other models.
- Build upon this hypothesis to interpret each package of the Osa Mélange in the context of its sedimentary facies and environment of deposition.
- Develop a comprehensive model for Osa Mélange formation.

10.1.1. Discussion of setting of deposition

As discussed in Chapter 6, a seamount chain's flexural moat is the preferred setting for initial formation of the Osa Mélange because it allows the accumulation of the significant volumes of quartz-poor, volcanoclastic sediment observed by this study. This subsection expands on the discussion in Chapter 6 and evaluates alternative settings for Osa Mélange formation to show why a flexural moat origin is the best fit for the available observations. Six potential settings for mélangé formation are considered:

- In-situ deposition of olistostromes onto the forearc slope.
- Tectonic disruption of the upper plate in the hanging wall of the subduction zone.
- Tectonic disruption of volcanic edifices on the lower plate during subduction.
- Tectonic disruption of normal ocean floor during subduction.
- Deposition of olistostromes into the trench, followed by accretion to the upper plate.
- Deposition of olistostromes into the flexural moat surrounding a seamount complex, followed by accretion to the upper plate.

Chapters 6 and 8 describe the Osa Mélange as consisting predominantly of sedimentary rocks, mostly in the form of volcanoclastic pelites and sandstones, as a matrix to blocks of basalt, chert and carbonate. These matrix sediments are predominantly composed of dark brown clays, basaltic lithic clasts, and pyroxene grains, with very little (0% to 5% ± 2%) quartz. Clarke *et al.* (2018) estimates that the present volume of the Osa Mélange is $23.0 - 24.6 \times 10^3 \text{ km}^3$; this volume underestimates the total volume of mélangé accreted as significant subduction erosion on the base of the forearc has removed portions of the Osa Mélange (Vannucchi *et al.*, 2013). Hauff *et al.* (2000b) and Buchs *et al.* (2009) determined that the basalt blocks have a Galapagos

ocean-island-basalt affinity. Material derived from the upper (Caribbean) plate is also reported in the mélange (Buchs *et al.*, 2009) but represents a very minor constituent (3 blocks, and some intermediate-composition clasts from Punta Campanario, reported in Buchs *et al.*, [2009]; 3 blocks reported in this study). Any mechanism of forming the Osa Mélange must be capable of producing significant quantities of quartz-poor volcanoclastic sediment, the majority of which is derived from Galapagos-affinity seamounts, and allow for the addition of rare intermediate-composition exotic blocks.

10.1.1.1. In-situ deposition of olistostromes onto the forearc slope

Olistostromes may occur within plates due to slope instabilities, usually caused by rapid uplift, change in slope angle, or volcanic or seismic activity (Delteil *et al.*, 2006). For such an olistostrome to occur, the source area must contain lithified or partially lithified rocks to be broken up into olistoliths. The forearc is a highly unstable region, undergoing subsidence or uplift, depending on the nature of the adjacent subduction zone and local features on the incoming plate undergoing subduction. The forearc is located above the Wadati-Benioff zone and as such may be the location of the epicentre of megathrust earthquakes and is also – by definition – close to the volcanic arc which may be another source of instability.

The geology of the forearc slope is critical for the occurrence of olistostromes. In fact, for an olistostrome to be deposited on the forearc slope, it must stall prior to reaching the trench, otherwise it would become a trench-fill deposit. Throughout the Cenozoic, the southern Central American region has consisted of the uplifted oceanic plateau of the Caribbean Large Igneous Province and the volcanic arcs above the Middle America Subduction Zone (Montes *et al.*, 2012). No metamorphic basement, orogenic, or cratonic rocks are exposed within the potential source area of such as olistostrome. As such, the dominant lithologies that can be expected to constitute the forearc are:

- Basalt from Caribbean Large Igneous Province (CLIP).
- Diverse basaltic – granitic composition igneous rocks from the arc.
- Volcanoclastic/epiclastic rocks from dissection of the arc/CLIP.
- Shallow water sediments similar to those found in Terraba basin.

DISCUSSION

The presence of a mature arc system producing dioritic and granitic rocks means that quartz will be abundant in derived sediments. Basalt blocks derived from the Caribbean Large Igneous Province will have an oceanic plateau-like geochemistry (e.g. flat REE trends) and a Galapagos signature (e.g. Hoernle *et al.*, 2002; 2004). The CLIP constitutes is overlain by both the volcanic arc and the overlying sediments and, as such, exposures from which CLIP basalt could be derived may be limited.

The Fila Costeña fold and thrust belt deformed the Terraba forearc basin sediments deposited from the Eocene to the Holocene (Chapter 2). The Terraba sedimentary succession does not contain olistostrome units and lacks blocks derived from the CLIP or the arc. It consists of bioclastic limestones, turbidites, and arc-derived volcanoclastics which differs significantly from the lithologies in the Osa Mélange. The Terraba basin/Fila Costeña can, therefore, be excluded as a source region for the Osa Mélange and cannot share a provenance. The outer forearc high (separating the forearc slope from the forearc basin) at the time consisted of the Late Cretaceous-early Eocene proto-arc of the Golfito Complex (Buch *et al.*, 2010). At present, the Golfito complex has not been eroded sufficiently to expose plutonic rocks; it can, therefore, be assumed that plutonic rocks were not exposed in this arc during the Eocene. No known exposures of the Caribbean Large Igneous Province are present near the Osa Peninsula. The lithologies of Osa Mélange are therefore inconsistent with an in-situ origin on the forearc slope.

10.1.1.2. Tectonic disruption of the upper plate in the hanging wall of the subduction zone

Meschede *et al.* (1999) proposed that the Osa Mélange was formed by tectonic disruption of the Caribbean Plate hanging wall (consisting of the Caribbean Large Igneous Province) by subduction erosion. Subduction erosion is a tectonic process which typically destroys its products as they are carried with the descending slab into the mantle. However, examples of rock units representing an erosive subduction channel do exist (e.g. Vannucchi *et al.*, 2008). This process primarily deforms the rocks already present in the

forearc, although some mixing with material exotic to the forearc may be facilitated within the subduction channel.

The forearc of the Middle America Subduction Zone near the Osa Peninsula at present has been interpreted as a “depositional forearc,” i.e. a forearc that has been deposited as a response to an extreme erosive event that consumed the pre-existing structure. As a consequence, most of the submarine portion of the forearc wedge now consists solely of sedimentary terrigenous rocks (Vannucchi *et al.*, 2016a). The catastrophic tectonic erosion was triggered by subduction of the Cocos Ridge and therefore the presence of a depositional forearc is a recent – within the last 2.5 Ma – development in the history of this margin (Vannucchi *et al.*, 2013, 2016a). Before the subduction of the Cocos Ridge, the forearc consisted predominantly of the Caribbean Large Igneous Province and its underlying oceanic crust, as well as the roots of the Golfito volcanic arc.

Tectonic erosion of this forearc would, therefore, produce a rock unit composed predominantly of CLIP basalt, possibly including some plutonic arc-related rocks, and a terrigenous sedimentary component.

As such, the Osa Mélange cannot be considered the product of tectonic erosion of the upper plate as:

- The basalt blocks in the Osa Mélange share greatest affinity with ocean island basalts and not with the Caribbean Large Igneous Complex (Buchs *et al.*, 2009).
- The Osa Mélange consists primarily of sedimentary rocks in the form of pelites and cherts which are definitively distinguished from gouged basalts by the presence of microfossils.
- The mélange also contains blocks of carbonates, which would be absent from the hanging wall at depth.

10.1.1.3. Tectonic disruption of volcanic edifices on the lower plate during subduction

Vannucchi *et al.*'s (2006) model instead argues that extensive tectonic disruption – resulting in dismemberment and mixing – effected volcanic edifices on the incoming plate to form the Osa Mélange. This would have been accomplished during the process of subduction and accretion. The resultant rock unit

DISCUSSION

would, therefore, contain the same constituent components as the seamount complex reconstituted into a *mélange*.

This model predicts that the Osa *Mélange* would mostly be composed of basaltic blocks similar to the Osa Igneous Complex, with volcanoclastic and sedimentary material as a minor component because – while an important constituent of seamount flanks – seamount flanks are dominantly settings of sediment bypass, not deposition (Leslie *et al.*, 2002). Siliciclastic sediment produced from a seamount complex would be rich in basalt lithic clasts, pyroxene grains, and clays and lack a significant proportion of quartz. Blocks of carbonate are also attributed to the seamount complex, implying that these seamounts grew to sufficient size to sustain a carbonate complex. Inclusion of material from other sources, such as the Caribbean Large Igneous Province or the Central American arc, is not predicted by this model, and their presence is used by Buchs *et al.* (2009) to oppose this hypothesis in favour of deposition in the Middle America Trench. However, tectonic incorporation of upper plate lithologies from the hanging wall into the subduction channel is conceivable, but unlikely due to the concurrent accretion of the Osa Igneous Complex which would have occupied the hanging wall at this time. Similarly, the high volumes of sedimentary material in the *mélange* constituting the matrix and some intermediate – felsic blocks described by Buchs *et al.* (2009) and Clarke *et al.* (2018) also argue against this hypothesis. However, the petrology of this sediment is consistent with a seamount source due to the lack of quartz and predominance of pyroxene grains.

10.1.1.4. Tectonic disruption of normal ocean floor during subduction

Conceivably, the Osa *Mélange* may have been formed by tectonic disruption of the oceanic plate in the absence of any seamount edifice. A *mélange* formed in this setting would be composed of the dismembered remnants of the oceanic crust – e.g. MORB basalt (likely containing pillow structures), dolerite, gabbro, and serpentinite (e.g. Dilek, 2003) – and its overlying sediments, typified by the “ocean plate stratigraphy” (OPS) detailed in Isozaki *et al.* (1990). However, no workers have proposed this hypothesis for

the formation of the Osa Mélange. Accretion and mélange formation in this setting is most often observed in long-established accretionary subduction zones, such as Japan and the Aleutians (Kusky *et al.*, 1997a, b).

While recent work has refuted the earlier (Penrose [Anonymous, 1972 cited in Dilek and Furnes, 2014]) inference that the well-established ophiolite sequence is representative of the internal structure of normal oceanic crust (e.g. Dilek, 2003; MacLeod *et al.*, 2013), the fast spreading rate of the East Pacific Rise – which formed the Farallon crust subducting beneath the Osa Peninsula until ~13 Ma – has drawn comparisons with the Oman ophiolite (Nicolas and Boudier, 2003) and is inferred to consist of Penrose-like pseudostratigraphy of sheeted dykes, gabbros and serpentinitised harzburgites and dunites (Dilek, 2003; Nicolas and Boudier, 2003).

Ocean plate stratigraphy is a generalised succession of oceanic sediments and is recognised in accretionary complexes and mélanges around the world (e.g. Kusky *et al.*, 1997a, b; Maruyama *et al.*, 2010). This succession is formed as the oceanic plate is transported through depositional environments as it migrates from the mid-ocean ridge to the trench. It consists, at its base, of mid-ocean ridge basalt overlain by, and sometimes intercalated with, deep-sea pelagic cherts deposited near or at a mid-ocean ridge. If the height of the mid-ocean ridge exceeds the carbonate compensation depth, pelagic limestones may be deposited. These pelagic sediments are overlain by hemi-pelagic mudstones as they approach a continental margin, and are finally covered by significant volumes of siliciclastic sediment in the form of shales, sandstones, conglomerates and olistostromes (Maruyama *et al.*, 2010).

Accretionary complexes formed this way preserve their constituent lithologies and their internal structures, even if the stratigraphic order is obscured during mélange formation (Kimura *et al.*, 2012). However, the Osa Mélange does not contain lithologies consistent with this setting of mélange formation. The basalt blocks analysed by Buchs *et al.* (2009) show that the basalts within the Osa Mélange have an ocean island basalt affinity, not a mid-ocean ridge affinity. The presence of even some OIB affinity basalts in a purely oceanic setting cannot be simply explained. There is also no evidence of pillow structures within the basalt blocks, nor a

DISCUSSION

sheeted dyke-like internal structure within the basalt megablocks. The sedimentary facies of the Osa Mélange is also markedly different from facies within typical ocean plate stratigraphy. Volcanoclastic sediment is ubiquitous throughout the Osa Mélange while absent from OPS, and 10^{-2} – 10^2 m blocks are present in every unit of the mélange, whereas they may only be found in the terminal trench-fill facies of OPS.

10.1.1.5. Deposition of olistostromes into the trench, followed by accretion to the upper plate

The high proportion of sedimentary material within the Osa Mélange was recognised by Buchs *et al.* (2009) who proposed that the mélange was originally deposited within the Middle America Trench and therefore constitutes a trench-fill deposit. Trench-fill sedimentation is a commonly ascribed process of mélange formation (e.g. Prohoroff *et al.*, 2012). This setting of formation adequately accounts for the volume and proportion of sediment within the mélange and explains the presence of arc-derived clasts. Ocean trenches may contain a diverse range of sediments and therefore investigation into the processes operating within trenches and their products is warranted here in order to evaluate whether it can explain the features observed in the Osa Mélange.

The diversity of sedimentary facies deposited in ocean trenches is a result of the varied morphology of the trench and forearc and numerous potential sources of sediment. The morphology of ocean trenches is predominantly controlled by sediment supply and convergence rate; however, this may be complicated by features in and adjacent to the trench, such as seamount re-entrants, structural blockages such as subducting seamounts and sediment fans, and submarine canyons (Underwood and Bachman, 1982). The downgoing plate may also cut by bend faults: large normal faults formed due to lithospheric flexure as the slab is bent (Ranero *et al.*, 2005). Trenches are bounded on the continent side by the forearc slope and the oceanward side by the flexural bulge (Husson *et al.*, 2012).

Sedimentation in ocean trenches is dominated by reworking of the continental margin. Large submarine canyons leading into the trench are a common feature in some margins and are a

prominent feature in the northern portion of the Middle America Trench (Ranero *et al.*, 2008). These allow sediment to bypass the slope and are a major source of sediment to the trench. Modern trench sediments are highly variable but typically consist of interbedded sandy turbidites and mudstones. Other sediment sources include background hemi-pelagic fallout, unconfined sediment flows on the slope, and mass wasting of the forearc slope into the trench. Mass wasting may occur by processes such as oversteepening of the forearc or ground movement during earthquakes. Some trench floors feature an axial channel where reworking of sediment is common, however non-channelised longitudinal flow occurs along most trench floors (Underwood and Bachman, 1982).

Accreted trench fill deposits have been recognised in many active and fossil subduction zone margins and are well described (e.g. Prohoroff *et al.*, 2012; Platt, 2015). The nature of the subduction zone environment in accretionary margins typically preserves trench fill sediments subsequent to intense deformation and re-ordering of stratigraphy. Accreted trench-fill deposits are generally found in accretionary prisms and generally have a long along-axis extent. They are typically dominated by turbidites and hemi-pelagites, plus material from the forearc slope in the case of mass wasting from the margin edge (Underwood and Bachman, 1982). Due to the high volumes of sediment deposited in the trench and the tectonic stacking of successive generations of trench-fill deposits, significant volumes of sediment may be accreted in this setting.

Buchs *et al.* (2009) attribute the Osa Mélangé to a trench-fill origin on the basis of a high proportion of sedimentary material and the presence of intermediate-composition igneous rocks attributed the Central American arc. However, the sedimentary facies within the Osa Mélangé is not typical of trench-fill deposits. The mélangé consists of significant volumes of volcanoclastic pelitic sediment containing no appreciable quartz content, and there is no evidence of turbidites throughout much of the mélangé; the only turbidites in the San Pedrillo Unit are the broken formation of turbidites in the Punta San Pedrillo Package. It is also not energetically feasible for >1 metre blocks of intermediate-composition igneous rocks to be transported to the trench from the arc while finer-grained sediment was not.

DISCUSSION

During the formation of the Osa Mélange, Costa Rica was far from the South American plate or any other potential source of continental sediment (Meschede and Barckhausen, 2001). Therefore, the primary source of terrigenous sediment in the trench would have been the volcanic arc. During the Late Eocene – Oligocene – when Buchs *et al.* (2009) interpret the San Pedrillo Unit was accreted – the Cordillera de Talamanca was beginning to build while the extinct Golfito arc was being denuded. As such, significant volumes of Golfito-derived material – including quartz-rich sediment – would be expected to have been deposited in Middle America Trench. Material from the active Cordillera de Talamanca could not have been transported to the trench without passing through the Terraba forearc basin now uplifted and exposed in the Fila Costeña fold and thrust belt, which contains no blocks of arc-derived igneous rocks.

Buchs *et al.* (2009) infer that the basalt blocks in the mélange are derived from the collapse of the already-accreted Osa Igneous Complex into the adjacent trench, triggered by the subduction of further seamounts. This setting satisfactorily explains the presence of high volumes of sediment, basalt blocks genetically linked to the Osa Igneous Complex, and the diverse block assemblages in the Cocolito and Punta San Pedrillo Packages. However, with the exception of very rare intermediate-composition blocks, no component can be attributed to the autochthonous upper plate.

The Middle America Subduction Zone has subducted Galapagos-hotspot-derived seamounts throughout its history (Hauff *et al.*, 1997, 2000a; Hoernle *et al.*, 2002). These subducting seamounts may have formed structural blockages that restricted the deposition of trench-sediments and starved the Osa region of sediment from the arc. However, as the deposition and accretion of the mélange are inferred to be a long-lived event, sustained obstruction of sediment by bathymetric highs on the incoming plate is infeasible.

Buchs *et al.*'s (2009) model of formation is also unfeasible because it requires rapid switches between accretionary and erosive behaviour without significant changes in sediment volume at the trench or plate velocity (cf. Clift and Vannucchi, 2004). They hypothesise that in the Eocene during the accretion of the

Osa Igneous Complex, subducting seamounts were accreted and did not trigger mass wasting from the forearc slope, however in the late Eocene – Oligocene, seamounts were subducted, causing subduction erosion and mass wasting into the trench. Prior to the mass wasting, no changes to the sediment thickness of the incoming plate is inferred and plate velocity is not inferred to change until the breakup of the Farallon Plate at ~23 Ma (Meschede and Barckhausen, 2001).

10.1.1.6. Deposition of olistostromes into the flexural moat surrounding a seamount complex, followed by accretion to the upper plate

Since no other conceivable setting of Osa Mélange formation remains, it is proposed in Clarke *et al.* (2018) that a broad sediment basin – a flexural moat or debris apron – surrounding the seamount complex from which the Osa Igneous Complex is derived is the most likely source for Osa Mélange material. Flexural moats form due to flexural bending of the oceanic crust to isostatically accommodate the mass of the seamount complex (Watts, 1994). However, since no other accreted moat deposit has been reported and in-situ flexural moats are highly inaccessible due to their location at great depths within the oceans, comprehensive petrological analysis of these deposits has not been conducted.

Flexural moats are composed mostly of material shed from the volcanic edifice mixed with pelagic and hemi-pelagic ocean sediment, and as such contains a high proportion of basalt and basalt-derived siliciclastic sediment, pelagic and hemi-pelagic mudstones, pelagic chert, and reef carbonates if the seamount is sufficiently large. Seismic imaging of seamount moats reveals that they are underlain by a layer of pelagic oceanic sediment deposited before the growth of the seamount. This pelagic layer also extends underneath the seamount edifice itself (Leslie *et al.*, 2002), and may facilitate severing from the downgoing slab and accretion. Since most large blocks and clasts remain close to the sediment source (Leslie *et al.*, 2002), and since most siliciclastic sediment is produced while the volcanic edifice is active, the sedimentary facies is indicative of the distance from the edifice and the time of deposition relative to the volcanic activity.

DISCUSSION

A key characteristic of these deposits is the lack of significant proportions of quartz grains, that are ubiquitous in terrigenous siliciclastic sediments. Instead, these deposits contain a high proportion of pyroxene grains and basalt lithic clasts. These deposits are predominantly composed of turbidites and debris avalanche deposits, meaning that clast size in these deposits are highly variable and may contain large blocks, although these blocks do not constitute the principal component. Mega-blocks up to hundreds of metres in scale derived from flank collapse have been well documented (Oehler *et al.*, 2008). These basins are commonly located away from continental margins, and therefore lack terrigenous input; however, if a moat is located close to a continental margin – as in the Canaries – continental material may be included in the moat deposit.

These characteristics match well with Osa Mélange, as the pelitic matrix is rich in pyroxene grains while lacking a significant quartz content. The common occurrence of debris flow deposits in flexural moats account for the pervasive block-in-matrix texture of the mélange and the lithologies which constitute these blocks – mostly basalt and carbonate – matches with the lithologies of blocks within the mélange. The presence of intermediate – felsic blocks attributed to the arc by Buchs *et al.* (2009) is simply explained in this hypothesis by incorporation while the moat was in the Middle America Trench. While this study attributes the majority of the material in the Osa Mélange to the seamounts from which the Osa Igneous Complex is derived, should future research find a greater proportion of material attributed to derived from the arc, this would not be incompatible with this hypothesis.

10.1.2. Recognition of relict sedimentary facies from moat in Osa Mélange

As the formation of the Osa Mélange is best explained by the flexural moat model (Clarke *et al.*, 2018), further inferences can be made between individual packages of the Osa Mélange and the sedimentary facies within flexural moats, allowing the original stratigraphy to be reconstructed. No way-up indicator structures have been preserved and existing biostratigraphic analysis

(Buchs *et al.*, 2009) lacks the precision to provide insight into the internal stratigraphy of the Osa M lange.

Flexural moats have been studied through seismic stratigraphy (e.g. Leslie *et al.*, 2002) and by submersible observations (e.g. Morgan *et al.*, 2007). These studies have revealed distinct sedimentary facies formed as the adjacent seamount evolves and distance from the seamount edifice varies. Seamount flexural moat deposits are seldom the product of only one seamount edifice. Seamounts continue to erode and contribute sediment after they cease to be magmatically active, and so multiple seamounts – at different stages in their evolution – may contribute sediment to the moat. This may result in an interfingering relationship between different moat facies. In the most extreme example, the distal portion of the moat around the youngest seamount may find itself located above the hotspot centre as the plate migrates over the hotspot. In this case, distal moat facies may be overlain by the lava flows forming the volcanic edifice itself (Leslie *et al.*, 2002). As such, proximal and distal sediments from primitive and late-stage seamounts may be intercalated without tectonic involvement. Growth of the seamount edifice may result in horizontal shortening of the moat wedge accommodated by thrust faults, a process referred to by flexural moat workers as “accretion” (Morgan *et al.*, 2007) but distinctly different from the subduction accretion referred to throughout this thesis. Therefore, thrust faults and tectonic interleaving of strata cannot be exclusively attributed to the subduction and accretion process.

10.1.2.1. *Facies in moats*

Leslie *et al.* (2002) defined 4 distinct facies within the Hawaiian moat on the basis of seismic reflection character:

- A basal pelagic unit composed of “normal” oceanic sediment.
- A proximal unit composed of debris avalanches and slumps.
- A distal unit composed of debris flows.
- A turbiditic facies composed of volcanoclastic turbidites.

As seamount complexes are formed on pre-existing oceanic plates, they are underlain by normal oceanic sediments, as described by Isozaki *et al.* (1990). This oceanic sediment will represent an incomplete succession of ocean plate stratigraphy

DISCUSSION

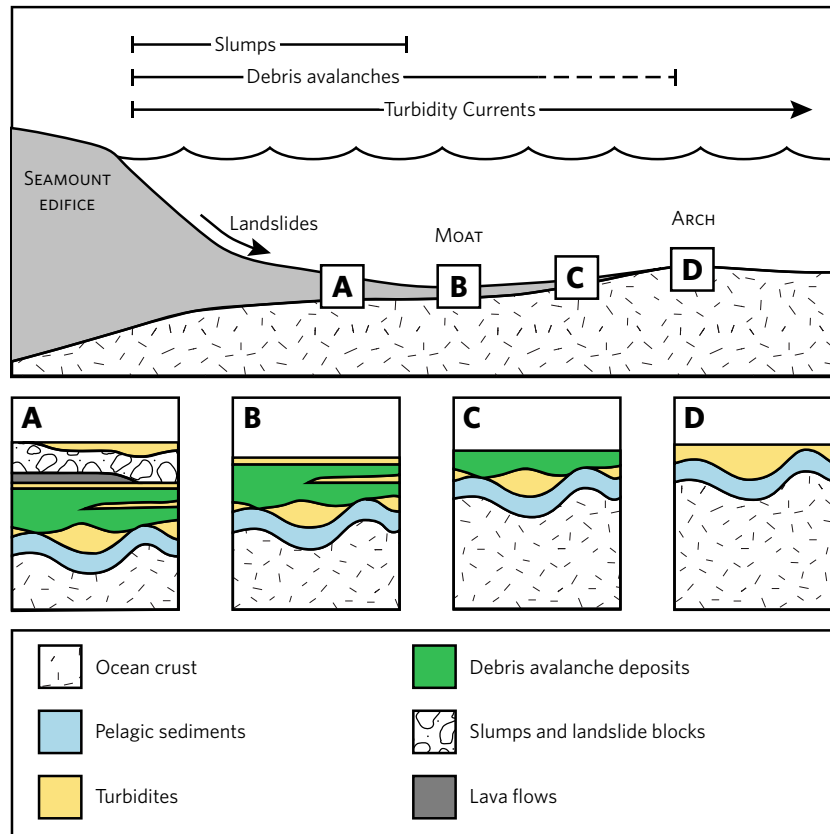


FIG. 10.1. Cross section through a seamount complex showing the variety of sediments deposited in seamount flexural moats (from Leslie *et al.*, 2002). **A:** Thick accumulations of sediments (including slump deposits) deposited in the proximal zone of the flexural moat. **B:** Debris avalanche deposits and turbidites deposited along the moat axis. **C:** Gradually thinning volcanoclastic debris as the setting of deposition becomes more distal. **D:** Mixture of distal turbidites and background pelagic sedimentation at the distal-most portion of the flexural moat.

(Isozaki *et al.*, 1990) and will typically only contain the pelagic portion (e.g. Leslie *et al.*, 2002). This pelagic layer maintains a near-constant thickness below the seamount complex and moat and drapes the topography of the oceanic basement (Leslie *et al.*, 2002).

The flexural moat-fill deposit is wedge-shaped, thins away from the chain of volcanic edifices, and is thickest near the scarps of slope failures. The proximal unit is deposited on, or close to, the lower slope of the seamount flanks and exhibits a highly

seismically chaotic texture. This unit is composed of poorly sorted volcanoclastic proximal debris avalanche and debris flow deposits and may contain megablocks derived from the catastrophic collapse of the seamount flanks. This unit is characterised by its chaotic, blocky fabric and lack of continuous reflections in seismic imaging (Leslie *et al.*, 2002).

The distal facies is composed of more distal debris avalanche and debris flow deposits with defined bedding. It is deposited within the moat basin and away from flanks of the seamount edifice and is interbedded with turbidites towards the outer arch. This unit may also contain megablocks (Leslie *et al.*, 2002). Turbidites are deposited extensively within the moat and on the outer arch. These turbidites are composed primarily of volcanoclastic material and vary in grain-size with distance from the edifice (Leslie *et al.*, 2002).

Although seismic reflectors typically dip towards the volcanic edifice, suggesting sediments were deposited during active subsidence, ten Brink and Watts (1985) and Rees *et al.* (1993) describe a “ponded” unit of sediment with horizontal reflectors overlying the preceding moat sediments. This “ponded” unit lies close to the volcanic edifice and is formed after the cessation of subsidence. The presence of continuous reflectors in this unit suggests that it is formed of bedded sediment, not the debris avalanche deposits of preceding units.

In addition to varying with distance from the volcanic edifices, the facies within the moat also varies with the evolution of the seamount from inception to extinction. Young, volcanically active edifices are more unstable and prone to collapse, producing debris avalanches and megablocks (Leslie *et al.*, 2002). If the seamount builds up to sufficient height, it may be colonised by carbonate reefs, adding carbonate blocks/material to the volcanoclastic sediment. Very large, particularly subaerial, seamounts may feature protracted sediment transport pathways, yielding more texturally and compositionally mature sediment. As the magmatism shuts off, debris avalanches and debris flows become less common and moat sedimentation becomes dominated by turbidites and background pelagic sedimentation (Leslie *et al.*, 2002). The growth stage of seamount moats typically produce a coarsening upwards sequence as the volcanic front migrates over the oceanic plate.

DISCUSSION

This may be overlain by a fining upwards sequence as the volcanic front moves away from that point of the moat (Leslie *et al.*, 2002).

If the seamount complex is subducted, the flexural moat will be buried beneath trench-fill sediments as the moat enters the trench. The process of subducting a seamount is likely to also cause instability in the seamount flanks, which will directly contribute seamount-derived material into the trench-fill deposit.

10.1.2.2. Interpretation of each package of the Osa Mélange in terms of sedimentary criteria

The subdivided units of the Osa Mélange vary in the lithology, size, shape, alignment, and abundance of their block populations – as described in detail in Chapter 8.4 – but all contain the same pyroxene-rich/quartz-poor sedimentary matrix, used by Clarke *et al.* (2018) to attribute this mélange to a seamount flexural moat. Given that these units are distinguished on the basis of their distinctive facies characteristics, these units can be attributed to their setting of deposition within the flexural moat system. While few thrust faults are directly observed, the high degree of shearing and internal folding suggests that stratigraphic order may have been extensively disrupted during subduction and accretion. Additionally, thrust faults have been observed to develop in-situ in flexural moats during the growth phase of the seamount edifice (Morgan *et al.*, 2007).

The pelagic and hemipelagic clays and cherts within the Bahia Drake Package are interpreted to represent formerly interbedded sediments that have been tectonically dismembered during the subduction and accretion process. These pelagic and hemipelagic lithologies contain planktonic foraminifera and clay – silt-sized siliciclastic grains, suggesting that the Bahia Drake Package was deposited in a largely quiescent environment. However, the presence of carbonate blocks containing fragmented, shallow-water (Buchs *et al.*, 2009) microfossils and rare basalt blocks indicate that the seamount edifice did contribute some material. Therefore, the Bahia Drake Package represents the distal portion of flexural moat dominated by distal flows and background abyssal sedimentation punctuated by larger turbidites and debris flows which bring the basalt and carbonate blocks. The presence of the

igneous and carbonate blocks precludes an association with the underlying pelagic “pre-moat” unit. The presence of carbonate blocks indicates that the source seamount was sufficiently large to maintain a carbonate complex.

In contrast, the Cocolito Package contains a high proportion of 10^{-2} – 10^2 metre-sized blocks consisting of carbonate, chert, some basalt, and one block of granodiorite. This variety in block lithologies suggests they were sourced from a mature seamount system colonised by carbonate reefs. Since the provenance of the granodiorite block is ambiguous (Chapter 9), its relationship to the origin of the *mélange* must be interpreted with precautions. If it originated from the upper plate, it may have been added to the Cocolito Package after it was deposited; however, if it originated from the seamount complex itself, it could have added alongside the basalt blocks. The presence of chlorite in this block – rare elsewhere in the *mélange* – may suggest that it was tectonically eroded from the upper plate and carried into the Cocolito Package by return flow within the subduction channel. The grain size of the matrix in this package is variable between clay-sized and granule-sized, suggesting variability in the energy of the flows and sorting during transport. The Cocolito Package is therefore interpreted as representing the proximal portion of the flexural moat, receiving both debris flows and turbidites. While layering within the turbidites was destroyed during the tectonisation process, the grain-size sorting remains.

The highly volcanoclastic-rich Punta Marengo Package contains predominantly igneous blocks, including blocks of gabbro, and these blocks can reach up to several hundreds of metres in size. As such, these units must have been deposited during catastrophic events involving the collapse and mobilisation of large sections of the seamount flanks. The thin unit of chert-rich material – mapped as the Playa Danta Sub-Package – may have been tectonically interleaved with the Punta Marengo Package during subduction and accretion or it may have been entrained in the debris avalanche. Similar to the granodiorite block in the Cocolito Package, the dacite block in the Punta Marengo Package may have been incorporated after the deposition of the unit if derived from the upper plate, or it may have been a part of the flank collapse flow if it originated from the seamount complex.

DISCUSSION

The Campanario Package lacks significant blocks and, where present, blocks tend to be blocks and mega-blocks of carbonate with a high aspect ratio; what siliciclastic material is present generally does not exceed pebble-sized clasts. This package is therefore interpreted as representing either the “ponded” unit described by Rees *et al.* (1993) or distal moat facies; although unlike the Bahia Drake Package, the Campanario Package does not contain a significant proportion of chert and is instead composed almost entirely of hemi-pelagic mudstones. Therefore, it is interpreted that the Campanario Package formed closer to the Central American and South American margins and therefore represents the ponded/distal moat equivalent of the hemi-pelagic mudstone unit of Isozaki *et al.*'s (1990) Ocean Plate Stratigraphy. This would imply that the Campanario Package postdates the Bahia Drake Package, and may have been deposited after the growth and denudation of the seamount had largely ceased.

The broken formation of greywacke turbidites that characterise the Punta San Pedrillo Package is notable due to its difference from the other units of the Osa Mélange. Large, up to several metre-scale blocks are present in this package, although they are confined to mega-breccia beds and are enclosed within a very poorly sorted matrix. These greywackes contain a great diversity of clast populations, potentially exceeding the diversity of the rest of the mélangé. Included within these greywackes are dacitic lithic clasts and zoned plagioclase grains. The roundness and sub-roundness of many of these clasts are indicative of long transport distances in rivers and along the shoreline and has been noted by Buchs *et al.* (2009). It is therefore tentatively interpreted that the Punta San Pedrillo Unit was deposited as the flexural moat of the Osa seamounts entered the Middle America Trench and was subducted, accounting for the contribution of both terrigenous and seamount-derived sediment into this package. The relict preservation of sedimentary structures is not observed in any other package of the San Pedrillo Unit, while the mudstone injection structures into the sandstone and conglomerate beds suggests that this unit was not more indurated prior to deformation, thereby implying that it underwent less tectonism.

10.1.3. Integrated model of Osa Melange formation

Based on the evidence provided throughout this thesis, the following subsection provides a comprehensive model for the formation, deformation, and emplacement of the Osa Melange and other nearby features of importance. To accomplish this, this subsection combines information from pre-existing literature (Chapter 2) with the findings of this doctoral project (Chapters 6, 7, 8, 9, and 10).

10.1.3.1. Cretaceous

At ~84 Ma, the Middle America Subduction Zone initiated on the western margin of Caribbean Large Igneous Province, separating the newly-formed Caribbean Plate from the Farallon Plate. The formation of this subduction zone left some Galapagos-derived volcanic edifices – such as the oceanic plateau that would become the Inner Osa Igneous Complex and the seamount that would become the Guerra Unit of the Osa Igneous Complex – on the Farallon Plate, and as this plate began to subduct beneath the Caribbean Plate, these edifices converged on the Caribbean Large Igneous Province. As the Farallon Plate continued to migrate over the Galapagos hotspot, the other seamounts that would become part of the Osa Igneous Complex, including the Vaquedano Unit (Buchs *et al.*, 2009) that would be the last to accrete, began to form. As these seamounts grew to become large volcanic edifices, their mass caused the creation of a flexural moat basin in which the Osa Melange was deposited, developed shallow marine carbonate complexes to contribute carbonate blocks to the melange, and may have become subaerially exposed.

At the same time, the Golfito arc developed above the Middle America Subduction Zone and started to produce volcanic rocks of basaltic to basaltic-andesitic composition.

10.1.3.2. Palaeocene

In the middle Palaeocene, the oceanic plateau that would become the Inner Osa Igneous Complex impacted with the Caribbean Plate resulting in tectonic erosion of almost the entire section of forearc, meaning that the subsequent accretion of the Inner Osa Igneous Complex would juxtapose the Golfito arc immediately against the accreted rock unit. This was followed

DISCUSSION

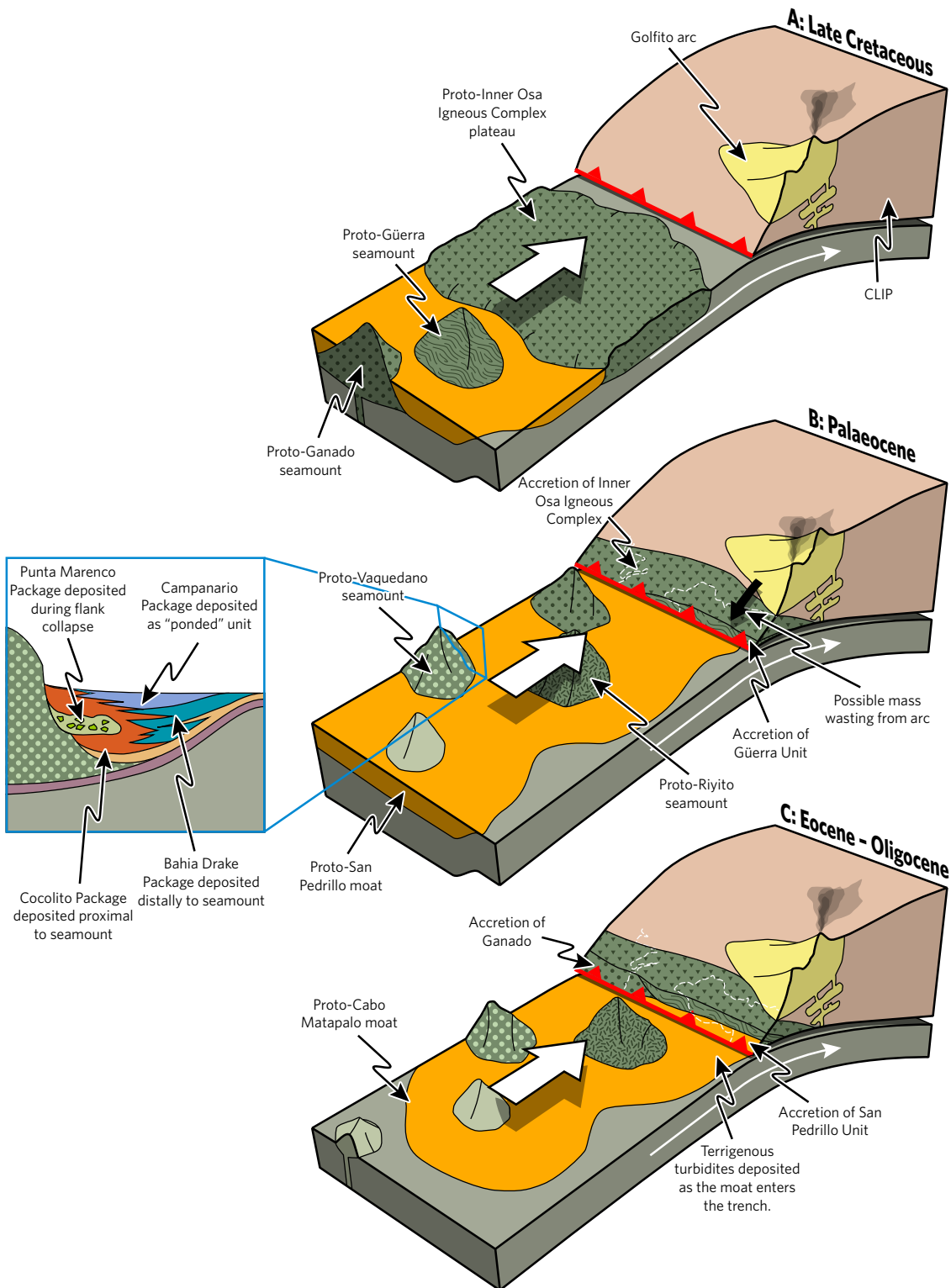
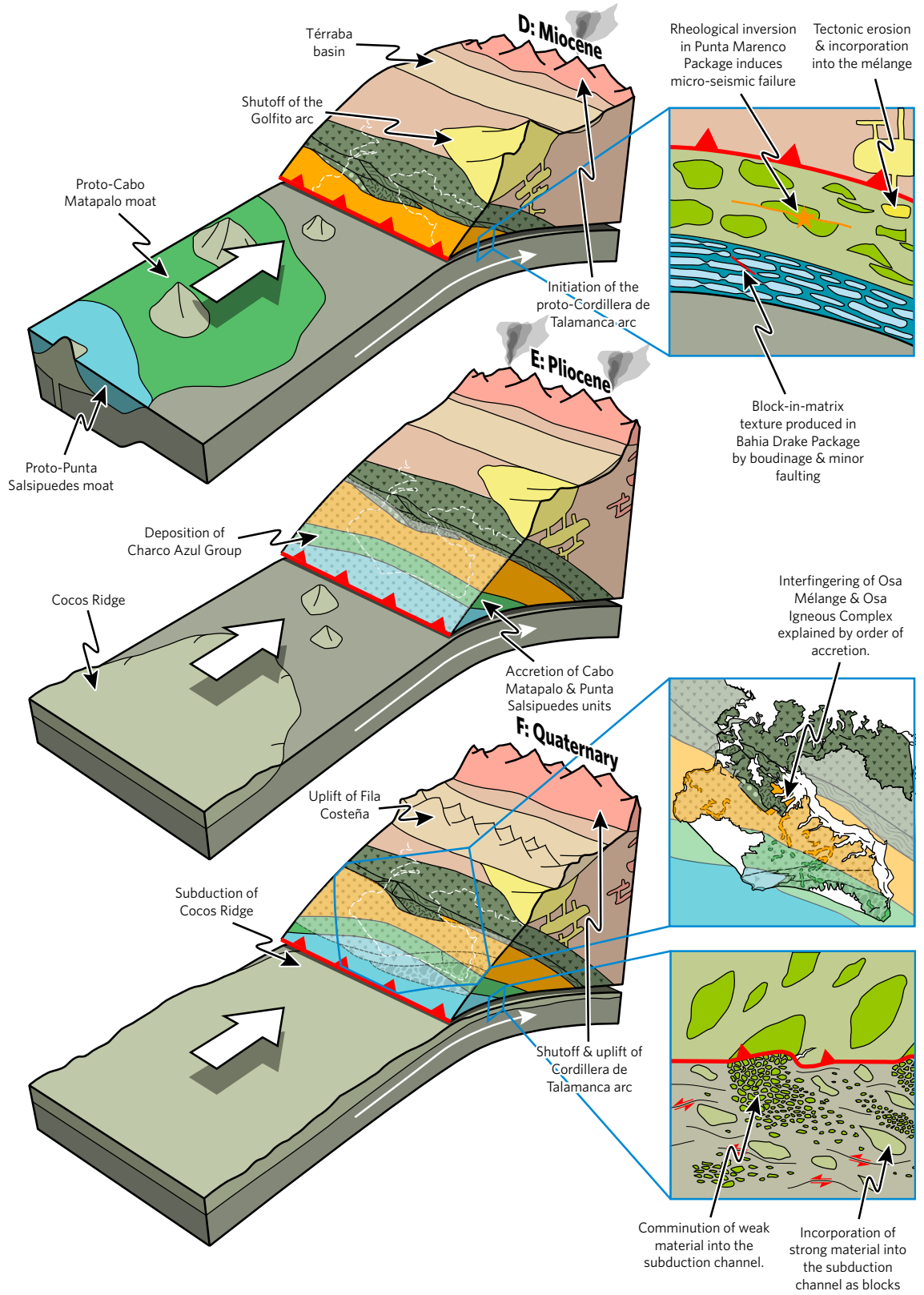


FIG. 10.2. (Caption overleaf.)



DISCUSSION

FIG. 10.2 (CONTINUED) Unified model of Osa Mélange formation in the context of the regional tectonics of the southwestern Caribbean. **A:** Initiation of the Middle America Subduction Zone leads to the development of the Golfito arc and the convergence between the oceanic plateau that will become the Inner Osa Igneous Complex and the Caribbean Plate. **B:** The Inner Osa Igneous Complex and Güerra unit are subducted and accreted while possible mass wasting from the arc bring dacite blocks into the trench. Meanwhile the flexural moat deposit that will become the San Pedrillo Unit is deposited and enters the trench at its leading edge. **C:** The San Pedrillo Unit begins to accrete from the incoming flexural moat; this begins as some seamounts are yet to be subducted. **D:** The San Pedrillo Unit subduct and accretes, with rheological inversion occurring in the Punta Marenco Package and dismemberment occurring in the Bahía Drake Package. Meanwhile, the Golfito arc shuts off and the Cordillera de Talamanca arc initiates, indirectly forming the Térraba basin. **E:** The Cabo Matapalo and Salsipuedes units are accreted and the Charco Azul cover sediments are deposited. Meanwhile, the Farallon Plate breaks up and the Cocos Ridge begins to form. **F:** Subduction of the Cocos Ridge causes uplift of the Osa Mélange, Fila Costeña fold and thrust belt, and Cordillera de Talamanca arc. It also causes enhanced subduction erosion from the base of the forearc, entraining material from the Osa Mélange into the subduction channel. White arrows indicate convergence direction.

by the subduction and underplating of the proto-Güerra seamount to form the Güerra Unit of the Osa Igneous Complex (Buchs *et al.*, 2009).

During this time, the flexural moat deposit that would become the San Pedrillo Unit of the Osa Mélange formed by mass wasting from the flanks of the seamounts that would become the Osa Igneous Complex. In the proximal area around the seamounts, debris avalanches and turbidites dominate sedimentation and deposit blocks of carbonate and basalt from the seamount flanks within a pelitic and sandstone matrix. It is in this environment that the Cocolito Package was formed. Catastrophic flank collapse events contribute megablocks of basalt and gabbro within a volcanoclastic matrix to the moat, producing rock units such as the Punta Marenco Package. In the distal moat, pelagic and hemi-pelagic cherts and mudstones intermix with distal turbidites containing

blocks of seamount-derived basalt and carbonate to form rock units such as the Bahia Drake Package. As growth of the seamount ceases, deposition of “ponded” sediments consisting of bedded turbidites and hemi-pelagic mudstones and carbonates occurs, resulting in the formation of Campanario Package. As the initial formation of the *mélange* occurred on the incoming plate prior to subduction, the first extensional phase of deformation interpreted by Vannucchi *et al.* (2006) to be the result of underthrusting may have occurred due to burial within the thick sediment pile of the moat basin. Hydrothermal fluids derived from the seamounts and circulating seawater resulted in ocean floor metamorphism and the first phase of alteration prior to subduction.

As the flexural moat approached and entered the Middle America Trench, sedimentation from the Caribbean Plate resulted in trench-fill turbidites being deposited on top of the flexural moat, producing the Punta San Pedrillo Package. If the dacitic blocks are derived from parts of the Golfito arc which have since been entirely eroded then they may have been inputted into the Osa *Mélange* at this point.

Subduction of the Osa seamounts and their surrounding moat sediments results in accretion of both the seamounts to form the Osa Igneous Complex and the moat to form the San Pedrillo Unit. The accretion of seamounts may have been facilitated by an underlying layer of pelagic and moat-fill sediments which prevented strong attachment to the incoming plate. The proto-Ganado and proto-Riyito seamounts (Buchs *et al.*, 2009) accreted after the initial accretion of the proto-San Pedrillo moat in the latest Palaeocene, resulting in the inter-fingering of the units observed on the maps of Vannucchi *et al.* (2006) and Buchs *et al.* (2009), however, the absence of any moat sediments intercalated with the Osa Igneous Complex suggests that some tectonic erosion occurred when these seamounts subducted – concurrent with the accretion elsewhere – to remove any accreted moat material ahead of the subducting seamount.

Like Vannucchi *et al.* (2006), this model for *mélange* formation describes direct accretion of the Osa *Mélange* from the incoming plate and does not involve two-stage accretion as described in Buchs *et al.* (2009). The Buchs *et al.* (2009) model requires rapid switching between subduction accretion and subduction erosion

DISCUSSION

— from accretion of the Osa seamounts, to subduction erosion and mass wasting to deposit the Osa Mélange in the Middle America Trench, and back to accretion to accrete the Osa Mélange within a timeframe of 11 Ma — without providing a cause to explain these behaviours. There is no evidence of dramatic changes to the plate velocity at this time and Buchs *et al.* (2009) does not infer or provide a mechanism for significant changes in the thickness of oceanic sediment; the two dominant controls on erosive or accretionary behaviour (Clift and Vannucchi, 2004). However, some recycling of already-accreted material from either the Osa Mélange or the Osa Igneous Complex can be accounted for in this model.

10.1.3.3. Eocene – Oligocene

Contrary to Vannucchi *et al.* (2006), this model suggests that significant portions of the Osa Mélange were frontally accreted, rather than being subducted and underplated. Where underplating did occur, the mélange was only subducted to shallow depths. Cloos and Shreve (1988b) distinguish between frontal accretion and underplating on the basis of deformation structures. Frontally accreted material is characterised by compressional structures including thrust faults, chaotic mixing, and reorientation of blocks to be parallel with the compressional foliation. In contrast,

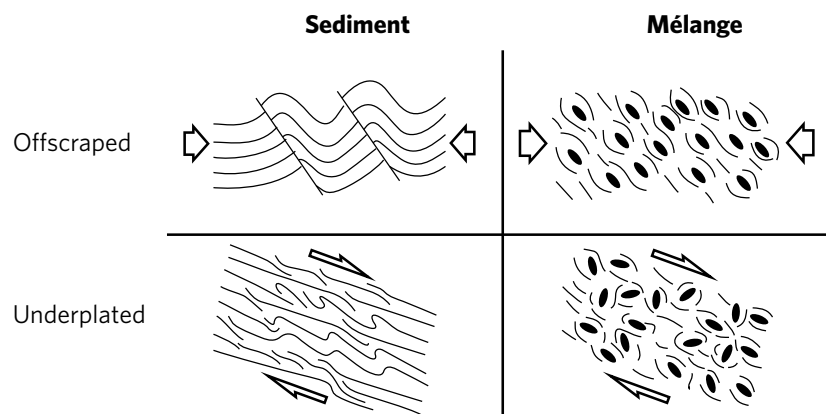


FIG. 10.3. Style of deformation expected in material that has been frontally accreted (off-scraped) and underplated, showing the structures expected for mélanges and bedded sediments (from Cloos and Shreve, 1988b).

underthrust material undergoes moderate to extreme shear within the subduction channel and is therefore characterised by a shear fabric – such as scaly fabric – slip parallel to bedding surfaces, rotation of blocks, and asymmetric structures preserving the kinematics of the shear. Evidence for both processes exists within the Osa Mélange, with the Bahia Drake, Campanario, and Punta Marengo packages displaying evidence of dominant underplating while the Cocolito and Punta San Pedrillo packages display evidence of dominant frontal accretion.

The process of boudinage and dismemberment of the previously interbedded cherts and pelites of the distal moat into the aligned, high aspect ratio chert blocks of the Bahia Drake Package occurred by layer-parallel extension in the form of boudinage likely occurring on the incoming plate prior to subduction followed by layer-parallel compression – likely during initial subduction – faulting out the necks of the boudins and creating the block-in-matrix texture. Subsequent shearing during underplating resulted in long-axis-parallel sliding, further destroying the original stratigraphy.

In the Punta Marengo Package, fracturing of the basalt and gabbro megablocks alongside fluidisation of the unconsolidated volcanoclastic matrix led to the development of matrix injection structures at the margins of the blocks, while intense fracturing led to the development of the brick-like fracturing pattern. As this package was underplated, concurrent induration of the surrounding volcanoclastic matrix and weakening of the basalt blocks resulted in an inversion of the typical rheological relationship (Chapter 7). At this point, the matrix became stronger and stiffer than the blocks. Stresses therefore concentrated in the matrix while stress in the blocks was more readily accommodated through permanent strain. This strain took the form of brecciation and cataclasis which differed from the earlier dense fracturing by its pervasiveness, comminution and gouge development, and geometric irregularity. Despite the lower stresses concentrated in the blocks, through-going fractures still occurred where the lower stresses in the blocks were sufficient to exceed the lower block strength while the greater stresses in the matrix were insufficient to exceed the matrix strength. This fracturing may have taken the form of microseismic events – analogous to

DISCUSSION

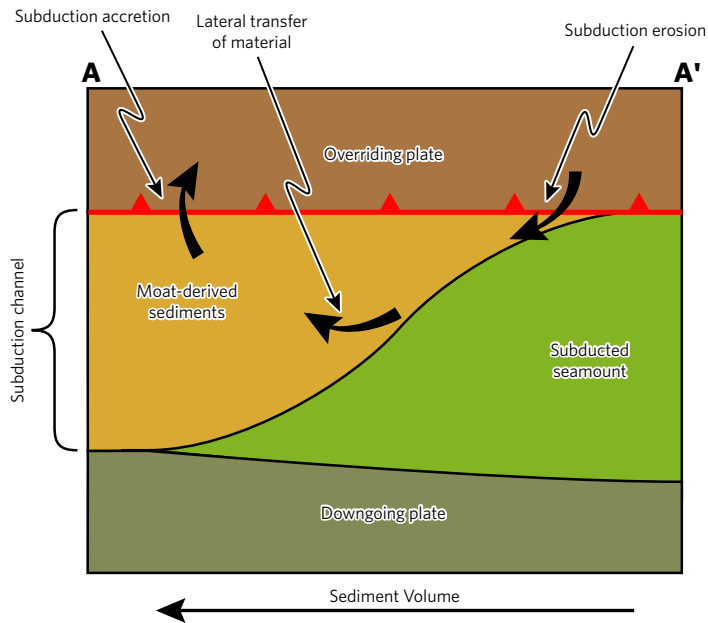
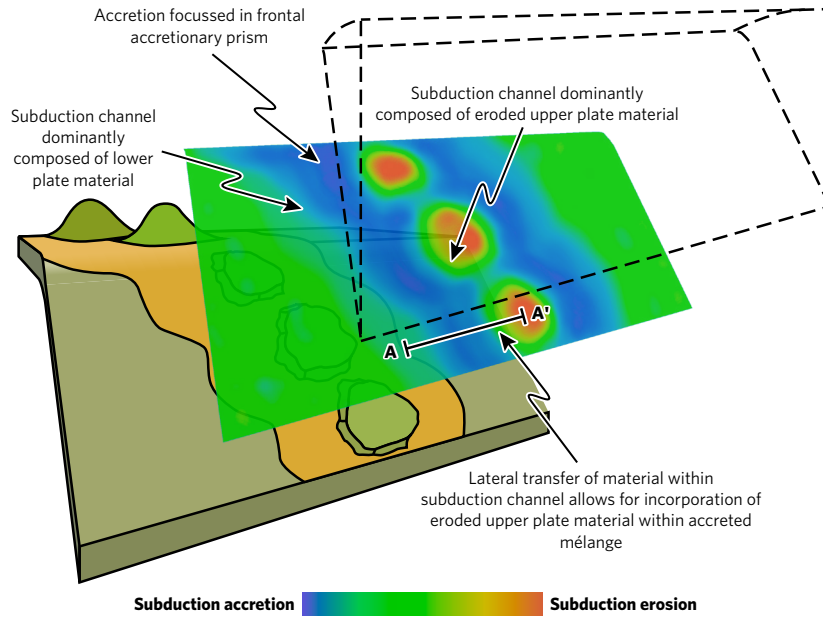


FIG. 10.4. Heterogeneity of subduction channel composition around a subducting seamount chain as a result of heterogeneous subduction erosion and accretion. **A - A'**: Lateral transfer of tectonically eroded material around subducted seamounts into accreting region of the subduction zone.

tremors — and may have primed the subduction interface for a larger, through-going rupture.

As subduction of seamounts typically promotes erosion at the contact between the subducting edifice and the upper plate (Ranero and von Huene, 2000), Clarke *et al.* (2018) infer that subduction of seamount complexes with flexural moat deposits promote concurrent accretion and erosion immediately adjacent to each other. In this case, erosion and incorporation of upper plate blocks into the subduction channel above the subducting seamount may be followed by accretion back to the upper plate above the moat (Fig. 10.4). This mechanism may explain the presence of eroded upper plate blocks in otherwise accretionary complexes — such as in the Franciscan Mélange of California (Ernst, 2015) — without invoking margin-scale shifts in erosive and accretionary behaviour. This process may account for the incorporation of the granodiorite block into the mélange, as no plutonic or intermediate – felsic rocks are exposed in the Golfito Complex and this block has a higher metamorphic grade than its surrounding matrix, suggesting it may have been incorporated by erosion of the arc roots in the hanging wall of the subduction zone.

The Osa Igneous Complex and the San Pedrillo Unit continued to be concurrently accreted, with the proto-Vaquedano seamount (Buchs *et al.*, 2009) — the terminal unit of the Osa Igneous Complex — accreting at ~38 Ma (Buchs *et al.*, 2009) and the San Pedrillo Unit ceasing to accrete at ~31 Ma (Vannucchi *et al.*, 2006). At ~38 Ma, the Golfito arc ceases to be active, marking the start of a ~10 Ma hiatus in Central American arc magmatism. This time also marked the beginning of deposition in the Térraba basin, which would deform in the Fila Costeña fold and thrust belt. In the late Oligocene, the proto-Cabo Matapalo Unit started to form on the incoming Farallon plate, likely also in the flexural moat of a seamount complex. However, this seamount complex must have contained larger carbonate complexes than the seamounts which formed the Osa Igneous Complex, accounting for the increased proportion of carbonate blocks in the Cabo Matapalo Unit. This includes deposition of calc-turbidites not seen in the San Pedrillo Unit.

DISCUSSION

10.1.3.4. *Miocene*

At ~28 Ma, early magmatism in the proto-Cordillera de Talamanca arc defines the start of the Miocene – recent arc front in Central America (Montes *et al.*, 2012). During the early – middle Miocene, the Farallon Plate broke into the Cocos and Nazca plates (~23 Ma [Meschede and Barckhausen, 2001]) – with the Osa seamounts now being situated on the Cocos Plate while they were subducting – and the Cocos Ridge began to form (~20 – 22 Ma [Meschede and Barckhausen, 2001]) marking the end of seamount-and-moat production by the Galapagos hotspot. After an ~20 Ma hiatus in accretion, likely due to the absence of significant flexural moats around the seamounts, the proto-Cabo Matapalo moat entered the subduction zone and began to accrete. The pervasive recrystallisation of the abundant calcite blocks (Vannucchi *et al.*, 2006) suggests that this unit was underthrust, rather than being frontally accreted. Why the seamounts around which the proto-Cabo Matapalo and proto-Salsipuedes moats formed did not accrete while the Osa seamounts now forming the Osa Igneous Complex did accrete is so-far unresolved. As the seamounts themselves did not accrete, the process of concurrent accretion and erosion around a subducting seamount and moat may be applicable here. As interpreted by Vannucchi *et al.* (2006), the Cabo Matapalo Unit underwent extensive layer parallel extension during subduction and underplating, before being sheared and thrust during the process of accretion. The accretion of the Cabo Matapalo and Salsipuedes units leads to uplift of the margin and eventual subaerial exposure of the Osa Peninsula.

At ~8.5 Ma, the Panama Fracture Zone formed (Meschede and Barckhausen, 2001; Morell, 2015), initially intersecting with the Middle America Trench to the north of the Osa Peninsula, meaning that the plate subducting beneath the Osa Peninsula at this time was the Nazca Plate. As the Salsipuedes Unit may not have accreted by this time, the Salsipuedes Unit may have been accreted from the slower-moving Nazca Plate and not the Farallon and Cocos plates like the other units of the Osa Mélange. This slow-down of convergence to the east of the Panama Fracture Zone is also responsible for the shut-off of magmatism in the Cordillera de Talamanca arc (Morell, 2015).

10.1.3.5. *Pliocene – Quaternary*

The sedimentary cover of the Charco Azul Group started to be deposited over the Osa Mélange in the Pliocene as the margin subsided due to subduction erosion and submerged the Osa Peninsula below sea level. This subsidence rapidly reversed with the arrival of the Cocos Ridge at the Middle America Subduction Zone at ~2.5 Ma (Morell, 2015), causing significant uplift and subaerial exposure of the Osa Peninsula, inversion of Térraba basin and uplift of the resultant Fila Costeña fold and thrust belt, along with the now-extinct Cordillera de Talamanca arc. Despite this uplift to accommodate the subduction of the high-bathymetry Cocos Ridge, subduction erosion from the base of the Caribbean Plate was intensified by Cocos Ridge subduction. The style of this subduction erosion was strongly controlled by the extreme heterogeneity of the Osa Mélange in the upper plate. As described in Chapter 8, highly structurally anisotropic packages such as the Bahia Drake Package are incorporated in part as poly-lithologic blocks because its strong fabric controls the propagation of hydrofractures and therefore tectonic erosion, while incorporation of more isotropic packages, such as the Punta Marengo and Cocolito packages, is controlled more by the rheology of each component, with the weaker component being more readily comminuted while the stronger component forms larger blocks within the subduction channel mélange.

DISCUSSION

10.2. IS THE OSA MÉLANGE REALLY A MÉLANGE?

Despite its name, the Osa Mélange is superficially unlike most well-studied mélanges, such as the Franciscan Mélange in the USA (Wakabayashi, 2011), the Mugi Mélange in Japan (Kimura *et al.*, 2012), and the Gwna Mélange in Wales (Kawai *et al.*, 2008). The most notable differences are the lack of a pervasive foliation – historically regarded by some workers (e.g. Hsü, 1968) as an essential characteristic of mélanges – the very low metamorphic grade, and the ubiquitous dark grey colour of most lithologies making the block-in-matrix texture non-trivial to discern. It is likely these reasons why some previous workers (Meschede *et al.*, 1999; Vannucchi *et al.*, 2006) described the mélange as consisting mostly of tectonised basalt. Whether the Osa Mélange is a mélange *sensu stricto* is a question of ancillary importance to this thesis.

As described in Chapter 4, this thesis adopts the mélange definition of Silver and Beutner (1980) that mélanges must exhibit a block-in-matrix texture, be of sufficient scale to be mappable on a regional-scale geological map, and must be “internally fragmented and mixed.” This definition does not contend that a pervasive foliation or a tectonic mechanism of breakup are essential characteristics of mélanges. The Osa Mélange, having an outcropping area of ~1,000 km², certainly meets the size requirements to be considered a mélange. It also exhibits a block-in-matrix texture throughout, with only the Punta San Pedrillo Package displaying incomplete stratal breakup. As stated above, the lack of a pervasive shear foliation and the olistostomal origin do not disqualify this rock unit from being termed a mélange.

While exotic blocks are not deemed an essential component of a mélange by many workers (e.g. Silver and Beutner, 1980; Wakabayashi, 2011; Festa *et al.*, 2012), some workers do consider their presence important for distinguishing between mélanges and other block-in-matrix rock units. The presence of exotic blocks demonstrates unequivocally that the rock unit has undergone “extra-formational mixing.” If the intermediate – felsic blocks in the mélange are derived from the Central American arc, then their position within a mélange predominantly composed of seamount-derived material deposited in the oceanic realm certainly qualifies them to be termed “exotic blocks,” even by the most restrictive of definitions (see Beutner, 1975).

However, any igneous block within a sedimentary *mélange* could be considered exotic to its depositional setting, especially the gabbro blocks which require significant exhumation to be available for erosion. Therefore, the seamount-derived basaltic blocks may be considered exotic to their depositional setting (the flexural moat).

No evidence exists for mixing between *mélange* packages, despite the contacts between packages being poorly defined. This allows for partial reconstruction of the stratigraphy of the flexural moat and interpretation of the facies by analysis of lithologies present and the size and shape of included blocks (Chapter 10.1).

The Bahia Drake Package – while it does contain rare basalt and carbonate olistoliths – is mostly composed of high aspect-ratio blocks of chert within a pelitic matrix. This fabric is interpreted to have formed by tectonic dismemberment of interbedded sediments by pinching out of boudin necks and minor faulting, with the ductile pelite flowing into the newly created spaces. As such, this unit is considered to be mostly composed of dismembered formation (*sensu* Raymond, 1984).

The Cocolito Package bears more resemblance to other olistostromal *mélanges* – such as sections of the Gwna *Mélange* in Wales (Horák and Evans, 2010) – due to the diversity of its block populations. This package contains blocks of basalt, carbonate, chert, sandstone, granodiorite and serpentinite with no discernible pattern to their occurrence. The presence of granodiorite and serpentinite in this package indicate mixing with material exotic to the flexural moat environment of deposition. Similarly, the Punta Marengo Package contains basalt, gabbro, and dacite megablocks, all of which – especially the gabbro and dacite – can be considered “exotic blocks.”

The Campanario Package, which is composed mostly of pelite with some rare carbonate blocks, is for-the-most-part devoid of blocks. The carbonate blocks that are present have a high aspect ratio, usually display pinch-and-swell structures, and sometimes occur as trains of aligned blocks. These blocks are interpreted to be produced by tectonic dismemberment – similar to the Bahia Drake Package – and therefore this package is regarded, at most, to be a dismembered formation, if it can at all be categorised as a block-in-matrix rock unit. The Punta San Pedrillo Package

DISCUSSION

consists of intensely faulted and boudinaged turbidites and lacks a fully developed block-in-matrix texture, making this a broken formation (*sensu* Raymond, 1984).

The Osa Mélange can, therefore, be described as a *mélange sensu stricto*, according both to the definition of Silver and Beutner (1980) and more restrictive definitions (e.g. Raymond, 1984) which require the presence of exotic blocks. However, this is a *mélange* which contains broken formations (e.g. Punta San Pedrillo Package) and not all sections of the *mélange* can be described as *mélange* themselves (e.g. Campanario Package). While exotic material is not considered a requirement for the rock unit to be termed a *mélange* in this thesis (after Silver and Beutner, 1980), its presence in the Osa Mélange indicates the extra-formational mixing that occurred during the formation of this *mélange*. This *mélange* features mixing of seamount-derived lithologies, abyssal sediment, and arc-derived volcanics and plutonics from both the Farallon and Caribbean plates. It therefore fully justifies the term “*mélange*.”

10.3. WHAT IS THE RELATIONSHIP BETWEEN THE OSA MÉLANGE AND THE CARIBBEAN LARGE IGNEOUS COMPLEX?

Hoernle *et al.* (2004) recognised that the Caribbean Large Igneous Province (CLIP) consists of a composite of Galapagos-derived volcanic edifices, and the Nicoya Complex in northwestern Costa Rica represents one of these accreted oceanic plateaus. However, the Inner Osa Igneous Complex — also derived from an accreted oceanic plateau with Galapagos affinity — is not considered part of the CLIP. Therefore, a definitional issue arises as to what igneous units may be considered part of the CLIP. Indeed, the many igneous complexes exposed along the southern Central American margin are variably regarded as parts or not parts of the CLIP. For example, the Inner Osa Igneous Complex is regarded as exotic to the CLIP on the basis of a lack of overlying arc rocks and its clear accretion to the Caribbean plate (Buchs *et al.*, 2009). However, the Osa Igneous Complex shares similar geochemistry with the CLIP (Hauff *et al.*, 2000a) and magmatism within the Osa Igneous Complex overlapped with magmatism within the CLIP and partially occurred before the initiation of the Middle America Subduction Zone separated the CLIP from other Galapagos products on the Farallon plate (Buchs *et al.*, 2009; Pindell and Kennan, 2009). Similarly, the Nicoya Complex is also shown to have formed on the Farallon plate coeval with the eruption of the CLIP and the Inner Osa Igneous Complex and have been located on the Farallon side of the nascent Middle America Subduction Zone prior to its accretion (Hoernle *et al.*, 2004). However, the Nicoya Complex is commonly regarded as part of the CLIP while the Inner Osa Igneous Complex is not. Allocation to the CLIP is not restricted to material located on the Caribbean Plate, as significant tracts of CLIP are present in Colombia and on Gorgona Island on the South American Plate. These were accreted from the Farallon Plate in the Maastrichtian, after the initiation of the Middle America Subduction Zone (Whattam and Stern, 2015).

The Caribbean Large Igneous Province is generally defined as an up-to-20 km thick accumulation of mostly basaltic material located within the Caribbean realm — although not restricted to the Caribbean Plate — and erupted and emplaced/accreted during the Cretaceous (Denyer and Gazel, 2009). It exhibits plateau-like geochemistry (e.g. flat REE patterns and MORB-like trace

DISCUSSION

elements) and Galapagos-hotspot-affinity Hf, Nd and Pb isotope ratios (Thomson *et al.*, 2003). Amongst the accreted igneous promontories in western Costa Rica, the Herradura Complex — which exhibits Galapagos-derived seamount-related geochemical affinity (Hauff *et al.*, 2000a) — is structurally juxtaposed between unexposed CLIP basement and the Nicoya Complex (also considered CLIP) but is not itself regarded as part of the CLIP. The Herradura Complex is similar in geochemistry and inferred genesis to the outer units of the Osa Igneous Complex.

The rocks of the Osa Peninsula differ from the surrounding rocks attributed to the CLIP by the seamount-affinity of parts of the outer units of the Osa Igneous Complex and the timing of accretion in the Cenozoic, rather than the Cretaceous. Given that the CLIP is composed of an amalgam of volcanic edifices of a range of sizes (Hoernle *et al.*, 2004), exclusion of seamount-derived units — especially when they occur within the geographic area of the CLIP as the Herradura Complex does — is an arbitrary distinction not reflective of the shared origin of these units. Exclusion of the Inner Osa Igneous Complex, which is derived from an

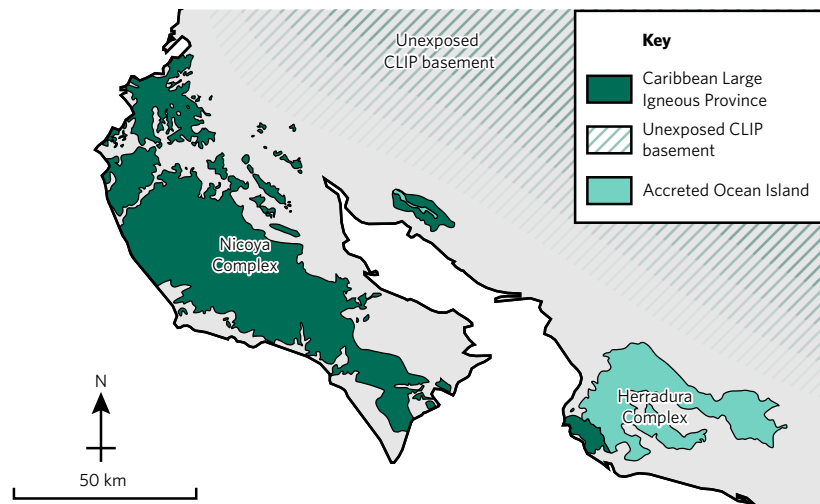


FIG. 10.5. Outcrop patterns of the Nicoya and Herradura complexes showing how the seamount-derived Herradura complex which is not considered part of the Caribbean Large Igneous Province is juxtaposed between the Nicoya Complex — which is considered part of the CLIP — and the unexposed CLIP basement (modified from Denyer and Gazel, 2009).

oceanic plateau similar to the Nicoya Complex, cannot be justified on compositional grounds.

Despite being erupted coeval with the latter stages of eruption of the CLIP, the seamounts of the Osa Igneous Complex accreted from the Farallon plate later than other CLIP edifices, with the Vaquedano Unit of the Osa Igneous Complex accreting at ~38 Ma (Buchs *et al.*, 2009). While differences in timing of accretion suggest physical separation on the incoming plate, the use of the Cretaceous – Palaeogene boundary in the definition of the CLIP is ultimately arbitrary and does not account for the continuity of magmatism from the Galapagos hotspot. I, therefore, advocate that the Osa Igneous Complex be considered part of the

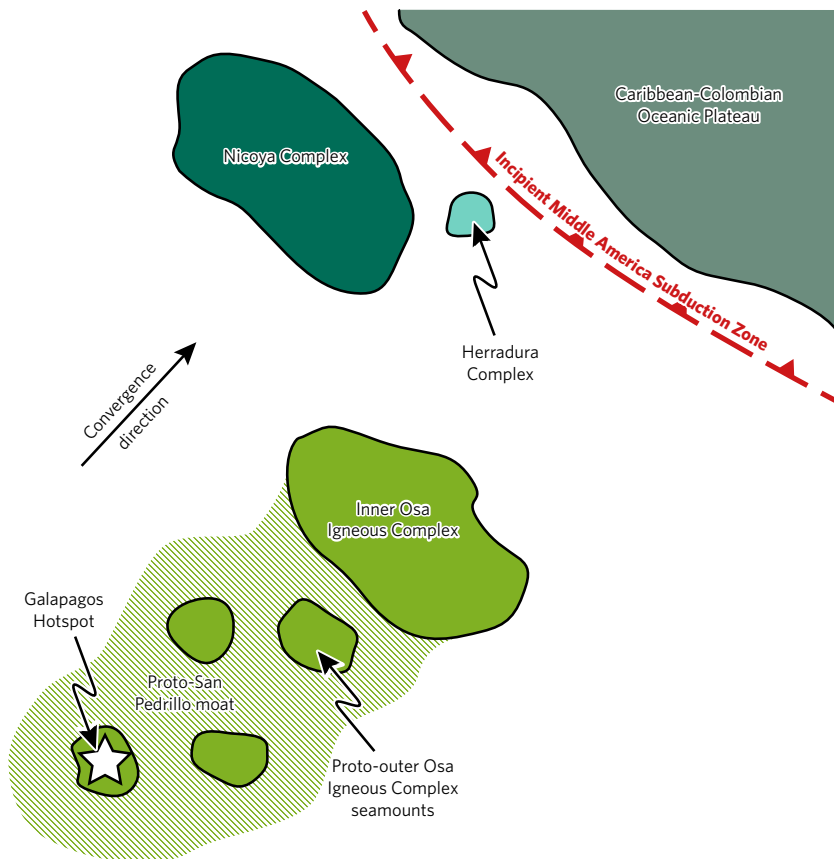


FIG. 10.6. Sketch of the relative locations of the Nicoya and Inner Osa Igneous Complex oceanic plateaus in the Campanian at the time of Middle America Subduction Zone initiation.

DISCUSSION

CLIP and recognised as the last component of the late Cretaceous Galapagos magmatic province to have been accreted.

While the Osa Mélange is predominantly composed of sediment and therefore cannot be considered part of the CLIP *sensu stricto*, its origin as a component of the proto-Osa Igneous Complex seamount system implies that it is integrally related to the terminal CLIP magmatism. The minor sedimentary component of the Nicoya Complex is commonly included as part of the CLIP (Denyer and Gazel, 2009). Similarly, I advocate that the Osa Mélange be considered an adjunct unit to the CLIP.

10.4. WHAT IS THE EFFECT OF MÉLANGE FABRICS AND RHEOLOGY ON SLIP AT THE PLATE BOUNDARY?

Mélanges are inferred to be present in subduction channels around the world (Vannucchi *et al.*, 2012). They may enter the channel either by underthrusting of existing block-in-matrix material present on the incoming plate – for example debris-flows filling the trench, but also formed far from it, such as in a flexural moat (Clarke *et al.*, 2018) – or by tectonic erosion of upper plate material, which may mix with subducted sediment. Subduction channel mélanges may, therefore, differ greatly from each other; both because of the origin of the material and because this material may enter the subduction zone at varying degree of lithification. In the case of underthrust mélanges, blocks may be lithified if mass-wasted from the forearc or incoming plate edifices, but they may also be formed from unlithified/partially lithified beds of more indurate sediment that has been tectonically dismembered through the subduction process. In this case, the matrix will initially consist of poorly consolidated sediment (Vannucchi *et al.*, 2012). In contrast, tectonically eroded blocks will generally

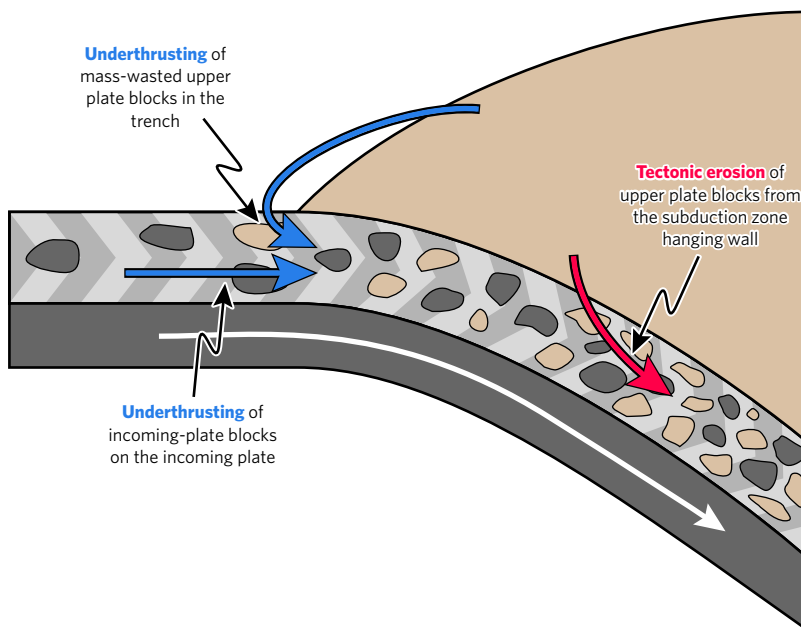


FIG. 10.7. Mechanisms of material addition to the subduction channel, showing underthrusting of both incoming plate sediments and mass-wasted upper plate material deposited in the trench, and tectonic erosion of upper plate material from the base of the subduction zone hanging wall.

DISCUSSION

be lithified and may have a pre-existing internal fabric which will control the shape and internal structure of the blocks (Chapter 8). This pre-existing fabric will not only influence the following deformation character of the rock assemblage in the subduction channel, but also the processes that control the incorporation of this material in the channel itself. Chapter 8 describes in detail how the structure and rheological relationships of the blocks and matrix in the upper plate influence the nature of subduction erosion. While stronger material will more likely be incorporated as intact blocks, weaker material is more likely to be comminuted. In this case, comminution implies that the weaker material will be broken into smaller blocks than its stronger counterparts, but also that especially weak material may be comminuted into a gouge which will mix with the typically clay-rich matrix. Because of this, blocks incorporated into the subduction channel will be stronger and have a higher Young's modulus than their new matrix (c.f. Chapter 8), although these physical properties may evolve as the blocks are deformed in the subduction channel. The presence of tectonically eroded upper plate material may, therefore, change the composition and material properties of the subduction

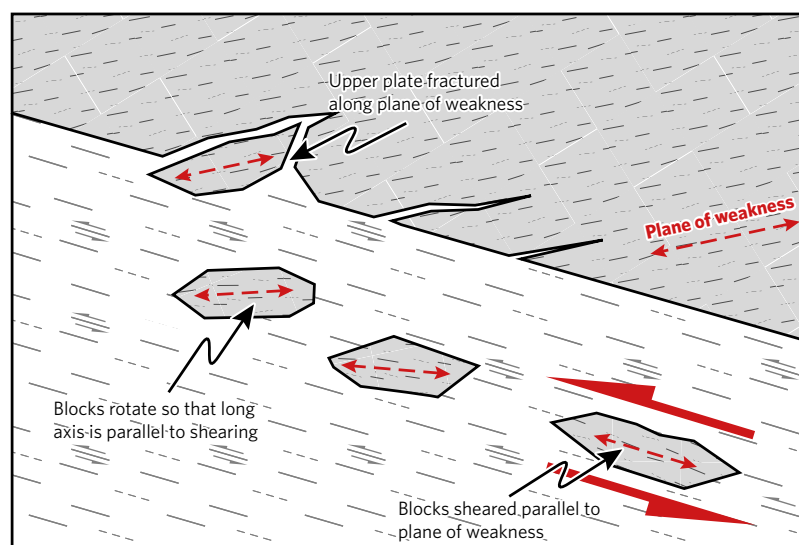


FIG. 10.8. Tectonic erosion and incorporation of blocks into the subduction channel produces blocks broken along their plane of weakness with their long axis parallel to this plane. These blocks therefore preferentially reorientate in the shear zone such that they are sheared in their plane of weakness.

channel, therefore influencing its capacity to host stable aseismic slip, slow transient slip, and mega-thrust earthquakes. This section discusses the influence of the upper plate contribution to the subduction channel on the nucleation and propagation of unstable and stable slip on the plate interface fault.

10.4.1. Influence of incorporated Osa Mélange material on slip nucleation at the plate boundary

Nucleation of both slow transient slip and mega-thrust earthquakes occurs by the rupture of asperities (Chapter 3) (Byerlee and Brace, 1968 cited in Kopp, 2013; Cloos, 1992). Subduction erosion typically occurs at margins with a heterogeneous seafloor related to the presence of topography and/or the lack of a continuous and thick sediment accumulation at the trench, meaning that erosive subduction zones are likely to feature abundant asperities and barriers, potentially increasing the amount of creep and small transient slip events. In the case of the Middle America Subduction Zone near the Osa Peninsula, the subduction of the Cocos Ridge induces plate interface heterogeneity which likely suppresses the nucleation of large earthquakes (Wang and Bilek, 2014), while the area of ocean floor to the north of the Cocos Ridge, which is ~40% covered by seamounts (Fig. 2.2) (Ranero and von Huene, 2000), provides asperities from which seismic ruptures may nucleate.

Incorporation of rigid blocks from the upper plate also acts to lock the subduction zone and may, therefore, produce asperities (Fagereng and Sibson, 2010). In this case, individual blocks are usually insufficiently large to induce plate interface locking, but a subduction channel mélange composed of rigid blocks — especially if block-to-matrix ratios are high — may interact to promote locking (Fagereng and Sibson, 2010). The block-to-matrix ratio in an erosive subduction zone is controlled by the rate of subduction erosion and the rate of sediment subduction. The rheology of the resultant blocks also influences whether the blocks are strong enough to lock the subduction zone. However, not all upper plate material is likely to form blocks in the subduction channel, and the weak matrix of the Osa Mélange is likely to be comminuted into a gouge and mixed with the subduction channel matrix. While the rate of subduction erosion at the Middle

DISCUSSION

America Subduction Zone near the Osa Peninsula is well defined, ($1.2 \times 10^6 \text{ km}^3$ of forearc material in $\sim 0.3 \text{ Ma}$ [Vannucchi *et al.*, 2013]), the amount of sediment subducted remains unconstrained.

The effect on slip behaviour of incorporating each package of the Osa Mélange (as described in Chapter 8) is described below:

- Incorporation of the Bahia Drake Package, with its high block-to-matrix ratio, high structural anisotropy, and chert-rich pelitic matrix will result in a relatively high block-to-matrix ratio in the subduction channel mélange; however, due to their pre-existing fractures, the fractured chert blocks are unlikely to sustain sufficient strain to lock the subduction zone.
- The Cocolito Package, featuring moderate block-to-matrix ratios and a range of matrix grain-sizes from clay-sized to granule-sized, may result in a relatively moderate block-to-matrix ratio in the subduction channel. The deformed and fractured carbonate blocks common in the Cocolito Package mean the blocks are likely insufficiently rigid to act as asperities.
- In the Punta Marengo Package, the weakening of the blocks described in Chapter 7 will lead to the blocks being comminuted into the matrix – likely as small blocks rather than as a gouge – while the indurated matrix forms larger blocks. Block-to-matrix ratios in the Punta Marengo Package are moderate but as both the blocks and the matrix from the mélange have the potential to become blocks in the subduction channel, the resultant subduction channel mélange will have a high block-to-matrix ratio. Channel blocks derived from the indurated mélange matrix will have a high strength and therefore have the potential to promote locking of the subduction zone, whereas blocks derived from the basalt blocks will fail readily.
- Incorporation of the Campanario Package, which is mostly composed of mechanically weak pelite (Chapter 8), will mostly occur by comminution into small blocks and gouge, producing a low block-to-matrix ratio in the subduction channel.
- The conglomerates and sandstones of the Punta San Pedrillo Unit will likely be incorporated as blocks into the subduction channel, producing a high block-to-matrix ratio in the channel.

Therefore, material derived from the Punta Marengo Package or the Punta San Pedrillo Package — or their equivalents at depth — has the potential of causing sufficient interaction and locking to promote seismicity in the manner predicted by Fagereng and Sibson (2010). Other packages are likely to introduce heterogeneity but not contribute to locking, thereby impeding the nucleation of slippage.

However, as demonstrated in Chapter 7, the mechanical properties of blocks and matrix within a *mélange* may evolve as a result of further deformation and chemical alteration. Igneous blocks which have maintained their strength and Young's modulus — such as the gabbro, dacite and granodiorite blocks as well as any basalt blocks that were less affected by the weakening described in Chapter 7 than the basalt blocks in the Punta Marengo Package — may now be susceptible to rheological inversion. Additionally, rheologically inverted Osa *Mélange* blocks in the Punta Marengo Package may exhibit a normal rheological relationship once incorporated into the weaker-still matrix of the subduction channel *mélange*. While hydrothermal alteration will be less effective at weakening sedimentary rocks due to their mineralogical stability, mechanical weakening by fracturing and brecciation may still affect these rocks. Lithification of the subducted sedimentary matrix, as well as incorporation of upper-plate-derived gouges, may act to strengthen the matrix while weakening of the blocks occurs to produce an inverted rheological relationship.

Chapter 7 describes how high block proportions will promote potentially seismic failure even if the rheological relationship between blocks and matrix is inverted, while high matrix proportions in the inverted rheological relationship do not favour aseismic slip as predicted for the normal rheological relationship by Fagereng and Sibson (2010). Chapter 7 also describes how the more negative the difference in Young's modulus — i.e. the more compliant the blocks are compared to the matrix — the less strain the model can accommodate before failure of one component occurs. The process of rheological inversion, therefore, weakens the plate interface as a whole; if the plate interface is maintained at a critical or close-to-critical stress, weakening its constituent materials can produce failure.

DISCUSSION

The anisotropy of upper plate rock units will control the shape of the fragments entrained into the subduction channel mélange as these blocks break along pre-existing planes of weakness. Therefore, blocks derived from highly anisotropic packages such as the Bahia Drake Package – or its equivalents at depth – will tend to have their long axis oriented parallel to their planes of weakness. Block rotation during shearing will reorientate these block to be sheared along their weakest plane (Fig. 10.8). Pre-existing fractures and heterogeneity – especially those oriented favourably for reactivation – will concentrate stresses and weaken the blocks, as shown in Chapter 7.

Chapter 7 describes how failure of a weakened block – which may be accompanied by small, low-frequency seismic emissions analogous to tremors during initial rupture and sliding – increases the loading on the intact surrounding matrix while simultaneously offering little impediment to further deformation. This – combined with the decreased resistance to strain due to the presence of weak blocks described above – weakens the plate interface such that it is unable to remain locked and nucleates a through-going rupture; therefore failure of weak blocks primes the subduction zone for a larger rupture. If the plate interface is maintained at near-critical stress (e.g. Obara and Kato, 2016), this through-going rupture may occur as the weakened block fails, meaning that these blocks control rupture nucleation on the plate interface. If the blocks or the matrix contain sufficient quantities of velocity-weakening material, this rupture may take the form of an earthquake; otherwise, it may produce slow transient slip or a slow earthquake (Ide *et al.*, 2007).

10.4.2. Influence of incorporated Osa Mélange material on slip propagation at the plate boundary

The subduction of the high relief seafloor of the Cocos Ridge and nearby seamounts introduces features which may act as small asperities or barriers to propagating ruptures and leads to a poor potential for large megathrust earthquakes (e.g. Wang and Bilek, 2014). In addition to this, the tectonic erosion of the Osa Mélange into the subduction channel produces heterogeneity which complicates the stress field which promotes the arrest of seismic

rupture and the promotion of slow slip (Saffer and Wallace, 2015). This degree of structural heterogeneity is modulated by the style of incorporation into the subduction channel (Chapter 8) which is in turn controlled by the strength and fabric of the upper plate. Incorporation of Osa M \acute{e} lange material as large blocks results in large perturbations in the local stress field which may deflect or arrest a rupture, whereas incorporation of weaker material as a gouge that mixes with the matrix produces a more homogeneous stress field which is favourable to rupture propagation.

Rupture through a heterogeneous material may be deflected around obstacles and form dilational or contractional jogs, as observed in exhumed subduction channels (Vannucchi *et al.*, 2012 and references therein). These fault jogs require additional energy to overcome and may lead to the arrest of the rupture (Sibson, 1985, 1986). Fig. 7.5 shows how, in the normal rheological relationship, the shear stress maxima are concentrated at the tips of the blocks in the direction of shearing, whereas when the rheological relationship is inverted, the stress maxima are located at an angle oblique to the direction of shearing. In the normal rheological relationship, the stress minima are located at the same angle as the stress maxima in the inverted relationship. This angle is determined by the aspect ratio of the blocks, with higher aspect ratio blocks concentrating stresses closer to the plane of shearing (Fig. 10.9). Ruptures propagating through a subduction channel m \acute{e} lange composed of low aspect ratio blocks will, therefore, be more likely to arrest, or be tortuous and contain more fault jogs, than a rupture propagating through a m \acute{e} lange composed of aligned high aspect ratio blocks.

While friction experiments on Osa M \acute{e} lange materials were outside of the remit of this doctoral project, typical frictional behaviours of common minerals – as described in 3.3 – can be used to estimate the effect of incorporating these materials on the velocity behaviour of the plate interface. For example, both smectite and illite are shown to be velocity-strengthening under the pressure-temperature conditions of the upper subduction channel, while quartz and calcite may exhibit velocity-weakening behaviour (e.g. Blanpied *et al.*, 1995; Saffer and Marone, 2003; Han *et al.*, 2010; Saffer *et al.*, 2012). Skarbek *et al.* (2012) predicted that the velocity-dependent behaviour of the subduction interface is

DISCUSSION

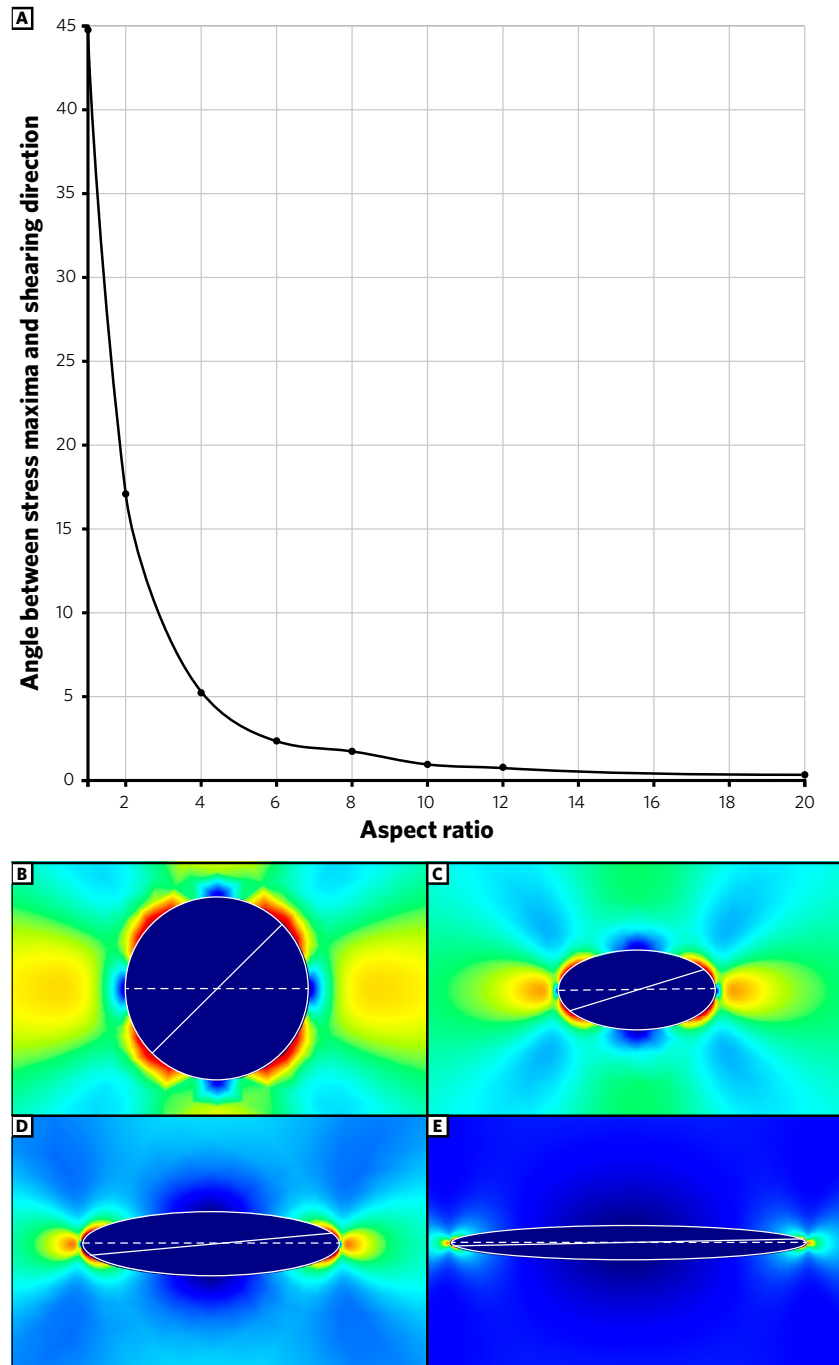


Fig. 10.9. Relationship between the angle of stress maxima relative to the direction of shearing, and the aspect ratio of the block. **A:** Relationship shows an approximately power-law relationship. **B:** Where aspect ratio = 1:1, angle = $\sim 45^\circ$. **C:** Where aspect ratio = 2:1, angle = $\sim 17^\circ$. **D:** Where aspect ratio = 4:1, angle = $\sim 5^\circ$. **E:** Where aspect ratio = 10:1, angle = $\sim 1^\circ$.

determined by the proportion of velocity-weakening and velocity-strengthening material which constitutes the subduction channel. The primary influencing factor on whether the plate interface exhibits velocity-strengthening or velocity-weakening behaviour will be the subducted sediment, as this will likely remain the largest single fraction of the plate interface, even after significant tectonic erosion, due to the extreme compositional heterogeneity of the upper plate. Kurzwski *et al.* (2016) report that the sediment being subducted offshore the Osa Peninsula consists of layers of silty clay and calcareous ooze, with the calcareous ooze developing velocity-weakening frictional behaviour once subducted >6 km.

The predominant lithology present in the Osa Mélange is clay-rich pelite containing varying proportions of volcanoclastic material, which constitutes the matrix throughout the mélange. While quartz grains are rare throughout the Osa Mélange, quartz veins, as well as silicified microfossils and amorphous silica are common. Chert and carbonate are also major lithological components of the mélange and collectively constitute the majority of the blocks. Incorporation of the Bahia Drake Package which contains high proportions of chert blocks and some carbonate blocks may have the potential to promote velocity-weakening behaviour. Due to the high block-to-matrix ratio of the Cocolito Package, the carbonate blocks are unlikely to contribute sufficient velocity-weakening material to influence slip behaviour. Both the altered basalt blocks and the volcanoclastic matrix of the Punta Marengo Package are predominantly composed of clays, and therefore a velocity-strengthening behaviour is expected. Incorporation of the Campanario Package will mostly contribute clay-rich pelite which will likely promote velocity-strengthening behaviour. Rare carbonate blocks may contribute velocity-weakening material, but in insufficient quantities to significantly influence slip behaviour. The turbiditic sandstones and conglomerates of the Punta San Pedrillo Package are mostly composed of igneous-derived lithic clasts with very little quartz. The extremely compositionally heterogeneous nature of this package precludes accurate estimation of the velocity-dependent behaviour of this material, although the high proportion of igneous-derived clasts may suggest velocity-weakening behaviour would be expected. The considerably

DISCUSSION

high proportions of carbonate blocks in the Cabo Matapalo Unit and the Salsipuedes Unit are likely to promote velocity-weakening behaviour once incorporated.

10.5. CRITICAL EVALUATION OF RESEARCH PROCESS AND RECOMMENDATIONS FOR FUTURE WORK

This section evaluates the effectiveness of the research in this doctoral project, the challenges faced, and the strength of the hypotheses presented in this thesis. Crucially, it addresses the weaknesses of these hypotheses, why the models presented in this thesis continue to be favoured, and presents falsifiability tests that may be conducted to determine the strength of these hypotheses. Finally, it presents recommendations for future research on the Osa Mélange and other similar rock units based on the conclusions and experiences of this project.

10.5.1. Critical evaluation of research methods and processes

The methodologies favoured for this study were predominantly those that are well established with the new methodology of determining structural anisotropy by image analysis of field photos developed as a low-cost alternative to traditional methods.

10.5.1.1. Evaluation of mapping techniques

Fieldwork in Costa Rica was limited by the quality and scarcity of the outcrop. Exposure is largely limited to the coasts and is only sufficiently consistent to map on the northern coast from Bahia Drake to Punta San Pedrillo and the southern tip of the Osa Peninsula near Cabo Matapalo. Inland exposure is present in some river valleys but is strongly weathered by tropical conditions and local wildlife presents a sufficient hazard that thorough investigation of these river valleys is not safe to attempt during solo fieldwork. As such, only a small portion of the Osa Mélange could be studied and, due to the heterogeneity and non-stratigraphic nature of the mélange, a comprehensive three-dimensional model cannot be formed. This heterogeneity and non-stratigraphic nature also prevented accurate inference of the subsurface geology of the mélange beyond 20 – 50 metres depth. Entry into the Corcovado National Park, which contains outcrops reported by Vannucchi *et al.* (2006) and Buchs *et al.* (2009), is now prohibited without a registered guide on authorised paths, and was deemed insufficiently important to warrant application for a scientific exemption as previous studies did not report findings differing significantly from areas outside of the national park. The Cabo

DISCUSSION

Matapalo Unit, although preliminarily studied in the field, was not studied in detail due to time limitations and our focus on the San Pedrillo Unit. Despite these limitations, the area studied was sufficiently large to ensure that a representative view of the *mélange* was formed. The methodology used to map the area was effective at discriminating between different *mélange* packages and developing an understanding of the three-dimensional relationships and evolution of the packages with the appropriate level of confidence.

Distinguishing between lithologies in the field is confounded by the similar colour, grain-size and fabric of all lithologies and the ubiquitous tropical weathering. The majority of the *mélange* presents as black – dark grey/brown, fine-grained and with brecciated and stockwork veined texture. The chert blocks appear superficially similar to their surrounding pelitic matrix as they contain a high proportion of clay and are only distinguishable by their strength, resistance to weathering, and angular surface texture. Volcanoclastic sandstone and pelite is derived from the same basaltic material as the basalt blocks and therefore has similar colour and mineralogy, and due to the fine-grained nature of both, they are frequently indistinguishable without microscopic study. Lithological identification was therefore confirmed by thin section analysis after fieldwork and this was compared to photographs and recorded observations of other areas to aid mapping after completion of the fieldwork.

10.5.1.2. Evaluation of sampling strategy

Wherever possible, efforts were made to choose samples which are representative of the whole and those from a broad geographical area.

Triaxial deformation tests required boulder-sized samples that were not extracted using a hammer as this would introduce unwanted new fractures. These samples were therefore collected from float. Great care was taken to choose samples that matched the lithology in outcrop; however, this was confounded by the superficial similarity of the rocks in the *mélange*. It is therefore not possible to be certain that the location that the sample was collected at matches the location of this rock in outcrop and

therefore the allocation of these samples to either the blocks or the matrix — made by field observation of outcrop — must contain uncertainty. However, petrographical analysis of these samples supports this allocation. The physical size and weight of these samples severely limited the number of samples that could be collected. The weight of these samples and the difficulty of the terrain limited sample collection locations to within 1.5 km of road or boat access.

Only samples of rock that is physically resistant enough to form prominent outcrops and samples that retain their cohesion were suitable for point-load analysis. Therefore the weakest material in the *mélange* could not be tested, resulting in a sampling bias towards stronger material. Some samples collected for point-load analysis were necessarily extracted from the outcrop using a hammer and chisel, potentially introducing new fractures. The difficulty of extracting samples from outcrop and the fact that some samples were collected from float precluded the orientation of these samples. Associating orientations of structures to the regional palaeo-stress field and therefore to tectonic events is confounded by the large strong blocks within the relatively compliant matrix, leading to highly complex local stress field around each block and development of the mostly chaotic foliation which is observed to wrap around the blocks. The samples selected for triaxial testing were as large as could be manually carried by a physically fit human over rough terrain and a local assistant was employed to assist with recovery of these samples. The use of mechanical equipment in the extraction and recovery of these samples should be investigated for future research.

10.5.1.3. Evaluation of light microscopy techniques

The highly altered nature of the samples added significant complications to light microscopy analysis as original mineralogy was often absent or partially destroyed, with chemically resistant minerals remaining as relics, while other minerals form pseudomorphs to which close attention was paid. As such, petrological analysis and estimation of normative mineralogy were not possible. Similarly, the complexity of the internal structures and the difficulty of extracting oriented samples prevented quantitative structural analysis. Because of this pervasive alteration,

DISCUSSION

only qualitative analysis such as recognition of key minerals and descriptions of the rock texture was possible. However, the detailed and complex micro-texture of these rocks – which is hard to discern in the field or in hand specimen – is shown vividly in thin section. Unambiguously distinguishing between the volcanoclastic pelites and sandstones and the altered basalts is also possible in thin section and difficult in the field or in hand specimen. Discerning cross-cutting relationships between the abundant, thin veins is also only possible by microstructural analysis.

Due to the challenging and ambiguous appearance of the Osa Mélange lithologies in the field, light microscopic analysis aided identification of lithologies for the purpose of mapping. However, only 70 thin sections were used for this purpose. A greater number of thin sections could have increased the resolution of the mapping study.

10.5.1.4. Evaluation of rock mechanics experimental techniques

While the samples used in this study were packaged for transportation in as secure a manner as was possible, some new fractures may have been formed during transport from the outcrop to the laboratory. The sawing, coring and lathing to produce the prepared sample for testing may have also introduced unavoidable further fractures. The samples tested by triaxial compression were restricted to those which survived sample preparation. Those which did not survive sample preparation failed along pre-existing weaknesses, therefore introducing a bias towards stronger material in the samples tested. Notches in the top surface of the prepared samples may – if unaddressed – have concentrated stress at their tips, producing a sample failure at a lower stress than the real peak stress of the material. This was mitigated by filling these flaws with plaster, although elastic deformation of the plaster may still have transferred some of this increased stress.

During the weighing of the samples for the density/porosity tests, fragments of the samples broke off during water saturation, therefore introducing inaccuracy into the measurements. This effect affected each sample differently, and it was not possible to attribute the fragments back to the sample from which they were derived. However, as the total weight of the broken fragments

represented less than 1% of the total weight of the samples, this error was considered negligible.

During triaxial deformation tests, confining fluid leaked into the sample. This likely occurred due to rupture of the jacket as the sample failed or through degradation of the latex seal at high temperature and pressure conditions. If oil had infiltrated and saturated the sample it would have acted as a pore fluid and altered the test results. As no oil infiltration was found in a sample placed under test conditions but not loaded, it is assumed that infiltration occurred during loading (without sufficient time to achieve saturation) or after the completed test, and would therefore not have affected the test results.

The physical size of the samples for triaxial testing — as large as could be carried unassisted by a physically fit human over rough terrain — was not sufficient to yield enough sub-samples to test exhaustively under a range of conditions or orientations. The size also limited the number of such samples that could be recovered and the range of lithologies that could be tested. As such, experiments were limited to three pressure/temperature conditions and the effect of temperature, anisotropy, strain rate and pore fluid pressure could not be measured. A more thorough investigation of the physical properties of these materials across different experimental conditions would require mechanical excavation and transport of samples not available as part of this study.

After triaxial deformation, some of the samples were damaged en route to being thin sectioned. As such, microscopic analysis of fracture surface features and gouges was not possible for all samples; however, analysis of unaffected samples was treated as representative of the sample set.

Inherent in the process of point load analysis — due to analysing a greater number of smaller samples relative to other methods — is a poorly quantifiable degree of error, especially when analysing highly heterogeneous material such as *mélange* rocks. However, while the precision of this method is low relative to other methods which may have been used, the benefits of its low cost and potential advantages in accuracy were deemed to outweigh the disadvantages in precision. To minimise these errors, sub-samples possessing significant through-going fractures were

DISCUSSION

discarded and the platens were positioned away from minor fractures or veins.

As triaxial experiments did not reveal significant changes in the rheological relationships under different P/T conditions, future rock mechanics analysis of the Osa Mélange should prioritise coverage of the full range of mélangé lithologies in ambient P/T conditions over detailed characterisation of a few materials by triaxial testing. Using a portable point-load tester in the field may be an option to minimise the amount of material needed to be recovered, saving money and physical exertion. Characterisation of the frictional properties of mélangé lithologies would also be directly relevant to understanding the effects of these lithologies on slip and seismicity within the subduction zone. As such, either rotary or triaxial shear experiments on synthetic gouges produced from Osa Mélange lithologies is recommended.

10.5.1.5. Evaluation of numerical modelling methodology

The numerical modelling used in this thesis is linearly elastic. As such, it cannot account for plastic or brittle behaviour in response to the applied stresses and cannot yield or produce a fracture. Instead, failure of the modelled material is inferred in post-processing to occur when the modelled concentrated stress exceeds the independently assessed yield stress of the material. In Chapter 7, the yield stress considered was both the experimentally measured yield stress of the altered basalt block and the volcanoclastic matrix, and systematic arbitrary values used to construct Fig. 7.6. The effects of other characteristics, such as block aspect ratio, rotation, proximity to other blocks, and Poisson's ratio were not accounted for during this study. These numerical experiments modelled elliptical blocks within a homogeneous matrix, and – besides one fracture in some models – no pre-existing defects were modelled. This was done to simplify the experiments, but it will result in differences with nature as the inevitable defects found in natural samples will concentrate stresses and may result in failure at a lower applied stress. Some small numerical error is present in the model data – as seen in Fig. 7.6 – although a sufficient number of similar experiments were performed to provide a statistical basis for the observed

pattern. These errors are likely the result of meshing and a fine mesh was used to minimise this effect.

10.5.1.6. Evaluation of geochemical techniques

As Chapter 9 describes a pilot study, only a small subset of samples were analysed for major and trace element geochemistry. As such, geochemical analysis of the full range of block lithologies was not possible. This study attempted to define the provenances of the basaltic and dacitic blocks, and therefore an approximately equal number of each lithology was tested; this is not indicative of the overall block proportions. Geochemical analysis of a truly representative sample of Osa Mélange lithologies was outside of the remit of this study. All samples are highly altered and are heavily cut by calcite, zeolite and quartz veins which, due to their narrow width and stockwork orientations, are inextricable from the host rock; this has likely highly modified the concentrations of fluid-mobile elements. A comprehensive study of the geochemistry of the lithologies of the Osa Mélange – including isotopic analysis of these rocks – may have benefited this doctoral study, but was not attempted due to other research being prioritised.

The flexural moat/debris apron hypothesis for the formation of the Osa Mélange is contingent on the predominant provenance for material in the mélange being the incoming (Farallon) plate. This model includes provision for upper plate material to form a minor component of the mélange – either through mass-wasting on the surface of the forearc or tectonic erosion of subduction zone hanging wall – which accounts for rare granodiorite and dacite blocks reported by Buchs *et al.* (2009). Single grain analysis of pyroxene grains (e.g. Nisbet and Pearce, 1977; Horozal *et al.*, 2017) in the volcanoclastic matrix would allow for the provenance analysis of a significantly greater number of clasts, allowing for the relative proportions of material of each provenance to be more accurately assessed. Such analysis would require comparison with pyroxene grains from the Osa Igneous Complex, Caribbean Large Igneous Complex, and Golfito arc. This analysis is recommended as future work.

DISCUSSION

10.5.1.7. Evaluation of image analysis techniques

The quality of the photographs and the trace of the blocks is the dominant control on the quality of the image analysis used in this study. The difficulty in distinguishing between the blocks and the matrix in many localities made precisely demarcating the block boundaries challenging. While attempts were made to mitigate the effects of perspective by choosing photographs that are approximately orthogonal to the rock surface, the effect of perspective could not be entirely eliminated. The process of tracing blocks naturally biases the data towards larger blocks, as smaller fragments may be too small or too numerous to trace accurately. The process of fitting ellipses to each block – performed automatically by ImageJ – represents approximately elliptical blocks well but cannot accurately represent more complex block geometries, especially in the case of folded blocks. In some cases, due to the size and number of the blocks in the frame of the photograph, some blocks which were truncated by the edge of the frame could not be excluded from analysis. Because the structural anisotropy technique detailed in Chapter 5.6 was developed after the 2016 field campaign, the photographs taken on that campaign did not contain a compass to allow orientation. As such, the structural anisotropy data could not be oriented to the cardinal orientations and was therefore detrended to remove the artefact of the camera orientation.

The method of determining structural anisotropy by image analysis detailed in Chapter 5.6 possesses some distinct limitations and caveats to its use. Firstly, the structural anisotropy ellipse produced by this method is a two-dimensional slice through the three-dimensional ellipsoid of the true anisotropy, and no means exist to discern the orientation of this slice with respect to the true anisotropy ellipsoid. This method can, therefore, offer only a minimum value for structural anisotropy. The results of this method are also independent of the size of the blocks and the block to matrix ratios; this is a strength of the method as it can compare anisotropies across scales, but it must be accounted for when interpreting the results. The scale of the anisotropy is an important consideration, as the value of anisotropy may vary across scales. The method used for drawing the

structural anisotropy ellipse assumes a perfect elliptical shape to the data cloud, which is a good fit in most cases in the Osa Mélange and simplifies the data. However the fit may not be ideal in all cases, especially if the data cloud presents as an “hourglass” shape; as this will not affect the structural anisotropy value, this was not considered. The choice of the 95th percentile to use for the SA₉₅ value was arbitrary but fitted well with the data. The process of detrending has a 5° resolution, which was deemed acceptable given the precision of the input data; this may have introduced some errors into SA₉₅ value, but these are considered negligible. The use of structural anisotropy as a proxy for mechanical anisotropy in Chapter 8 is premised on the relationship between structural features and mechanical properties outlined in Chapter 5.6. While blocks are the dominant structural characteristic of mélangé units, their shape and orientation are not the only factors determining their mechanical anisotropy and the structural anisotropy technique does not account for the orientations of fractures or the crystallographic anisotropy.

10.5.2. Critical evaluation of hypotheses and conclusions

10.5.2.1. Evaluation of the flexural moat hypothesis for Osa Mélange origin

The model of Osa Mélange formation by accretion of a seamount flexural moat basin — as described in Chapter 6 and Chapter 8 — fits the observation that the Osa Mélange is composed mostly of quartz-poor sedimentary material. Accretion of flexural moat deposits to the overriding plate has not been described before in other convergent margins, despite ~17% of modern global subduction zones subducting major bathymetric features (Vannucchi *et al.* 2016b), approximately 54% of which display a flexural moat visible on gravity data (see Table 10.1). This may be due to accreted moat deposits being ascribed to other settings, or it may suggest that accretion of moats is not a globally significant process. While the subduction channel hypothesis predicts that significantly increased thicknesses of sediment in a flexural moat should promote subduction accretion, this process has not been directly observed and further research should determine if it is geodynamically possible.

DISCUSSION

The inferred presence of a flexural moat around the Osa seamounts and the presence of carbonate blocks implies that the Osa seamounts were large enough to both induce crustal flexure and support a carbonate complex. The greater proportion of carbonate blocks in the Cabo Matapalo and Punta Salsipuedes units suggests that the seamounts which produced these units were larger than the seamounts which produced the San Pedrillo Unit. However, unlike the seamounts preserved in the Osa Igneous Complex which temporally coincide with the San Pedrillo Unit, the seamounts which produced the Cabo Matapalo and Salsipuedes units were not accreted. Such larger seamounts would likely also exhibit larger flexural moats, promoting increased accretion. The relative size of the seamounts which produced the San Pedrillo, Cabo Matapalo and Salsipuedes units and their effect on subduction accretion remains unresolved.

The presence of blocks of basalt and carbonate containing fragmented, shallow-water (Buchs *et al.*, 2009) microfossils within the otherwise quiescent, deep marine facies of the Bahia Drake Package is incongruous but may be explained by sporadic mass wasting events that bring blocks typically only deposited in the proximal portion of the moat into the more distal regions. Geochemical analysis of the basalt blocks by Hauff *et al.* (2000a), Buchs *et al.* (2009), and Chapter 9 have in total analysed a

RIDGE	HAS MOAT?	LENGTH
Hawaii-Emperor	Yes	635
Loisville	Yes	225
Hikurangi	No	140
Carnegie	No	330
Nazca	Yes	185
Cocos Ridge	No	185
Juan Fernandez	Yes	120
Java	No	450
Izu-Bonin	Yes	140

TABLE 10.1. Table showing the length of subduction zones worldwide that are subducting large high relief features (e.g. aseismic ridges, oceanic plateaus) (from Vannucchi *et al.*, 2016b) with the addition of whether these features have accompanying flexural moats.

maximum of 15 basalt blocks; this analysis can therefore not preclude the possibility that a greater number of blocks are derived from the Caribbean plate – either the arc or the Caribbean Large Igneous Province – than is currently estimated. The dacitic blocks feature ambiguous geochemistry and have no obvious source, with the most likely potential sources being a portion of the Golfito arc that has since been eroded or is no longer exposed, or a minor felsic component of the Osa seamounts. If these dacitic blocks are derived from the upper plate, then a mechanism of emplacing them within the Punta Marenco and Cocolito packages is required, as no evidence exists in the Osa Mélange for mixing between packages. As explained in Chapter 9, the Cordillera de Talamanca arc is unlikely to be the source for the dacitic rocks in the Osa Mélange; however, should these blocks be derived from this arc, it would necessitate that the Osa Mélange formed more recently than currently understood by Vannucchi *et al.* (2006), Buchs *et al.* (2009), and Clarke *et al.* (2018).

The absence of a significant felsic component in the Central American arc prior to the Miocene and the presence of the basaltic Caribbean Large Igneous Province in the upper plate means that the terrigenous sediment entering the Middle America Trench would itself be poor in quartz and is unlikely to resemble the accreted trench-fill found on the edges of mature continental crust, such as in Japan (e.g. Yamamoto *et al.*, 2011). However, the extreme predominance of igneous blocks derived from Galapagos seamounts (Hauff *et al.*, 2000a; Buchs *et al.*, 2009) and the highly localised outcrop pattern of the Osa Mélange favour a moat-derived origin for the mélange over a trench-derived origin.

Tests of the moat hypothesis should focus on the distribution of igneous blocks and their relationship to the Osa Igneous Complex. The moat hypothesis predicts that basalt blocks be derived from nearby seamounts, with most material originating at the closest seamount. However, the trench-fill hypothesis of Buchs *et al.* (2009) predicts that blocks are indiscriminately derived from Osa Igneous Complex. A greater number of igneous blocks should be analysed to quantify the proportion derived from the upper plate, as a high proportion would argue for a trench origin. This model also predicts that the depositional and accretionary ages of the San Pedrillo Unit should decrease systematically towards

DISCUSSION

the Middle America Trench. Paleontological analysis of the microfossils found in the cherts and carbonates may reveal faunal associations with Caribbean plate. Similarly, further geochemical analysis (e.g. Murray *et al.*, 1990) of the cherts and pelites may better constrain the provenances of these materials. Discerning and quantifying the proportion of material derived from the Caribbean Plate is important as, while the model does account for a minor component of terrigenous material, it predicts that the majority of the Osa Melange will be composed of material from the Galapagos-derived Osa seamounts.

10.5.2.2. Evaluation of the rheological inversion process and other deformation processes interpreted to occur during subduction

The depth to which the Osa Melange was subducted is poorly constrained, although the maximum depth is set by the lack of metamorphic recrystallisation and the rarity of greenschist facies minerals. Whether particular sections of the Osa Melange were frontally accreted or subducted to a shallow depth prior to accretion is often ambiguous, although evidence exists for both processes. Analysis of twinning patterns in calcite veins by Meschede *et al.* (1999) is used to determine that the lower limit of the maximum temperature reached was ~200 – 250 °C. However, this temperature only reflects the temperature at the time the veins formed and does not necessarily represent peak metamorphism. XRD analysis of zeolite mineral species to discern pressure and temperature conditions of veining was not attempted.

Chapter 7 presents the concept of inversion of the typical melange rheological relationship based on the observation that the volcanoclastic matrix of the Punta Marengo Package is now significantly stronger and has a higher Young's modulus than the altered basalt blocks it encloses. However, Fig. 8.7 shows that the matrix of the Punta Marengo Package is anomalous in its high strength, and that the matrix of other packages is weaker than its enclosing blocks (see Chapter 8). Processes unique to the altered basalt and volcanoclastic pelite must, therefore, be responsible for the induration of the matrix. The cause of this induration is not well understood, but is suspected to be the result of reactions between the volcanoclastic minerals and the subduction zone

fluids. Similar reactions between volcanoclastic material and fluids in other settings (e.g. Jackson *et al.*, 2017) have been reported to result in induration. Further analysis into the cause of this induration is warranted.

The present mechanical properties are regarded as representative of the mechanical properties during subduction because their deformation structures corroborate their relative strength and Young's modulus. However, despite care being taken during sampling to select samples that are minimally affected by visible weathering, alteration by tropical weather conditions likely had some effect on mechanical properties. Shear fractures cutting alteration fronts (as is visible in Fig. 7.3) indicates that a significant proportion of the alteration occurred before or coeval with deformation. Crucially, as the inversion of the rheological relationship involves volcanoclastic matrix that has been significantly indurated, it cannot be explained by differential weakening due to weathering.

The relationship between brittle fracture and seismicity within subduction zones is not well understood, with slip at a range of velocities being possible once a shear fracture has initiated. As such, in Chapter 7, brittle failure events are assumed to equate to seismic events. Since the rupture area for fractured blocks described in Chapter 7 is typically no larger than hundreds of square metres, these events are analogous to tremors. This chapter hypothesises that these tremor events load the subduction interface and may trigger a mega-thrust earthquake. More research into the relationships between tremors and large earthquakes, especially regarding the depths both phenomena occur at, is necessary to test this hypothesis. Further numerical analysis of the stress vectors during deformation and fracturing of blocks is also required to determine the propensity for fractures to propagate or arrest at block boundaries.

10.5.2.3. Evaluation of the inferred mechanisms of tectonic erosion and incorporation

In order to predict how the active tectonic erosion of the Osa Mélangé into the Middle America Subduction Zone influences the subduction interface processes, Chapter 8 predicts the

DISCUSSION

form in which each lithology will be incorporated. This follows the principles that:

1. The subduction channel is a viscous layer into which upper plate material may be abraded, allowing mixing of material from the downgoing slab with tectonically eroded material from the upper plate (*sensu* Cloos and Shreve, 1988b; Vannucchi *et al.*, 2012).
2. Tectonic erosion is accomplished by fluid-induced fracturing of the upper plate above a subduction zone (von Huene *et al.*, 2004).
3. The weakest of the two materials will be more readily comminuted while the strongest will be more prone to fracturing into larger blocks (Bearman *et al.*, 1997).
4. Where significant pre-existing weaknesses exist in the rock unit and are oriented such that they may be reactivated by stresses in the subduction zone, new fractures follow these weaknesses and preferentially erode this area.
5. Preferential tectonic erosion of one component creates irregularities on the upper surface of the subduction channel which increase stresses on the other component, increasing its rate of tectonic erosion.
6. Ready comminution of weaker components and fracturing of stronger components equilibrate to produce an approximately smooth upper subduction channel surface.

While principle 4 follows logically from well-understood theories of weakness reactivation (e.g. White *et al.*, 1986; Alaminiz-Alvarez *et al.*, 1998), additional research to numerically model hydrofractures in the complex fabric of the upper plate would provide a test for this principle and demonstrate the importance of upper plate structure in the process of tectonic erosion. Principles 5 and 6 follow logically from the subduction channel hypothesis of Cloos and Shreve (1988a), although these may also be tested by additional numerical modelling. As tectonic erosion of the Osa Melange is occurring at a shallow depth within the subduction system, the mechanical properties of these rocks measured at the surface are assumed not to differ significantly from the mechanical properties at depth. Once this material is incorporated into the subduction channel, its behaviour and influence on seismicity

will be dependant on its strength, Young's modulus, and frictional properties (see Chapters 7 and 8).

10.5.2.4. The effect of tropical weathering

The influence of the pervasive tropical weathering on the rocks of the Osa Mélange cannot be quantified and remains an important consideration in this research. The effects of low-temperature hydrothermal alteration on the ocean floor, within the subduction channel, and at depth in the forearc cannot be adequately distinguished from this tropical weathering. Since all samples were collected from the coast where the action of waves maintains a mostly fresh rock surface, the effects of tropical weathering are discounted with cautions. This weathering likely contributed to the pervasive alteration of the primary mineralogy to clays, which furthered the modification of the mobile element chemistry. It likely also affected the mechanical properties of the rocks as clay alteration products are generally weaker than the primary mineralogy. However, as this weathering intensifies the effects of the hydrothermal alteration – which is likely more active at depth – these rocks at the surface are still considered good analogues for the rocks at depth.

10.5.3. Recommendations for future work

1. Detailed study of the Cabo Matapalo and Salsipuedes units

High-resolution mapping, petrology and microstructural analysis – similar to the work done on the San Pedrillo Unit in this study – should be conducted on the younger two units of the Osa Mélange. This should address the issues of how and where these carbonate-rich units formed while no record remains of the seamounts from which they may be derived. The moat hypothesis – developed for the San Pedrillo Unit – may not be directly applicable to the Cabo Matapalo and Salsipuedes units.

2. Additional study of the San Pedrillo Unit in areas inaccessible to the 2016 field campaign.

Additional field campaigns to the Osa Peninsula would benefit study of this mélange. The primary benefit of additional field campaigns would be to address issues and questions raised during

DISCUSSION

the laboratory analysis and apply new methods developed during the analysis process, such as including cardinal orientation data in the structural anisotropy analysis. Fieldwork undertaken by more than one worker would allow study of exposure in river valleys to be accomplished safely. Authorised study in the Corcovado National Park and Caño Island would allow a more complete investigation of the Osa Mélangé and the study of a thrust fault reported by Vannucchi *et al.* (2006).

3. Oriented structural anisotropy

Any future fieldwork on the Osa Mélangé should include oriented photographs such that the structural anisotropy ellipses can be oriented to match the fabric and be presented on the geological map, as was demonstrated on the Gwna Mélangé in Chapter 5.6.

4. Detailed petrology of the indurated matrix

The mechanism by which the volcanoclastic matrix in the Punta Marengo Package became indurated remains unknown and deserves investigation. XRD or Raman spectroscopy of these rocks to determine the mineralogical content should be conducted alongside SEM analysis of the clay microtexture.

5. Single grain provenance of pyroxenes in the matrix

Geochemical provenance analysis of the abundant pyroxene grains in the matrix using the methodology of Nisbet and Pearce (1977) and Horozal *et al.* (2017), alongside comparison with the Osa Igneous Complex, Golfito and Cordillera de Talamanca arcs, and the Caribbean Large Igneous Province, will likely provide a more statistically viable means of quantifying the relative inputs of material from these sources. This provides a test for the moat hypothesis as it predicts that the significant majority of material will be derived from the same source as the Osa Igneous Complex.

6. Geochemical provenance of the cherts and pelites

Using the methodology of Murray *et al.* (1990), geochemical analysis of the cherts and pelites may be used to determine their provenance. Samples from the Osa Mélangé should be compared with other chert samples from the Osa Igneous Complex and

Azuero Complex to provide constraints on the specific chemistry of sediments formed at Galapagos-derived seamounts and on the Caribbean Large Igneous Province respectively.

7. Geochemical provenance of the basalt blocks

Following the pilot study reported in Chapter 9, geochemical provenance analysis should be performed on a range of basalt blocks from throughout the Osa Melange. This study should aim to sample a significantly greater number of blocks than the 15 that have currently been studied. The methodologies of Hauff *et al.* (2000a) and Buchs *et al.* (2009, 2016) should be applied to these blocks to discern their provenance and distinguish between which unit of the Osa Igneous Complex they share most geochemical similarity with.

8. Detailed geochemical provenance of the dacitic blocks

The geochemical data already collected for the dacitic blocks and reported in Chapter 9 should be supplemented by isotopic analysis to further discriminate between potential sources.

9. Faunal analysis of microfossils in the chert and carbonate blocks

Buchs *et al.* (2009) report the presence of shallow-water microfossils in the carbonate blocks. Species-level identification should be made of these microfossils and should be compared with the faunal assemblages of the western Caribbean margin throughout the Eocene – Miocene to determine if species endemic to the Caribbean are found in the melange. This would also help assess the proportion of upper plate material in the melange.

10. Determine the mechanical anisotropy of Osa Melange lithologies

The structural anisotropy method (Chapter 5.6) was developed in lieu of mechanical anisotropy analysis. However, mechanical anisotropy – especially tensile and compressive strength anisotropy – would be useful for predicting future deformation for this material in the subduction channel.

11. Determine crystallographic preferred orientation of Osa Melange lithologies

EBSD analysis would allow the crystallographic preferred orientation of melange lithologies to be discerned, which would be useful for discerning the anisotropy of the materials and complement the structural anisotropy method detailed in Chapter 5.6. This technique would be especially applicable to characterising the deformation in the melange matrix.

12. Higher resolution strength map

The strength map presented in Fig. 8.4 could be significantly improved by more data, both of the strength at given locations and the variety of different block strengths. This analysis may necessitate using a portable point load tester in the field to reduce the number of large samples that need to be recovered.

13. Comprehensive characterisation of the mechanical properties of melange blocks and matrix

The detailed characterisation of the mechanical properties of the altered basalt and volcanoclastic matrix reported in Chapter 7 should be expanded to include all major block and matrix lithologies. Triaxial tests are not necessary for this study as the priority should be comparison between lithologies which can be suitably accomplished using the unconfined compressive strength (UCS) test. This detailed characterisation can complement the point load strength data collected for the strength map.

14. Quantification of structural anisotropy as a proxy for mechanical anisotropy

Structural anisotropy analysis should be conducted on rock samples for which the mechanical anisotropy is well characterised to determine if structural anisotropy can function as a quantitative proxy for mechanical anisotropy.

15. Analysis of propagation and arrest of fractures within blocks undergoing rheological inversion.

Numerical modelling of blocks in matrix undergoing shear and rheological inversion (Chapter 7) should be expanded to include

analysis of the stress vectors around the block as the rheologies change to determine if a fracture is likely to arrest or propagate into the matrix.

16. Influence of non-homogenous materials on block and matrix deformation in subduction channels

In reality, *mélange* lithologies are highly heterogeneous. Therefore, in addition to the numerical modelling used in Chapter 7, similar models should also study the influence of non-homogeneous block and matrix on the deformation in the subduction channel. In particular, a model investigating a block whose strength and Young's modulus increases towards its core may more accurately represent the blocks in the Punta Marengo Package.

17. Determine the effect of block aspect ratio and rotation, distance between blocks, and difference in Poisson's ratio on the rheological inversion envelope.

The numerical modelling used to produce Fig. 7.6 should be expanded to study the effect of other variables on whether the block or the matrix breaks first at different values of difference in strength and difference in Young's modulus.

18. Numerical modelling of tectonic erosion by hydrofracturing of the upper plate

Numerical modelling of different *mélange* fabrics in the upper plate (Fig. 8.10) and the propagation paths of induced hydrofractures will allow testing of the hypothesis that the structure of the upper plate represents a control on the style of tectonic erosion.

THIS PAGE INTENTIONALLY LEFT BLANK.

CHAPTER 11. CONCLUSION

Analysis of the Osa Mélange has revealed that locally thick accumulations of sediment in oceanic features such as seamount flexural moats can promote subduction accretion when they are subducted, even in otherwise erosive subduction zones like the Middle America Subduction Zone. The accreted products of these sediment-rich oceanic features can be recognised by their lack of terrigenous sediment such as quartz, as well as lithic clasts/blocks derived from continental settings. Seamount flexural moat deposits may contain mass-wasted megablocks of basalt within a volcanoclastic matrix and accreted moats may possess a relict stratigraphy that can be reconstructed by comparison to extant moats (Chapter 10.1). These deposits may include volcanoclastic-rich debris-avalanches deposited proximal to the seamount edifice, and interbedded pelites, cherts, and distal turbidites in the distal moat basin. The Osa Mélange is the first recognised accreted flexural moat deposit and formed around the seamounts which now constitute the adjacent Osa Igneous Complex (Clarke *et al.*, 2018).

While on the incoming plate, seafloor alteration processes began to weaken the basalt blocks. Once the moat deposit was subducted, the basalt blocks continued to weaken as a result of chemical alteration and mechanical brecciation while its surrounding matrix lithified and indurated. This eventually led to the blocks becoming weaker than the matrix, resulting in an inversion of the typically conceived rheological relationship of mélanges (e.g. Fagereng and Sibson, 2010). Rheological inversion can modify the seismic potential of the plate interface by weakening the subduction channel. Failure of a weakened block increases the stress on its intervening matrix and neighbouring blocks, therefore priming the subduction zone for a larger, through-going rupture (Chapter 7).

The interbedded cherts and pelites deposited in the distal moat have been thoroughly dismembered during the subduction and accretion process. Combined with accreted debris avalanche deposits, the dismembered bedded sediments provide a wide range of fabrics in the upper plate. Since tectonic erosion in a

CONCLUSION

subduction zone occurs by hydrofracturing of the hanging wall, the complex fabric and material properties of the upper plate control the size, shape, and internal structure of blocks tectonically eroded into the subduction channel (Chapter 8). Slip and seismicity in the subduction channel beneath the Osa Melange are controlled by the structure and material properties of the tectonically eroded blocks in addition to the material properties of the subducted sediment and the relief of the downgoing plate. On the whole, the eroded material entering the subduction channel is expected to suppress seismic activity and favour transient aseismic slip and stable sliding; leading to a reduced seismic hazard around the Osa Peninsula.

REFERENCES

- Abbate, E., Bortolotti, V. & Passerini, P. 1970. Olistostromes and Olistoliths. *Sedimentary Geology*, 4, 521 – 557.
- Abbate, E. & Sagri, M. 1970. The eugeosynclinal sequences. *Sedimentary Geology*, 4, 251 – 340, [https://doi.org/10.1016/0037-0738\(70\)90018-7](https://doi.org/10.1016/0037-0738(70)90018-7).
- Abbott, R.N. & Bandy, B.R. 2008. Amphibolite and blueschist-greenschist facies metamorphism, Blue Mountain inlier, eastern Jamaica. *Geological Journal*, 43, 525 – 541, <https://doi.org/10.1002/gj.1126>.
- Abercrombie, R.E., Antolik, M., Felzer, K. & Ekström, G. 2001. The 1994 Java tsunami earthquake: Slip over a subducting seamount. *Journal of Geophysical Research: Solid Earth*, 106, 6595 – 6607, <https://doi.org/10.1029/2000JB900403>.
- Abratis, M. & Wörner, G. 2001. Ridge collision, slab-window formation, and the flux of Pacific asthenosphere into the Caribbean realm. *Geology*, 29, 127, [https://doi.org/10.1130/0091-7613\(2001\)029<0127:RCSWFA>2.0.CO;2](https://doi.org/10.1130/0091-7613(2001)029<0127:RCSWFA>2.0.CO;2).
- Abratis, M. 1998. Geochemical variations in magmatic rocks from southern Costa Rica as a consequence of Cocos Ridge subduction and uplift of the Cordillera de Talamanca.
- Adamek, S., Frohlich, C. & Pennington, D. 1988. Seismicity of the Caribbean – Nazca Boundary: Constraints on Microplate Tectonics of the Panama Region. *Journal of Geophysical Research*, 93, 2053 – 2075.
- Alaniz-Alvarez, S.A., Nieto-Samaniego, Á.F. & Tolson, G. 1998. A graphical technique to predict slip along a pre-existing plane of weakness. *Engineering Geology*, 49, 53 – 60, [https://doi.org/10.1016/S0013-7952\(97\)00071-9](https://doi.org/10.1016/S0013-7952(97)00071-9).
- Almeyda-Zambrano, A.M., Broadbent, E.N. & Durham, W.H. 2010. Social and environmental effects of ecotourism in the Osa Peninsula of Costa Rica: the Lapa Rios case. *Journal of Ecotourism*, 9, 62 – 83, <https://doi.org/10.1080/14724040902953076>.
- Alvarado, G.E., Denyer, P. & Sinton, C.W. 1997. The 89 Ma Tortugal komatiitic suite, Costa Rica: Implications for a common geological origin of the Caribbean and Eastern Pacific region from a mantle plume. *Geology*, 25, 439, [https://doi.org/10.1130/0091-7613\(1997\)025<0439:TMTKSC>2.3.CO;2](https://doi.org/10.1130/0091-7613(1997)025<0439:TMTKSC>2.3.CO;2).
- Alvarado, G.E., Denyer, P., et al. 2009. Endeavor research into evolving paradigms around Ophiolites : The case of the oceanic igneous complexes of Costa Rica Área de Amenazas y Auscultación Sísmica y Volcánica ; Department of Geological Sciences , Rutgers University. *Revista geologica América Central*, 40, 49 – 73.

- Angiboust, S., Kirsch, J., Oncken, O., Glodny, J., Monié, P. & Rybacki, E. 2015. Probing the transition between seismically coupled and decoupled segments along an ancient subduction interface: CATACLASIS ON THE SUBDUCTION INTERFACE. *Geochemistry, Geophysics, Geosystems*, 16, 1905 – 1922, <https://doi.org/10.1002/2015GC005776>.
- Arias, O. 2011. Redefinición de la Formación Tulín (Maastrichtiano-Eoceno Inferior) del Pacífico Central de Costa Rica. *Revista Geológica de América Central*, <https://doi.org/10.15517/rgac.v0i28.7783>.
- Arroyo, I.G., Grevemeyer, I., Ranero, C.R. & von Huene, R. 2014. Interplate seismicity at the CRISP drilling site: The 2002 Mw 6.4 Osa Earthquake at the southeastern end of the Middle America Trench. *Geochemistry, Geophysics, Geosystems*, 15, 3035 – 3050, <https://doi.org/10.1002/2014GC005359>.
- Aubouin, J., von Huene, R., et al. 1982. Leg 84 of the Deep Sea Drilling Project. Subduction without accretion: Middle America Trench off Guatemala. *Nature*, 297.
- Bachmann, R., Oncken, O., Glodny, J., Seifert, W., Georgieva, V. & Sudo, M. 2009. Exposed plate interface in the European Alps reveals fabric styles and gradients related to an ancient seismogenic coupling zone. *Journal of Geophysical Research*, 114, <https://doi.org/10.1029/2008JB005927>.
- Bacon, C.D., Silvestro, D., Jaramillo, C., Smith, B.T., Chakrabarty, P. & Antonelli, A. 2015. Biological evidence supports an early and complex emergence of the Isthmus of Panama. *Proceedings of the National Academy of Sciences*, 112, 6110 – 6115, <https://doi.org/10.1073/pnas.1423853112>.
- Baier, J., Audétat, A. & Keppler, H. 2008. The origin of the negative niobium tantalum anomaly in subduction zone magmas. *Earth and Planetary Science Letters*, 267, 290 – 300, <https://doi.org/10.1016/j.epsl.2007.11.032>.
- Bailey, E. & McCallien, W.J. 1950. The Ankara Mélange and the Anatolian Thrust. *Nature*, 166, 938 – 940, <https://doi.org/10.1038/166938a0>.
- Bailey, E.B. & McCallien, W.J. 1954. XI.—Serpentine Lavas, the Ankara Mélange and the Anatolian Thrust. *Transactions of the Royal Society of Edinburgh*, 62, 403 – 442, <https://doi.org/10.1017/S0080456800009340>.
- Bailey, E.B. & McCallien, W.J. 1962. Liguria Nappe: Northern Apennines. *Transactions of the Royal Society of Edinburgh*, 65, 315 – 333.
- Bailey, E.B. & McCallien, W.J. 1963. XIII.—Liguria Nappe: Northern Apennines. *Transactions of the Royal Society of Edinburgh*, 65, 315 – 333, <https://doi.org/10.1017/S0080456800012552>.
- Barber, A.J. 2013. The origin of mélanges: Cautionary tales from Indonesia. *Journal of Asian Earth Sciences*, 76, 428 – 438, <https://doi.org/10.1016/j.jseaes.2012.12.021>.

- Barckhausen, U., Ranero, C.R., von Huene, R., Cande, S.C. & Roeser, H.A. 2001. Revised tectonic boundaries in the Cocos Plate off Costa Rica: Implications for the segmentation of the convergent margin and for plate tectonic models. *Journal of Geophysical Research: Solid Earth*, 106, 19207 – 19220, <https://doi.org/10.1029/2001JB000238>.
- Baumgartner, P.O. & Denyer, P. 2006. Evidence for middle Cretaceous accretion at Santa Elena Peninsula (Santa Rosa Accretionary Complex), Costa Rica. *Geologica Acta*, 4, 179 – 191.
- Bearman, R.A., Briggs, C.A. & Kojovic, T. 1997. The application of rock mechanics parameters to the prediction of comminution behaviour. 10.
- Berkland, J.O., Raymond, L.A., Kramer, J.C., Moores, E.M. & O'Day, M. 1972. What is Franciscan. *American Association of Petroleum Geologists Bulletin*, 56, 2295 – 2302.
- Berrangé, J.P., Bradley, D.R. & Snelling, N.J. 1989. K/Ar age dating of the ophiolitic Nicoya Complex of the Osa Peninsula, southern Costa Rica. *Journal of South American Earth Sciences*, 2, 49 – 59.
- Berrangé, J.P. & Thorpe, R.S. 1988. The geology, geochemistry and emplacement of the Cretaceous – Tertiary ophiolitic Nicoya Complex of the Osa Peninsula, southern Costa Rica. *Tectonophysics*, 147, 193 – 220, [https://doi.org/10.1016/0040-1951\(88\)90187-4](https://doi.org/10.1016/0040-1951(88)90187-4).
- Bettelli, G. & Vannucchi, P. 2003. Structural style of the offscraped Ligurian oceanic sequences of the Northern Apennines: new hypothesis concerning the development of mélange block-in-matrix fabric. *Journal of Structural Geology*, 25, 371 – 388.
- Beutel, E.K. 2009. Tectonophysics Magmatic rifting of Pangaea linked to onset of South American plate motion. *Tectonophysics*, 468, 149 – 157, <https://doi.org/10.1016/j.tecto.2008.06.019>.
- Beutner, E.C. 1975. Tectonite and mélange – A distinction: Comment and reply: COMMENT. *Geology*, 3, 358 – 358, [https://doi.org/10.1130/0091-7613\(1975\)3<358a:TAMDCA>2.0.CO;2](https://doi.org/10.1130/0091-7613(1975)3<358a:TAMDCA>2.0.CO;2).
- Bilek, S.L., Schwartz, S.Y. & DeShon, H.R. 2003. Control of seafloor roughness on earthquake rupture behavior. *Geology*, 31, 455, [https://doi.org/10.1130/0091-7613\(2003\)031<0455:COSROE>2.0.CO;2](https://doi.org/10.1130/0091-7613(2003)031<0455:COSROE>2.0.CO;2).
- Blanpied, M.L., Lockner, D.A. & Byerlee, J.D. 1995. Frictional slip of granite at hydrothermal conditions. *Journal of Geophysical Research: Solid Earth*, 100, 13045 – 13064, <https://doi.org/10.1029/95JB00862>.
- Broch, E. 1983. Estimation of strength anisotropy using the point-load test. *International Journal of Rock Mechanics and Mining Sciences & Geomechanics Abstracts*, 20, 181 – 187, [https://doi.org/10.1016/0148-9062\(83\)90942-7](https://doi.org/10.1016/0148-9062(83)90942-7).

- Brueckner, H.K., Avé Lallemant, H.G., et al. 2009. Metamorphic reworking of a high pressure–low temperature mélange along the Motagua fault, Guatemala: A record of Neocomian and Maastrichtian transpressional tectonics. *Earth and Planetary Science Letters*, 284, 228 – 235, <https://doi.org/10.1016/j.epsl.2009.04.032>.
- Buchs, D.M. 2008. Late Cretaceous to Eocene Geology of the South Central American Forearc Area (Southern Costa Rica and Western Panama): Initiation and Evolution of an Intra-Oceanic Convergent Margin. PhD Thesis, Université de Lausanne, Switzerland.
- Buchs, D.M., Arculus, R.J. & Baumgartner, P.O. 2011. Oceanic intraplate volcanoes exposed : Example from seamounts accreted in Panama. *Geology*, 39, 335 – 338, <https://doi.org/10.1130/G31703.1>.
- Buchs, D.M., Arculus, R.J., Baumgartner, P.O., Baumgartner-Mora, C. & Ulianov, A. 2010. Late Cretaceous arc development on the SW margin of the Caribbean Plate: Insights from the Golfito, Costa Rica, and Azuero, Panama, complexes. *Geochemistry, Geophysics, Geosystems*, 11, 1 – 35, <https://doi.org/10.1029/2009GC002901>.
- Buchs, D.M., Baumgartner, P.O., Baumgartner-Mora, C., Bandini, A.N., Jackett, S.-J., Diserens, M.-O. & Stucki, J. 2009. Late Cretaceous to Miocene seamount accretion and melange formation in the Osa and Burica Peninsulas (Southern Costa Rica): episodic growth of a convergent margin. Geological Society, London, Special Publications, 328, 411 – 456, <https://doi.org/10.1144/SP328.17>.
- Buchs, D.M., Hoernle, K., Hauff, F. & Baumgartner, P.O. 2016. Evidence from accreted seamounts for a depleted component in the early Galapagos plume. *Geology*, 383 – 386, <https://doi.org/10.1130/G37618.1>.
- Burke, K. 1988. Tectonic Evolution of the Caribbean. *Annual Review of Earth and Planetary Sciences*, 16, 201 – 239.
- Burton, K.W., Ling, H.-F. & O’Nions, R.K. 1997. Closure of the Central American Isthmus and its effect on deep-water formation in the North Atlantic. *Nature*, 386, 382.
- Butler, R.W.H., Bond, C.E., Shipton, Z.K., Jones, R.R. & Casey, M. 2008. Fabric anisotropy controls faulting in the continental crust. *Journal of the Geological Society*, 165, 449 – 452, <https://doi.org/10.1144/0016-76492007-129>.
- Calahorra, A., Sallares, V., Collot, J., Sage, F. & Ranero, C. 2008. Nonlinear variations of the physical properties along the southern Ecuador subduction channel: Results from depth-migrated seismic data. *Earth and Planetary Science Letters*, 267, 453 – 467, <https://doi.org/10.1016/j.epsl.2007.11.061>.

- Callaway, C. 1905. The Eastern Gneisses of the Scottish Highlands. *Geological Magazine*, 1, 90 – 90.
- Cecca, C., Giovagnoli, C., Manni, R., Mariotti, N., Nicosia, U. & Santantonio, M. 1981. Tithonian 'Ammonitico Rosso' near Bolognola (Marche - Central Apennines): A Shallow Water Nodular Limestone.
- Chemenda, A.I., Burg, J.-P. & Mattauer, M. 2000. Evolutionary model of the Himalaya–Tibet system: geopoembased on new modelling, geological and geophysical data. *Earth and Planetary Science Letters*, 174, 397 – 409, [https://doi.org/10.1016/S0012-821X\(99\)00277-0](https://doi.org/10.1016/S0012-821X(99)00277-0).
- Chemenda, A.I., Mattauer, M. & Bokun, A.N. 1996. Continental subduction and a mechanism for exhumation of high-pressure metamorphic rocks: new modelling and field data from Oman. *Earth and Planetary Science Letters*, 143, 173 – 182, [https://doi.org/10.1016/0012-821X\(96\)00123-9](https://doi.org/10.1016/0012-821X(96)00123-9).
- Chen, J., Niemeijer, A.R. & Spiers, C.J. 2017. Microphysically Derived Expressions for Rate-and-State Friction Parameters, a , b , and D : Microphysically Derived RSF Parameters. *Journal of Geophysical Research: Solid Earth*, 122, 9627 – 9657, <https://doi.org/10.1002/2017JB014226>.
- Clarke, A.P. 2014. Discerning the Age of NW – SE Trending Mafic Dykes at Llanbadrig, N. Anglesey through Geochemical and Structural Analysis. MGeol. University of Leicester.
- Clarke, A.P., Vannucchi, P. & Morgan, J. 2018. Seamount chain–subduction zone interactions: Implications for accretionary and erosive subduction zone behavior. *Geology*, 46, 367 – 370, <https://doi.org/10.1130/G40063.1>.
- Clift, P.D. & Vannucchi, P. 2004. Controls on tectonic accretion versus erosion in subduction zones: Implications for the origin and recycling of the continental crust. *Review of Geophysics*, 42, <https://doi.org/10.1029/2003RG000127>.
- Cloos, M. & Shreve, R.L. 1988a. Subduction-channel model of prism accretion, melange formation, sediment subduction, and subduction erosion at convergent plate margins: 1. Background and description. *Pure and Applied Geophysics*, 128, 455 – 500, <https://doi.org/10.1007/BF00874548>.
- Cloos, M. & Shreve, R.L. 1988b. Subduction-channel model of prism accretion, melange formation, sediment subduction, and subduction erosion at convergent plate margins: 2. Implications and discussion. *Pure and Applied Geophysics*, 128, 501 – 545, <https://doi.org/10.1007/BF00874549>.
- Cloos, M. 1982. Flow melanges: Numerical modeling and geologic constraints on their origin in the Franciscan subduction complex, California. *Geological Society of America Bulletin*, 93, 330, [https://doi.org/10.1130/0016-7606\(1982\)93<330:FMNMG>2.0.CO;2](https://doi.org/10.1130/0016-7606(1982)93<330:FMNMG>2.0.CO;2).

- Cloos, M. 1992. Thrust-type subduction-zone earthquakes and seamount asperities: A physical model for seismic rupture. *Geology*, 20, 601, [https://doi.org/10.1130/0091-7613\(1992\)020<0601:TTSZEA>2.3.CO;2](https://doi.org/10.1130/0091-7613(1992)020<0601:TTSZEA>2.3.CO;2).
- Coates, A.G., George, T., Dowsett, H.J., Survey, U.S.G. & Bybell, L.M. 1992. Closure of the Isthmus of Panama : The near-shore marine record of Costa Rica and western Panama. 814 – 828.
- Coats, R.R. 1962. Magma Type and Crustal Structure in the Aleutian Arc. In: Macdonald, G. A. & Kuno, H. (eds) *Geophysical Monograph Series*. Washington, D. C., American Geophysical Union, 92 – 109., <https://doi.org/10.1029/GM006p0092>.
- Coleman, P.J. 1975. On Island Arcs. *Earth-Science Reviews*, 11, 47 – 80.
- Collettini, C., Niemeijer, A., Viti, C. & Marone, C. 2009. Fault zone fabric and fault weakness. *Nature*, 462, 907 – 910, <https://doi.org/10.1038/nature08585>.
- Collot, J.-Y., Ribodetti, A., Agudelo, W. & Sage, F. 2011. The South Ecuador subduction channel: Evidence for a dynamic mega-shear zone from 2D fine-scale seismic reflection imaging and implications for material transfer: Ecuador dynamic subduction channel. *Journal of Geophysical Research: Solid Earth*, 116, n/a-n/a, <https://doi.org/10.1029/2011JB008429>.
- Cowan, D.S. 1974. Deformation and metamorphism of the Franciscan subduction zone complex northwest of Pacheco Pass, California. *Bulletin of the Geological Society of America*, 85, 1623 – 1634, [https://doi.org/10.1130/0016-7606\(1974\)85<1623:DAMOTF>2.0.CO;2](https://doi.org/10.1130/0016-7606(1974)85<1623:DAMOTF>2.0.CO;2).
- Cowan, D.S. 1978. Origin of blueschist-bearing chaotic rocks in the Franciscan Complex, San Simeon, California. *Geological Society of America Bulletin*, 89, 1415, [https://doi.org/10.1130/0016-7606\(1978\)89<1415:OBCRI>2.0.CO;2](https://doi.org/10.1130/0016-7606(1978)89<1415:OBCRI>2.0.CO;2).
- Cowan, D.S. 1990. Kinematic analysis of shear zones in sandstone and mudstone of the Shimanto belt, Shikoku, SW Japan. *Journal of Structural Geology*, 12, 431 – 441, [https://doi.org/10.1016/0191-8141\(90\)90032-T](https://doi.org/10.1016/0191-8141(90)90032-T).
- Cowan, D.S.D. 1985. Structural styles in Mesozoic and Cenozoic mélanges in the western Cordillera of North America. *Geological Society of America Bulletin*, 96, 451 – 462, [https://doi.org/10.1130/0016-7606\(1985\)96<451:SSIMAC>2.0.CO;2](https://doi.org/10.1130/0016-7606(1985)96<451:SSIMAC>2.0.CO;2).
- Cruz-Uribe, A.M., Marschall, H., Gaetani, G.A. & Le Roux, V. 2018. Generation of alkaline magmas in subduction zones by partial melting of mélange diapirs – an experimental study. 46, 2 – 5.
- Dahlen, F.A. 1990. Critical taper model of fold-and-thrust belts and accretionary wedges. *Annual Review of Earth and Planetary Sciences*, 18, 55 – 99.

- Das, S. & Watts, A.B. 2009. Effect of Subducting Seafloor Topography on the Rupture Characteristics of Great Subduction Zone Earthquakes. In: Lallemand, S. & Funicello, F. (eds) *Subduction Zone Geodynamics*. Berlin, Heidelberg, Springer Berlin Heidelberg, 103 – 118., https://doi.org/10.1007/978-3-540-87974-9_6.
- de Boer, J.Z., Drummond, M.S., Bordelon, M.J., Defant, M.J., Bellon, H. & Maury, R.C. 1995. Cenozoic magmatic phases of the Costa Rican island arc (Cordillera de Talamanca). In: Mann, P. (ed.) *Geologic and Tectonic Development of the Caribbean Plate Boundary in Southern Central America*. Geological Society of America.
- de Jong, K. 1974. Melange (Olistostrome) near Lago Titicaca, Peru. *American Association of Petroleum Geologists Bulletin*, 58, 729 – 741.
- Dela Pierre, F., Festa, a. & Irace, a. 2007. Interaction of tectonic, sedimentary, and diapiric processes in the origin of chaotic sediments: An example from the Messinian of Torino Hill (Tertiary Piedmont Basin, northwestern Italy). *Geological Society of America Bulletin*, 119, 1107 – 1119, <https://doi.org/10.1130/B26072.1>.
- Delteil, J., de Lepinay, B.M., Morgans, H.E.G. & Field, B.D. 2006. Olistostromes marking tectonic events, East Coast, New Zealand. *New Zealand Journal of Geology and Geophysics*, 49, 517 – 531, <https://doi.org/10.1080/00288306.2006.9515185>.
- Dengo, G. 1962. Tectonic-igneous sequence in Costa Rica. In: Engle, A. E. J. & James, H. J. (eds) *Petrological Studies (A Volume in Honor of A. F. Buddington)*. Boulder, Colorado, Geological Society of America, 133 – 161.
- Denyer, P. & Gazel, E. 2009. The Costa Rican Jurassic to Miocene oceanic complexes: Origin, tectonics and relations. *Journal of South American Earth Sciences*, 28, 429 – 442, <https://doi.org/10.1016/j.jsames.2009.04.010>.
- Di Marco, G. 1994. Les terrains accrétés du Costa Rica: évolution tectonostratigraphique de la marge continentale de la plaque caraïbe. *Mémoires de Géologie*, Lausanne.
- Di Marco, G., Baumgartner, P.O. & Channell, J.E.T. 1995. tectonostratigraphic subdivision of Costa Rica and western Panama.
- Dickinson, W.R. 1970. Relations of Andesites, Granites, and Derivative Sandstones to Arc-Trench Tectonics. *Reviews of Geophysics and Space Physics*, 8, 813 – 860.
- Dietz, R.S. & Holden, J.C. 1970. Reconstruction of Pangaea: Breakup and Dispersion of Continents, Permian to Present. *Journal of Geophysical Research*, 75, 4939 – 4956.

- Dilek, Y. & Furnes, H. 2014. Ophiolites and Their Origins. *Elements*, 10, 93 – 100, <https://doi.org/10.2113/gselements.10.2.93>.
- Dilek, Y. 2003. Ophiolite concept and its evolution. In: Special Paper 373: Ophiolite Concept and the Evolution of Geological Thought. Geological Society of America, 1 – 16., <https://doi.org/10.1130/0-8137-2373-6.1>.
- Dott, R.H. 1965. Mesozoic-cenozoic tectonic history of the southwestern Oregon coast in relation to cordilleran orogenesis. *Journal of Geophysical Research*, 70, 4687 – 4707, <https://doi.org/10.1029/JZ070i018p04687>.
- Duarte, J.C., Schellart, W.P. & Cruden, A.R. 2015. How weak is the subduction zone interface?: How weak is the subduction interface? *Geophysical Research Letters*, 42, 2664 – 2673, <https://doi.org/10.1002/2014GL062876>.
- Duncan, R.A. & Hargraves, R.B. 1984. Plate tectonic evolution of the Caribbean region in the mantle reference frame. In: Geological Society of America Memoirs. Geological Society of America, 81 – 94., <https://doi.org/10.1130/MEM162-p81>.
- Echeverría, L.M. & Aitken, B.G. 1986. Pyroclastic rocks: another manifestation of ultramafic volcanism on Gorgona Island, Colombia. *Contributions to Mineralogy and Petrology*, 92, 428 – 436, <https://doi.org/10.1007/BF00374425>.
- Eden, C.P. & Andrews, J.R. 1990. Middle to Upper Devonian melanges in SW Spain and their relationship to the Meneage Formation in south Cornwall. In: Proceedings of the Ussher Society – Annual Conference of the Ussher Society, January 1990. 217 – 222.
- Ernst, W.G. & Seki, Y. 1967. Petrologic comparison of the franciscan and sanbagawa metamorphic terranes. *Tectonophysics*, 4, 463 – 478, [https://doi.org/10.1016/0040-1951\(67\)90011-X](https://doi.org/10.1016/0040-1951(67)90011-X).
- Ernst, W.G. 1965. Mineral Parageneses in Franciscan Metamorphic Rocks, Panchoe Pass, California. *Geological Society of America Bulletin*, 76, 879 – 914.
- Ernst, W.G. 1970. Tectonic Contact between the Franciscan Mélange and the Great Great Valley sequence Franciscan group. *Journal of Geophysical Research*, 75, 886 – 901.
- Ernst, W.G. 1971. Petrologic Reconnaissance of Franciscan Metagraywackes from the Diablo Range, Central California Coast Ranges. *Journal of Petrology*, 12, 413 – 437.
- Ernst, W.G. 2015. Franciscan geologic history constrained by tectonic/olistostromal high-grade metamafic blocks in the iconic California Mesozoic-Cenozoic accretionary complex. *American Mineralogist*, 100, 6 – 13, <https://doi.org/10.2138/am-2015-4850>.

- Fagereng, A. & Sibson, R.H. 2010. Melange rheology and seismic style. *Geology*, 38, 751 – 754, <https://doi.org/10.1130/G30868.1>.
- Federico, L., Crispini, L., Scambelluri, M. & Capponi, G. 2007. Ophiolite mélangé zone records exhumation in a fossil subduction channel. *Geology*, 35, 499 – 502, <https://doi.org/10.1130/G23190A.1>.
- Festa, A. 2011. Tectonic, sedimentary, and diapiric formation of the Messinian mélangé: Tertiary Piedmont Basin (northwestern Italy). In: *Geological Society of America Special Papers*. Geological Society of America, 215 – 232., [https://doi.org/10.1130/2011.2480\(10\)](https://doi.org/10.1130/2011.2480(10)).
- Festa, A., Dilek, Y., Pini, G.A., Codegone, G. & Ogata, K. 2012. Mechanisms and processes of stratal disruption and mixing in the development of mélanges and broken formations: Redefining and classifying mélanges. *Tectonophysics*, 568 – 569, 7 – 24, <https://doi.org/10.1016/j.tecto.2012.05.021>.
- Festa, A., Pini, G.A., Dilek, Y. & Codegone, G. 2010. Mélanges and mélangé-forming processes: A historical overview and new concepts. *International Geology Review*, 52, 1040 – 1105, <https://doi.org/10.1080/00206810903557704>.
- Fisher, D.M., Gardner, T.W., Sak, P.B., Sanchez, J.D., Murphy, K. & Vannucchi, P. 2004. Active thrusting in the inner forearc of an erosive convergent margin, Pacific coast, Costa Rica. *Tectonics*, 23, <https://doi.org/10.1029/2002TC001464>.
- Fitton, J.G., Saunders, a. D., Norry, M.J., Hardarson, B.S. & Taylor, R.N. 1997. Thermal and chemical structure of the Iceland plume. *Earth and Planetary Science Letters*, 153, 197 – 208, [https://doi.org/10.1016/S0012-821X\(97\)00170-2](https://doi.org/10.1016/S0012-821X(97)00170-2).
- Flores, K.E., Skora, S., Martin, C., Harlow, G.E., Rodríguez, D. & Baumgartner, P.O. 2015. Metamorphic history of riebeckite- and aegirine-augite-bearing high-pressure-low-temperature blocks within the Siuna Serpentinite Mélange, northeastern Nicaragua. *International Geology Review*, 57, 943 – 977, <https://doi.org/10.1080/00206814.2015.1027747>.
- Flores. 1955. Discussion. In: *Proceedings of the 4th World Petroleum Conference*, Rome. 120 – 121.
- Forastelli, M.R. & Aguilar, J.E.A. 2013. *Socio-Economic Panorama of the Osa and Golfito Cantons: Trends and Challenges for Sustainable Development (Executive Summary)*.
- Forbes Inskip, N. D., Meredith, P. G., Chandler, M. R., & Gudmundsson, A. (2018). Fracture properties of Nash Point shale as a function of orientation to bedding. *Journal of Geophysical Research: Solid Earth*, 123. <https://doi.org/10.1029/2018JB015943>

- Foulger, G.R. & Anderson, D.L. 2005. A cool model for the Iceland hotspot. *Journal of Volcanology and Geothermal Research*, 141, 1 – 22, <https://doi.org/10.1016/j.jvolgeores.2004.10.007>.
- Franklin, J.A. 1985. Suggested method for determining point load strength. *International Journal of Rock Mechanics and Mining Sciences & Geomechanics Abstracts*, 22, 51 – 60, [https://doi.org/10.1016/0148-9062\(85\)92327-7](https://doi.org/10.1016/0148-9062(85)92327-7).
- Franklin, J.A., Vogler, U.W., Szlavin, J., Edmond, J.M. & Bieniawski, Z.T. 1977. Suggested Methods for Determining Water-Content, Porosity, Density, Absorption and Related Properties and Swelling and Slake-Durability Index Properties.
- Frisch, W., Meschede, M. & Sick, M. 1992. Origin of the Central American ophiolites: Evidence from paleomagnetic results. *Geological Society of America Bulletin*, 104, 1301 – 1314, [https://doi.org/10.1130/0016-7606\(1992\)104<1301:OOTCAO>2.3.CO;2](https://doi.org/10.1130/0016-7606(1992)104<1301:OOTCAO>2.3.CO;2).
- Fuentes, P., Díaz-Alvarado, J., Fernández, C., Díaz-Azpiroz, M. & Rodríguez, N. 2016. Structural analysis and shape-preferred orientation determination of the mélangé facies in the Chañaral mélangé, Las Tórtolas Formation, Coastal Cordillera, northern Chile. *Journal of South American Earth Sciences*, 67, 40 – 56, <https://doi.org/10.1016/j.jsames.2016.02.001>.
- Gale, A., Dalton, C.A., Langmuir, C.H., Su, Y. & Schilling, J.-G. 2013. The mean composition of ocean ridge basalts: MEAN MORB. *Geochemistry, Geophysics, Geosystems*, 14, 489 – 518, <https://doi.org/10.1029/2012GC004334>.
- Gallitelli, P. 1955. Clay Minerals of the Argille Scagliose of the Modenese Apennines. *Clay Minerals*, 2, 275 – 280, <https://doi.org/10.1180/claymin.1955.002.13.09>.
- Gansser, A. 1955. *New Aspects Of The Geology In Central Iran*. World Petroleum Congress.
- Gao, X. & Wang, K. 2017. Rheological separation of the megathrust seismogenic zone and episodic tremor and slip. *Nature*, 543, 416 – 419, <https://doi.org/10.1038/nature21389>.
- Garcia, M.O. & Davis, M.G. 2001. Submarine growth and internal structure of ocean island volcanoes based on submarine observations of Mauna Loa volcano, Hawaii. *Geology*, 29, 163, [https://doi.org/10.1130/0091-7613\(2001\)029<0163:SGAISO>2.0.CO;2](https://doi.org/10.1130/0091-7613(2001)029<0163:SGAISO>2.0.CO;2).
- Gardner, T.W., Fisher, D.M., Morell, K.D. & Cupper, M.L. 2013. Upper-plate deformation in response to flat slab subduction inboard of the aseismic Cocos Ridge, Osa Peninsula, Costa Rica. *Lithosphere*, 5, 247 – 264, <https://doi.org/10.1130/L251.1>.

- Gardner, T.W., Verdonck, D., Pinter, N.M., Slingerland, R., Furlong, K.P., Bullard, T.F. & Wells, S.G. 1992. Quaternary uplift astride the aseismic Cocos Ridge, Pacific coast, Costa Rica. *GSA Bulletin*, 104, 219 – 232, [https://doi.org/10.1130/0016-7606\(1992\)104<0219:QUATAC>2.3.CO;2](https://doi.org/10.1130/0016-7606(1992)104<0219:QUATAC>2.3.CO;2).
- Gazel, E., Carr, M.J., Hoernle, K., Feigenson, M.D., Szymanski, D., Hauff, F. & van den Bogaard, P. 2009. Galapagos-OIB signature in southern Central America: Mantle refertilization by arc-hot spot interaction. *Geochemistry, Geophysics, Geosystems*, 10, <https://doi.org/10.1029/2008GC002246>.
- Gerya, T.V. & Stöckhert, B. 2002. Exhumation rates of high pressure metamorphic rocks in subduction channels: The effect of Rheology: Exhumation rates of high pressure metamorphic rocks in subduction channels. *Geophysical Research Letters*, 29, 102-1-102 – 104, <https://doi.org/10.1029/2001GL014307>.
- Gerya, T.V. 2002. Exhumation rates of high pressure metamorphic rocks in subduction channels: The effect of Rheology. *Geophysical Research Letters*, 29, 1261 – 1261, <https://doi.org/10.1029/2001GL014307>.
- Gibbons, W. & McCarroll, D. 1993. *Geology of the Country around Aberdaron, Including Bardsey Island*. HMSO, British Geological Survey Memoirs Series.
- Goodchild, J.G. 1892. Note on a Granite Junction in the Ross of Mull. *Geological Magazine*, 9, 447 – 463.
- Government of Costa Rica. 1965. 1:50,000 Sheets “Llorona” and “Sierpe”.
- Greenly, E. 1919. *The Geology of Anglesey*. HMSO, London.
- Grevemeyer, I., Kopf, A.J., et al. 2004. Fluid flow through active mud dome Mound Culebra offshore Nicoya Peninsula, Costa Rica: evidence from heat flow surveying. *Marine Geology*, 207, 145 – 157, <https://doi.org/10.1016/j.margeo.2004.04.002>.
- Han, R., Hirose, T. & Shimamoto, T. 2010. Strong velocity weakening and powder lubrication of simulated carbonate faults at seismic slip rates. *Journal of Geophysical Research*, 115, <https://doi.org/10.1029/2008JB006136>.
- Handschumacher, D.W. 1976. Post-Eocene Plate Tectonics of the Eastern Pacific. In: Sutton, G. H. (ed.) *The Geophysics of the Pacific Ocean Basin and Its Margin: A Volume in Honor of George P. Woollard*. Washington, American Geophysical Union.
- Harris, R., Sakaguchi, A. & Petronotis, K. 2012. Costa Rica Seismogenesis Project, Program A Stage 2 (CRISP-A2): sampling and quantifying lithologic inputs and fluid inputs and outputs of the seismogenic zone. *IODP Scientific Prospectus*, 344, 76, <https://doi.org/doi:10.2204/iodp.sp.344.2012>.

- Harris, R.N., Grevemeyer, I., et al. 2010a. Thermal regime of the Costa Rican convergent margin: 1. Along-strike variations in heat flow from probe measurements and estimated from bottom-simulating reflectors: Costa Rica convergent margin heat flow. *Geochemistry, Geophysics, Geosystems*, 11, n/a-n/a, <https://doi.org/10.1029/2010GC003272>.
- Harris, R.N., Sakaguchi, A., et al. 2013. Expedition 344 summary 1. 344, <https://doi.org/10.2204/iodp.proc.344.101.2013>.
- Harris, R.N., Spinelli, G., Ranero, C.R., Grevemeyer, I., Villinger, H. & Barckhausen, U. 2010b. Thermal regime of the Costa Rican convergent margin: 2. Thermal models of the shallow Middle America subduction zone offshore Costa Rica: Costa Rica subduction thermal model. *Geochemistry, Geophysics, Geosystems*, 11, <https://doi.org/10.1029/2010GC003273>.
- Hastie, A. R., Kerr, a. C., Pearce, J. a. & Mitchell, S.F. 2007. Classification of Altered Volcanic Island Arc Rocks using Immobile Trace Elements: Development of the Th Co Discrimination Diagram. *Journal of Petrology*, 48, 2341 – 2357, <https://doi.org/10.1093/petrology/egm062>.
- Hastie, A.R., Kerr, A.C., et al. 2010. Geochronology, geochemistry and petrogenesis of rhyodacite lavas in eastern Jamaica: A new adakite subgroup analogous to early Archaean continental crust? *Chemical Geology*, 276, 344 – 359, <https://doi.org/10.1016/j.chemgeo.2010.07.002>.
- Hastie, A.R., Mitchell, S.F., Treloar, P.J., Kerr, A.C., Neill, I. & Barfod, D.N. 2013. Lithos Geochemical components in a Cretaceous island arc: The Th / La – (Ce / Ce *) Nd diagram and implications for subduction initiation in the inter-American region on Jamaica Proto-Caribbean. *LITHOS*, 162 – 163, 57 – 69, <https://doi.org/10.1016/j.lithos.2012.12.001>.
- Hauff, F., Hoernle, K., Bogaard, P. van den, Alvarado, G. & Garbeschönberg, D. 2000a. Age and geochemistry of basaltic complexes in western Costa Rica: Contributions to the geotectonic evolution of Central America. *Geochemistry, Geophysics, Geosystems*, 1, <https://doi.org/10.1029/1999GC000020>.
- Hauff, F., Hoernle, K., Schmincke, H.-U. & Werner, R. 1997. A Mid Cretaceous origin for the Galápagos hotspot: volcanological, petrological and geochemical evidence from Costa Rican oceanic crustal segments. *Geologische Rundschau*, 86, 141 – 155, <https://doi.org/10.1007/PL00009938>.
- Hauff, Hoernle, K., Tilton, G., Graham, D.W. & Kerr, a. C. 2000b. Large volume recycling of oceanic lithosphere over short time scales: Geochemical constraints from the Caribbean Large Igneous Province. *Earth and Planetary Science Letters*, 174, 247 – 263, [https://doi.org/10.1016/S0012-821X\(99\)00272-1](https://doi.org/10.1016/S0012-821X(99)00272-1).

- Haug, G.H., Tiedemann, R., Zahn, R. & Ravelo, A.C. 2001. Role of Panama uplift on oceanic freshwater balance. *Geology*, 29, 207, [https://doi.org/10.1130/0091-7613\(2001\)029<0207:ROPUOO>2.0.CO;2](https://doi.org/10.1130/0091-7613(2001)029<0207:ROPUOO>2.0.CO;2).
- Hayashi, N. & Tsutsumi, A. 2010. Deformation textures and mechanical behavior of a hydrated amorphous silica formed along an experimentally produced fault in chert: FRICTIONAL PROPERTIES OF CHERT. *Geophysical Research Letters*, 37, n/a-n/a, <https://doi.org/10.1029/2010GL042943>.
- Hayes, G.P., Herman, M.W., et al. 2014. Continuing megathrust earthquake potential in Chile after the 2014 Iquique earthquake. *Nature*, 512, 295.
- He, C., Luo, L., Hao, Q.-M. & Zhou, Y. 2013. Velocity-weakening behavior of plagioclase and pyroxene gouges and stabilizing effect of small amounts of quartz under hydrothermal conditions: Unstable sliding of gabbroic gouge. *Journal of Geophysical Research: Solid Earth*, 118, 3408 – 3430, <https://doi.org/10.1002/jgrb.50280>.
- Hensen, C., Wallmann, K., Schmidt, M., Ranero, C.R. & Suess, E. 2004. Fluid expulsion related to mud extrusion off Costa Rica – A window to the subducting slab. *Geology*, 32, 201, <https://doi.org/10.1130/G20119.1>.
- Herzberg, C., Asimow, P.D., et al. 2007. Temperatures in ambient mantle and plumes: Constraints from basalts, picrites, and komatiites: mantle temperatures inferred from volcanoes. *Geochemistry, Geophysics, Geosystems*, 8, 1 – 34, <https://doi.org/10.1029/2006GC001390>.
- Hibbard, J. & Karig, D.E. 1987. Sheath-like folds and progressive fold deformation in tertiary sedimentary rocks of the Shimanto accretionary complex, Japan. *Journal of Structural Geology*, 9, 845 – 857, [https://doi.org/10.1016/0191-8141\(87\)90085-X](https://doi.org/10.1016/0191-8141(87)90085-X).
- Hilde, W.C. 1983. Sediment subduction versus accretion around the Pacific. *Tectonophysics*, 99, 381 – 397.
- Hirose, H. & Obara, K. 2005. Repeating short- and long-term slow slip events with deep tremor activity around the Bungo channel region, southwest Japan. *Earth, Planets and Space*, 57, 961 – 972, <https://doi.org/10.1186/BF03351875>.
- Hobbs, B.E., Ord, A. & Teyssier, C. 1986. Earthquakes in the ductile regime? *Pure and Applied Geophysics PAGEOPH*, 124, 309 – 336, <https://doi.org/10.1007/BF00875730>.
- Hoernle, K., Bogaard, P.V., Werner, R., Lissinna, B., Alvarado, G. & Garbe-Schönberg, D. 2002. Missing history (16 – 71 Ma) of the Galápagos hotspot: Implications for the tectonic and biological evolution of the Americas. *Geological Society of America Bulletin*, 30, 795 – 798, [https://doi.org/10.1130/0091-7613\(2002\)030<0795](https://doi.org/10.1130/0091-7613(2002)030<0795).

- Hoernle, K., Hauff, F. & van den Bogaard, P. 2004. 70 m.y. history (139-69 Ma) for the Caribbean large igneous province. *Geology*, 32, 697 – 700, <https://doi.org/10.1130/G20574.1>.
- Hoernle, K., Werner, R., Morgan, J.P., Garbeschönberg, D., Bryce, J. & Mrazek, J. 2000. Existence of complex spatial zonation in the Galapagos plume for at least 14 m.y. *Geology*, 28, 435 – 438, [https://doi.org/10.1130/0091-7613\(2000\)28<435:Eocszi>2.0.Co;2](https://doi.org/10.1130/0091-7613(2000)28<435:Eocszi>2.0.Co;2).
- Hollocher, K., Robinson, P., Walsh, E. & Roberts, D. 2012. Geochemistry Of Amphibolite-Facies Volcanics And Gabbros Of The Støren Nappe In Extensions West And Southwest Of Trondheim, Western Gneiss Region, Norway: A Key To Correlations And Paleotectonic Settings. *American Journal of Science*, 312, 357 – 416, <https://doi.org/10.2475/04.2012.01>.
- Horák, J.M. & Evans, J. a. 2010. Early Neoproterozoic limestones from the Gwna Group, Anglesey. *Geological Magazine*, 148, 78 – 88, <https://doi.org/10.1017/S0016756810000464>.
- Horne, G.S. 1969. Early Ordovician Chaotic Deposits in the Central Volcanic Belt of Northeastern Newfoundland. *Geological Society of America Bulletin*, 80, 2451 – 2464.
- Horozal, S., Kim, G.-Y., et al. 2017. Sedimentary and structural evolution of the Eastern South Korea Plateau (ESKP), East Sea (Japan Sea). *Marine and Petroleum Geology*, 85, 70 – 88, <https://doi.org/10.1016/j.marpetgeo.2017.04.014>.
- Hsü, K.J. 1968. Principles of Mélanges and Their Bearing on the Franciscan-Knoxville Paradox. *Geological Society of America Bulletin*, 79, 1063 – 1074, [https://doi.org/10.1130/0016-7606\(1968\)79](https://doi.org/10.1130/0016-7606(1968)79).
- Hsü, K.J. 1974. Mélanges and their distinction from Olistostromes. In: Dott, R. H. J. & Shaver, R. H. (eds) *Modern and Ancient Geosynclinal Sedimentation*. Society of Economic Palaeontologists and Mineralogists Special Publication, 19, 321 – 333.
- Husson, L., Guillaume, B., Funicello, F., Faccenna, C. & Royden, L.H. 2012. Unraveling topography around subduction zones from laboratory models. *Tectonophysics*, 526 – 529, 5 – 15, <https://doi.org/10.1016/j.tecto.2011.09.001>.
- Hyndman, R.D., Yamano, M. & Oleskevich, D.A. 1997. The seismogenic zone of subduction thrust faults. *The Island Arc*, 6, 244 – 260.
- Ide, S., Beroza, G.C., Shelly, D.R. & Uchide, T. 2007. A scaling law for slow earthquakes. *Nature*, 447, 76 – 79, <https://doi.org/10.1038/nature05780>.
- Ikari, M.J., Saffer, D.M. & Marone, C. 2007. Effect of hydration state on the frictional properties of montmorillonite-based fault gouge. 112, 1 – 12, <https://doi.org/10.1029/2006JB004748>.

- Ikari, M.J., Saffer, D.M. & Marone, C. 2009. Frictional and hydrologic properties of clay-rich fault gouge. *Journal of Geophysical Research*, 114, <https://doi.org/10.1029/2008JB006089>.
- Instituto Nacional de Estadística y Censos. 2011. Costa Rica Census 2011.
- Isozaki, Y., Maruyama, S. & Furuoka, F. 1990. Accreted oceanic materials in Japan. *Tectonophysics*, 181, 179 – 205, [https://doi.org/10.1016/0040-1951\(90\)90016-2](https://doi.org/10.1016/0040-1951(90)90016-2).
- ISRM. 2014. The ISRM Suggested Methods for Rock Characterization, Testing and Monitoring: 2007-2014. R, U. (ed.). Springer International Publishing, SpringerLink : Bücher.
- Ito, Y., Obara, K., Shiomi, K., Sekine, S. & Hirose, H. 2007. Slow Earthquakes Coincident with Episodic Tremors and Slow Slip Events. *Science*, 315, 503 – 506, <https://doi.org/10.1126/science.1134454>.
- J Eardley & Max G White. 1947. Flysch and Molasse. *GSA Bulletin*, 58, 979 – 990, [https://doi.org/10.1130/0016-7606\(1947\)58\[979:FAM\]2.0.CO;2](https://doi.org/10.1130/0016-7606(1947)58[979:FAM]2.0.CO;2).
- Jackson, J.B.C., Jung, P., Coates, A.G. & Collins, L.S. 1993. Diversity and Extinction of Tropical American Mollusks and Emergence of the Isthmus of Panama. *Science, New Series*, 260, 1624 – 1626.
- Jackson, M.D., Mulcahy, S.R., Chen, H., Li, Y., Li, Q., Cappelletti, P. & Wenk, H.-R. 2017. Phillipsite and Al-tobermorite mineral cements produced through low-temperature water-rock reactions in Roman marine concrete. *American Mineralogist*, 102, 1435 – 1450, <https://doi.org/10.2138/am-2017-5993CCBY>.
- James, D.M.D. 1972. Sedimentation across an intra-basinal slope: the garnedd-wen formation (ashgillian), west central Wales. *Sedimentary Geology*, 7, 291 – 307.
- James, D.M.D. 1973. The Garnedd-wen Formation (Ashgillian) of the Towyn-Abergynolwyn district, Merionethshire. *Geological Magazine*, 110, 145 – 152.
- James, D.M.D. 1975. Caradoc turbidites at Poppit Sands (Pembrokeshire), Wales. *Geological Journal*, 12, 295 – 304.
- James, K.H. 2002. A Simple Synthesis of Caribbean Geology. In: 16th Caribbean Geological Conference, Abstracts. Barbados.
- James, K.H. 2005. A simple synthesis of Caribbean geology. In: Transactions of the 16th Caribbean Geological Conference. Barbados, *Caribbean Journal of Earth Sciences*, 39, 69 – 82.
- James, K.H. 2006. Arguments for and against the Pacific origin of the Caribbean Plate: discussion, finding for an inter-American origin. 25.

- James, K.H. 2009. Evolution of Middle America and the in situ Caribbean Plate model. *Geological Society, London, Special Publications*, 328, 127 – 138, <https://doi.org/10.1144/SP328.4>.
- Johnston, S.T. & Thorkelson, D.J. 1997. Cocos-Nazca slab window beneath Central America. *Earth and Planetary Science Letters*, 146, 465 – 474, [https://doi.org/10.1016/S0012-821X\(96\)00242-7](https://doi.org/10.1016/S0012-821X(96)00242-7).
- Jongens, R., Bradshaw, J.D. & Fowler, A.P. 2003. The balloon Melange, north-west Nelson: Origin, structure, and emplacement. *New Zealand Journal of Geology and Geophysics*, 46, 437 – 448, <https://doi.org/10.1080/00288306.2003.9515019>.
- Jung, H., Green II, H.W. & Dobrzhinetskaya, L.F. 2004. Intermediate-depth earthquake faulting by dehydration embrittlement with negative volume change. *Nature*, 428, 545 – 549, <https://doi.org/10.1038/nature02412>.
- Kagan, Y.Y. 1997. Are earthquakes predictable? *Geophysical Journal International*, 131, 505 – 525, <https://doi.org/10.1111/j.1365-246X.1997.tb06595.x>.
- Kamenetsky, V.S., Gurenko, A.A. & Kerr, A.C. 2010. Composition and temperature of komatiite melts from Gorgona Island, Colombia, constrained from olivine-hosted melt inclusions. *Geology*, 38, 1003 – 1006, <https://doi.org/10.1130/G31143.1>.
- Kano, K., Nakaji, M. & Takeuchi, S. 1991. Asymmetrical melange fabrics as possible indicators of the convergent direction of plates: a case study from the Shimanto Belt of the Akaishi Mountains, central Japan. *Tectonophysics*, 185, 375 – 388, [https://doi.org/10.1016/0040-1951\(91\)90455-2](https://doi.org/10.1016/0040-1951(91)90455-2).
- Kano, K., Nakaji, M. & Takeuchi, S. 1991. Asymmetrical melange fabrics as possible indicators of the convergent direction of plates: a case study from the Shimanto Belt of the Akaishi Mountains, central Japan. *Tectonophysics*, 185, 375 – 388, [https://doi.org/10.1016/0040-1951\(91\)90455-2](https://doi.org/10.1016/0040-1951(91)90455-2).
- Karig, D.E. 1974. Tectonic Erosion at Trenches. *Earth and Planetary Science Letters*, 21, 209 – 212.
- Karner, S.L., Chester, F.M., Kronenberg, A.K. & Chester, J.S. 2003. Subcritical compaction and yielding of granular quartz sand. *Tectonophysics*, 377, 357 – 381, <https://doi.org/10.1016/j.tecto.2003.10.006>.
- Katsumata, A. & Kamaya, N. 2003. Low-frequency continuous tremor around the Moho discontinuity away from volcanoes in the southwest Japan: deep tremor in the southwest Japan. *Geophysical Research Letters*, 30, 20-1-20 – 24, <https://doi.org/10.1029/2002GL015981>.
- Katz, H.R. 1968. Potential oil formations in New Zealand, and their stratigraphic position as related to basin evolution. *New Zealand journal of geology and Geophysics*, 11, <https://doi.org/10.1080/00288306.1968.10420242>.

- Kawai, T., Windley, B.F., Terabayashi, M., Yamamoto, H., Isozaki, Y. & Maruyama, S. 2008. Neoproterozoic glaciation in the mid-oceanic realm: An example from hemi-pelagic mudstones on Llanddwyn Island, Anglesey, UK. *Gondwana Research*, 14, 105 – 114, <https://doi.org/10.1016/j.gr.2007.12.008>.
- Kawasaki, I., Asai, Y. & Tamura, Y. 2001. Space–time distribution of interplate moment release including slow earthquakes and the seismo-geodetic coupling in the Sanriku-oki region along the Japan trench. *Tectonophysics*, 330, 267 – 283, [https://doi.org/10.1016/S0040-1951\(00\)00245-6](https://doi.org/10.1016/S0040-1951(00)00245-6).
- Kawasaki, I., Asai, Y., et al. 1995. The 1992 Sanriku-Oki, Japan, Ultra-Slow Earthquake. *Journal of Physics of the Earth*, 43, 105 – 116, <https://doi.org/10.4294/jpe1952.43.105>.
- Kear, D. & Waterhouse, B.C. 1967. Onerahi chaos-breccia of Northland. *New Zealand journal of geology and Geophysics*, 10, 629 – 646, <https://doi.org/10.1080/00288306.1967.10431082>.
- Keigwin, L.D. 1978. Pliocene closing of the Isthmus of Panama, based on biostratigraphic evidence from nearby Pacific Ocean and Caribbean Sea cores. *Geology*, 6, 630, [https://doi.org/10.1130/0091-7613\(1978\)6<630:PCOTIO>2.0.CO;2](https://doi.org/10.1130/0091-7613(1978)6<630:PCOTIO>2.0.CO;2).
- Kelleher, J. & McCann, W. 1976. Buoyant zones, great earthquakes, and unstable boundaries of subduction. *Journal of Geophysical Research*, 81, 4885 – 4896, <https://doi.org/10.1029/JB081i026p04885>.
- Kerr, A.C. & Tarney, J. 2005. Tectonic evolution of the Caribbean and north-western South America: The case for accretion of two Late Cretaceous oceanic plateaus. *Geology*, 33, 269, <https://doi.org/10.1130/G21109.1>.
- Kerr, A.C., Marriner, G.F., Arndt, N.T., Tarney, J., Nivia, A., Saunders, A.D. & Duncan, R.A. 1996. The petrogenesis of Gorgona komatiites, picrites and basalts: new field, petrographic and geochemical constraints. *Mafic Magmatism through Time*, 37, 245 – 260, [https://doi.org/10.1016/0024-4937\(95\)00039-9](https://doi.org/10.1016/0024-4937(95)00039-9).
- Kerr, A.C., White, R.V., Thompson, P.M.E., Tarney, J. & Saunders, A.D. 2003. No Oceanic Plateau – No Caribbean Plate? The Seminal Role of an Oceanic Plateau in Caribbean Plate Evolution. In: Bartolini, C., Buffler, R. T. & Blickwede, J. (eds) *The Circum-Gulf of Mexico and the Caribbean: Hydrocarbon Habitats, Basin Formation, and Plate Tectonics: AAPG Memoir 79*. 126 – 168.
- Kimura, G., Yamaguchi, A., et al. 2012. Tectonic mélange as fault rock of subduction plate boundary. *Tectonophysics*, 568 – 569, 25 – 38, <https://doi.org/10.1016/j.tecto.2011.08.025>.

- Kirby, M.X. & MacFadden, B. 2005. Was southern Central America an archipelago or a peninsula in the middle Miocene? A test using land-mammal body size. *Palaeogeography, Palaeoclimatology, Palaeoecology*, 228, 193 – 202, <https://doi.org/10.1016/j.palaeo.2005.06.002>.
- Kirby, M.X., Jones, D.S. & Macfadden, B.J. 2008. Lower Miocene Stratigraphy along the Panama Canal and Its Bearing on the Central American Peninsula. *PLoS one*, 3, <https://doi.org/10.1371/journal.pone.0002791>.
- Kitamura, Y., Sato, K., et al. 2005. Mélange and its seismogenic roof décollement: A plate boundary fault rock in the subduction zone - An example from the Shimanto Belt, Japan. *Tectonics*, 24, 1 – 15, <https://doi.org/10.1029/2004TC001635>.
- Kodaira, S., No, T., et al. 2012. Coseismic fault rupture at the trench axis during the 2011 Tohoku-oki earthquake. *Nature Geoscience*, 5, 646 – 650, <https://doi.org/10.1038/ngeo1547>.
- Kolarsky, R.A., Mann, P. & Montero, W. 1995. Island arc response to shallow subduction of the Cocos Ridge, Costa Rica. In: *Geological Society of America Special Papers*. Geological Society of America, 235 – 262., <https://doi.org/10.1130/SPE295-p235>.
- Kopp, H. 2013. Invited review paper: The control of subduction zone structural complexity and geometry on margin segmentation and seismicity. *Tectonophysics*, 589, 1 – 16, <https://doi.org/10.1016/j.tecto.2012.12.037>.
- Kopp, H. 2013. Invited review paper: The control of subduction zone structural complexity and geometry on margin segmentation and seismicity. *Tectonophysics*, 589, 1 – 16, <https://doi.org/10.1016/j.tecto.2012.12.037>.
- Kostoglodov, V., Singh, S.K., Santiago, J.A., Franco, S.I., Larson, K.M., Lowry, A.R. & Bilham, R. 2003. A large silent earthquake in the Guerrero seismic gap, Mexico: a large silent earthquake in the Guerrero seismic gap. *Geophysical Research Letters*, 30, <https://doi.org/10.1029/2003GL017219>.
- Krohe, A. 2017. The Franciscan Complex (California, USA) – The model case for return-flow in a subduction channel put to the test. *Gondwana Research*, 45, 282 – 307, <https://doi.org/10.1016/j.gr.2017.02.003>.
- Kurzawski, R.M., Stipp, M., Niemeijer, A.R. & Behrmann, J.H. 2016. Earthquake nucleation in weak subducted carbonates. *Nature Geoscience*, <https://doi.org/10.1038/ngeo2774>.
- Kusky, T. & Bradley, D. 1999. Kinematic analysis of mélange fabrics: examples and applications from the McHugh Complex, Kenai Peninsula, Alaska. *Journal of Structural Geology*, 21, 1883 – 1796.

- Kusky, T.M., Bradley, D.C. & Haeussler, P. 1997b. Progressive deformation of the Chugach accretionary complex, Alaska, during a paleogene ridge-trench encounter. *Journal of Structural Geology*, 19, 139 – 157, [https://doi.org/10.1016/S0191-8141\(96\)00084-3](https://doi.org/10.1016/S0191-8141(96)00084-3).
- Kusky, T.M., Bradley, D.C., Haeussler, P.J. & Karl, S. 1997a. Controls on accretion of flysch and mélangé belts at convergent margins: Evidence from the Chugach Bay thrust and Iceworm mélangé, Chugach accretionary wedge, Alaska. *Tectonics*, 16, 855 – 878, <https://doi.org/10.1029/97TC02780>.
- Lallemand, S.E., Schnürle, P. & Malavieille, J. 1994. Coulomb theory applied to accretionary and nonaccretionary wedges: Possible causes for tectonic erosion and/or frontal accretion. *Journal of Geophysical Research: Solid Earth*, 99, 12033 – 12055, <https://doi.org/10.1029/94JB00124>.
- Langseth, M.G., Von Huene, R., Nasu, N. & Okada, H. 1981. Subsidence of the Japan Trench forearc region of Northern Honshu. *Oceanologica Acta*, 4, 173 – 179.
- Lash, G.G. 1987. Diverse melanges of an ancient subduction complex. *Geology*, 15, 652, [https://doi.org/10.1130/0091-7613\(1987\)15<652:DMOAAS>2.0.CO;2](https://doi.org/10.1130/0091-7613(1987)15<652:DMOAAS>2.0.CO;2).
- Lay, T., Kanamori, H. & J. Ruff, L. 1982. The Asperity Model and the Nature of Large Subduction Zone Earthquakes.
- Le Bas, M.J.L., Maitre, R.W.L., Streckeisen, A., Zanettin, B. & IUGS Subcommittee on the Systematics of Igneous Rocks. 1986. A Chemical Classification of Volcanic Rocks Based on the Total Alkali-Silica Diagram. *Journal of Petrology*, 27, 745 – 750, <https://doi.org/10.1093/petrology/27.3.745>.
- Lear, C.H., Rosenthal, Y. & Wright, J.D. 2003. The closing of a seaway: ocean water masses and global climate change. *Earth and Planetary Science Letters*, 210, 425 – 436, [https://doi.org/10.1016/S0012-821X\(03\)00164-X](https://doi.org/10.1016/S0012-821X(03)00164-X).
- Leslie, A.G., Krabbendam, M., Gillespie, M.R. & British Geological Survey. 2012. BGS Classification of Lithodemic Units: Proposals for Classifying Tectonometamorphic Units and Mixed-Class Units : British Geological Survey Report RR/12/002.
- Leslie, S.C., Moore, G.F., Morgan, J.K. & Hills, D.J. 2002. Seismic stratigraphy of the Frontal Hawaiian Moat : implications for sedimentary processes at the leading edge of an oceanic hotspot trace. *Marine Geology*, 184, 143 – 162.
- Lindquist, E.S. & Goodman, R.E. 1994. Strength and Deformation Properties of a Physical Model Melange. In: ARMA-1994-0843 – 1st North American Rock Mechanics Symposium. ARMA, American Rock Mechanics Association, 8.

- Liu, M.-Q., Li, Z.-H. & Yang, S.-H. 2017. Diapir versus along-channel ascent of crustal material during plate convergence: Constrained by the thermal structure of subduction zones. *Journal of Asian Earth Sciences*, 145, 16 – 36, <https://doi.org/10.1016/j.jseaes.2017.02.036>.
- Lloyd, G.E. 1991. Crystallographic textures. *Mineralogical Magazine*, 55, 331 – 345.
- Louis, L., David, C., Metz, V., Robion, P., Menéndez, B. & Kissel, C. 2005. Microstructural control on the anisotropy of elastic and transport properties in undeformed sandstones. *International Journal of Rock Mechanics and Mining Sciences*, 42, 911 – 923, <https://doi.org/10.1016/j.ijrmms.2005.05.004>.
- Lowrie, A., Aitken, T., Grim, P. & McRaney, L. 1979. Fossil spreading center and faults within the Panama Fracture Zone. *Marine Geophysical Researches*, 4, 153 – 166, <https://doi.org/10.1007/BF00286402>.
- Macdonald, G.A. & Katsura, T. 1964. Chemical Composition of Hawaiian Lavas. *Journal of Petrology*, 5, 82 – 133, <https://doi.org/10.1093/petrology/5.1.82>.
- MacLeod, C.J., Johan Lissenberg, C. & Bibby, L.E. 2013. ‘Moist MORB’ axial magmatism in the Oman ophiolite: The evidence against a mid-ocean ridge origin. *Geology*, 41, 459 – 462, <https://doi.org/10.1130/G33904.1>.
- Maltman, A.J. 1975. Ultramafic rocks in Anglesey their non-tectonic emplacement. *Journal of the Geological Society*, 131, 593 – 603, <https://doi.org/10.1144/gsjgs.131.6.0593>.
- Manea, V.C., Leeman, W.P., Gerya, T., Manea, M. & Zhu, G. 2014. Subduction of fracture zones controls mantle melting and geochemical signature above slabs. *Nature Communications*, 5, <https://doi.org/10.1038/ncomms6095>.
- Mann, P., Draper, G. & Lewis, J.F. 1991. An overview of the geologic and tectonic development of Hispaniola. In: *Geological Society of America Special Papers*. Geological Society of America, 1 – 28., <https://doi.org/10.1130/SPE262-pl>.
- Marschall, H.R. & Schumacher, J.C. 2012. Arc magmas sourced from mélange diapirs in subduction zones. *Nature Geoscience*, 5, 862 – 867, <https://doi.org/10.1038/ngeo1634>.
- Marshall, L.G., Webb, S.D., Sepkoski, J.J. & Raup, D.M. 1982. Mammalian Evolution and the Great American Interchange. *Science*, 215, 1351, <https://doi.org/10.1126/science.215.4538.1351>.
- Maruyama, S., Kawai, T. & Windley, B.F. 2010. Ocean plate stratigraphy and its imbrication in an accretionary orogen: the Mona Complex, Anglesey-Lleyn, Wales, UK. *Geological Society, London, Special Publications*, 338, 55 – 75, <https://doi.org/10.1144/SP338.4>.

- Mccarthy, J. & Scholl, D.W. 1985. Mechanisms of subduction accretion along the central Aleutian Trench. *Geological Society of America Bulletin*, 96, 691 – 701.
- McMath, J. 1947. The Composite Intrusion of Sròn Bheag, Ardnamurchan. *Geological Journal*, 84.
- Medley, E. 1994. The Engineering Characterization of Melanges and Similar Block-in- Matrix Rocks (Bimrocks). Doctoral thesis, University of California at Berkeley.
- Medley, E.W. & Zekkos, D. 2011. Geopractitioner approaches to working with antisocial mélanges. In: *Geological Society of America Special Papers*. Geological Society of America, 261 – 277., [https://doi.org/10.1130/2011.2480\(13\)](https://doi.org/10.1130/2011.2480(13)).
- Melgar, D., Fan, W., et al. 2016. Slip segmentation and slow rupture to the trench during the 2015, M w 8.3 Illapel, Chile earthquake: SLIP DURING THE M w 8.3 Illapel Earthquake. *Geophysical Research Letters*, 43, 961 – 966, <https://doi.org/10.1002/2015GL067369>.
- Menegon, L., Pennacchioni, G., Heilbronner, R. & Pittarello, L. 2008. Evolution of quartz microstructure and c-axis crystallographic preferred orientation within ductilely deformed granitoids (Arolla unit, Western Alps). *Journal of Structural Geology*, 30, 1332 – 1347, <https://doi.org/10.1016/j.jsg.2008.07.007>.
- Meschede, M. & Barckhausen, U. 2001. The relationship of the Cocos and Carnegie ridges: Age constraints from Paleogeographic reconstructions. *International Journal of Earth Sciences*, 90, 386 – 392, <https://doi.org/10.1007/s005310000155>.
- Meschede, M. & Frisch, W. 1998. A plate-tectonic model for the Mesozoic and Early Cenozoic history of the Caribbean plate. *Tectonophysics*, 296, 269 – 291, [https://doi.org/10.1016/S0040-1951\(98\)00157-7](https://doi.org/10.1016/S0040-1951(98)00157-7).
- Meschede, M. 1998. The impossible Galapagos connection: geometric constraints for a near-American origin of the Caribbean plate. *Geologische Rundschau*, 87, 200 – 205, <https://doi.org/10.1007/s005310050202>.
- Meschede, M., Zweigel, P., Frisch, W. & Völker, D. 1999. Mélange formation by subduction erosion: the case of the Osa Mélange in southern Costa Rica. *Terra Nova*, 11, 141 – 148.
- Mitchell, S.F. 2003. Sedimentology and Tectonic Evolution of the Cretaceous Rocks of Central Jamaica: Relationships to the Plate Tectonic Evolution of the Caribbean. In: Bartolini, C., Buffler, R. T. & Blickwede, J. (eds) *The Circum-Gulf of Mexico and the Caribbean: Hydrocarbon Habitats, Basin Formation, and Plate Tectonics*. AAPG Memoir 79, 605 – 623.

- Montes, C., Bayona, G., et al. 2012. Arc-continent collision and orocline formation: Closing of the Central American seaway. *Journal of Geophysical Research*, 117, B04105 – B04105, <https://doi.org/10.1029/2011JB008959>.
- Moore, D.E. & Lockner, D.A. 2011. Frictional strengths of talc-serpentine and talc-quartz mixtures. *Journal of Geophysical Research*, 116, <https://doi.org/10.1029/2010JB007881>.
- Moore, J.C. & Byrne, T. 1987. Thickening of fault zones: A mechanism of melange formation in accreting sediments. *Geology*, 15, 1040 – 1043, [https://doi.org/10.1130/0091-7613\(1987\)15<1040](https://doi.org/10.1130/0091-7613(1987)15<1040).
- Moore, J.C. 1989. Tectonics and hydrogeology of accretionary prisms: role of the décollement zone. *Journal of Structural Geology*, 11.
- Moore, E. 1970. Ultramafics and Orogeny, with Models of the US Cordillera and the Tethys. *Nature*, 228, 837 – 842, <https://doi.org/10.1038/228837a0>.
- Morell, K.D. 2015. Late Miocene to recent plate tectonic history of the southern Central America convergent margin: Tectonic history of central america. *Geochemistry, Geophysics, Geosystems*, 16, 3362 – 3382, <https://doi.org/10.1002/2015GC005971>.
- Morell, K.D., Gardner, T.W., Fisher, D.M., Idleman, B.D. & Zellner, H.M. 2013. Active thrusting, landscape evolution, and late Pleistocene sector collapse of Baru Volcano above the Cocos-Nazca slab tear, southern Central America. *Bulletin of the Geological Society of America*, 125, 1301 – 1318, <https://doi.org/10.1130/B30771.1>.
- Moreno, M., Melnick, D., et al. 2011. Heterogeneous plate locking in the South-Central Chile subduction zone: Building up the next great earthquake. *Earth and Planetary Science Letters*, 305, 413 – 424, <https://doi.org/10.1016/j.epsl.2011.03.025>.
- Morgan, J.K., Clague, D.A., Borchers, D.C., Davis, S. & Milliken, K.L. 2007. Mauna Loa's submarine western flank: Landsliding, deep volcanic spreading, and hydrothermal alteration. *Geochemistry, Geophysics, Geosystems*, 8, <https://doi.org/10.1029/2006GC001420>.
- Murauchi, S. & Ludwig, W.J. 1980. Crustal Structure of the Japan Trench: The Effect of Subduction of Ocean Crust. In: *Initial Reports of the Deep Sea Drilling Project, Volume 56/57*. Washington, D.C, U.S. Government Printing Office, 463 – 469.
- Murray, R.W. 1994. Chemical criteria to identify the depositional environment of chert : general principles and applications. 0738.
- Naha, K. 1961. Precambrian Sedimentation around Ghatsila in East Singhbhum, Eastern India. *Proceedings of the National Institute of Sciences of India*, 27A, 361 – 372.

- Naughton, L. 1993. Conservation versus Artisanal Gold Mining in Corcovado National Park, Costa Rica: Land Use Conflicts at Neotropical Wilderness Frontiers. Yearbook, Conference of Latin Americanist Geographers, 4, 47 – 55.
- Needham, D.T. 1987. Asymmetric extensional structures and their implications for the generation of melanges. *Geological Magazine*, 124, 311, <https://doi.org/10.1017/S0016756800016642>.
- Needham, D.T. 1995. Mechanisms of mélange formation: Examples from SW Japan and southern Scotland. *Journal of Structural Geology*, 17, 971 – 985, [https://doi.org/10.1016/0191-8141\(94\)00132-J](https://doi.org/10.1016/0191-8141(94)00132-J).
- Newkirk, D.R. & Martin, E.E. 2009. Circulation through the Central American Seaway during the Miocene carbonate crash. *Geology*, 37, 87 – 90, <https://doi.org/10.1130/G25193A.1>.
- Nicolas, A. & Boudier, F. 2003. Where ophiolites come from and what they tell us. In: Special Paper 373: Ophiolite Concept and the Evolution of Geological Thought. Geological Society of America, 137 – 152., <https://doi.org/10.1130/0-8137-2373-6.137>.
- Nielsen, S.G. & Marschall, H.R. 2017. Geochemical evidence for mélange melting in global arcs. *Science Advances*, 3, 1 – 6.
- Nisbet, E.G. & Pearce, J.A. 1977. Clinopyroxene composition in mafic lavas from different tectonic settings. *Contributions to Mineralogy and Petrology*, 63, 149 – 160, <https://doi.org/10.1007/BF00398776>.
- Nisbet, E.G., Cheadle, M.J., Arndt, N.T. & Bickle, M.J. 1993. Constraining the potential temperature of the Archaean mantle: A review of the evidence from komatiites. *Lithos*, 30, 291 – 307, [https://doi.org/10.1016/0024-4937\(93\)90042-B](https://doi.org/10.1016/0024-4937(93)90042-B).
- O’Dea, A., Lessios, H.A., et al. 2016. Formation of the Isthmus of Panama. *Science Advances*, 2, 1 – 12.
- Obara, K. & Kato, A. 2016. Connecting slow earthquakes to huge earthquakes. *Science*, 353, 253 – 257, <https://doi.org/10.1126/science.aaf1512>.
- Okada, Y., Kasahara, K., Hori, S., Obara, K., Sekiguchi, S., Fujiwara, H. & Yamamoto, A. 2004. Recent progress of seismic observation networks in Japan —Hi-net, F-net, K-NET and KiK-net —. *Earth, Planets and Space*, 56, xv–xxviii, <https://doi.org/10.1186/BF03353076>.
- Onishi, C.T. & Kimura, G. 1995. Change in fabric of melange in the Shimanto Belt, Japan: Change in relative convergence? *Tectonics*, 14, 1273 – 1289, <https://doi.org/10.1029/95TC01929>.

- Orange, D. 1990. Criteria helpful in recognizing shear-zone and diapiric mélanges: Examples from the Hoh accretionary complex, Olympic Peninsula, Washington. *Geological Society of America Bulletin*, 102, 935 – 951.
- Osborne, A.H., Newkirk, D.R., Groeneveld, J., Martin, E.E., Tiedemann, R. & Frank, M. 2014. The seawater neodymium and lead isotope record of the final stages of Central American Seaway closure: CAS CLOSURE ND AND PB. *Paleoceanography*, 29, 715 – 729, <https://doi.org/10.1002/2014PA002676>.
- Osinowo, O.O., Chapman, M., Bell, R. & Lynn, H.B. 2017. Modelling Orthorhombic Anisotropic Effects for Reservoir Fracture Characterization of a Naturally Fractured Tight Carbonate Reservoir, Onshore Texas, USA. *Pure and Applied Geophysics*, 174, 4137 – 4152, <https://doi.org/10.1007/s00024-017-1620-0>.
- Ozawa, S., Murakami, M., et al. 2002. Detection and Monitoring of Ongoing Aseismic Slip in the Tokai Region, Central Japan. *Science*, 298, 1009 – 1012, <https://doi.org/10.1126/science.1076780>.
- Page, B.M. 1963. Gravity Tectonics Near Passo Della Cisa, Northern Apennines, Italy. *GSA Bulletin*, 74, 655 – 671, [https://doi.org/10.1130/0016-7606\(1963\)74\[655:GTNPDC\]2.0.CO;2](https://doi.org/10.1130/0016-7606(1963)74[655:GTNPDC]2.0.CO;2).
- Pearce, J.A. & Cann, J.R. 1973. Tectonic setting of basic volcanic rocks determined using trace element analyses, I. 19, 290 – 300.
- Pearce, J.A. & Norry, M.J. 1979. Mineralogy and Petrogenetic Implications of Ti, Zr, Y, and Nb Variations in Volcanic Rocks. 47, 33 – 47.
- Pindell, J. 1992. Regional Synopsis of Gulf of Mexico and Caribbean Evolution. In: *Mesozoic and Early Cenozoic Development of the Gulf of Mexico and Caribbean Region: A Context for Hydrocarbon Exploration*. 13th Annual, 251 – 274., <https://doi.org/10.5724/gcs.92.13.0251>.
- Pindell, J., Kennan, L., Maresch, W.V., Stanek, K.-P., Draper, G. & Higgs, R. 2005. Plate-kinematics and crustal dynamics of circum-Caribbean arc-continent interactions: Tectonic controls on basin development in Proto-Caribbean margins. In: *Special Paper 394: Caribbean-South American Plate Interactions, Venezuela*. Geological Society of America, 7 – 52., <https://doi.org/10.1130/0-8137-2394-9.7>.
- Pindell, J., Kennan, L., Stanek, K.P., Maresch, W.V. & Draper, G. 2006. Foundations of Gulf of Mexico and Caribbean evolution: eight controversies resolved. *Geologica Acta*, 40.

- Pindell, J.L. & Kennan, L. 2009. Tectonic evolution of the Gulf of Mexico, Caribbean and northern South America in the mantle reference frame: an update. Geological Society, London, Special Publications, 328, 1.1-55, <https://doi.org/10.1144/SP328.1>.
- Pindell, J.L. 1994. Evolution of the Gulf of Mexico and the Caribbean. 13 – 39.
- Pini, G.A. 1999. Tectonosomes and Olistostromes in the Argille Scagliose of the Northern Apennines, Italy. Boulder, Colo, Geological Society of America, Special paper, 335.
- Platt, J.P. 2015. Origin of Franciscan blueschist-bearing melange at San Simeon, central California coast. *International Geology Review*, 57, 843 – 853, <https://doi.org/10.1080/00206814.2014.902756>.
- Plunder, A., Agard, P., Chopin, C., Pourteau, A. & Okay, A.I. 2015. From subduction initiation to continental subduction platform. *Lithos*, 226, 233 – 254, <https://doi.org/10.1016/j.lithos.2015.01.007>.
- Polat, A. & Casey, J.F. 1995. A structural record of the emplacement of the Pozanti-Karsanti ophiolite onto the Menderes-Taurus block in the late Cretaceous, eastern Taurides, Turkey. *Journal of Structural Geology*, 17, 1673 – 1688, [https://doi.org/10.1016/0191-8141\(95\)00061-H](https://doi.org/10.1016/0191-8141(95)00061-H).
- Prieto, G.A., Florez, M., Barrett, S.A., Beroza, G.C., Pedraza, P., Blanco, J.F. & Poveda, E. 2013. Seismic evidence for thermal runaway during intermediate-depth earthquake rupture: seismic evidence for thermal runaway. *Geophysical Research Letters*, 40, 6064 – 6068, <https://doi.org/10.1002/2013GL058109>.
- Prohoroff, R., Wakabayashi, J. & Dumitru, T. a. 2012. Sandstone matrix olistostrome deposited on intra-subduction complex serpentinite, Franciscan Complex, western Marin County, California. *Tectonophysics*, 568 – 569, 296 – 305, <https://doi.org/10.1016/j.tecto.2012.05.018>.
- Protti, M., Giendel, F. & McNally, K. 1995. Correlation between the age of the subducting Cocos plate and the geometry of the Wadati-Benioff zone under Nicaragua and Costa Rica. In: Mann, P. (ed.) *Geologic and Tectonic Development of the Caribbean Plate Boundary in Southern Central America*. Geological Society of America.
- Protti, M., Guñdel, F. & McNally, K. 1994. The geometry of the Wadati-Benioff zone under southern Central America and its tectonic significance: results from a high-resolution local seismographic network. *Physics of the Earth and Planetary Interiors*, 84, 271 – 287, [https://doi.org/10.1016/0031-9201\(94\)90046-9](https://doi.org/10.1016/0031-9201(94)90046-9).

- Ranero, C. & von Huene, R. 2000. Subduction erosion along the Middle America convergent margin. *Nature*, 404, 748 – 752, <https://doi.org/10.1038/35008046>.
- Ranero, C.R., Grevemeyer, I., et al. 2008. Hydrogeological system of erosional convergent margins and its influence on tectonics and interplate seismogenesis: CONVERGENT MARGINS AND TECTONICS. *Geochemistry, Geophysics, Geosystems*, 9, n/a-n/a, <https://doi.org/10.1029/2007GC001679>.
- Ranero, C.R., Villaseñor, A., Morgan, J.P. & Weinrebe, W. 2005. Relationship between bend-faulting at trenches and intermediate-depth seismicity. *Geochemistry, Geophysics, Geosystems*, 6, <https://doi.org/10.1029/2005GC000997>.
- Rau, W.W. & Grocock, G.R. 1974. Information Circular 51: Piercement Structure Outcrops along the Washington Coast (1974).
- Raymond, L.A. & Terranova, T. 1984. Prologue The melange problem – a review. In: Raymond, L. A. (ed.) *Melanges: Their Nature, Origin, and Significance*.
- Raymond, L.A. 1975. Tectonite and Melange – A Distinction. *Geology*, 3, 7 – 9.
- Raymond, L.A. 1984. Classification of melanges. In: Raymond, L. A. (ed.) *Melanges: Their Nature, Origin, and Significance*. Geological Society of America.
- Rees, B.A., Detrick, R. & Coakley, B.J. 1993. Seismic stratigraphy of the Hawaiian flexural moat. *Geological Society of America Bulletin*, 105, 189 – 205, [https://doi.org/10.1130/0016-7606\(1993\)105<0189:SSOTHF>2.3.CO;2](https://doi.org/10.1130/0016-7606(1993)105<0189:SSOTHF>2.3.CO;2).
- Reynolds, S.H. 1928. Breccias. *The Geological Magazine*, 65.
- Ridd, M.F. 1964. Succession and structural interpretation of the Whangara-Waimata area, Gisborne, New Zealand. *New Zealand journal of geology and Geophysics*, 7, 279 – 298, <https://doi.org/10.1080/00288306.1964.10420175>.
- Rigo de Righi, M. & Cortesini, A. 1964. Gravity tectonics in foothills structure belt of southeast Turkey. *AAPG Bulletin*, 48, 1911 – 1937.
- Robertson, H.F. & Pickett, A. n.d. Palaeozoic-Early Tertiary Tethyan evolution of melanges, rift and passive margin units in the Karaburun Peninsula (western Turkey) and Chios Island (Greece). 40.
- Rubinstein, J.L., La Rocca, M., Vidale, J.E., Creager, K.C. & Wech, A.G. 2008. Tidal Modulation of Nonvolcanic Tremor. *Science*, 319, 186 – 189, <https://doi.org/10.1126/science.1150558>.
- Ruiz, S., Metois, M., et al. 2014. Intense foreshocks and a slow slip event preceded the 2014 Iquique Mw 8.1 earthquake. *Science*, 345, 1165 – 1169, <https://doi.org/10.1126/science.1256074>.

- Ryan, W.B.F., Carbotte, S.M., et al. 2009. Global Multi-Resolution Topography synthesis: Global Multi-Resolution Topography Synthesis. *Geochemistry, Geophysics, Geosystems*, 10, n/a-n/a, <https://doi.org/10.1029/2008GC002332>.
- Saffer, D.M. & Bekins, B.A. 2002. Hydrologic controls on the morphology and mechanics of accretionary wedges. *Geology*, 30, 271, [https://doi.org/10.1130/0091-7613\(2002\)030<0271:HCOTMA>2.0.CO;2](https://doi.org/10.1130/0091-7613(2002)030<0271:HCOTMA>2.0.CO;2).
- Saffer, D.M. & Marone, C. 2003. Comparison of smectite- and illite-rich gouge frictional properties: application to the updip limit of the seismogenic zone along subduction megathrusts. *Earth and Planetary Science Letters*, 215, 219 – 235, [https://doi.org/10.1016/S0012-821X\(03\)00424-2](https://doi.org/10.1016/S0012-821X(03)00424-2).
- Saffer, D.M. & Wallace, L.M. 2015. The frictional, hydrologic, metamorphic and thermal habitat of shallow slow earthquakes. *Nature Geoscience*, 8, 594 – 600, <https://doi.org/10.1038/ngeo2490>.
- Saffer, D.M., Lockner, D.A. & McKiernan, A. 2012. Effects of smectite to illite transformation on the frictional strength and sliding stability of intact marine mudstones: FRICTION AND SMECTITE TRANSFORMATION. *Geophysical Research Letters*, 39, n/a-n/a, <https://doi.org/10.1029/2012GL051761>.
- Sage, F., Collot, J.-Y. & Ranero, C.R. 2006. Interplate patchiness and subduction-erosion mechanisms: Evidence from depth-migrated seismic images at the central Ecuador convergent margin. *Geology*, 34, 997 – 997, <https://doi.org/10.1130/G22790A.1>.
- Sagiya, T., Nishimura, T. & Iio, Y. 2004. Heterogeneous crustal deformation along the central-northern Itoigawa-Shizuoka Tectonic Line Fault system, Central Japan. *Earth, Planets and Space*, 56, 1247 – 1252, <https://doi.org/10.1186/BF03353347>.
- Saito, T. 1976. Geologic significance of coiling direction in the planktonic foraminifera *Pulleniatina*. *Geology*, 4, 305, [https://doi.org/10.1130/0091-7613\(1976\)4<305:GSOCDI>2.0.CO;2](https://doi.org/10.1130/0091-7613(1976)4<305:GSOCDI>2.0.CO;2).
- Sakaguchi, A., Chester, F., et al. 2011. Seismic slip propagation to the updip end of plate boundary subduction interface faults: Vitrinite reflectance geothermometry on Integrated Ocean Drilling Program NanTro SEIZE cores. *Geology*, 39, 395 – 398, <https://doi.org/10.1130/G31642.1>.
- Saleeby, J. 2011. Geochemical mapping of the Kings-Kaweah ophiolite belt, California-Evidence for progressive melange formation in a large offset transform-subduction initiation environment. In: *The Geological Society of America Special Paper 480*. 31 – 73., [https://doi.org/10.1130/2011.2480\(02\)](https://doi.org/10.1130/2011.2480(02)).

- Sanchez-Azofeifa, G.A., Rivard, B., Calvo, J. & Moorthy, I. 2002. Dynamics of Tropical Deforestation Around National Parks: Remote Sensing of Forest Change on the Osa Peninsula of Costa Rica. *Mountain Research and Development*, 22, 352 – 358, [https://doi.org/10.1659/0276-4741\(2002\)022\[0352:DOTDAN\]2.0.CO;2](https://doi.org/10.1659/0276-4741(2002)022[0352:DOTDAN]2.0.CO;2).
- Saunders, A.D., Tarney, J., Kerr, A.C. & Kent, R.W. 1996. The formation and fate of large oceanic igneous provinces. *Lithos*, 37, 81 – 95, [https://doi.org/10.1016/0024-4937\(95\)00030-5](https://doi.org/10.1016/0024-4937(95)00030-5).
- Savage, M.K. 1999. Seismic anisotropy and mantle deformation: What have we learned from shear wave splitting? *Reviews of Geophysics*, 37, 65 – 106, <https://doi.org/10.1029/98RG02075>.
- Scherwath, M., Kopp, H., et al. 2010. Fore arc deformation and underplating at the northern Hikurangi margin, New Zealand. *Journal of Geophysical Research*, 115, 1 – 23, <https://doi.org/10.1029/2009JB006645>.
- Scholl, D.W., Kirby, S.H., von Huene, R., Ryan, H., Wells, R.E. & Geist, E.L. 2015. Great (\geq Mw8.0) megathrust earthquakes and the subduction of excess sediment and bathymetrically smooth seafloor. *Geosphere*, 11, 236 – 265, <https://doi.org/10.1130/GES01079.1>.
- Scholl, D.W., Marlow, M.S. & Cooper, A.K. 1977. Sediment subduction and offscraping at Pacific margins. In: Talwani, M. & Pitman, W. C. (eds) *Maurice Ewing Series*. Washington, D. C., American Geophysical Union, 199 – 210., <https://doi.org/10.1029/ME001p0199>.
- Scholz, C.H. 1998. Earthquakes and friction laws. *Nature*, 391, 37 – 42, <https://doi.org/10.1038/34097>.
- Serrano, L., Ferrari, L., Martínez, M.L., Petrone, C.M. & Jaramillo, C. 2011. An integrative geologic, geochronologic and geochemical study of Gorgona Island, Colombia: Implications for the formation of the Caribbean Large Igneous Province. *Earth and Planetary Science Letters*, 309, 324 – 336, <https://doi.org/10.1016/j.epsl.2011.07.011>.
- Shackleton, R.M. 1954. The Structure and Succession of Anglesey and the Lleyn Peninsula. *Advancement of Science*, 41, 106 – 108.
- Shervais, J.W., Choi, S.H., Sharp, W.D., Ross, J., Zoglman-Schuman, M. & Mukasa, S.B. 2011. Serpentinite matrix mélange: Implications of mixed provenance for mélange formation. In: *Geological Society of America Special Papers*. Geological Society of America, 1 – 30., [https://doi.org/10.1130/2011.2480\(01\)](https://doi.org/10.1130/2011.2480(01)).
- Shimamoto, T. 1986. Transition Between Frictional Slip and Ductile Flow for Halite Shear Zones at Room Temperature. *Science*, 231, 711 – 714, <https://doi.org/10.1126/science.231.4739.711>.

- Shreve, R.L. & Cloos, M. 1986. Dynamics of sediment subduction, melange formation, and prism accretion. *Journal of Geophysical Research*, 91, 10229 – 10229, <https://doi.org/10.1029/JB091iB10p10229>.
- Sibson, R.H. 1985. Stopping of earthquake rupture at dilational jogs. *Nature*, 316.
- Sibson, R.H. 1986. Rupture Interaction with Fault Jogs. In: Das, S., Boatwright, J. & Scholz, C. H. (eds) *Earthquake Source Mechanics*. American Geophysical Union, Geophysical Monograph Series, 37.
- Silver, E.A. & Beutner, E.C. 1980. Melanges. *Geology*, 8, 32 – 34, [https://doi.org/10.1130/0091-7613\(1980\)8<32:M>2.0.CO;2](https://doi.org/10.1130/0091-7613(1980)8<32:M>2.0.CO;2).
- Singleton, J.S. & Cloos, M. 2013. Kinematic analysis of mélangé fabrics in the Franciscan Complex near San Simeon, California: Evidence for sinistral slip on the Nacimiento fault zone? *Lithosphere*, 5, 179 – 188, <https://doi.org/10.1130/L259.1>.
- Sinton, W., Duncan, A., Denyer, P., Rica, D.C. & Jose, S. 1997. Nicoya Peninsula, Costa Rica: A single suite of Caribbean oceanic plateau magmas. 102.
- Skarbek, R.M., Rempel, A.W. & Schmidt, D.A. 2012. Geologic heterogeneity can produce aseismic slip transients: Geologic heterogeneity and aseismic slip. *Geophysical Research Letters*, 39, n/a-n/a, <https://doi.org/10.1029/2012GL053762>.
- Sparkes, R., Tilmann, F., Hovius, N. & Hillier, J. 2010. Subducted seafloor relief stops rupture in South American great earthquakes: Implications for rupture behaviour in the 2010 Maule, Chile earthquake. *Earth and Planetary Science Letters*, 298, 89 – 94, <https://doi.org/10.1016/j.epsl.2010.07.029>.
- Spooner, E.T.C. & Fyfe, W.S. 1973. Sub-sea-floor metamorphism, heat and mass transfer. *Contributions to Mineralogy and Petrology*, 42, 287 – 304, <https://doi.org/10.1007/BF00372607>.
- Sutherland, R., Stagpoole, V., et al. 2009. Reactivation of tectonics, crustal underplating, and uplift after 60 Myr of passive subsidence, Raukumara Basin, Hikurangi-Kermadec fore arc, New Zealand: Implications for global growth and recycling of continents. *Tectonics*, 28, 1 – 23, <https://doi.org/10.1029/2008TC002356>.
- Svitek, T., Vavryčuk, V., Lokajíček, T. & Petružálek, M. 2014. Determination of elastic anisotropy of rocks from P- and S-wave velocities: numerical modelling and lab measurements. *Geophysical Journal International*, 199, 1682 – 1697, <https://doi.org/10.1093/gji/ggu332>.
- Talbot, C.J. & Brunn, V.V. 1989. Melanges, intrusive and extrusive sediments, and hydraulic arcs. *Geology*, 17, 446 – 448, [https://doi.org/10.1130/0091-7613\(1989\)017<0446](https://doi.org/10.1130/0091-7613(1989)017<0446).

- Taylor, J.H. 1934. The Mountsorrel Granodiorite and Associated Igneous Rocks. *The Geological Magazine*, 71.
- Tembe, S., Lockner, D.A. & Wong, T.-F. 2010. Effect of clay content and mineralogy on frictional sliding behavior of simulated gouges: Binary and ternary mixtures of quartz, illite, and montmorillonite. *Journal of Geophysical Research*, 115, <https://doi.org/10.1029/2009JB006383>.
- ten Brink, U.S. & Watts, A.B. 1985. Seismic stratigraphy of the flexural moat flanking the Hawaiian Islands. *Nature*, 317, 421 – 424, <https://doi.org/10.1038/317421a0>.
- Tepp, G., Ebinger, C.J., et al. 2018. Seismic Anisotropy of the Upper Mantle Below the Western Rift, East Africa. *Journal of Geophysical Research: Solid Earth*, <https://doi.org/10.1029/2017JB015409>.
- Thielmann, M., Rozel, A., Kaus, B.J.P. & Ricard, Y. 2015. Intermediate-depth earthquake generation and shear zone formation caused by grain size reduction and shear heating. *Geology*, 43, 791 – 794, <https://doi.org/10.1130/G36864.1>.
- Thompson, P.M.E., Kempton, P.D., et al. 2003. Hf–Nd isotope constraints on the origin of the Cretaceous Caribbean plateau and its relationship to the Galápagos plume. *Earth and Planetary Science Letters*, 217, 59 – 75, [https://doi.org/10.1016/S0012-821X\(03\)00542-9](https://doi.org/10.1016/S0012-821X(03)00542-9).
- Trechmann, C.T. 1948. Some Puzzling Features of Alpine and West Indian Metamorphic Rocks. *Geological Magazine*, 85, 297, <https://doi.org/10.1017/S0016756800075816>.
- Ujiie, K., Yamaguchi, A., Kimura, G. & Toh, S. 2007. Fluidization of granular material in a subduction thrust at seismogenic depths. *Earth and Planetary Science Letters*, 259, 307 – 318, <https://doi.org/10.1016/j.epsl.2007.04.049>.
- Underwood, M.B. & Bachman, S.B. 1982. Sedimentary facies associations within subduction complexes 4500 If.
- Vannucchi, P. & Bettelli, G. 2002. Mechanisms of subduction accretion as implied from the broken formations in the Apennines, Italy. 1, 835 – 838.
- Vannucchi, P., Fisher, D.M., Bier, S. & Gardner, T.W. 2006. From seamount accretion to tectonic erosion: Formation of Osa Mélangé and the effects of Cocos Ridge subduction in southern Costa Rica. *Tectonics*, 25, n/a-n/a, <https://doi.org/10.1029/2005TC001855>.
- Vannucchi, P., Morgan, J.P. & Balestrieri, M.L. 2016b. Subduction erosion, and the de-construction of continental crust: The Central America case and its global implications. *Gondwana Research*, 40, 184 – 198, <https://doi.org/10.1016/j.gr.2016.10.001>.

- Vannucchi, P., Morgan, J.P., Silver, E.A. & Kluesner, J.W. 2016a. Origin and dynamics of depositional subduction margins Paola. *Geochemistry Geophysics Geosystems*, 17, 2825 – 2834, <https://doi.org/10.1002/2016GC006406>.
- Vannucchi, P., Remitti, F. & Bettelli, G. 2008. Geological record of fluid flow and seismogenesis along an erosive subducting plate boundary. *Nature*, 451, 699 – 703, <https://doi.org/10.1038/nature06486>.
- Vannucchi, P., Sage, F., Phipps Morgan, J., Remitti, F. & Collot, J.-Y. 2012. Toward a dynamic concept of the subduction channel at erosive convergent margins with implications for interplate material transfer. *Geochemistry, Geophysics, Geosystems*, 13, 1 – 24, <https://doi.org/10.1029/2011GC003846>.
- Vannucchi, P., Sak, P.B., Morgan, J.P., Ohkushi, K. & Ujiie, K. 2013. Rapid pulses of uplift, subsidence, and subduction erosion offshore Central America: Implications for building the rock record of convergent margins. *Geology*, 41, 995 – 998, <https://doi.org/10.1130/G34355.1>.
- Vannucchi, P., Ujiie, K., Stronck, N., Malinverno, A. & the Expedition 334 Scientists. 2011. Costa Rica Seismogenesis Project, Program A Stage 1 (CRISP-A1): Expedition 344 of the riserless drilling platform from and to Puntarenas, Costa Rica. In: *Proceedings of the Integrated Ocean Drilling Program Volume 334 Expedition Reports*. Integrated Ocean Drilling Program Management International, Inc., for the Integrated Ocean Drilling Program, 16.
- Vollmer, F.W. & Bosworth, W. 1984. Formation of melange in a foreland basin overthrust setting: Example from the Taconic Orogen. In: *Geological Society of America Special Papers*. Geological Society of America, 53 – 70., <https://doi.org/10.1130/SPE198-p53>.
- von Huene, R. & Culotta, R. 1989. Tectonic erosion at the front of the Japan Trench convergent margin. *Tectonophysics*, 160, 75 – 90.
- von Huene, R. & Ranero, C.R. 2003. Subduction erosion and basal friction along the sediment-starved convergent margin off Antofagasta, Chile. 108, <https://doi.org/10.1029/2001JB001569>.
- von Huene, R., Ranero, C.R. & Vannucchi, P. 2004. Generic model of subduction erosion. *Geology*, 32, 913 – 913, <https://doi.org/10.1130/G20563.1>.
- Wakabayashi, J. & Dilek, Y. 2011. *Mélanges: Processes of Formation and Societal Significance*, <https://doi.org/10.1130/2011.CITATIONS>.
- Wakabayashi, J. 2011. *Mélanges of the Franciscan Complex, California: Diverse structural settings, evidence for sedimentary mixing, and their connection to subduction processes*. In: Wakabayashi, J. & Dilek, Y. (eds) *Mélanges: Processes of Formation and Societal Significance*. Geological Society of America.

- Wakabayashi, J. 2012. Subducted sedimentary serpentinite mélanges: Record of multiple burial–exhumation cycles and subduction erosion. *Tectonophysics*, 568 – 569, 230 – 247, <https://doi.org/10.1016/j.tecto.2011.11.006>.
- Walther, C.H.E. 2003. The crustal structure of the Cocos ridge off Costa Rica. *Journal of Geophysical Research: Solid Earth*, 108, 1 – 21, <https://doi.org/10.1029/2001JB000888>.
- Wang, K. & Bilek, S.L. 2014. Invited review paper: Fault creep caused by subduction of rough seafloor relief. *Tectonophysics*, 610, 1 – 24, <https://doi.org/10.1016/j.tecto.2013.11.024>.
- Ward, W.H., Burland, J.B. & Gallois, R.W. 1968. Geotechnical Assessment of a Site at Mundford, Norfolk, for a large Proton Accelerator. *Géotechnique*, <https://doi.org/10.1680/geot.1968.18.4.399>.
- Warren, C.J., Beaumont, C. & Jamieson, R. a. 2008. Formation and exhumation of ultra-high-pressure rocks during continental collision: Role of detachment in the subduction channel. *Geochemistry, Geophysics, Geosystems*, 9, n/a-n/a, <https://doi.org/10.1029/2007GC001839>.
- Watts, A.B. 1994. Crustal Structure, Gravity-Anomalies and Flexure of the Lithosphere in the Vicinity of the Canary-Islands. *Geophysical Journal International*, 119, 648 – 666, <https://doi.org/10.1111/j.1365-246X.1994.tb00147.x>.
- Weatherall, P., Marks, K.M., et al. 2015. A new digital bathymetric model of the world's oceans: New Digital Bathymetric Model. *Earth and Space Science*, 2, 331 – 345, <https://doi.org/10.1002/2015EA000107>.
- Wegner, W., Worner, G., Harmon, R.S. & Jicha, B.R. 2011. Magmatic history and evolution of the Central American Land Bridge in Panama since Cretaceous times. *Geological Society of America Bulletin*, 123, 703 – 724, <https://doi.org/10.1130/B30109.1>.
- Wells, D.L. & Coppersmith, K.J. 1994. New Empirical Relationships among Magnitude, Rupture Length, Rupture Width, Rupture Area, and Surface Displacement. *Bulletin of the Seismological Society of America*, 84, 974 – 1002.
- Whattam, S. a. & Stern, R.J. 2015. Late Cretaceous plume-induced subduction initiation along the southern margin of the Caribbean and NW South America: The first documented example with implications for the onset of plate tectonics. *Gondwana Research*, 27, 38 – 63, <https://doi.org/10.1016/j.gr.2014.07.011>.
- Whattam, S.A. & Stern, R.J. 2016. Arc magmatic evolution and the construction of continental crust at the Central American Volcanic Arc system. *International Geology Review*, 58, 653 – 686, <https://doi.org/10.1080/00206814.2015.1103668>.

- White, S.H., Bretan, P.G. & Rutter, E.H. 1986. Fault-Zone Reactivation: Kinematics and Mechanisms. *Philosophical Transactions of the Royal Society A: Mathematical, Physical and Engineering Sciences*, 317, 81 – 97, <https://doi.org/10.1098/rsta.1986.0026>.
- Willbold, M., Hegner, E., Stracke, A. & Rocholl, A. 2009. Continental geochemical signatures in dacites from Iceland and implications for models of early Archaean crust formation. *Earth and Planetary Science Letters*, 279, 44 – 52, <https://doi.org/10.1016/j.epsl.2008.12.029>.
- Williams, T.P.T. 2007. The role of Annie Greenly in the elucidation of the geology of Anglesey. Geological Society, London, Special Publications, 281, 319 – 324, <https://doi.org/10.1144/SP281.21>.
- Wilson, G. 1938. The Evolution of Granodioritic Rocks of the South-Eastern End of the Kopaonik Batholith, Yugoslavia. *The Geological Magazine*, 75.
- Winchester, J.A. & Floyd, P.A. 1977. Geochemical discrimination of different magma series and their differentiation products using immobile elements. *Chemical Geology*, 20, 325 – 343, [https://doi.org/10.1016/0009-2541\(77\)90057-2](https://doi.org/10.1016/0009-2541(77)90057-2).
- Woo, S., Lee, H., Han, R., Chon, C.-M., Son, M. & Song, I. 2015. Frictional properties of gouges collected from the Yangsan Fault, SE Korea. *Journal of the geological society of Korea*, 51, 569, <https://doi.org/10.14770/jgsk.2015.51.6.569>.
- Wood, M. 2012. The Historical Development of the Term ‘Mélange’ and Its Relevance to the Precambrian Geology of Anglesey and the Llyn Peninsula in Wales, UK. *Journal of Geography (Chigaku Zasshi)*, 121, 168 – 180, <https://doi.org/10.5026/jgeography.121.168>.
- Wright, J.E. & Wyld, S.J. 2011. Late Cretaceous subduction initiation on the eastern margin of the Caribbean-Colombian Oceanic Plateau: One Great Arc of the Caribbean (?). *Geosphere*, 7, 468 – 493, <https://doi.org/10.1130/GES00577.1>.
- Zhang, Z. & Jin, M. 1979. Two kinds of melange and their tectonic significance in Xiangcheng-Derong area, southwestern Sichuan. *Scientia Geological Sinica*, 7, 205 – 214.
- Zheng, Y., Zhao, Z. & Chen, Y. 2013. Continental subduction channel processes: Plate interface interaction during continental collision. *Chinese Science Bulletin*, 58, 4371 – 4377, <https://doi.org/10.1007/s11434-013-6066-x>.

THIS PAGE INTENTIONALLY LEFT BLANK.

APPENDIX 1: GEOCHEMICAL DATA

Electronic appendix material can be accessed via Royal Holloway's website.

- **Osa Mélange Dataset.xlsx**
- Comparison Datasets
 - Azuero
 - **Azuero - Buchs et al 2011.xlsx**
 - Cordillera de Talamanca
 - **Talamanca - Abratis 1998.xlsx**
 - Golfito
 - **Golfito Complete - Buchs 08.xlsx**
 - Nicoya, Santa Elena, Herradura, and Quepos
 - **Nicoya Santa Elena - Whattam et al 2016.xlsx**
 - **Nicoya Santa Elena Herradura Quepos - Hauff et al 1997.xlsx**
 - Osa Igneous Complex
 - **Osa Igneous Complex - Buchs et al 2016.xlsx**
 - Osa Mélange
 - **Osa Melange - Buchs 2008.xlsx**

THIS PAGE INTENTIONALLY LEFT BLANK.

APPENDIX 2: STRUCTURAL ANISOTROPY DATA

Electronic appendix material can be accessed via Royal Holloway's website.

- Campanario
 - Campanario 1
 - **Campanario 1.xlsx**
 - **Photo.jpg**
 - **Trace.tif**
 - Campanario 2
 - **Campanario 2.xlsx**
 - **Photo.jpg**
 - **Trace.tif**
- Cocolito
 - Cocolito 1
 - **Cocolito 1.xlsx**
 - **Photo.jpg**
 - **Trace.tif**
 - Cocolito 2
 - **Cocolito 2.xlsx**
 - **Photo.jpg**
 - **Trace.tif**
 - Cocolito 3
 - **Cocolito 3.xlsx**
 - **Photo.jpg**
 - **Trace.tif**
 - Cocolito 4
 - **Cocolito 4.xlsx**
 - **Photo.jpg**
 - **Trace.tif**
 - Cocolito 5
 - **Cocolito 5.xlsx**
 - **Photo.jpg**
 - **Trace.tif**

- Cocolito 6
 - **Cocolito 6.xlsx**
 - **Photo.jpg**
 - **Trace.tif**
- Cocolito 7
 - **Cocolito 7.xlsx**
 - **Photo.jpg**
 - **Trace.tif**
- Drake
 - Drake 1
 - **Drake 1.xlsx**
 - **Photo.jpg**
 - **Trace.tif**
 - Drake 2
 - **Drake 2.xlsx**
 - **Photo.jpg**
 - **Trace.tif**
 - Drake 3
 - **Drake 3.xlsx**
 - **Photo.jpg**
 - **Trace.tif**
 - Drake 4
 - **Drake 4.xlsx**
 - **Photo.jpg**
 - **Trace.tif**
 - Drake 5
 - **Drake 5.xlsx**
 - **Photo.jpg**
 - **Trace.tif**
 - Drake 6
 - **Drake 6.xlsx**
 - **Photo.jpg**
 - **Trace.tif**
- Marengo
 - Marengo 1
 - **Marengo 1.xlsx**
 - **Photo.jpg**
 - **Trace.tif**

- Marengo 2
 - **Marengo 2.xlsx**
 - **Photo.jpg**
 - **Trace.tif**
- Marengo 3
 - **Marengo 3 - Generation 1.xlsx**
 - **Marengo 3 - Generation 2.xlsx**
 - **Photo.jpg**
 - **Trace - Generation 1.tif**
 - **Trace - Generation 2.tif**

THIS PAGE INTENTIONALLY LEFT BLANK.

APPENDIX 3: TRIAXIAL EXPERIMENT DATA

*Electronic appendix material can be accessed via Royal
Holloway's website.*

- Altered basalt
 - **60-60 Osa 16 - 146a.xlsx**
 - **120-60 Osa 16 - 146c.xlsx**
- Cocos ridge basalt
 - **60-60 Cocos 12 - 2.xlsx**
- Volcanoclastic matrix
 - **60-60 Osa 16 - 147b.xlsx**
 - **120-60 Osa 16 - 147h.xlsx**
 - **120-120 Osa 16 - 147e.xlsx**